

Graduation Report

Driver's acceptance of trajectory type in trajectory-driven Haptic Shared Control



Driver's acceptance of trajectory type in trajectory-driven Haptic Shared Control

Master of Science Thesis

by E.P.J. Ghys

to obtain the degree of Master of Science at the Delft University of Technology, to be defended publicly on Thursday July 9, 2020 at 13:00.

Student number: 4368568

Thesis committee: Prof. M. Mulder, TU Delft, chair
Dr. D. M. Pool. TU Delft, supervisor

Dr. D. M. Pool, TU Delft, supervisor Ir. S. Barendswaard, TU Delft, supervisor

Dr. M. M. van Paassen, TU Delft, additional committee member

Dr. J. C. F. de Winter, TU Delft, examiner

An electronic version of this thesis is available at http://repository.tudelft.nl/.



Preface

This graduation report contains my entire master thesis and thereby concludes my studies at the Delft University of Technology. I am very grateful that I got to work on such a popular and relatable topic, as automation in car driving is becoming more advanced every day. Initially, the intention behind my research was to investigate personalisation in haptic shared control depending on the age of the driver, however, along the way we took several turns, jumped through some hoops, and ended up with an entirely different research goal. This processed showed me that being a researcher is not as straightforward as I thought it would be.

During my entire thesis I could always count on the help and supervision of Daan and Sarah, who often reassured me about the track of my research and helped me countless times when the simulator broke down. Thank you Daan and Sarah for always helping me and thank you Max, for always showing great enthusiasm and interest in my work.

At last I would like to thank my family and friends. Thank you for participating in my experiment and thank you for helping me find even more participants. It was amazing to see your enthusiasm about my experiment and your interest in finding and understanding the results.

E.P.J. Ghys Delft, July 2020

Contents

	Lis	t of A	Abbreviations	vii
	Lis	t of S	Symbols	хi
ı	Sci	ienti	fic Article	1
Ш	Pr	relim	ninary Graduation Report	31
	1	Intr	roduction	33
	2	Lite	erature Survey	35
		2.1	Haptic Shared Control	35
			2.1.1 Meshed Controller	35
			2.1.2 Four-Design-Choice Architecture	36
			2.1.3 Other Control Strategies	38
			2.1.4 Conclusion	38
		2.2	Personalisation Types	
			2.2.1 Level of Haptic Authority	38
			2.2.2 Ratio Haptic Feedback & Haptic Support	39
			2.2.3 Human Compatible Reference	39
			2.2.4 Conclusion	
		2.3	Driving Behaviour Classification	
			2.3.1 Normal vs. Aggressive Behaviour	
			2.3.2 Track Path Classification	
			2.3.3 Trajectory Type Classification	
			2.3.4 Conclusion	
		2.4	Driver Grouping	
			2.4.1 Driving Habits of the Elderly	
			2.4.2 Different Effects of ADAS	
			2.4.3 Gender And Age	
			2.4.4 Conclusion	
		2.5	Method Trade-off	45
	3	Res	search Objective and Questions	47
	4	Pre	. ,	49
		4.1	Simulation Setup	49
			4.1.1 Driver Model	49
			4.1.2 Trajectory tuning	
			4.1.3 Four-Design-Choice-Architecture	53
			4.1.4 Joining of driver and controller	
			4.1.5 Collaboration between parties	
			4.1.6 Conflict torques	
		4.2	Results	
			4.2.1 Conflict Torque Analysis	
			4.2.2 New Centerline Trajectory	
			4.2.3 Updated Simulations	
		4.3	Verification	
			4.3.1 Code Verification	65

vi

	4.4 Validation. 4.5 Discussion 4.6 Conclusion	68
5	Proposal Final Experiment	71
	5.1 Apparatus	
	5.3 Subjects and Instructions	
	5.4 Experiment Design	
	5.5 Hypotheses	74
6	Conclusion	75
Bil	oliography	77
Α	Simulation Results	81
В	Individual Driver Results	85
С	Questionnaire data 1	151
D	Briefing and Consent Form 1	155
Е	Attempts at New Conflict Definition	159

List of Abbreviations

AD Automated Driving

ADAS Advanced Driver Assistance Systems

COG Centre of Gravity
D Manual Driving

FDC Four-Design-Choice

FDCA Four-Design-Choice-Architecture

FoV Field of View

HCR Human Compatible ReferenceHMI Human-Machine Interaction

HSC Haptic Shared Control

iFDCA Four-Design-Choice with individualized Human Compatible Reference

LoHA Level of Haptic Authority LoHS Level of Haptic Support

mFDCA Four-Design-Choice with averaged Human Compatible Reference

NMS Neuromuscular SystemSRR Steering Reversal Rate

SoHF Strength of Haptic Feedback

TDCA Total Four-Design-Choice-Architecture

TLC Time-to-Lane-Crossing TwL Two-Level Controller

List of Symbols

 Γ_d Desired steering torque driver model[Nm]

 Γ_s Torque feedback driver model [Nm]

 Δ Euclidean distance [m] $\Delta \psi$ Error in heading [rad]

 Δs_{lat} Error in lateral position [m]

eta Sideslip angle [rad] δ Road width [m]

 δ_{driver} Steering wheel angle by driver in simulations [rad]

 δ_{far} Far angle [rad] δ_{near} Near angle [rad]

 $\delta_s(t)$ Desired steering angle simplified driver model [rad]

 δ_{total} Total steering wheel angle Four-Design-Choice and driver combined in simulations [rad]

 $\overrightarrow{\delta}_R$ Reference steering angle of car [rad]

 $\delta_R(t)$ Reference steering angle of car at nearest point [rad] $\hat{\delta}_{SW}$ Desired steering wheel angle driver model [rad]

 δ_{SW} Steering wheel angle driver model [rad]

heta Steering wheel angle [rad] $\kappa(t)$ Current curvature $[m^{-1}]$ τ Steering wheel torque [Nm] τ_p Time delay driver model [sec]

 τ_{v} Time delay simplified driver model [sec]

 $\psi_{car}(t)$ Heading of car at time t [rad]

 $\hat{\psi}_{car}(t + t_{LH})$ Predicted heading of car at look-ahead time t_{LH} [rad]

 ψ_L Heading angle driver model [rad] $\overrightarrow{\psi}_R$ Reference heading of car [rad]

 $\psi_R(t)$ Reference heading of car at nearest point [rad]

 $\psi_R(t + t_L H)$ Predicted reference heading of car at look-ahead time t_{LH} [rad]

 B_w Steering wheel friction coefficient [Nms/rad]

D Lateral position error gain [N]

 D_{far} Far angle distance [m]

G_C Compensation part driver model [-]

 G_NM Neuromuscular dynamics driver model [-]

 G_p Anticipation part driver model [-]

x Contents

 H_{NM} Neuromuscular dynamics [-]

J Vehicle yaw moment of inertia $[kgm^{-1}]$ J_{cost} Cost resulting from cost function [-]

 J_w Steering wheel inertia [kgm^2]

 K_{ψ} Heading error gain Four-Design-Choice-Architecture [Nm/deg]

 K_c Compensation gain driver model [-]

 K_{co-dr} Collaboration gain driver [-]

 K_{co-fdc} Collaboration gain Four-Design-Choice-Architecture [-]

 K_f Feedback gain Meshed controller [-]

 K_{LoHS} Level of Haptic Support Four-Design-Choice-Architecture [Nm/rad]

 K_p Anticipation gain driver model [-]

 K_r Angle to torque coefficient driver model [-]

 K_{SoHF} Strength of Haptic Feedback Four-Design-Choice-Architecture [-]

 K_s Lateral error gain Four-Design-Choice-Architecture [N] K_t Driver steering wheel holding stiffness driver model [-]

 K_w Steering wheel spring constant [Nm/rad]

M Total mass of vehicle [kg] $O_{conflict}$ Occurrence of conflict [-] P Heading error gain [Nm/deg]

R Radius of curve [m] R_s Steering gear ratio [-] $T_D(t)$ Driver torque [Nm]

 T_{driver} Driver steering wheel torque in simulations [Nm]

 T_{FDCA} Torque output of Four-Design-Choice-Architecture in simulations [Nm]

 T_L Compensation rate driver model [-]

 T_l Compensation frequency band driver model [-]

 $T_{LoHS}(t)$ Haptic support torque Four-Design-Choice-Architecture [Nm]

 $T_M(t)$ Feedback torque Meshed Controller [Nm] T_N Neuromuscular time constant driver model [-]

 $T_{SoHF}(t)$ Haptic feedback torque Four-Design-Choice-Architecture [Nm]

 $T_{TDCA}(t)$ Total Four-Design-Choice-Architecture torque[Nm]

 $T_{tot}(t)$ Total torque [Nm]

 T_{total} Total torque of Four-Design-Choice and driver combined in simulations [Nm]

V Longitudinal velocity vehicle [m/s] V_x Longitudinal velocity vehicle [m/s]

 $X_{car}(t)$ X-position of car at time t [m]

 $\hat{X}_{car}(t + t_{LH})$ Predicted X-position of car at look-ahead time t_{LH} [m]

 \vec{X}_R Reference X-position of car [m]

 $X_R(t)$ Reference X-position of car at nearest point [m]

 $X_R(t + t_L H)$ Predicted reference X-position of car at look-ahead time t_{LH} [m]

Contents xi

 $Y_{car}(t)$ Y-position of car at time t [m]

 $\hat{Y}_{car}(t + t_{LH})$ Predicted Y-position of car at look-ahead time t_{LH} [m]

 \overrightarrow{Y}_R Reference Y-position of car [m]

 $Y_R(t)$ Reference Y-position of car at nearest point [m]

 $Y_R(t + t_{LH})$ Predicted reference Y-position of car at look-ahead time t_{LH} [m]

 c_f Front cornering stiffness [N/rad] c_r Rear cornering stiffness [N/rad]

m Number of data points along curve [-]

 l_f Distance from centre of gravity to front axle [m] l_r Distance from centre of gravity to rear axle [m]

 l_s Near point distance driver model[m]

r Yaw rate [rad/s]

t time [s]

 t_{LH} Look-ahead time Meshed Controller [s] s_{lat} Lateral position of vehicle on road [m]

*s*_{latHCR} Lateral position on road of HCR trajectory [m]

*s*_{lattotal} Lateral position of combined trajecotry by HCR and driver [m]

v Vehicle speed driver model [m/s] y_L Lateral deviation driver model [m]

I

Scientific Article

Drivers' acceptance of trajectory type in trajectory-driven Haptic Shared Control

Author: E.P.J. Ghys
Dep. Control and Simulation, Aerospace Engineering
Delft University of Technology, Delft, The Netherlands
Email: e.p.j.ghys@student.tudelft.nl

Abstract—Haptic shared control is a driving assistance system that allows for continuous communication between the driver and the automation through a physical control device, such as the steering wheel. Previous research has proposed the Four-Design-Choice-Architecture, a control system with a feedforward loop that opens possiblities for personalisation to the driver. The goal of this research is therefore to understand how changing the reference trajectory and the feedforward gain influences the acceptance of the system. This investigation consists of an offline simulation platform and a human-in-the-loop experiment in which the most popular driving group, R3L5 drivers, and the optimal curve cutters group, R2L1 and R2L2 drivers, were subjected to four different reference trajectories and two feedforward gains. The reference trajectories consisted of the industry standard centerline trajectory, a completely personalised trajectory and the classaverage trajectories of the drivers' own class and the other group's class. The feedforward gains consisted of the heuristically tuned value of 0.92 and the lower 0.5 to give the drivers a higher workload. The results showed that complete personalisation consistently leads to less conflict for all drivers, however, drivers that adapt their driving style to the guidance also reach low conflict values for the class-average guidance of their own class. Furthermore, it was found that acceptance is not linked to optimal trajectories, i.e., less steering input needed and more dynamically safe trajectories. The results also showed that the higher feedforward gain of 0.92 is beneficial with respect to the lower gain as it reduces conflicts up to 86.91% and is rated consistently higher in subjective questionnaires. Future research should focus on understanding which drivers need the complete personalisation and on how to optimise the feedforward gain.

Index Terms—Haptic Shared Control, Human-Machine Interaction, Acceptance, Conflict, Personalisation, Feedforward, Adaptation

I. Introduction

Haptic shared control (HSC) is a type of Advanced Driver Assistance System (ADAS) for highly automated vehicles in which the driver and vehicle automation communicate through a physical control device [1] [2]. Instead of removing the driver from the control loop – which is a widely favoured strategy in autonomous vehicles [3] [4] – haptic shared control allows the driver to stay relevant and knowledgeable about the system's intentions and shortcomings [5]. Studies so far have shown that haptic shared

control is capable of increasing safety [6] and decreasing control activity [7] compared to manual driving, however, it also may lead to an increase in driver torque [8]. This increase in driver torque is often experienced as a nuisance by drivers and is caused by a misalignment of intention between both the driver and the controller [7] [9]. This misalignment is often referred to as a conflict and is detrimental for the acceptance of the haptic shared control systems. Acceptance is an essential requirement and is defined in [10] as "the degree to which an individual intends to use a system and, when available, to incorporate the system in his/her driving". It is therefore critical that acceptance is increased, which is accomplished by the reduction of conflict.

As haptic shared control will provide a key bridge in the development period until fully autonomous cars are realised, researchers have developed a great interest in shared control with the steering wheel as haptic surface [5] [11] [12]. As a way to minimise conflicts and thus optimise acceptance, past research has mostly focused on what type of controller drivers prefer in terms of structure. Most early research on haptic shared control was focused on an architecture that only provided feedback torques to the drivers [5] [13]. The results of these studies were very promising in terms of reduced control activity, however, more recently, it was found that feedback torque is experienced by drivers as punishing [14]. A following study found that drivers therefore prefer a controller that also anticipates the upcoming curve with feedforward torques [14]. More specifically, the recently proposed Four-Design-Choice-Architecture (FDCA) [15] is able to reduce conflicts by a factor of 2.3 compared to the older, feedbackonly controllers [14].

So far, however, the focal point of HSC research for curve driving has mostly been on control structures and less on the curve negotiation behaviour of the architecture. Research by [16] has shown that drivers operating an automated vehicle prefer a system that matches their own curve driving style both in terms of lateral acceleration and Time-to-Lane Crossing (TLC) or is at least very similar in both areas. The Time-to-Lane Crossing is a measure of perceived risk by the driver, where a large TLC indicates a safe trajectory [17] [18]. This of course raises the question

whether acceptance of haptic shared control can further be improved by changing the driving style of the haptic shared controller. Most research concerning haptic shared control assumes that the controller should follow a centerline trajectory through curves [5] [13], however, centerline driving is generally not natural to drivers [19]. The earlier mentioned FDCA, however, differs from these traditional controllers as it allows changing the reference trajectory to independently set paths, opening the opportunity to test different driving styles. [15].

According to [19], the driving population can be categorised into seven different curve negotiation styles. The full classification, based on a rule-based classifier, is shown in Figure 1. Each style or class is characterised by a different lateral path through the curve. Some classes, such as class 1 and 2, are more efficient or optimal than other classes due to their lower lateral acceleration and higher TLC and thus require less steering input.

Based on this categorisation, together with the variable FDCA, the goal of this research is to investigate how haptic shared control acceptance is influenced by changing the reference trajectory of the control system. Specifically, this is investigated by a conflict torque analysis of predictive simulations and a fixed-speed human-in-the-loop experiment, in which two driver groups from [19] are assessed: the most popular driving style and the more efficient curve cutters. These drivers are subjected to a fully personalised reference trajectory, as well as a class-average trajectory of their own and the other driver group. These are then tested to compare with the industry standard, the centerline path. For each condition, different torques are analysed together with subjective acceptance ratings.

With respect to the research goal, both the completely personalised and class average trajectories are tested to understand how the level of personalisation influences acceptance, whereas the centerline trajectory, the industry standard, is added for reference. It will be researched if drivers can be tricked into liking certain trajectories and if the efficiency of the different trajectories influences this decision. Additionally, after the conclusions of [14], two different levels of guiding feedforward torques are tested to understand what type of collaboration is preferred by drivers.

The paper is structured parallel to the methodology followed to answer the research objective. Section II explains the simulation platform, designed to replicate the collaboration between driver and haptic shared controller, followed by the experiment hypotheses deducted from them. Section III provides the details of the conducted experiment, including the simulator, software set-up and hypotheses. In Section IV the results of the experiments are presented, followed by the discussion and conclusion in, respectively, Section V and VI.

II. SIMULATIONS

From a research perspective, computer simulations and experiments go hand in hand. Simulations raise questions that experiments are capable of answering, while experiments also validate the models and assumptions on which the simulations are built [20]. Simulations are therefore included in this research as they add supplementary knowledge on the collaboration between drivers and haptic shared and could be a valuable asset for the experiment design. More specifically, these simulations help in gaining a deeper understanding on how drivers may react to the different steering wheel inputs created by the HSC systems and whether they follow these contributions or oppose them. In this paper, the simulation results are used to derive hypotheses for the final experiment.

A. Set-up

Because of the symbiotic relationship between the simulations and the experiment, it is essential that the simulations resemble the set-up of the experiment as closely as possible. This is achieved by implementing the same haptic shared control architecture, i.e., the Four-Design-Choice-Architecture, in both entities. This is crucial as each architecture has a different framework and structure, resulting in different forms of collaboration and perception for the drivers. Additionally, the architecture must be tuned correspondingly in both the simulations and experiments.

The one segment that evidently differs in the simulations is the lack of true human dynamic interaction. The driver is replaced by a driver model to mimic the driving task performed by a human driver.

1) Driver Model: In the computer simulations, a driver model that focuses on curve driving and that was designed to operate in combination with haptics [21] is used to represent the driver. The model, shown in Figure 2, combines two functional abilities drivers use when driving: perceptual and motor skills. The main advantage of this driver model involves the direct combination of the driver model with the vehicle dynamics, which eliminates the need for coordinate system transformations [21].

The workings of the driver model are mainly based on the differentiation between an anticipatory and compensatory part. The compensatory, closed-loop behaviour is designed to stabilise the heading and follow the centre of the road, while the anticipatory, open-loop part accounts for the needed steering to follow the curve based on the current road curvature $\kappa(t)$.

In order to calculate the resulting steering angles of both parts the near angle $\theta_{near}(t)$ and far angle $\theta_{far}(t)$ are computed respectively, see Figure 3. These calculations are simplified by making two assumptions: first, a constant curvature is assumed for the calculation of $\theta_{far}(t)$ and a straight road is assumed for the calculation of $\theta_{near}(t)$.

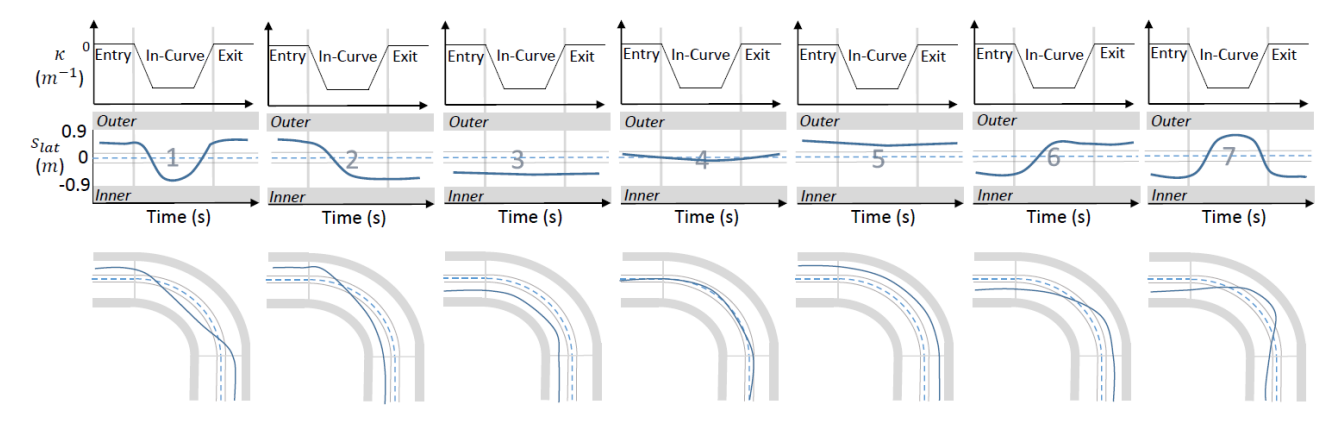


Fig. 1: The seven identified rule-based classes, taken from [19].

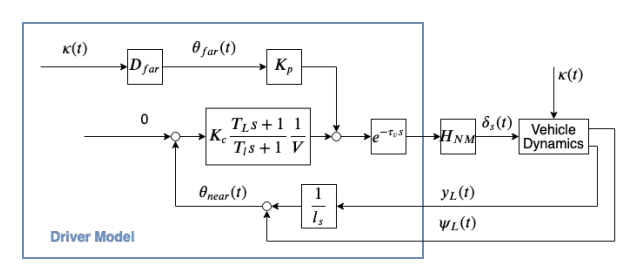


Fig. 2: The implemented driver model, adapted from [21].

Second, small angles are assumed, which simplifies computations, but also implies that the simulations are only valid for very small $\theta_{near}(t)$ and $\theta_{far}(t)$ angles, close to zero degrees.

Adhering to these assumptions, $\theta_{near}(t)$ is calculated from Figure 3, according to Equation (1), where y_L represents the lateral position error, ψ_L the heading error and l_s the look-ahead distance.

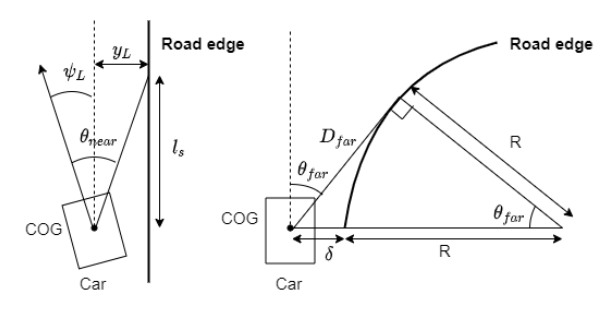


Fig. 3: The calculation of the compensatory near angle (left) and the anticipatory, tangent far angle (right), based on [21].

$$\theta_{near} = \tan\left(\frac{y_L}{l_s}\right) + \psi_L = \frac{y_L}{l_s} + \psi_L$$
 (1)

Note that all distances and angles in Figure 3 are determined from the centre of gravity (COG) of the vehicle. Furthermore, R represents the radius of the curve and δ

the distance between the COG of the vehicle and the road boundary. Similarly, the calculation of D_{far} and θ_{far} is given by Equations (2) and (3), respectively. Equation (2) is created by applying the Pythagorean theorem.

$$D_{far} = \sqrt{\delta^2 + 2\delta R} \tag{2}$$

$$\theta_{far} = \tan\left(\frac{D_{far}}{R(t)}\right) = \kappa(t) \cdot D_{far}$$
 (3)

After adding the anticipatory and compensatory parts, the driver model includes a visual processing delay, τ_p , after which the signal is processed by the neuromuscular dynamics of the driver in the H_{NM} -block of Figure 2. This block represents the neuromuscular dynamics as a simple first order system. At last, the desired steering wheel angle, $\delta_s(t)$ is used as the input to the vehicle dynamics. A linear bicycle model is implemented that uses $\delta_s(t)$ and current curvature $\kappa(t)$ as inputs and outputs side slip angle β , yaw rate r, heading angle ψ and offset from the centerline y_L [21]. This system is presented in Equations (4) to (10). Additional information on the different parameters is provided in Table I.

$$\begin{bmatrix} \dot{\beta} \\ \dot{r} \\ \dot{\psi}_L \\ \dot{y}_L \end{bmatrix} = \begin{bmatrix} a_{11c} & a_{12c} & 0 & 0 \\ a_{21c} & a_{22c} & 0 & 0 \\ 0 & 1 & 0 & 0 \\ V_x & l_s & V_x & 0 \end{bmatrix} \begin{bmatrix} \beta \\ r \\ \psi_L \\ y_L \end{bmatrix} + \begin{bmatrix} 0 \\ 0 \\ -V_x \\ -l_s V_x \end{bmatrix} \kappa + \begin{bmatrix} a_{15c} \\ a_{25c} \\ 0 \\ 0 \end{bmatrix} \delta_s$$
 (4)

$$a_{11c} = -\frac{2(c_j + c_r)}{MV_r}$$
 (5) $a_{12c} = \frac{2(c_r l_r + c_f l_f)}{MV_r^2} - 1$ (6)

$$a_{15c} = \frac{2c_f}{MV_x R_s}$$
 (7) $a_{21c} = \frac{2(c_r l_r + c_f l_f)}{J}$ (8)

$$a_{22c} = \frac{2(c_r l_r^2 + c_f l_f^2)}{JV_r} \quad (9) \qquad a_{25c} = \frac{2c_f l_f}{JR_s} \quad (10)$$

TABLE I: Parameters used for the driver model, taken from [21] and [22].

Parameter	Description	Value [Dimension]
l_f	Distance COG to front axle	1.127 [m]
l_r	Distance COG to rear axle	1.485 [m]
M	Total mass	$1476 \ [kg]$
J	Yaw moment of inertia	$1810 \ [kg \cdot m^2]$
c_f	Front cornering stiffness	65000 [N/rad]
c_r	Rear cornering stiffness	5700 [N/rad]
R_s	Steering gear ratio	16 [-]
l_s	Look-ahead distance	5 [m]
V_x	Longitudinal velocity	80 [km/h]

2) Trajectory Tuning: Trajectory-type classification puts drivers into one of the seven categories shown in Figure 1. The implemented driver model, however, has only limited capabilities to mimic these. It is therefore decided to design three variants of the driver model, each variant representing one of the seven classes. Despite the driver model lacking the ability to simulate pre-positioning behaviour before curves, the simulations do demonstrate how similar or opposing HCR-driver trajectories influence each other. Therefore, three opposing types of trajectories are selected for the simulations: centerline driving (class 4), curve cutting (class 2) and counter curve cutting (class 6). To mimic these behaviours, the remaining parameters must be tuned accordingly: the anticipation gain K_p , the compensation gain K_c , the lag time constant T_l and the lead time constant T_L of the stabilising loop. The result of this gain tuning can be found in Table II, where the parameter combinations for the three types of curve negotiation are shown.

TABLE II: Simulation parameters of the driver model of [21] used for different types of curve negotiation.

Driving Style	K_p	K_c	T_l	T_L
Centerline driving (class 4)	1.5	18	1	3
Curve cutting (class 2)	2.7	15	1	3
Counter curve cutting (class 6)	1.4	5	1	3

In these scenarios, the vehicle speed V_x is always fixed at 80 km/h and the curve radius at 204 m. This combination is chosen as it ensures a maximum centerline lateral acceleration equal to 2.41 ms^{-1} , which is the upper limit of allowed lateral acceleration for road design rules [23]. Furthermore, this scenario most closely resembles a highway scenario, where drivers are more inclined to use cruise control, making the constant velocity more plausible.

At last, an important remark must be made on this driver model. The model lacks true preview as its feed-forward acts on the current road curvature. Even if a curve is approaching, the model will still assume an infinite

straight road ahead. This differs from reality, where drivers will start to preposition the car seven seconds before the curve and turn into the curve already before the car COG enters the current section [24].

- 3) HSC Architecture: The HSC architecture implemented in both the simulations and experiments is the Four-Design-Choice-Architecture (FDCA). This architecture not only corrects deviations from the reference trajectory, but also guides the driver through curves [15]. The FDCA, depicted in Figure 4, consists of four main parts:
 - Human Compatible Reference (HCR): The HCR represents the path the controller intends to follow. The output of the Modelled Driver Trajectory block equals the trajectory $(\overrightarrow{X}_R, \overrightarrow{Y}_R)$, heading $\overrightarrow{\Psi}_R$ and steering angle $\overrightarrow{\delta}_R$ of the reference trajectory the HSC intends to follow. The Reference Selector block then selects the index of the point in the reference trajectory that is currently closest in distance to the car's position $(X_{car}(t), Y_{car}(t))$ and outputs the corresponding current reference position $(X_R(t), Y_R(t))$ and heading $\Psi_R(t)$ to the feedback loop and the steering angle $\delta_R(t)$ to the feedforward loop [14].
 - Strength of Haptic Feedback (SoHF): The SoHF determines the strength by which the control system corrects the driver if the vehicle deviates from the reference path [15]. The SoHF uses the HCR position $(X_R(t), Y_R(t))$ and heading $\Psi_R(t)$ as input and compares them to the car's current position $(X_{car}(t), Y_{car}(t))$ and heading $\Psi_{car}(t)$. This comparison consists of calculating the Euclidean distance, Δ , between the HCR's desired position and the vehicle's current position, which results in the error in lateral road position Δs_{lat} [14]. The exact calculation of Euclidean distance is given by Equation (11) [14].

$$\Delta s_{lat}(t) = \sqrt{(X_R(t) - X_{car}(t))^2 + (Y_R(t) - Y_{car}(t))^2}$$
(11)

The difference between the desired and actual heading is also computed, resulting in $\Delta\Psi$. Both Δs_{lat} and $\Delta\Psi$ are subsequently weighted by K_s and K_{Ψ} , respectively, after which they are added together and multiplied by gain K_{SoHF} to obtain the output of the SoHF block, the haptic feedback torque $T_{SoHF}(t)$.

• Level of Haptic Support (LoHS): The LoHS regulates how much the control system steers the vehicle in the reference direction [15]. Even when the car follows the reference trajectory and the feedback torque $T_{SoHF}(t)$ becomes zero, the feedforward torque $T_{LoHS}(t)$ still gives guidance to the driver due to its open-loop properties [14]. The LoHS uses the steering angle $\delta_R(t)$ of the HCR as input and multiplies this variable with gain a K_{LoHS} to obtain the feedforward torque $T_{LoHS}(t)$. K_{LoHS} thus regulates how much the control system contributes to the driving task.

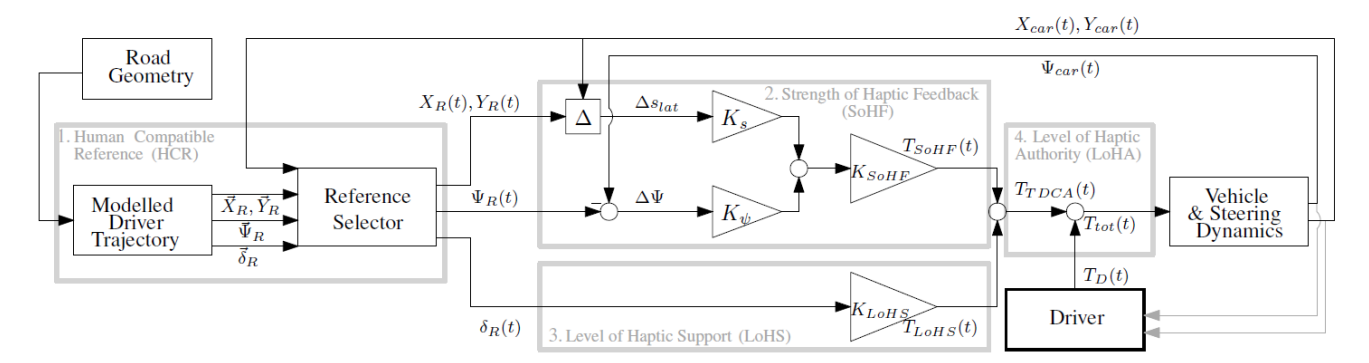


Fig. 4: The Four-Design-Choice architecture for haptic shared control [14].

• Level of Haptic Authority (LoHA): The LoHA regulates the balance between the steering wheel input of the human and the steering wheel input of the automation [15]. If the LoHA is high, it means that the haptic support is more difficult to override for the driver, which is felt by the driver as a stiffness around the optimal steering angle [15].

The Driver block visible in Figure 4 is replaced by the driver model, with one of the settings from Table II, for the simulations. In addition, the HCR is also generated using one of the three driver model settings. In total, this results in a total of nine test scenarios to be simulated. Some scenarios include the HCR and driver pursuing the same trajectory, while in other scenario their desired trajectories are very different.

In order to ensure proper trajectory tracking by the controller, the feedfoward gain K_{LoHS} and feedback gains K_s , K_{ψ} and K_{SoHF} are tuned identical to previous experiments. This tuning also depends on the simulated conditions, which is why the feedforward gain K_{LoHS} takes on two different values. Two different collaboration shares are compared to each other to see from which one the driver benefits most. This is elaborated on more in Section III. The result of the gain tuning is shown in Table III.

TABLE III: Simulation parameters of the FDCA.

Simulation gains	K_s	K_{ψ}	K_{SoHF}	K_{LoHS}
Tuning 1	0.08	0.03	1.5	0.92
Tuning 2	0.08	0.03	1.5	0.5

4) Joining of Driver and Architecture: The most complex part of the implementation of the FDCA is the connection between the driver model and vehicle dynamics. The driver model outputs a steering wheel angle that needs to be converted to steering torque, before it is added together with the FDCA torque. This total torque must then be transformed back to a steering wheel angle as it serves as the input to the vehicle dynamics. Figure 5 shows where these transformations take place. Steering wheel angle and torque are related to each other by a second-

order, rotational mass-spring-damper system, which will be used for the conversion in both directions. This system is tuned according to the steering wheel of the simulator, whose constants are shown in Table IV.

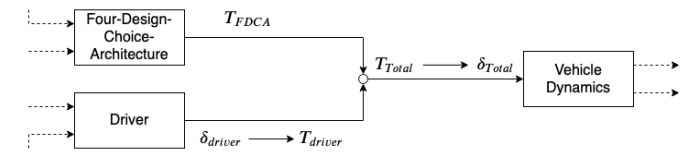


Fig. 5: Implementation of Four-Design-Choice-Architecture with driver model and vehicle dynamics.

TABLE IV: Steering wheel constants of the simulator.

Constants	
Inertia J_w	$0.005 \ [kg \cdot m^2]$
Friction constant B_w	$0.03 \ [2Nms/rad]$
Spring constant K_w	1 [Nm/rad]

As this second-order system becomes unstable for high frequencies as the output magnitude keeps increasing past the corner frequency, it was decided to approximate the conversion to guarantee stability. A low-pass filter was added to the differentiator of the steering wheel angle, which limits the impact of the higher frequency inputs. The transfer function is shown in Equation (12).

$$\frac{\dot{\theta}(s)}{\theta(s)} = \frac{s}{\frac{s}{20} + 1} \tag{12}$$

This angle-torque and torque-angle conversion is the last step in the implementation of simulation platform.

5) Conflict: The results of the computer simulations are simulated lateral position, steering wheel angle, and steering wheel torque time traces. The main metrics calculated from this data are the conflict torque, $T_{conflict}$, between the haptics and the driver and also their relative time of being in conflict during the simulation interval, $O_{conflict}$. These two parameters provide information on how the driver and FDCA react to each other, whether

their interaction is positive or negative. Therefore, the following definition is used in this paper:

$$O_{conflict} = \begin{cases} 1, & \text{if } T_{driver} \cdot T_{HSC} < 0 \\ & \&\& \ T_{driver} > 0.1 \cdot max |T_{HSC}| \\ 0, & \text{otherwise} \end{cases}$$

This definition entails that if the torque exerted by the driver on the steering wheel and the torque by the controller are in opposite directions and if the Weber fraction is satisfied, the driver and controller are in conflict. The Weber fraction is a threshold of noticeable sensory perception [25] and is tuned based on [26]. In other words, if the Weber fraction is not satisfied, then the driver is not able to feel the opposition of the automation. If their torques, however, are aimed in the same direction or the Weber fraction is not satisfied, then no conflict is present. Using the definition, at every time step it can be checked whether or not the driver and controller are in conflict. For each time step in conflict, the absolute conflict torque, $T_{conflict}$, is calculated by taking the absolute value of the difference between the FDCA torque and driver torque. Also, the time percentage, $O_{conflict}$, of being in conflict is calculated.

B. Results

In total, eighteen scenarios were simulated. These are all combinations of the driver and HCR either exhibiting centerline, curve cutting or counter curve cutting behaviour (9 cases), for two settings of the feedforward gain K_{LoHS} . An example simulation result can be found in Figure 6. For each scenario, a plot is made of the lateral positions of the programmed driver model and HCR and the resulting final trajectory the vehicle follows due to their collaboration. An identical plot of the individual torques is also generated.

The lateral position and torque plots in Figure 6 show the collaboration of the architecture and the driver model over the different time steps in the curve, however the most important aspect in the analysis is the amount of conflict time and conflict torque present in each simulated scenario. The amount of conflict indicates how much the driver complies with the controller, which is a possible indication of how much a driver would comply with the guidance in an experiment. The results of the analysis are split for both feedforward cases and are shown in Tables V and VI.

Starting with the analysis of the $K_{LoHS} = 0.5$ case in Table V, several levels of disagreement become apparent. The scenarios in which the driver and HSC are programmed to drive identical trajectories (diagonal elements) lead to low conflict. The conflict torque, $T_{conflict}$, values are consistently lower than 0.0190 Nm and also the conflict time, $O_{conflict}$, does not exceed 2.40%.

Conflicts are seen to increase when the driver and HSC follow different paths. These opposing scenarios show

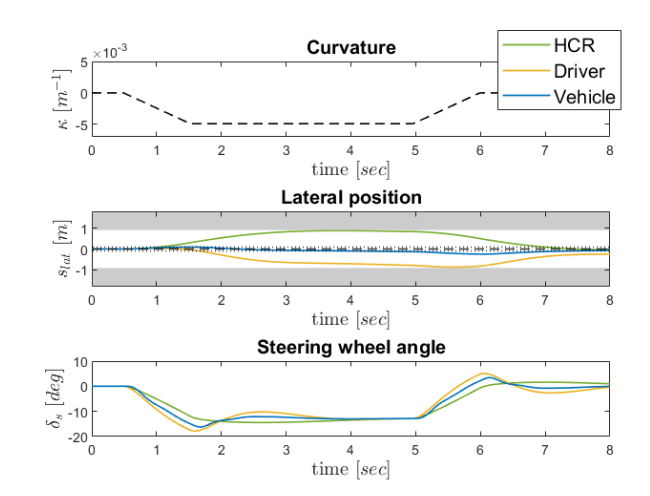


Fig. 6: Results of the simulated scenario where the HCR is programmed to follow a counter curve cutting trajectory and the driver model a curve cutting path for $K_{LoHS} = 0.5$.

two clear trends. First, scenarios that involve centerline driving show an excessive amount of conflict torque. Even the scenario where both the HCR and driver perform centerline driving, the conflict torque and time percentage are over twice as high compared to the other scenarios where driver and HCR follow the same path. Conflict torque in these non-centerline scenarios does not exceed 0.01 Nm and conflict time is consistently lower than 1%.

It is found that this is caused by oscillations in the steering wheel angle when the driver model, either implemented as driver or HCR, follows the centerline path. This is directly related to the centerline path having the highest closed-loop gain, K_c , of all three trajectories, see Table II. In order to avoid this artifact, as this is not a situation that would occur in real life, the K_c value was lowered to its current value of 18, despite originally being valued at 28. This K_c decreases oscillations, but also makes the resulting centerline trajectory less precise in its centerline trajectory that stayed within the centerline band, which is the centerline \pm 0.1m, but the new centerline trajectory leaves the centerline band and has a constant lateral position of 0.15m from the centerline.

Second, one would expect similar conflict values in contrasting scenarios. For example, the combinations of "driver curve cutting and HCR counter curve cutting" and "driver counter curve cutting and HCR curve cutting" are opposite, so similar conflict values are expected. However, the results of the simulations indicate an asymmetry. The former scenario shows a $T_{conflict}$ of 2.7037 Nm and a $O_{conflict}$ of 27.60%, while the latter shows 0.3985 Nm and 6.50% respectively. The driver model complies more with the HSC if the HSC follows a more optimal trajec-

tory, meaning a lower average lateral accelerations and a higher Time-to-Line-Crossing, with respect to its own programmed path, resulting in lower conflict values. If the guidance uses a less optimal trajectory, then the driver model fights the guidance and forces a more optimal path. This indicates that drivers may be more inclined to follow optimal trajectories.

At last, a comparison between the different feedforward gains shows that the same trends in conflict time and torque are present in both cases, but that conflict is consistently lower for the $K_{LoHS}=0.92$ case. Reviewing the earlier mentioned "driver curve cutting and HCR counter curve cutting" scenario, the $T_{conflict}$ value has lowered to 1.2040 Nm and $O_{conflict}$ to 22.60%, while the opposing scenario now shows a $T_{conflict}$ of 0.2538 Nm and a $O_{conflict}$ of 4.00%. This finding is in line with both [8] and [13], which both state that an increase in feedforward guidance lowers the conflicts the driver experiences with the haptics.

TABLE V: Conflict torque and time overview of the nine simulated scenarios for $K_{LoHS} = 0.5$.

Feedforward gain 0.5	Driver Centerline	Driver Curve cutting	Driver Counter curve cutting
HCR	0.0190 Nm	1.3828 Nm	0.2600 Nm
Centerline	2.40 %	23.80 %	6.90 %
HCR	3.6103 Nm	0.0090 Nm	$0.3985 \; \mathrm{Nm}$
Curve cutting	17.50 %	0.90 %	6.50 %
HCR Counter curve cutting	3.6762 Nm 32.00 %	2.7037 Nm 27.60 %	0.0090 Nm 0.50 %

TABLE VI: Conflict torque and time overview of the nine simulated scenarios for $K_{LoHS} = 0.92$.

Feedforward gain 0.92	Driver Centerline	Driver Curve cutting	Driver Counter curve cutting
HCR	0.0049 Nm $2.80 %$	1.2257 Nm	0.4807 Nm
Centerline		21.70 %	11.00 %
HCR	2.6840 Nm	0.0332 Nm	0.2538 Nm
Curve cutting	17.40 %	1.40 %	4.00 %
HCR Counter curve cutting	1.0686 Nm 25.30 %	1.2040 Nm 22.60 %	0.0040 Nm 0.50 %

The findings of these simulations are useful for the experiment as they contribute to the formulation of the hypotheses in Section III-I. In turn, the experiment will help validate the results of the simulations.

III. EXPERIMENT

A. Apparatus

The human-in-the-loop experiment was performed in the fixed-base driving simulator at the Human-Machine Interaction Lab of the Delft University of Technology. The hardware setup matched numerous earlier experiments [8] [14] [27]. The visual scenery was displayed using three LCD projectors, each covering a horizontal field-of-view of 180 deg and a vertical field-of view of 40 deg, at an update rate of 50 Hz and an image generation delay of 10 ms. A MOOG FCS Ecol800S actuator, operating at a rate of 2500 Hz, was employed for the generation of haptic torques on the steering wheel [27]. The set-up of the simulator is shown in Figure 7



Fig. 7: Simulator set-up at the Human-Machine Interaction Lab.

B. HSC Architecture

The haptic guidance that the participants felt on the steering wheel of the simulator was provided using an implementation of the Four-Design-Choice-Architecture. This architecture, shown in Figure 4, has the same structure as the FDCA implemented in the simulations, however, some small implementation differences can be found. First, for the experiment, the HCR is not longer derived from a driver model, but the reference trajectories are now created by averaging real driver data on the same raod from earlier measurements [19].

Second, the added angle-to-torque and torque-to-angle conversions needed in the simulations to connect the FDCA with the driver and vehicle dynamics are no longer necessary. The simulator software is set up in such a way that the FDCA torques are converted to steering wheel angles, after which they are added together with the measured steering wheel angle of the driver and used as the input to the bicycle model that represents the vehicle dynamics.

At last, an adaptation is made to the feedforward loop of the FDCA. In the initial testing stages of the experiment, it was found that the trajectory tracking of the implemented FDCA was subpar. Despite using the original gain tuning from [8] [14] [27], the architecture was not able to follow its programmed HCR, even without driver inputs. A solution had to be found for this issue, especially in order to reach fine-tuned individualised trajectories. It was therefore decided to re-identify the steering wheel dynamics, the second-order mass-spring-damper transfer function between the FDCA and the vehicle dynamics,

that converts the haptic shared control torque in a steering wheel angle, see Figure 8.

The steering wheel constants resulting from this system identification can be found in Table VII. Table VII shows a much higher inertia and friction coefficient value than the original identification, while the spring constant is halved and is now valued at $0.4984\ Nm/rad$. Additionally, the inverse steering wheel dynamics, with the same values from Table VII, are added to the feedforward loop as a prefiltering of the feedforward signal, before being multiplied with the feedforward gain, see Figure 8. The resulting steering wheel angle and trajectory tracking can be found in Figure 9. The yellow line represents the lateral position of the reference trajectory, the HCR, and the steering wheel angle to driver this path. The blue line is the output of the Four-Design-Choice-Architecture.

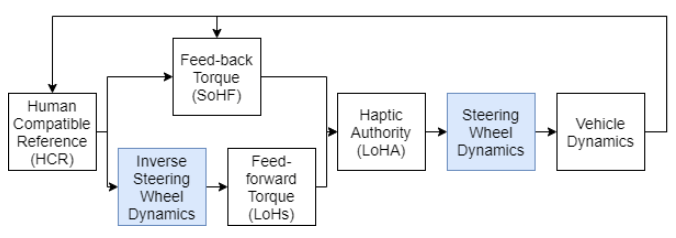


Fig. 8: Clarification of re-identified steering wheel dynamics and the added inverse steering wheel dynamics to the feedforward loop.

TABLE VII: Steering wheel constants of the simulator.

Constants	
Inertia J_w	$0.0258 \ [kg \cdot m^2]$
Friction constant B_w	$0.1114 \ [2Nms/rad]$
Spring constant K_w	$0.4984 \ [Nm/rad]$

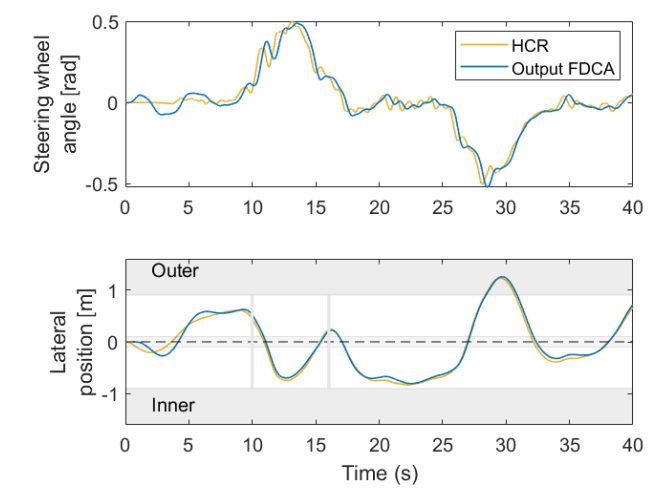


Fig. 9: The result of the addition of inverse steering wheel dynamics in the feedforward loop (no driver input present).

C. Road Design

The drivers that participated in the experiment were asked to drive a heavy sedan of 1.8 m width on a 3.6 m wide, single lane road. For each testing condition, the same trajectory was used with identical conditions. The vehicle had a fixed longitudinal speed, V_x , of 80 km/h and the objective of the drivers was to follow a trajectory consisting of six left and six right clothoidal turns. All turns had a radius, R, of 204 m. In between the curves, straight stretches of road were present to reset the drivers' positions on the road before curves. These sections were 240 m long.

D. Experimental Design

The experiment was split-up in two sessions, performed on separate days. The first day consisted of a manual driving experiment, in which drivers were asked to drive the curved road trajectory without any haptic shared controller. This in order to determine their manual driving style in both left and right curves. Additionally, this data was used to generate an individualised HCR. On the second day, about eight weeks later, drivers were asked to drive the same trajectory, however this time they were assisted by different variations of the FDCA.

- 1) Day 1: The manual driving experiment served as a selection procedure for the HSC experiment on the second day. Before the start of the experiment, the drivers were informed about the goal of the research, the experiment procedures and on that, based on their manual driving style, they might be asked to return for a second, longer experiment session. They were asked to sign a consent form and to fill out a questionnaire that asked about their driving experience, gaming habits and contact with Advanced Driver-Assistance Systems (ADAS). The experiment itself consisted of one training run, in which drivers could get acquainted with the steering wheel. This training run also consisted of six left and right curves, which was argued to be enough for familiarising. The actual experiment session consisted of two more identical trials on the 12-curve road. In total for each participant information was thus gathered for twelve left and twelve right curves.
- 2) Processing Phase: Based on these data and using the classifier of [19], it was determined what driving style the participants showed. The rule-based classifier of [19], shown in Figure 1 uses lateral position of the vehicle at curve-entry and the number of crossings over the centerline band to determine the driving style of participants. For each driver, the analysis was performed separately for left and right curves. It was also evaluated how consistent drivers are in their driving.
- 3) Day 2: The second day of the experiment consisted of a haptic shared control experiment with the Four-Design-Choice-Architecture. After the classification of all participants of Day 1, drivers that fit into the two

most meaningful class combinations were re-invited for the second experiment session: the most populated class combination and the most optimal class combination in terms of low lateral acceleration and high TLC [24] [28]. The most populated class combination are R3L5 drivers, who fit into class 3 [19] for right curves and class 5 [19] for left curves, and the most optimal class combination are the R2L1 drivers, who fall into class 2 for right curves and class 1 for left curves. This is because no R1L1 drivers have been found in previous research [19]. The simulations have indicated that drivers might be willing to follow more optimal trajectories than their own natural style and fight less optimal trajectories, therefore testing R2L1 drivers directly helps validating this hypothesis.

E. Experiment Conditions

The goal of this research is to understand driver's acceptance of HSC and to understand how far personalisation should go. This is clearly reflected in the experiment conditions. In total, eight different conditions are tested by each participant in session 2 of the experiment. These conditions vary in both reference trajectories of the HCR, as well as the value of the feedforward gain, K_{LoHS} . Four HCR's are tested:

- R4L4: This HCR represents the centerline trajectory and is the *baseline* condition as it represents the industry standard. However, previous research has not found any drivers who naturally follow this trajectory [19]. The R4L4 HCR is generated with the driver model also used by [8] [13].
- R3L5: This HCR is very interesting as previous research on manual driving has shown that 36% of drivers fall into this category [19], which makes it the most occurring class. The HCR is generated by averaging trajectories of R3L5 drivers from previous measurements [19].
- R2L1: This HCR represents the most optimal driver. The HCR is generated by averaging trajectories of R2L1 drivers from previous measurements [19].
- Personalised: This HCR is individualised for each driver and represents full personalisation. The reference is created by averaging each driver's own trajectory from the first experiment session. This condition helps answering the question whether drivers need absolute personalisation or if class-level personalisation is sufficient. The difference between both full personalisation and class-level personalisation is further shown in Figure 10, which shows all the fully personalised HCR's of the 16 R3L5 and 16 R2L1 drivers in colour. A variation is present for every driver. The class averaged HCR's are shown in black. For some drivers, the class averaged HCR is similar to their personalised guidance, while for others large differences are present.

These four reference trajectories are tested twice by each participant with two different feedforward gain settings:

- K_{LoHS} 0.5: A naive implementation of haptic shared control would assume an equal share to the driver and automation.
- K_{LoHS} 0.92: A recent study on the FDCA at the Delft University of Technology has shown that the feedforward loop is essential in the acceptance of the control system [14]. Shared control, however, is defined in [2] as "In shared control, human(s) and robot(s) are interacting congruently in a perception-action cycle to perform a dynamic task that either the human or the robot could execute individually under ideal circumstances", which shows that there is no definition on the exact share. Therefore, it is possible to increase the share of the feedforward loop, which could possibly increase acceptance, by increasing K_{LoHS} .

In this within-subject experiment, each participant received each condition in a random order, determined by a 4x4 Latin square matrix. Each participant performed two training runs: one run of manual driving and one driving with the baseline HSC condition, R4L4 HCR - K_{LoHS} 0.92. Furthermore, all other variables, such as FDCA tuning, speed and curve radius, were all identical to the simulations.

F. Participants and Instructions

Eighty-five subjects (13 women and 72 men) participated in the manual driving experiment, i.e., the first part of the study. The driver's ages ranged between 19 and 60 years (median = 24 years, IQR = 3 years) and all were in possession of a driving license for at least one year (median = 6.2 years, IQR = 3.7 years). After a selection based on their driving style, 32 drivers returned for the HSC experiment in the second experiment session. All subjects participated on a voluntary basis and no financial compensation was provided. Participants were asked to keep their hands at a "ten-to-two" position on the steering wheel and to drive as they normally would. The experiment was approved by the Human Research Ethics Committee (HREC) of the Delft University of Technology.

G. Variables & Metrics

The dependent measures used to analyse the drivers' acceptance over the different experiment conditions are divided in two categories: objective and subjective metrics. The objective variables consist of metrics that can be objectively measured, while the subjective variables are the result of the Van der Laan and CARS questionnaires the drivers were asked to fill out during the experiment.

1) Objective Variables:

• Driver torque: The driver torque is the torque exerted by the driver on the steering while driving with guidance. As the driver torque represents the driver's physical effort, it is therefore also a measure of how much the driver complies with the guidance or how

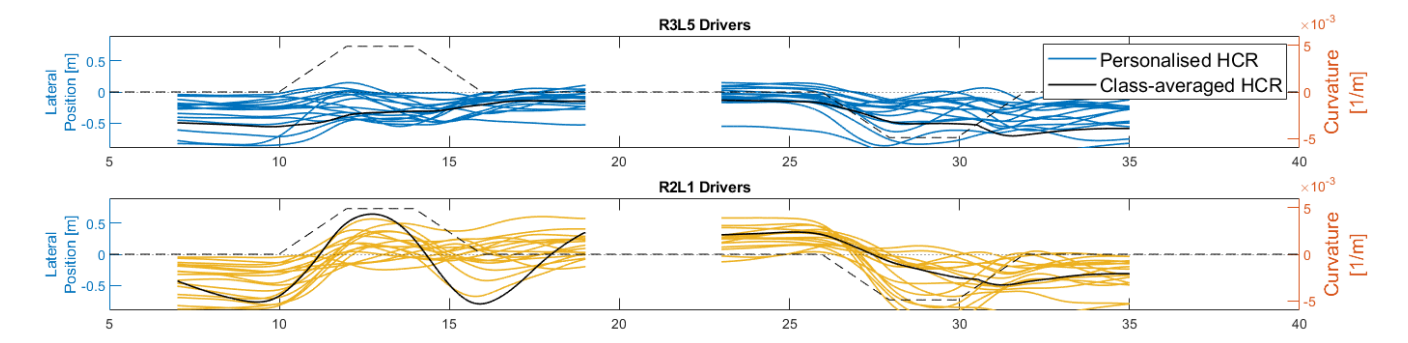


Fig. 10: Time traces of completely personalised HCR's and class-averaged HCR's for left and right curves.

much he/she opposes it. The amount of driver torque is also highly dependent on the feedforward gain.

- HSC torque: The haptic shared control torque is the total torque exerted on the steering wheel by the FDCA. It thus illustrates the combined torque of the feedforward and feedback loops.
- Feedback torque: The feedback torque is a contributor to the total HSC torque, however, this torque is perceived as punishing by the driver as it directly corrects any deviation from the reference trajectory. It therefore is likely correlated with the subjective assessment and acceptance by the driver, since a high feedback torque typically is very unpleasant to the driver [14].
- Conflict time: For each time step in the experiment, it is determined whether or not the driver and FDCA are in conflict. The definition of conflict is identical to the conflict definition in the simulations:

$$O_{conflict} = \begin{cases} 1, & \text{if } T_{driver} \cdot T_{HSC} < 0 \\ & \&\& \ T_{driver} > 0.1 \cdot max |T_{HSC}| \\ 0, & \text{otherwise} \end{cases}$$

Conflict time gives an indication of objective acceptance. The conflict time is calculated for each time step and is expressed as a percentage of time of the trial.

• Conflict torque: As in the simulations of Section II, the conflict torque equals the difference between the driver torque and HSC torque when a conflict is present. Conflict torque also gives an indication of objective acceptance and is therefore analysed side-by-side with the conflict time.

2) Subjective Variables:

• Van der Laan: The Van der Laan questionnaire [29] is filled out by participants in order for them to personally grade each experiment condition both on a "usefulness" and a "satisfaction" level. Nine features, four to describe the satisfaction level and five for the usefulness, are graded with a score between -2 and

- 2. These grades are then averaged to get the final usefulness and satisfaction levels.
- Controller Acceptance Rating Scale (CARS): The CARS scale is a subjective rating system that lets participants indicate the degree of deficiencies of the controller [30]. The scores range between 1 and 10, where a score of 1 indicates that the system is untrustworthy and improvement is necessary to guarantee safe operation, whereas a 10 shows that deficiencies are rare and the driver does not need to compensate for errors. The grade is also accompanied by a confidence rating: A, B or C [30].

H. Statistical Analysis

The statistical analysis for this research consists of two major parts. First for the objective measures, a two-way repeated-measures ANOVA with an additional between-subject variable is used for a full statistical comparison of all data. The two-way repeated-measures ANOVA is imperative as a result for the two independent variables: the HCR and the feedforward gain. The additional between-subject variable is included to account for the two different driver groups, i.e. R3L5 and R2L1. An ANOVA is a parametric test, which assumes that the data are normally distributed. This is checked by use of the Kolmogorov-Smirnov test. Sphericity is also checked and corrected for, if necessary, with the Greenhouse-Geisser correction.

If the data are not normally distributed, then a nonparametric test must be used. The Kruskal-Wallis test is used to understand differences between the two driver groups and the Friedman test to check the variations between the conditions. These non-parametric tests are used for the subjective measures as well.

I. Hypotheses

The combined knowledge gathered from the simulations and supplementary literature results in five hypotheses that this research aims to verify. One covers the first part of the experiment in which manual driving data are collected:

• H.I: The most prominent driver group will be R3L5, with more than 30% of the drivers falling into this

class, while no driver will naturally exhibit true centerline driving.

This hypothesis is fully based on previous research by [19], where for a similar experiment (45 participants) this was concluded

The remaining four hypotheses cover the haptic shared control experiment:

- H.II: The averaged class HCR of the natural driving class of the driver and the replay of the own trajectory will lead equivalent conflicts and subjective usefulness and satisfaction scores, indicating equal acceptance. This hypothesis is based on the research by [16], which concluded that drivers like their own trajectory as reference trajectory of a semi-automated system equally much as a similar trajectory.
- H.III: If the HCR follows a more optimal trajectory in terms of TLC (higher minimum TLC) and lateral acceleration (lower maximum lateral acceleration) than the driver's natural driving, then the conflict will be less and acceptance is increased compared to less optimal trajectories.
 - The analysis of the conflict torques in the simulates have clearly shown that a driver is likely to resist the HSC less if the HSC uses a more efficient trajectory than the driver normally would.
- H.IV: The centerline HCR will cause the highest driver torques and will have the worst subjective rating, leading to a low acceptance rate.

 Centerline driving does not come natural to to drivers [19], who prefer similar driving styles to their own in their controllers [16]. Additionally, the centerline tra
 - their controllers [16]. Additionally, the centerline trajectory is not efficient in terms of lateral acceleration or TLC [24]. Hence, the centerline guidance will be disliked.
- H.V: A higher feedforward gain will increase objective acceptance by reducing conflicts, but will result in lower subjective satisfaction and usefulness.
 - It was hypothesised before by [8], [13] and [14] that feedforward torques reduce conflict. However, a high feedforward gain is more noticeable and hard to ignore and might thus be perceived by drivers as a nuisance. So, objectively a high feedforward gain will reduce conflict, but subjectively this setting will rate lower.

IV. Results

The results are presented in four separate subsections. Section IV-A discusses the first experiment session and thus focuses on the findings of the manual driving behaviour of the participants. Sections IV-B, IV-C and IV-D examine the results of the second experiment session. Section IV-B presents the subjective ratings given by the drivers for the different test conditions, while Section IV-C presents the objective measures and aims at finding an objective way to measure acceptance. At last, Section IV-D includes an investigation of the collaborative driven trajectories and compares them to the manual driving

patterns of the participants to understand how drivers adapt their driving behaviour with HSC.

A. Manual Driving Patterns

In total eighty-five drivers participated in the manual driving experiment. Each participant's driving behaviour was analysed separately for left and right curves and classified according to the seven rule-based classes, as presented in Figure 1. The results of this classification are shown in Figure 11, where for every driver it is indicated in which left and right class their natural driving style fits. The figure also shows how the left and right curves relate to each other per driver.

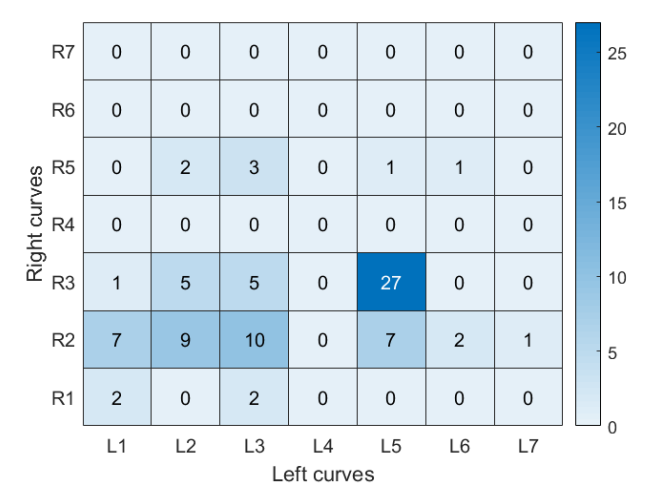
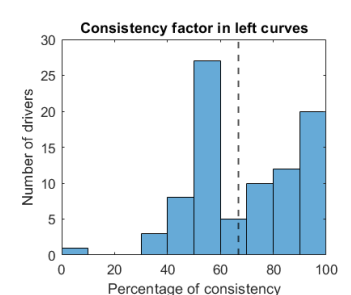


Fig. 11: Classification of driver behaviour in the manual driving experiment.

Figure 11 shows classification results in line with [19]. The most populated class is R3L5, and 27 out of 85 drivers, 32%, fit into this category. Moreover, curve cutting trajectories, i.e. class 1 and 2, are also relatively heavily populated, especially class 2 for right curves. More variation is present for left curves. In contrast to [19], two R1L1 drivers were found in the participant group. These drivers always drive the most optimal trajectory in terms of lateral acceleration and TLC. At last, no driver exhibits natural centerline driving behaviour (class 4).

Additionally, the consistency with which drivers negotiate their curves is investigated. The dominant class of each driver, as presented in Figure 11, was determined by checking which class occurred most in the six left and right curves of the first experiment session. Exactly how often this dominant class occurred helped mapping the consistency of the drivers towards their dominant class. The consistency values are shown in Figure 12. The figure shows a similar spread of consistency over left and right curves, with both medians at 67%. This demonstrates that the vast majority of drivers do have a consistent (>50%) preference for a certain class.



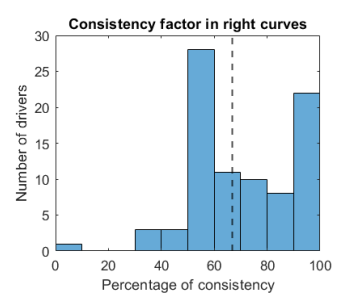


Fig. 12: Classification of driver behaviour in the manual driving experiment.

The original intent of the haptic shared control experiment was to test both R2L1 and R3L5 drivers. However, as can be seen from Figure 11, not enough R2L1 drivers were available to conduct a statistically powerful experiment. It was therefore decided to also include R2L2 drivers and group them together with the R2L1 drivers to form the 'curve cutters' group. It is, however, important to remember that these two driver groups have a different curve negotiating technique for left curves. If any deviating results are found for the subjective or objective measures of the haptic shared control experiment, it must be checked if this is due their different natural styles in left curves.

B. Subjective Measures

After each of the eight haptic shared control experiment conditions, the drivers were asked to provide an acceptance rating on the CARS scale and fill out a Van Der Laan questionnaire. This data was used to assess their subjective acceptance of the different conditions. The first measure is the CARS score the drivers used to rate the different testing conditions. The exact scores of all drivers (bars) together with the corresponding medians (vertical dashed lines) are shown in Figure 13. The figure shows that overall a higher feedforward, FF 0.92, received higher acceptance scores. The only exception is the R2L1 guidance, which is only rated a 7 by the R3L5 drivers. The Kruskal-Wallis test shows that this condition is the only one where both driver groups significantly differ in opinion, see Table X. The curve cutters especially rate R2L1 and the less efficient R3L5 high, followed closely by the personalised and centerline guidance. No significant differences are found between these ratings. The R3L5 drivers on the other hand rate their class average R3L5 and personalised guidance equally, as well as the slightly less efficient centerline trajectory. In the R2L1 case, the subjective ratings for the low feedforward setting surpass the score of the higher gain. A Friedman's test only shows significant differences for the 0.92 feedforward case ($\chi^2(3)$) = 15.070, p<0.05), but none for the 0.5 case. It is reasoned that the significant difference is caused by the low rating of the R2L1 guidance in high feedforward gains.

TABLE VIII: Results of the Kruskal-Wallis test for the CARS scale, where ** indicates a highly significant result (p<0.01), * indicates a significant result (0.01 \leq p \leq 0.05) and - indicates not significant (p>0.05).

Kruskal-Wallis			
Factor	df	Н	Sig.
R4L4-0.92	1	1.858	-
R4L4-0.50	1	0.161	-
R3L5-0.92	1	0.081	-
R3L5-0.50	1	0.315	-
R2L1-0.92	1	4.879	*
R2L1-0.50	1	0.041	-
Person0.92	1	1.659	-
Person0.50	1	0.000	-

A more detailed picture on subjective feel is provided by the Van Der Laan questionnaire, whose results are reorganised into the Satisfaction-Usefulness plots shown in Figure 14. The plots show the median of the satisfaction and usefulness scores per condition, together with the interquartile ranges. A good satisfaction and usefulness score means that the median of the condition is placed in the upper right corner of the plot. The curve cutters tend to rate the higher feedforward, FF 0.92, consistently higher on both the usefulness and satisfaction scale. Especially R3L5 - 0.92, R4L4 - 0.92 and Personalised - 0.92 rate high on usefulness with scores equal or higher than 1. These settings also rate 1 or higher on satisfaction, but are accompanied by Personalised - 0.5. The class average of these drivers, R2L1 - 0.92, is rated mediocre with a satisfaction score of 0.56 and a usefulness score of 0.85. By checking all individual curve cutters, it was found that this lower rating is present for all curve cutters and not only to the R2L2 drivers who might perceive the left curves as being too aggressive. This is a first indication that acceptance might not be linked to optimal trajectories, although no significant differences were found between conditions for the curve cutters.

The R3L5 drivers also rate FF 0.92 higher in general. Especially in terms of usefulness, R3L5 - 0.92, R4L4 - 0.92 and Personalised - 0.92 all rate a lot higher than the other conditions with values exceeding 0.85. In terms of satisfaction, once again R4L4 - 0.92 and Personalised - 0.92 rate highest with scores of 0.88 and 0.95 respectively. R2L1 - 0.92 rates very badly and has a negative satisfaction score as it feels very aggressive. The Friedman's test showed significant differences between conditions for both satisfaction ($\chi^2(3) = 8.293$, p<0.05) and usefulness ($\chi^2(3) = 11.178$, p<0.05).

The Kruskal-Wallis test for the satisfaction showed significant differences between the driver groups for both R2L1 - 92 and Personalised - 50. The former is explained by the negative satisfaction score, -0.42, by the R3L5 drivers, while the curve cutters still rate the satisfaction at 0.56. The latter is caused by a high satisfaction score by the curve cutters, 1.03, where it is hypothesised that

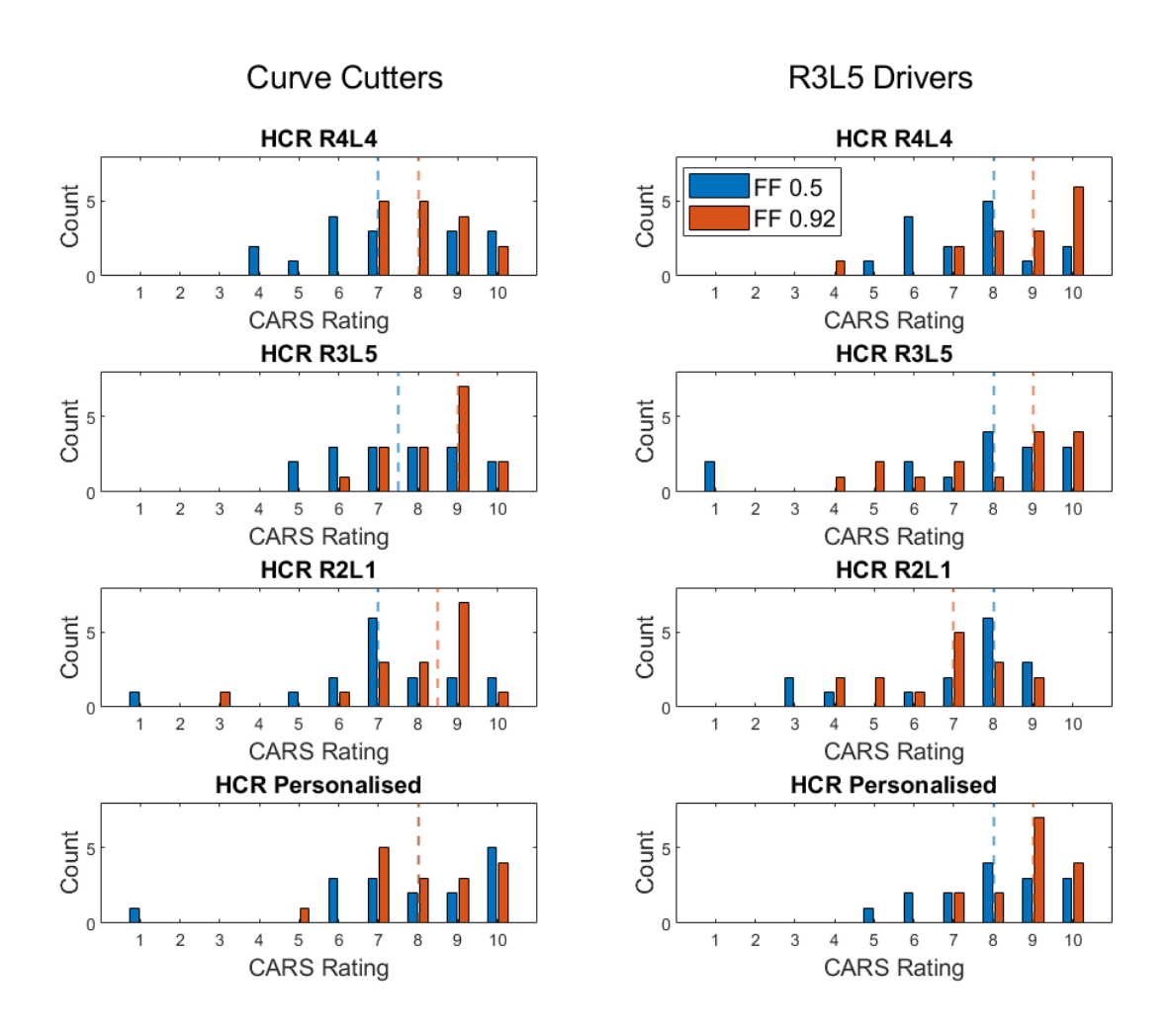


Fig. 13: Results of the CARS questionnaire and corresponding medians for both the curve cutters and R3L5 drivers.

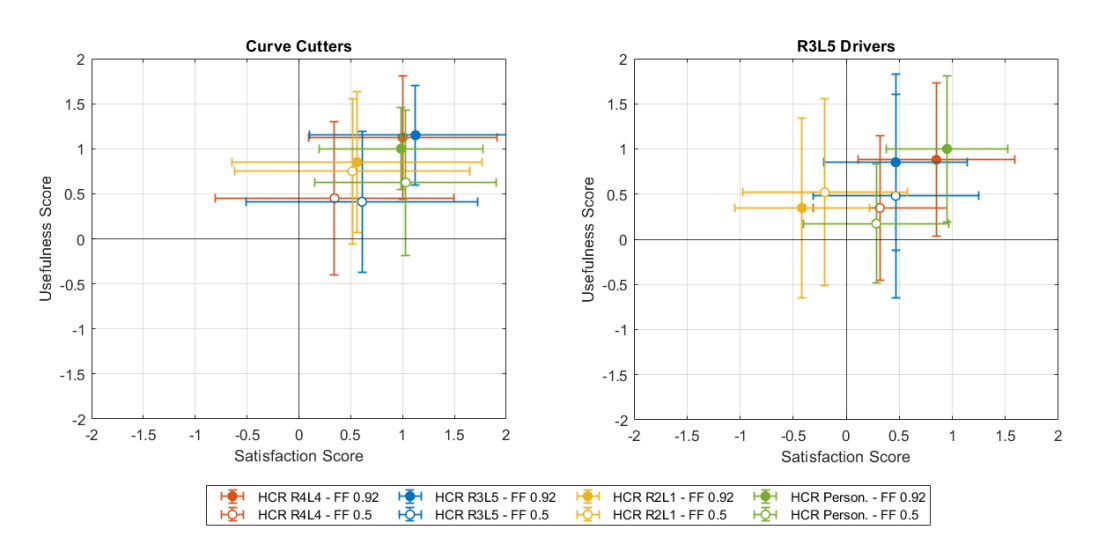


Fig. 14: Satisfaction-Usefulness plots resulting from the Van Der Laan questionnaire for both curve cutters and R3L5 drivers.

a "sloppy" personalised curve cutting guidance feels as a strong, less optimal trajectory. At last, the Kruskal-Wallis test for usefulness shows the same significant difference for the R2L1 - 92 condition. In conclusion, for the subjective measures, it seems that both driver groups prefer a completely individualised HCR or a group averaged HCR that is a bit less optimal than their own class.

TABLE IX: Results of the Kruskal-Wallis test for the Satisfaction scale, where ** indicates a highly significant result (p<0.01), * indicates a significant result ($0.01 \le p \le 0.05$) and - indicates not significant (p>0.05).

Kruskal-Wallis			
Factor	df	Н	Sig.
R4L4-0.92	1	0.294	-
R4L4-0.50	1	0.057	-
R3L5-0.92	1	3.666	-
R3L5-0.50	1	0.191	-
R2L1-0.92	1	4.851	*
R2L1-0.50	1	2.665	-
Person0.92	1	0.40	-
Person0.50	1	6.007	*

TABLE X: Results of the Kruskal-Wallis test for the Usefulness scale, where ** indicates a highly significant result (p<0.01), * indicates a significant result (0.01 \leq p \leq 0.05) and - indicates not significant (p>0.05).

Kruskal-Wallis			
Factor	df	Н	Sig.
R4L4-0.92	1	1.289	-
R4L4-0.50	1	0.101	-
R3L5-0.92	1	1.532	-
R3L5-0.50	1	0.142	-
R2L1-0.92	1	4.520	*
R2L1-0.50	1	0.404	-
Person0.92	1	0.000	-
Person0.50	1	3.723	-

C. Objective Measures

The objective measures aim at finding a way to assess acceptance in a more unbiased manner. An important adjustment compared to the subjective measures is that for the objective measures the left and right curves are analysed separately. This decision was made since the drivers' manual class for right and left curves might differ, as well as the HCR class for left and right. Significant differences in acceptance might thus be present for the different curve directions.

The results of the collaboration between driver and haptic shared control have been summarised per driver in plots such as Figure 15 and 16. Figure 15 shows a summary of an R2L1 driver reacting to the eight different conditions, while Figure 16 duplicates this for an R3L5 driver. These plots include the driver torque to measure the effort level of the driver and their willingness to follow the guidance. The plots also contain the complete haptic shared control torque, T_{HSC} , to show the forces exerted by the controller. The feedback torque, $T_{Feedback}$, is shown separately as this

torque is variable in contrast to the feedforward torque and represents the disagreement between the driver and controller. The feedback torque is also the force that is most perceived as punishing by the driver and is therefore essential in the acceptance discussion. At last, conflict time and torque are shown to better understand the disagreements between driver and HSC. For each driver the intermediate values of their six left and right curves are shown. Note that in Figures 15 and 16 a positive curvature, κ , represents a left curve.

These results per driver are subsequently brought together in driver groups in order to see trends in conflicts. These trends are subsequently analysed per experiment condition, per curve direction and more importantly per driving phase. Two driving phases are identified: a prepositioning and curve phase. The prepositioning phase was identified by [24] and has proven to be essential for a heightened acceptance of the guidance [14] [24]. Hence, for the analysis per curve, both a prepositioning phase of five seconds and the six-second curve phase itself are analysed. The results of this analysis per objective measure are shown in Figures 24, 25, 26 and 27.

1) Curve cutters - Right curves: First, the behaviour of the curve cutters in right curves is analysed. The curve cutters are a mixed group of R2L1 and R2L2 drivers, indicating that their manual driving style in right curves is equivalent and their preferences are thus expected to be identical. Figure 24 shows the exerted force by the drivers on the steering wheel. It is immediately visible that the driver torque is significantly higher if the feedforward gain is low, especially for the curve phase (F(2.057,61.698) =81.895, p<0.05)). This is expected, as a lower feedforward gain steers less in the curves and thus more input is needed from the driver. This trend is also clearly visible for the left curves and the R3L5 drivers. In the prepositioning phase, the curve cutters exert the most torque on the steering wheel for the R3L5 condition, an effect which is significant (F(1.966,58.975) = 10.969, p < 0.05)). The prepositioning guidance of the class 3 HCR pushes the driver towards the inner side of the curve, while a curve cutter has a natural inclination towards the outer side.

This perception is further supported by a much higher conflict time (increase of 57.50% for FF 0.5 and 82.30% for FF 0.92, F(3,90) = 9.186, p<0.05)) and torque (increase of 0.751 Nm for FF 0.5 and 0.629 Nm for FF 0.92, F(1.946,58383) = 8.659, p<0.05)) for this condition. It is also noticeable that both conflict time and torque are on average 13.17% lower for the FF 0.92 conditions. Furthermore, for this prepositioning phase, the R2L1 and personalised conditions are liked equally, since both align with the natural outer side inclination of the curve cutters. In the curve phase, the driver torque is also lowest for the R2L1 and personalised conditions, indicating a willingness to follow the guidance. The trend is confirmed with the lowest conflict values found for these two conditions.

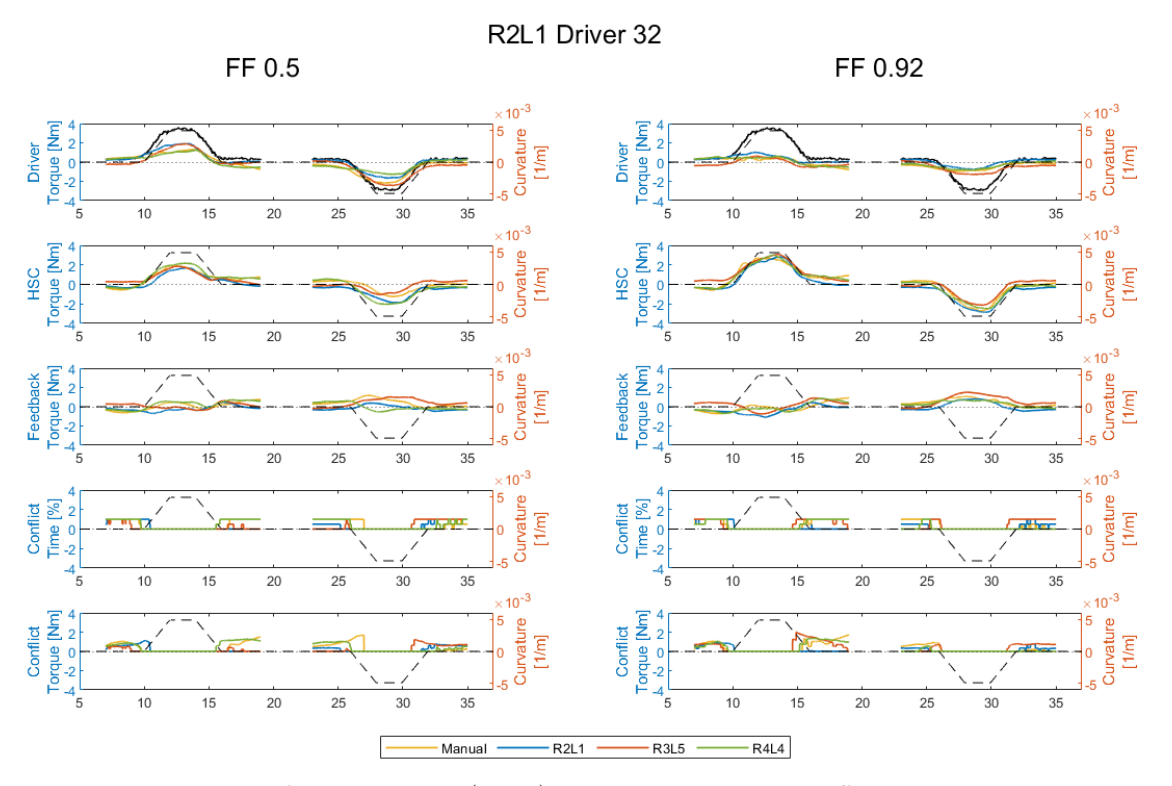


Fig. 15: Timeseries result of a curve cutter (R2L1) subjected to the eight different experiment conditions.

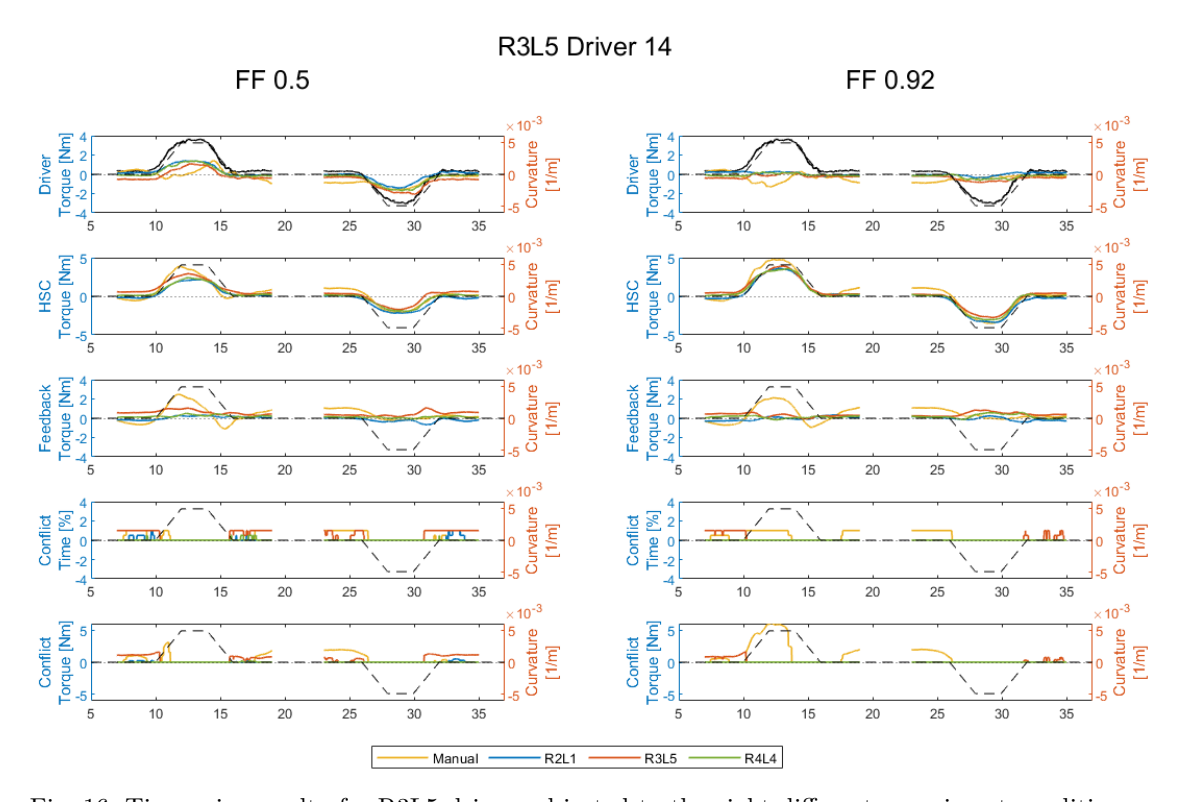


Fig. 16: Timeseries result of a R3L5 driver subjected to the eight different experiment conditions.

In this curve phase, the R3L5 condition results in the highest conflict torques (>0.450 Nm, F(1.618,48.537) = 4.296, p<0.05)) and times (>11.00%, F(1.699,50.979) = 4.988, p<0.05)), even though the driver torque is on lower than the other conditions with a value of only 0.395 Nm. It is hypothesised that this is a result of the large torque provided by the controller to follow the inner lane, small curvature path. The class 3 trajectory has the smallest curve radius and thus highest curvature value. Since the radius, R, and the yaw rate, $\dot{\psi}$, are related to each other and velocity, V_x , by Equation (13), a small radius results in a high yaw rate. A high yaw rate is proportional to a high steering angle and thus despite not agreeing with the guidance, the drivers do not need to exert high forces on the steering wheel to negotiate the curve.

$$\dot{\psi} = \frac{V}{R} \tag{13}$$

The full statistical analysis for driver torque, conflict time, conflict torque and feedback torque can be found in Tables XI, XII, XIII and XIV respectively. The normality and sphericity of every condition data sample were checked, a necessary requirement before an ANOVA test. The normality tests showed that some condition samples did not meet the normality requirement, however, it was decided to continue using the ANOVA test for these conditions as no alternatives for this specific test are available and ANOVA is considered robust against the lack of normality [31].

2) Curve cutters - Left curves: Second, the left curve behaviour of the curve cutters is analysed. As curve cutters are a mixed group of class 1 and class 2 drivers in left curves, the results must be interpreted carefully and it must be validated if trends are due to only a subpopulation group or if it is an common occurrence. In the prepositioning phase, the personalised condition is preferred as it results in the least amount of conflict (32.60% and 0.163) Nm for FF 0.5 and 1.10% and 0.006 Nm for FF 0.92) and the lowest driver torque (0.155 Nm for FF 0.5 and 0.108 Nm for FF 0.92). The R3L5 and R2L1 guidance are found to result in similar driver torque and conflict values. In the prepositioning phase this can be explained by both guidances pushing the driver to the outside of the upcoming curve, which is where the curve cutters want to be. In the curve phase, the personalised guidance is also liked best. It is found that in curves the conflict is highest for the R2L1 guidance with conflict torques up to 0.170 Nm (F(1.381,41.424) = 7.422, p < 0.05). This is surprising as it contradicts earlier findings that drivers like their own or a very similar driving style [16]. Since this might be due to the curve cutters consisting of two different types of drivers, the curve is analysed separately for both groups. The results of this detailed analysis are shown in Figure 17, which shows the conflict time and torque plots for the R2L1 and R2L2 drivers separately.

Despite the hypothesis that the dislike of the R2L1 guidance is caused mostly by the R2L2 drivers disliking the too aggressive (L1) left curve, Figure 17 shows that the origin of the high conflict values lies with the R2L1 drivers. After thorough analysis it was found that the high conflict values are the direct result of two factors and that conflict only occurs when both factors are rejected. The first factor is the similarity between the HCR and the manual driving of the driver. Figure 18 shows the manual trajectory of an R2L1 driver with high conflict values. It can be seen that this driver's manual trajectory, while in the same class, is less extreme in its behaviour than the class average R2L1 and therefore large deviations between the natural driving style and R2L1 guidance are present. The conflict torque for the driver in Figure 18 equals 2.091 Nm and the conflict time 52.60%.

However, the lack of similarity between HCR and driver trajectory on its own does not result in conflict. Only if the driver also refuses to adapt her/his driving behaviour and the resulting driven trajectory therefore does not deviate much from the driver's manual trajectory, then high conflict values are generally present. This is the second factor and is illustrated in Figure 19.

The figure shows two different drivers whose natural trajectories, from session 1 of the experiment, are very similar, however, their driven trajectories when subjected to an R2L1 HCR differ greatly. The resulting trajectories show that the top driver, driver 1, exhibits less adaptation in behaviour when driving, while the bottom driver, driver 2, changes her/his trajectory significantly. The top scenario results in large amounts of conflict time and torque, while the bottom driver almost experiences no conflict with the guidance due to her/his willingness to adapt. Another method to understand how much drivers adapt their behaviour is check the feedback torque, $T_{feedback}$, as this shows how much the driver deviates from the reference trajectory. Figure 27 also shows a high feedback torque for this condition because of those drivers that do not adapt their trajectories.

The conclusion of this extensive analysis for R2L1 drivers indicates that the relationship between HCR and manual driving trajectories is very important. However, even more crucial is the driver's willingness to adapt her/his trajectories. This will be analysed more in detail in Subsection IV-D by focusing on trajectories, despite the lack of hypotheses concerning this matter.

3) R3L5 drivers - Right curves: The same analysis is now performed for the R3L5 drivers. First the right curves are analysed, for which it is once again clear that a higher feedforward gain consistently results in lower conflict times and torques. This effect is only significant for the prepositioning phase (conflict time: F(1,30) = 38.028, p<0.05, conflict torque: F(1,30) = 26.636, p<0.05). During prepositioning, these drivers prefer a completely personalised guidance or the centerline HCR. The R2L1

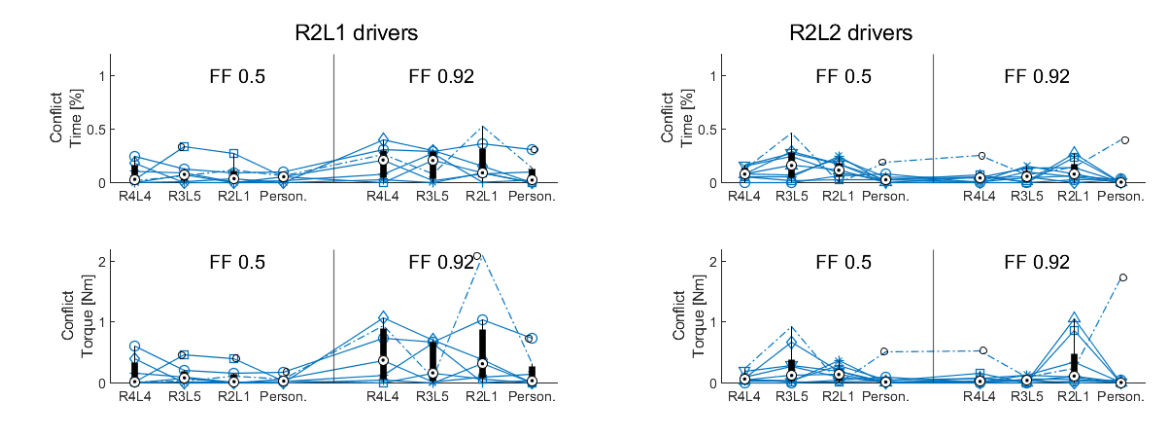


Fig. 17: Side-by-side analysis of conflict times and torques for R2L1 and R2L2 drivers.

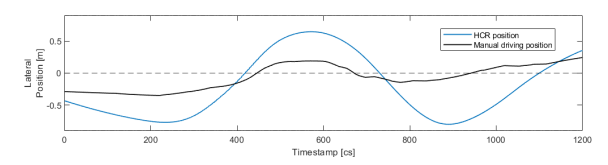


Fig. 18: Comparision of the R2L1 class average used for the R2L1 HCR and an individual driver (driver 25) classified as R2L1.

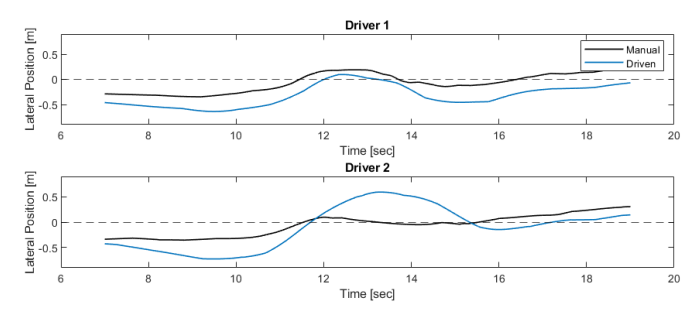


Fig. 19: Comparison of two drivers natural driving behaviour and their resulting, driven trajectories when subjected to R2L1 guidance, indicating their willingness to change their trajectories when collaboration with haptic shared control.

guidance shows the biggest mismatch (F(1.946,58.383) = 8.659, p<0.05)), which is caused due to the guidance pushing the driver towards to outer side of the upcoming curve, while the drivers natural inclination is to tend towards the inner side of the curve. This is also visible from the significant difference in conflict time and torque for the HCR between the driver groups (conflict time: F(3,90) = 7.881, p<0.05, conflict torque: F(1.946,58.383) = 11.870, p<0.05). The R3L5 drivers, however, also do not seem to like the R3L5 guidance in this scenario. The driver torque is relatively low (0.206 Nm for FF 0.5 and 0.226 Nm for FF 0.92), but the conflict torque and especially conflict

time show a clear increase in value relative to the other conditions. The conflict torque increased to 0.353 Nm and the conflict time to 62.10%. It is theorized that this is caused due to a wide variety in R3L5 drivers. A lot of drivers fall into class 3 as this class has loose constraints and does not differentiate between behaviours, such as a constant negotiation on the inner side of the curve or a progression from centerline to inner curve negotiation. The class average HCR might thus not suit everyone. This issue was already illustrated in Figure 10, where all the personalised HCR's are plotted against the class-average HCR for R3L5. This figure shows that some R3L5 drivers fluctuate their lateral position on the road, while others follow a more steady trend. After an additional analysis, it was found that indeed the high conflict values are caused by R3L5 drivers whose manual driving style differs in behaviour from the class averaged HCR and who refuse to adapt their driving style.

For the curve phase analysis, some differences in trends are noticeable between the high and low feedforward gain, however, these are not statistically significant. For the low feedforward gain, it seems like all conditions, with exception of the centerline guidance, result in the same amount of conflict of 0.074 Nm and 5.40% and thus no clear preference is present. The high feedforward case on the other hand shows no difference between R4L4, R2L1 or personalised guidance, yet shows a high conflict time (F(1.618,48.537) = 4.296, p<0.05)) and torque (F(1.699,50.979) = 4.296, p<0.05)) for the R3L5 HCR. Especially the high conflict torque, which is higher than 0.098 Nm, is surprising as the driver torque and feedback torque in this scenario are rather low. Furthermore, high conflict values typically indicate a lack of acceptance by the driver, while the subjective rating of this condition is among the highest, see Figures 13 and 14. Usually, it is the high feedback torque that causes high conflict torques and a subsequent low subjective rating as feedback torque is perceived by the driver as punishing. Since this is not the case in this scenario, the cause of the conflict is the feedforward torque. It is possible that these R3L5 drivers, who usually preposition on the inner side of the road, find themselves in a different position than usual with respect to the curve. Therefore, less steering may be needed to negotiate the curve, however, the feedforward is still strongly active due to the small radius of its trajectory. The drivers therefore correct the feedforward force, however this is very hard to perceive for the driver and does not feel punishing. This issue leads to believe that this is an artefact of the current conflict definition, which only checks for opposing signs of T_{driver} and T_{HSC} , but does not impose any limits on the driver torques (to understand if the driver is actively steering or following the guidance) or feedback torques. It should be investigated to find a more suitable, new conflict definition for HSC with separated feedforward and feedback cueing.

4) R3L5 drivers - Left curves: At last, the left curves for R3L5 drivers are analysed. The prepositioning again shows consistently lower conflict values for the higher feedforward gain (F(1,30) = 10.059, p<0.05)). The personalised guidance clearly causes the least conflict time and torque (85.60% and 0.108 Nm for FF 0.5, 48.40% and 0.063 Nm for FF 0.92), followed by the three other HCR's, for which no differences in conflict are found. This makes sense, especially for the R2L1 and R3L5 HCR's as their prepositioning is both towards the outer side of the curve, while it seems that R3L5 drivers are also accepting of a centerline prepositioning. This pattern is also visible in their right curves.

In the curve phase, a distinct difference in conflict between the low and high feedforward gain is present (F(1.634,49.012)=8.859, p<0.05)). The low feedforward gain shows no preference among the four guidances, all four result in equal conflict values. The conflict times do not exceed 9.10% and the conflict torques are all valued around 0.061 Nm. In the high feedforward case, all conditions except R2L1 result in similar conflict values. The conflict time of 8.20% and conflict torque of 0.270 Nm for the R2L1 are high, which is expected as the left guidance falls into class 1 and is therefore the most efficient and aggressive.

D. Driven Trajectories

The analysis of the objective measures has shown that conflicts are strongly dependent on the trajectory adaptation by the driver. Conflict was low when drivers adapted their trajectory, showing their willingness to follow the guidance. In case the driver agrees with the guidance and follows its lead, then the conflict values will be low, while if the driver fights the guidance and forcibly attempts to follow her/his own path, then high conflict values are expected. It is, however, not yet understood when or why a driver chooses to retain her/his own trajectory or to adapt her/his trajectory to align with the guidance. Figure 19 illustrates this issue for two drivers with a similar

natural driving trajectory, who adapt differently to the HCR R2L1 guidance. One driver largely sticks to her/his manual driving style, while the other changes her/his behaviour and reclassifies as a class 1 driver. As this is a very important aspect in the understanding of acceptance of haptic shared control, it is decided to investigate this behaviour a bit further despite the lack of any hypotheses surrounding this topic. It is investigated how many drivers change their behaviour, how they change their trajectories and if any trends are visible in these adaptations.

Figures 28 and 29 show the six left and right trajectories driven for the eight different test conditions, for an R2L1 and R3L5 driver respectively. These figures show that the R2L1 driver is very consistent in her/his driving style and persistently, for each guidance, maintains her/his original trajectory. The R3L5 driver, however, seems to be more prone to adapt to the haptic shared control. This driver's classification changes to R2L1 with an R2L1 guidance and to R3L1 for the R3L5 guidance.

To see if these tendencies are inherent to these specific drivers or group of drivers, the behaviour of all participants was reclassified after driving with the different haptic shared control variations. The results are summarised in Figures 20, 21, 22 and 23, each representing a different guidance. An example of this plot for the R2L1 HCR is shown in Figure 20. It shows that for the left and right curves and feedforward gains if the drivers' new class after reclassification (Day 2) is consistent with their original one (Day 1). Figure 20 shows how the curve cutters, both R2L1 and R2L2 drivers, are 84.38% consistent for right curves and 59.38% for left curves with R2L1 guidance. The R3L5 drivers on the other hand adapt to follow the guidance and end up in more efficient classes. A significant portion, 43.75% for FF 0.5 and 50.00% for FF 0.92, of the R3L5 drivers reclassifies as R2L1 drivers when following this guidance.

A similar analysis for the R3L5 HCR shows that the R3L5 drivers most often stick to their own class after reclassification, although up to 37.50% change their trajectory to the more efficient class 2 for left curves. This in contrast to the curve cutters who in this scenario, especially for the low feedforward gain, 25.00% of the time fall into class 5. The R4L4 guidance on the other hand has a large effect on drivers and changes both the behaviour of the curve cutters and the R3L5 drivers. In right curves, it makes the curve cutters less efficient and reduces up to 50.00% of them to class 3 drivers for the low feedforward gain. In left curves, the curve cutters also lose efficiency and often reclassify as class 3 (18.75% for FF 0.50 and 31.25% for FF 0.92) or even class 5 (25.00%for FF 0.50 and 12.50% for FF 0.92). The original R3L5 drivers however, gain efficiency and reclassify as more efficient classes for left curves with R4L4 guidance. At last, the personalised condition induces the most changes for left curves. Many of the R3L5 drivers reclassify as class 1

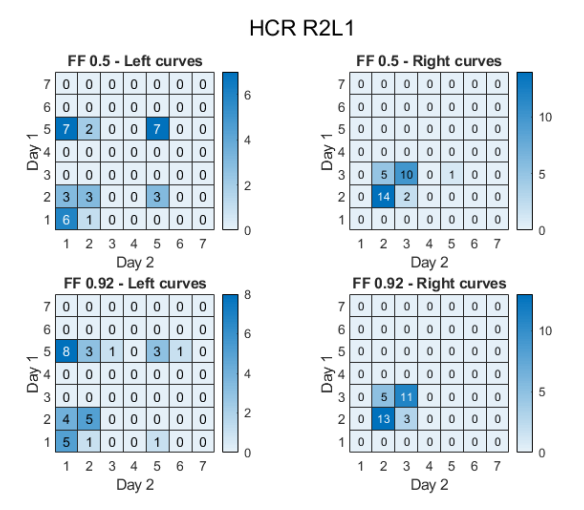


Fig. 20: Reclassification of all drivers after driving the R2L1 guidance.

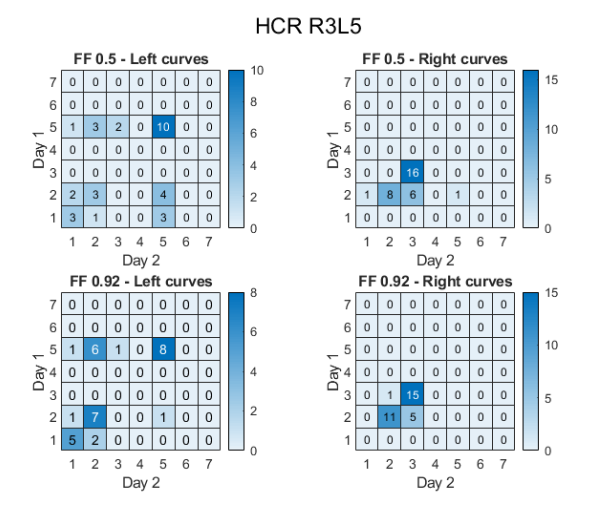


Fig. 21: Reclassification of all drivers after driving the R3L5 guidance.

or 2 (25.00% for FF 0.50 and 56.25% for FF 0.92) and the R2L2 drivers, part of the curve cutters, sometimes reclassify as class 1.

Finally, Table XV summarises the overall consistency of the different driver groups. It shows how consistent the drivers are in retaining their natural driving style after being subjected to all the different conditions. This as an attempt to see which driver groups are less willing to adapt to the HSC than others. It seems that most drivers, regardless of their manual driving class, change their driving habits when subjected to haptic shared control. Some groups are very adamant about the continuation of their own trajectory, such as R2L1 drivers in left curves, while other groups are more adaptive, such as R3L5 drivers in left curves. Future research should investigate

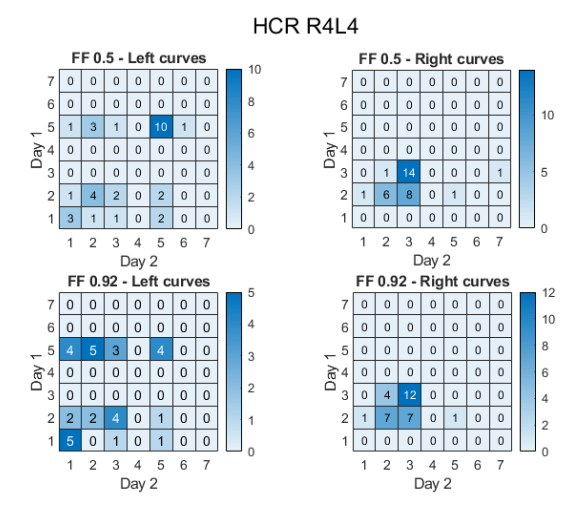


Fig. 22: Reclassification of all drivers after driving the R4L4 guidance.

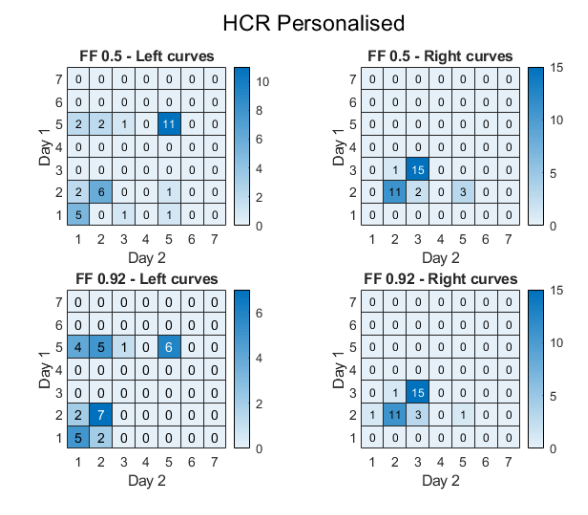


Fig. 23: Reclassification of all drivers after driving the Personalised guidance.

more in depth the link between these consistencies and the results of the objective measures. These showed a few R2L1 drivers that strongly disliked the R2L1 guidance, because their own class 1 trajectory deviated from the class-averaged class 1 trajectory and they refused to change their behaviour. Furthermore, the analysis of the left curves of R3L5 drivers showed low conflict values for all conditions, resulting in overall low conflict values. This might be linked to the R3L5 drivers being very willing to adapt their left curve behaviour as their consistency is only 43.18%.

V. Discussion

The goal of this research is to understand how haptic shared control acceptance is influenced by changing the reference trajectory and feedforward gain of the control

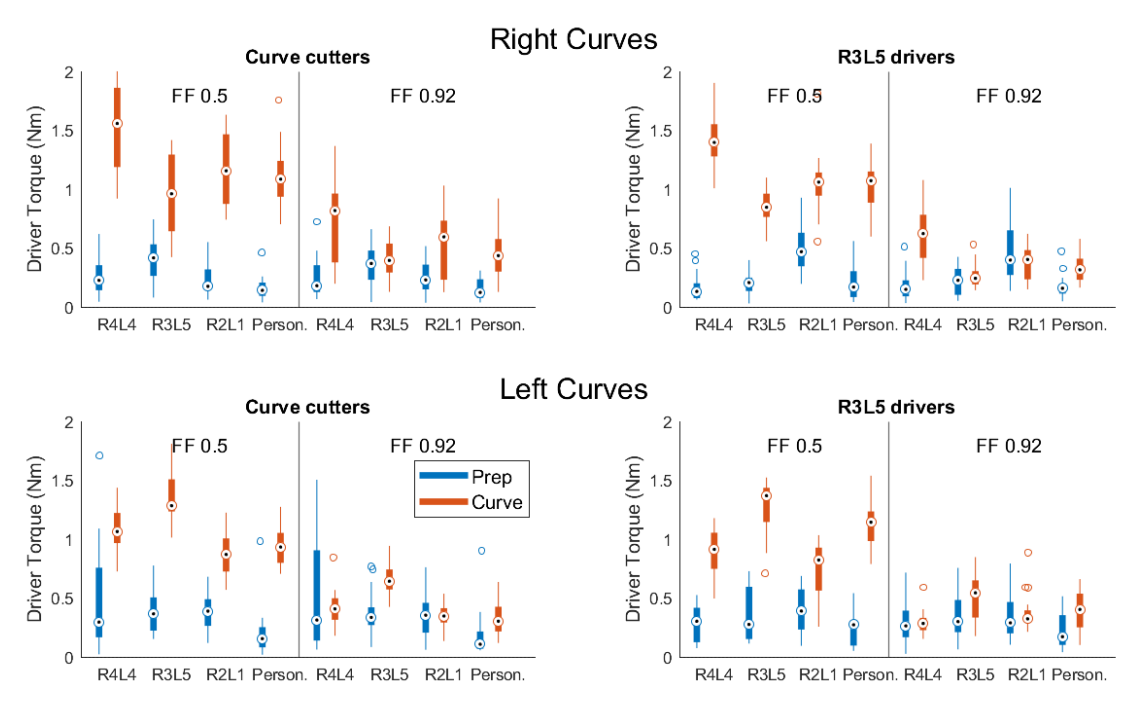


Fig. 24: Overview of driver torque for both driver groups in all conditions.

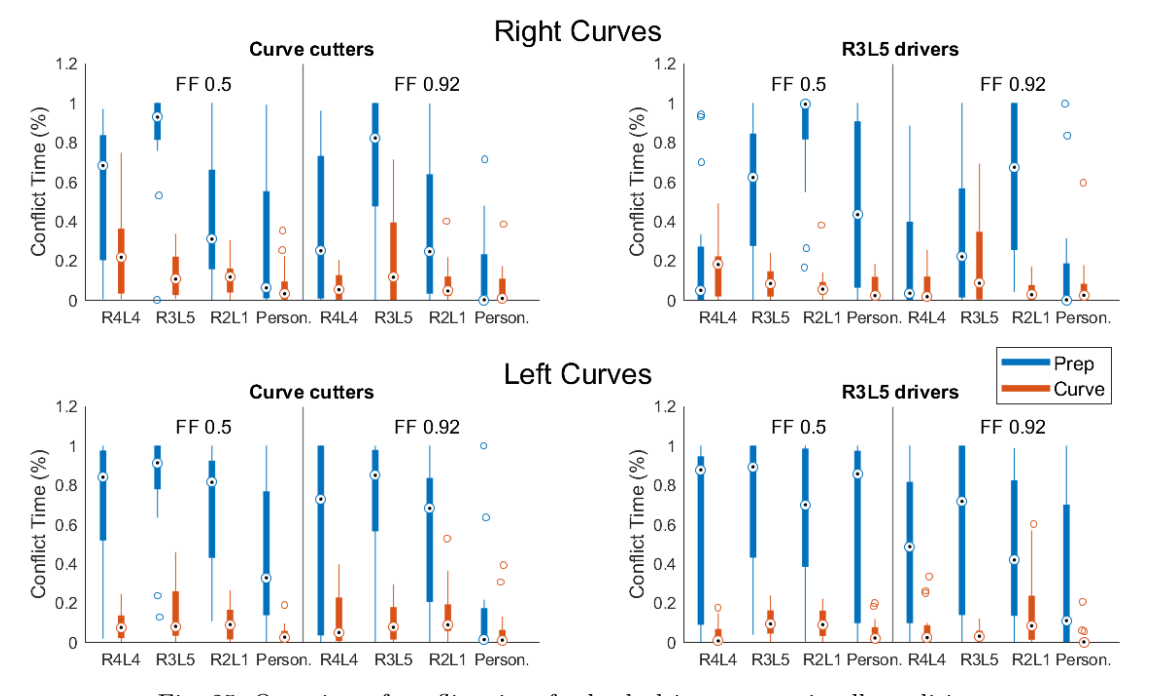


Fig. 25: Overview of conflict time for both driver groups in all conditions.

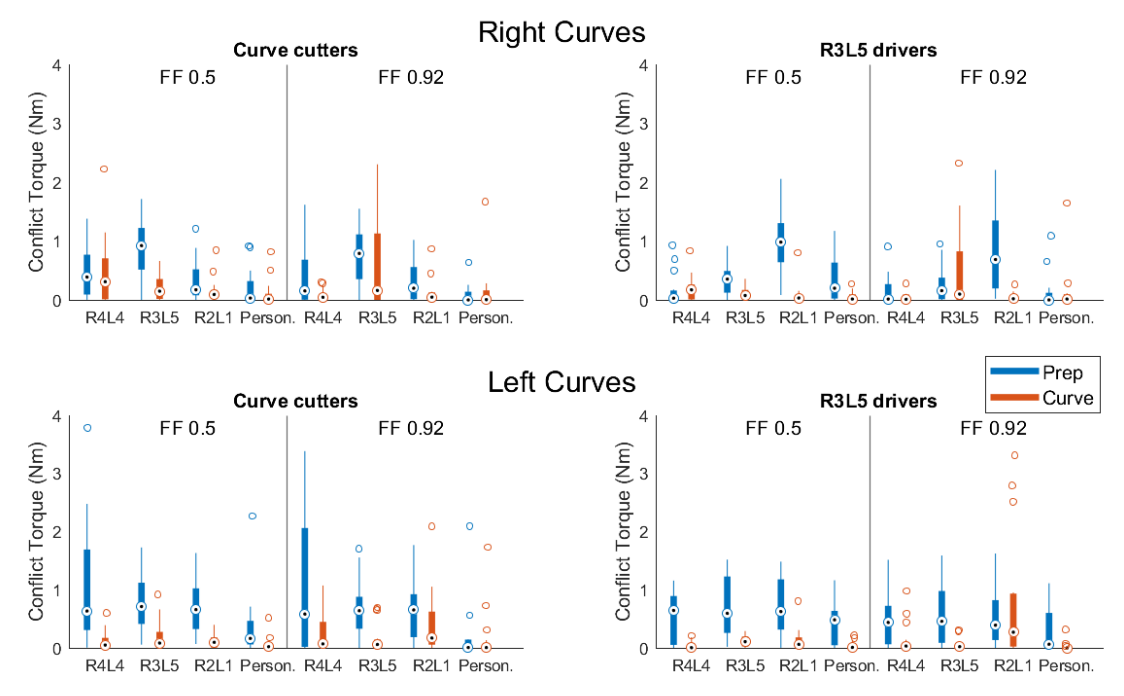


Fig. 26: Overview of conflict torque for both driver groups in all conditions.

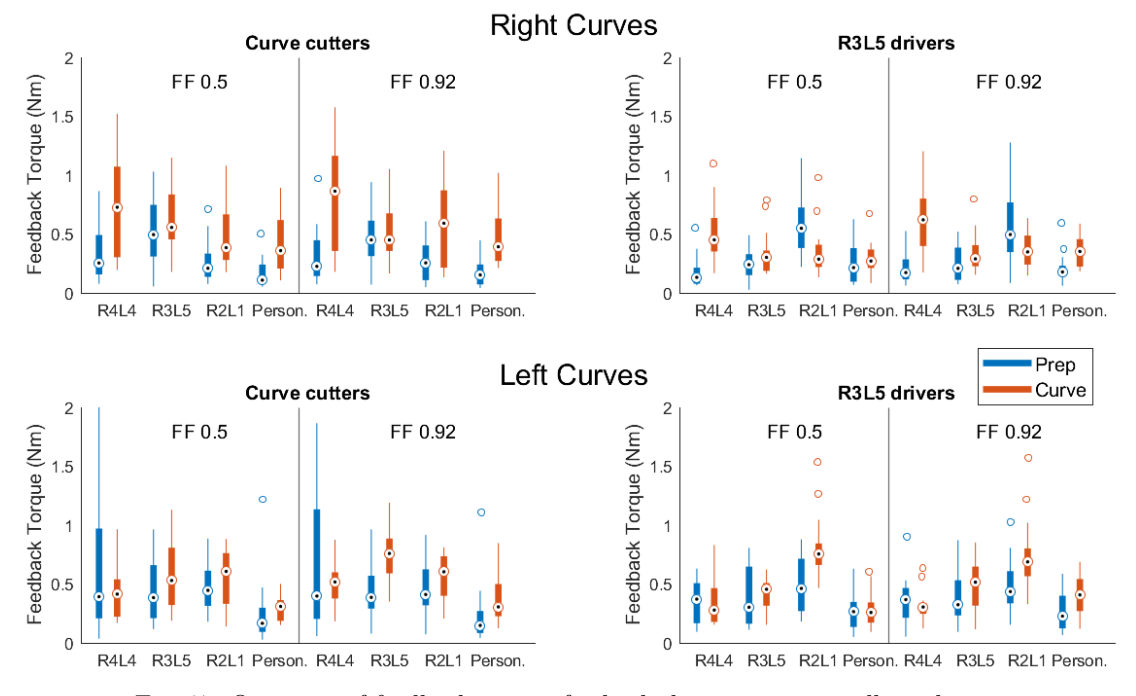


Fig. 27: Overview of feedback torque for both driver groups in all conditions.

significant result (p<0.01), * indicates a significant result $(0.01\le p\le 0.05)$ and - indicates not significant (p>0.05) (gg indicates that the Greenhouse-Geisser TABLE XI: Results of the two-way repeated-measures ANOVA with additional between-subject variable for the driver torque, where ** indicates a highly correction is used).

Oriver torque - ANOVA	_											
			П	eft					Щ	Right		
	PP			CRV			PP			CRV		
	Jp	H	d	Jp	দ	d	Jp	H	d	Jp	Ţ	d
	$1.379, 41.369^{2} \{gg\}$	5.283	*	$2.361, 70.823^{\circ} \{gg\}$	80.287	* *	$1.966, 58.975^{2}\{gg\}$	10.969	*	$2.057, 61.698^{2} \{gg\}$	81.895	* *
	1, 30	1.017	1	1, 30	707.895	* *	1, 30	2.178	ı	1, 30	1122.426	* *
ICR x FF	. 1	1.199	1	$2.146, 64.383^{\circ} \{gg\}$	19.950	* *	$2.268, 68.037^{2} \{gg\}$	0.309		2.632, 78.972	11.429	* *
ICR x Driver Group	$1.379, 41.369^{2} \{gg\}$	2.555	1	2.361, 70.823 ² {gg}	12.964	*	$1.966, 58.975^{2}\{gg\}$	12.339	*	$2.057, 61.698^{\circ} \{gg\}$	0.034	,
Driver Group	1, 30	1.176	,	1, 30	1.444	,	1, 30	0.189		1, 30	2.578	1

TABLE XII: Results of the two-way repeated-measures ANOVA with additional between-subject variable for the conflict time, where ** indicates a highly significant result (p<0.01), * indicates a significant result $(0.01\le p\le 0.05)$ and - indicates not significant (p>0.05) (gg indicates that the Greenhouse-Geisser correction is used).

			d	×	1	* *	1	1
			ĹΉ	4.296	0.950	18.095	0.233	3.610
	Right	CRV	Jp	$1.618, 48.537^{\circ} \{gg\}$	1, 30	$1,75.047^{\circ}\{gg\}$	$1.618, 48.537^{\circ} \{gg\}$	1, 30
			р	* *	* *	,	*	1
		PP	Ē	9.186	38.028	0.970	7.881	0.614
			df	3, 90	1, 30	3, 90	3, 90	1, 30
				*		* *	'	1
			ഥ	7.469	0.339	5.166	1.184	1.656
	Left	CRV	df	$2.339, 70.160^{\circ} \{ gg \}$	1,30	$2.434, 73.019^{\circ} \{ gg \}$	$2.339, 70.160^{\circ} \{ gg \}$	1,30
				d	*	*	*	
				ĹΉ	5.423	27.797	3.761	1.447
_		PP	Jp	$1.639, 49.167^{\circ} \{gg\}$	1, 30	$2.503, 75.077^{\circ} \{gg\}$	$1.639, 49.167^{\circ} \{gg\}$	1, 30
Conflict time - ANOVA				HCR	FF	HCR x FF	HCR x Driver Group 1.639, 49.167^{g	Driver Group

TABLE XIII: Results of the two-way repeated-measures ANOVA with additional between-subject variable for the conflict torque, where ** indicates a highly significant result (p<0.01), * indicates a significant result $(0.01 \le p \le 0.05)$ and - indicates not significant (p>0.05) (gg indicates that the Greenhouse-Geisser correction is used).

			d	*		* *	'	'
			ſΞĄ	4.988	0.561	14.456	0.284	2.951
	ght	CRV	df	$1.699, 50.979^{\circ} \{gg\}$	1, 30	$2.044, 90^{\circ} \{gg\}$	$1.699, 50.979^{\circ} \{gg\}$	1, 30
	Right		ď	*	* *	,	* *	,
			ſΞĄ	8.659	26.636	0.829	11.870	0.094
		PP	df	$1.946, 58.383^{\circ} \{ gg \}$	1, 30	2.190, 65.688	$1.946, 58.383^{\circ} \{gg\}$	1, 30
			d	* *	* *	* *	,	,
		됴	7.422	8.349	8.859	2.317	0.122	
	ff	CRV	Jp	$1.381, 41.424^{\circ} \{gg\}$	1,30	$1.634, 49.012^{\circ} \{gg\}$	$1.381, 41.424^{\circ} \{gg\}$	1, 30
	Left		d	*	* *	ı	ı	ı
				ഥ	5.390	10.059	1.087	2.758
		PP	Jp	$1.363, 40.888^{\circ} \{gg\}$	1,30	$2.184, 65.634^{\circ} \{gg\}$	$1.363, 40.888^{\circ} \{gg\}$	1, 30
Common norder and a structure				HCR	FF	HCR x FF	HCR x Driver Group	Driver Group

TABLE XIV: Results of the two-way repeated-measures ANOVA with additional between-subject variable for the feedback torque, where ** indicates a highly significant result (p<0.01), * indicates a significant result (0.01 \leq p \leq 0.05) and - indicates not significant (p>0.05) (gg indicates that the Greenhouse-Geisser correction is used).

Feedback torque - ANOVA	JVA											
			Lef	ft					Right	t		
	PP			CRV			PP			CRV		
	fp	Ĺ	d	fþ	ĹΤΙ	d	fþ	ſΉ	d	Jp	ĹΉ	d
HCR	$1.379, 41.379^{\circ} \{ gg \}$	6.424	* *	$1.687, 50.622^{\circ} \{ gg \}$	18.810	*	$1.885, 56.557^{\circ} \{gg\}$	9.756	* *	$1.555, 46.643^{\circ} \{ gg \}$	13.358	* *
PF	1, 30	0.002		1, 30	8.913	* *	1, 30	0.513		1, 30	4.285	×
ICR x FF	3, 90	0.550	,	3, 90	899.2	* *		0.656		3, 90	3.037	×
HCR x Driver Group	$1.379, 41.379^{\circ} \{ gg \}$	2.957		$1.687, 50.622^{\circ} \{gg\}$	6.818	* *		13.784	* *	$1.555, 46.643^{\circ} \{ gg \}$	0.554	ı
Priver Group	1.30	1 202	,	1.30	0.860	,	1.30	690 0	0.805	1.30	7 469	* *

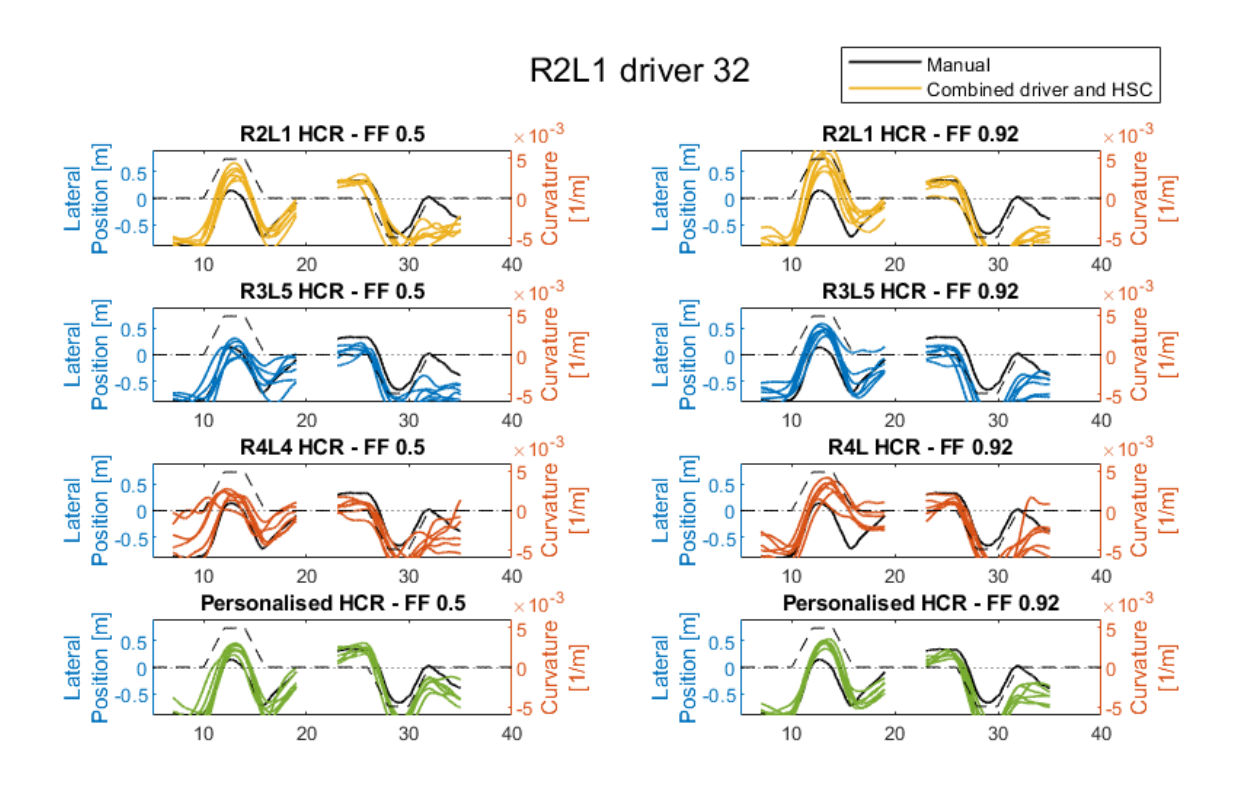


Fig. 28: Driven trajectories by an R2L1 driver subjected to the eight different experiment conditions.

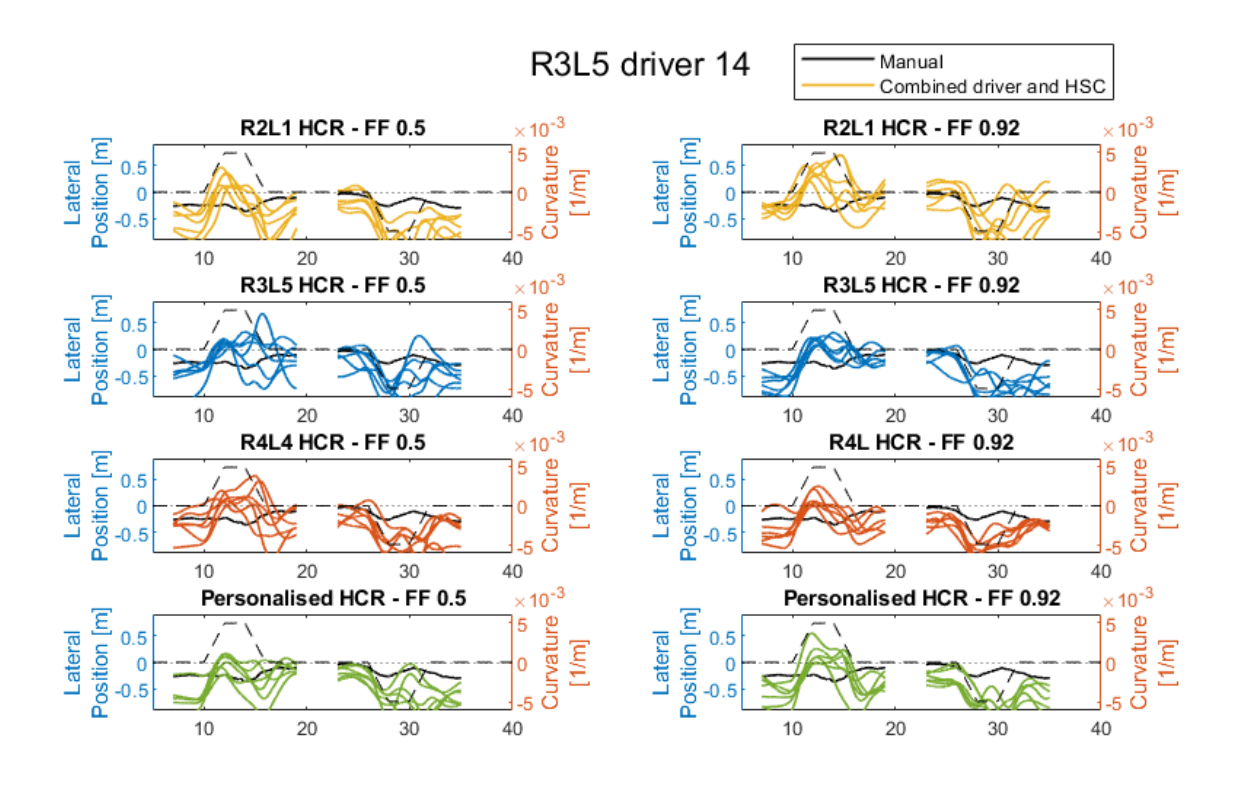


Fig. 29: Driven trajectories by an R2L1 driver subjected to the eight different experiment conditions.

TABLE XV: Consistency of the different driver groups towards their manual driving class.

Driver Group	Curve	Consistency
R2L1 drivers	Right	65%
102L1 drivers	Left	72.50%
R2L2 drivers	Right	67.50
102L2 drivers	Left	52.60%
R3L5 drivers	Right	80.68%
100L0 drivers	Left	43.18%

system. This is investigated by a computer simulation platform and a human-in-the-loop experiment in which two driver groups from [19] are assessed: the most popular driving style (n=16), R3L5 drivers, and the curve cutters (n=16), R2L1 and R2L2 drivers, whose driving style is optimal in terms of lateral acceleration and Time-to-Lane Crossing. These drivers were subjected to a fully personalised reference trajectory, as well as a class-average guidance of their own and the other driver group's class. These are then tested to compare with the industry standard, the centerline path. This relates back to the research goal as this helps to understand if complete personalisation is necessary and if the efficiency of the guiding trajectory influences this decision. The different levels of feedforward, K_{LoHS} , are added to understand the drivers' reaction to having a smaller and larger share of the control and thus also to a smaller or larger workload.

To help understand acceptance, five hypotheses were formulated. The first hypothesis H.I was that the natural driving style of more than 30% of drivers would fall into the R3L5 class and no natural centerline drivers would be found. This hypothesis was formulated based on [19] and can easily be accepted as the results of the experiment are completely in line with this previous study. Of the tested drivers, 32% is classified as the R3L5 category and no natural centerline drivers are found.

The remaining four hypotheses cover the haptic shared control experiment.

The second hypothesis H.II deals with the question whether or not drivers can be tricked into liking a similar driving style (class-average HCR) without needing full personalisation. This hypothesis is based on previous research by [16], but must be rejected. Complete personalisation significantly reduces conflicts for all drivers, however, some drivers show the same level of conflict and subjective acceptance for the class-average HCR. A structure was found that helps to understand this behaviour: If the natural driving trajectory of the driver is similar to the classaverage HCR (see Figure 10), then the level of conflict is low and personalisation is not necessary. In case both trajectories are different, then the level of conflict depends on the attitude of the driver. If the driver is willing to follow the guidance, then conflict is low and personalisation is not necessary. If the driver follows her/his own trajectory despite the HSC, then conflict values are high for this guidance and personalisation is necessary. In hindsight, we are able to determine why a driver may accept HSC, however, these findings do not give us the opportunity to predict whether a given driver may accept or reject the class-average HCR.

Future research in this area should therefore focus on understanding why certain drivers follow the guidance and why other drivers follow their own trajectory. It was found that the answer to the issue is related to the similarity between the natural driving style of the driver and the HCR (see Figure 10). It is therefore recommended to investigate a more detailed driver classification method that is able to capture more subtle differences in trajectories. Depending on the classification, personalisation could become obsolete as every driver's natural driving closely resembles a class-average HCR.

The third hypothesis H.III is based on the computer simulations generated at the beginning of this research and questions if drivers are more likely to follow optimal trajectories. These trajectories result in a minimum requirement for steering [28] and are found to be dynamically the safest [24]. However, this hypothesis must also be rejected. The analysis has shown that the R2L1 guidance, especially in left curves, often results in conflict values up to 0.270 Nm for the curve phase. Furthermore, the Satisfaction-Usefulness plots even indicate a negative satisfaction rating for this guidance by the R3L5 drivers. These results show that acceptance is not related to the optimal guidance. Despite the high conflict values and low subjective rating, 43.75% for K_{LoHS} and 50.00% for K_{LoHS} of R3L5 drivers reclassify as R2L1 drivers after being subjected to this guidance (see Figure 20). This demonstrates that despite the drivers fighting the optimal guidance, they are influenced and adopt a more optimal driving style.

The fourth hypothesis H.IV deals with the centerline guidance. Centerline guidance is the industry standard, however, no drivers exhibit this driving style naturally. This hypothesis is also rejected as it is not the most disliked reference, at least not by all drivers. The centerline guidance should be seen as a good middle ground. It was never rated or measured as the best guidance, but it also never annoyed the driver into huge conflict values as large as the R2L1 guidance.

The last hypothesis H.V discusses the two different feedforward gains. It was hypothesised based on [8] [13] and [14] that a higher feedforward torque would reduce conflict, however, higher feedforward is more noticeable and might be perceived as a nuisance. The hypothesis is rejected. The high K_{LoHS} does significantly reduce conflict time and torque up to 86.91%, however, it is not perceived as a nuisance and is rated consistently better in all subjective questionnaires. It can be concluded that the feedforward element is indeed essential for the acceptance of the guidance.

This study has only compared two different feedforward settings. It is therefore recommended that succeeding research focuses on finding the ideal feedforward gain K_{LoHS} . K_{LoHS} 0.92 was determined heuristically in previous studies [14] [27] [13], however, there is no scientific explanation for this value. K_{LoHS} 0.92 reduced conflicts and improved subjective acceptance compared to K_{LoHS} 0.50, however, there might be an even better combination of driver and HSC effort.

The analysis of the objective measures brought forward the importance of the adaptation of the driven trajectories with HSC. An additional analysis was performed that focused on the reclassification of drivers after being subjected to the different HSC guidances. It was found that a large share of drivers adapt their behaviour depending on the guidance, e.g. only 43.18% of R3L5 drivers is completely consistent throughout all conditions. Future research should focus on understanding why some drivers adapt and why others do not. This is linked to the results of H.II; If the natural driving style of the driver and the class-average HCR are different, then either the driver will follow the guidance (which results in being reclassified into a different class) or retain her/his own driving style.

In hindsight, it appears that the major limitations of this research are twofold.

First, the driver model used in the simulations is inadequate for this application as it does not exhibit prepositioning. The model acts on current curvature information, which means that before the curve starts, the model assumes an infinite straight road ahead. Every driver prepositions before a curve as it is an essential element for acceptance [24], however, this model is unable to capture that behaviour, resulting in trajectories that cannot be classified and less accurate predictions in simulations. Future work should find or design a driver model that is able to capture this prepositioning behaviour as it would greatly improve the validity of the simulations.

Second, the conflict definition used in this paper is incomplete. Some scenarios in which the driver torque and feedback torque are low do show high amounts of conflict. The detected conflicts were found to be caused by the feedforward torque, which is not perceived by the drivers as punishing. The scenarios for which this occurred also show high subjective ratings. Further research should focus on expanding this conflict definition. A suggestion would be to include a threshold for driver torque. Therefore, if the driver decides to follow the guidance and the driver torque is below this threshold, then the conflict is zero. Only if the driver makes a significant contribution on the steering wheel, then conflict is possible. This would also immediately show if the driver reclassifies her/his trajectories or pushing her/his own preferences.

VI. CONCLUSIONS

This research aimed at understanding how changing the reference trajectory and the feedforward gain of the haptic shared control influence its acceptance. It was investigated if complete personalisation is necessary and if acceptance is linked to optimal trajectories, i.e. minimal steering input required and dynamically safest. The different levels of feedforward, K_{LoHS} , are added to investigate the drivers reactions to smaller and larger shares of control. This was investigated by computer simulations and a human-in-theloop experiment in which the most popular driving style, R3L5 drivers, and the more optimal curve cutters, R2L1 and R2L2, were subjected to eight different test conditions. These participants were subjected to four reference trajectories: the industry standard centerline, a complete personalised trajectory and a class-average trajectory of their own and the other driving group. The results the following conclusions were drawn:

- Of the current driving population, more than 30% exhibits R3L5 driving, while centerline driving, the industry standard of all ADAS systems, is not found.
- Complete trajectory personalisation consistently leads to the lowest conflict times and torques, however, complete personalisation is not necessary for every driver. The drivers that decide to adapt their driving behaviour to follow the guidance have equal conflict values for the class-average trajectory of their own class. It is not known which drivers decide to adapt and which ones do not adapt.
- Acceptance is not linked to optimal trajectories.
 These trajectories are experienced as a nuisance and result in high conflict values and low subjective ratings.
- Even though centerline driving does not come natural to drivers, it is not the most disliked guidance.
 Centerline guidance offers a good middle ground.
- A higher feedforward gain, K_{LoHS} , reduces conflict up to 86.91% and is consistently rated better in the CARS and Van der Laan rating.
- Certain drivers have a tendency to adapt their driving style when subjected to HSC and are reclassified to other classes, often more optimal than their natural driving style. These adaptations are linked to the drivers needing complete personalisation (if they do not adapt) or only needing class-average personalisation (in case they adapt).

The results show that complete personalisation might not be necessary for every driver, but it does guarantee high acceptance levels for everyone. Furthermore, a high feedforward gain further increases acceptance. Future research should focus on understanding why drivers choose to adapt or not and on finding the ideal feedforward gain.

REFERENCES

[1] D. A. Abbink, M. Mulder, and E. R. Boer, "Haptic shared control: smoothly shifting control authority?," Cognition, Tech-

- nology Work, vol. 14(1), pp. 19-28, 2012.
- [2] D. A. Abbink, T. Carlson, M. Mulder, J. C. F. de Winter, F. Aminravan, T. L. Gibo, and E. R. Boer, "A topology of shared control system – finding common ground in diversity," *IEEE Transactions on Human-Machine Systems*, vol. 48(5), pp. 509–525, 2018.
- [3] F. Hartwich, M. Beggiato, and J. F. Krems, "Driving comfort, enjoyment and acceptance of automated driving effects of drivers' age and driving style familiarity," *Ergonomics*, vol. 61(8), pp. 1017–1032, 2018.
- [4] G. H. Walker, N. A. Stanton, and M. S. Young, "Where is computing driving cars," *International Journal of Human-Computer Interaction*, vol. 13(2), pp. 203–229, 2001.
- [5] M. Mulder, D. A. Abbink, and E. R. Boer, "Sharing control with haptics: Seamless driver support from manual to automatic control," *Human Factors and Ergonomics Society*, vol. 54(5), pp. 786–798, 2012.
- [6] P. G. Griffiths and R. B. Gillespie, "Sharing control between humans and automation using haptic interface: Primary and secondary task performance benefits," Human Factors: The Journal of the Human Factors and Ergonomics Society, vol. 47(3), pp. 574–590, 2005.
- [7] S. M. Petermeijer, D. A. Abbink, M. Mulder, and J. C. F. D. Winter, "The effect of haptic support systems on driver performance: A literature survey," *IEEE Transactions on Haptics*, vol. 8(4), pp. 467–479, 2015.
- [8] R. Boink, M. M. van Paassen, M. Mulder, and D. A. Abbink, "Understanding and reducing conflicts between driver and haptic shared control," *IEEE International Conference on Systems*, Man, and Cybernetics (SMC), pp. 1510–1515, 2014.
- [9] J. C. F. de Winter, N. A. Stanton, J. S. Price, and H. Mistry, "The effects of driving with different levels of unreliable automation on self-reported workload and secondary task performance," *International Journal of Vehicle Design*, vol. 70(4), pp. 297–324, 2016.
- [10] E. Adell, Driver Experience and Acceptance of Driver Support Systems - A Case of Speed Adaptation. PhD thesis, Department of Technology and Society, Lund University, 2009.
- [11] M. Mulder, D. M. Pool, D. A. Abbink, E. R. Boer, P. M. T. Zaal, F. M. Drop, K. van der El, and M. M. van Paassen, "Manual control cybernetics: State-of-the-art and current trends," *IEEE Transactions on Human-Machine Systems*, vol. 48(5), pp. 468–485, 2018.
- [12] F. Mars and J. Navarro, "Where we look when we driver with or without active steering wheel control," *PLoS One*, vol. 7(8), 2012. Art. no. e43858.
- [13] M. Mulder, D. A. Abbink, and E. R. Boer, "The effect of haptic guidance on curve negotiation behavior of young, experienced drivers," 2008 IEEE International Conference on Systems, Man and Cybernetics (SMC 2008), pp. 804–809, 2008.
- [14] W. Scholtens, S. Barendswaard, D. M. Pool, M. M. van Paassen, and D. A. Abbink, "A new haptic shared controller reducint steering conflicts," 2018 IEEE International Conference on Systems, Man, and Cybernetics (SMC), pp. 2705–2710, 2018.
- [15] M. M. van Paassen, R. P. Boink, D. A. Abbink, M. Mulder, and M. M. and, "Four design choices for haptic shared control," in Advances in Aviation Psychology, Volume 2 Using Scientific Methods to Address Practical Human Factors Needs (M. Vidulich, P. Tsang, and J. Flach, eds.), ch. 12, pp. 237–254, Routhledge New York, NY: Oxford University Press, 2017.
- [16] S. Griesche, E. Nicolay, D. Assmann, M. Dotzauer, and D. Kätner, "Should my car drive as i do? what kind of driving style do drivers prefer for the design of automated driving functions?," in Braunscheiger Symposium Automatisieringssysteme, Assistenzsysteme und eingebettete Systeme für Transportmittel (AAET), pp. 185–204, Deutches Zentrum für Luft- und Raumfahrt e.V., February 2016. ISBN 978-3-937655-37-6.
- [17] H. Godthelp, P. Milgram, and G. J. Blaauw, "The development of a time-related measure to describe driving strategy," *Human Factors The Journal of the Human Factors and Ergonomics Society*, vol. 26(3), pp. 257–268, 1984.
- [18] W. van Winsum, K. A. Brookhuis, and D. de Waard, "A comparison of different ways to approximate time-to-linecrossing (tlc)

- during car driving," Accident Analysis & Prevention, vol. 32(1), pp. 47–56, 2000.
- [19] S. Barendswaard, D. M. Pool, E. R. Boer, and D. A. Abbink, "A classification method for driver trajectories during curvenegotiation," 2019 IEEE International Conference on Systems, Man, and Cybernetics (SMC), pp. 3729–3734, 2019.
- [20] M. Greenwald, "Beyond benchmarking how experiments and simulations can work together in plasma physics," Computer Physics Communications, vol. 164, no. (1-3), pp. 1–8, 2004.
- [21] L. Saleh, P. Chevrel, F. Mars, J. Lafay, and F. Claveau, "Human-like cybernetic driver model for lane keeping," *IFAC Proceedings Volumes*, vol. 44, no. 1, pp. 4368–4373, 2011.
- [22] L. Saleh, P. Chevrel, F. Claveau, J. Lafay, and F. Mars, "Shared steering control between a driver and an automation: Stability in the presence of driver behavior uncertainty," *IEEE Transactions* on Intelligent Transportation Systems, vol. 14(2), pp. 974 – 983, 2013
- [23] W. Schofield, "Engineering surveying theory and examination problems for students," 2001.
- [24] S. Barendswaard, L. van Breugel, B. Schelfaut, J. Sluijter, L. Zuiker, D. M. Pool, E. R. Boer, and D. A. Abbink, "Effect of velocity and curve radius on driver steering behaviour before curve entry," 2019 IEEE International Conference on Systems, Man and Cybernetics (SMC), pp. 3866–3871, 2019.
- [25] J. P. Guilford, Psychometric Methods. McGraw-Hill Book Company, 2 ed., 1954.
- [26] J. Park, A. J. Doxon, W. R. Provancher, D. E. Johnson, and H. Z. Tan, "Haptic edge sharpness perception with a contact location display," *IEEE Transactions on Haptics*, vol. 5(4), pp. 323–331, 2012.
- [27] W. Vreugdenhil, S. Barendswaard, S. M. Petermeijer, C. Borst, and D. A. Abbink, "Complementing automotive haptic shared control with visual feedback for obstacle avoidance," Master's thesis, Faculty of Mechanical Engineering, Delft University of Technology, 2019.
- [28] E. R. Boer, "Tangent point oriented curve negotiation," Proceedings of the 1996 IEEE Intelligent Vehicles Symposium, pp. 7–12, 1996.
- [29] J. van der Laan, A. Heino, and D. de Waard, "A simple procedure for the assessment of acceptance of advance transport telematics," *Transportation Research Part C: Emerging Technologies*, vol. 5(1), pp. 1–10, 1997.
- [30] K. Lee, K. Kerns, R. Bone, and M. Nickelson, "Development and validation of the controller acceptance rating scale (cars): Results of empirical research," Proceedings of the 4th USA/Europe Air Traffic Management R&D Seminar, p. 1297, 2001.
- [31] A. Field, Discovering Statistics Using SPSS (Introducing Statistical Methods series), vol. 3. Sage Publications Ltd., 2005.

II

Preliminary Graduation Report

Introduction

This report is the first milestone of an extensive research in the individualisation of haptic shared controllers. Haptic shared control is a type of control architecture for highly automated vehicles in which the driver and vehicle automation communicate through the steering wheel. Instead of removing the driver from the control loop – which is a widely favoured strategy in autonomous vehicles – haptic shared control allows the driver to stay relevant and knowledgeable about the systems intentions and shortcomings (Mulder et al., 2012). Studies so far have shown that haptic shared control is capable of increasing safety (Griffiths and Gillespie, 2005) and decreasing control activity (Petermeijer et al., 2015) compared to manual driving, however, it also may lead to an increase in driver torque (Boink et al., 2014). This increase in driver torque is experienced as a nuisance by drivers and is caused by a misalignment of intention between both the driver and the controller (Petermeijer et al., 2015). This misalignment is often referred to as a *conflict*, which is detrimental for the acceptance of the haptic shared control.

In order to find a way to minimise conflicts and optimise acceptance of haptic shared control, past research has mostly focused on what type of controller drivers prefer in terms of structure. It was found that drivers actually prefer a controller which not only provides feedback torques to keep the vehicle on the reference trajectory, but also provides feedforward torques to anticipate an upcoming curve (Scholtens et al., 2018). So far, however, the focal point of research has never been on how the reference trajectory that the controller follows influences the acceptance of the driver. The aim of this research is therefore to investigate and learn to understand the relationship between the haptic shared controller's reference trajectory, the driver's natural preference and the acceptance of the haptic feedback by drivers. A second objective is to investigate whether individualisation is necessary and if so, how far should individualisation go?

This Preliminary Graduation Report provides an overview of all previous research in Chapter 2. It also includes a detailed research objective and research question in Chapter 3. As part of the methodology to answer the research question, a simulation platform is created, able to replicate the collaboration between driver and haptic shared controller. This is explained in Chapter 4. Finally, Chapter 5 delivers a proposal for the final experiment, a necessary step in reaching the objective, and this report is concluded in Chapter 6.

Literature Survey

To understand the motivation and goal behind this research, a literature survey is conducted that aims to map the importance of haptic shared control and the relevance of investigating personalisation in this field. The literature survey includes a summary on the relevance and different implementation possibilities of haptic shared controllers and discusses several personalisation strategies. Furthermore, an approach to driver behaviour classification is presented as well as a consideration on the selection of a suitable target group. Each section ends with an evaluation of the findings and discusses the subsequent implications for this research.

2.1. Haptic Shared Control

In recent years, researchers have developed a great interest in automated driving. It is expected that automated cars will increase driving comfort, safety and efficiency in the future (Hartwich et al., 2018, Walker et al., 2001). However, reaching fully autonomous systems has proven to be more difficult than anticipated (van Paassen, 2010), forcing the human driver into a supervisory role during this development period. The driver's tasks will as a consequence be reduced to monitoring the system and to intervene in case of (impending) failure. Humans show a poor ability to fulfil the role as supervisor (Kyriakidis et al., 2019) and thus depict a major weakness in the use of automated systems. This is therefore considered as one of the ironies of automation. Other problems related to the human as supervisor are complacency, over-reliance on the systems, and reduced situation awareness. Subsequently, this means that more automation ironically indicates a more critical and difficult role for the human (Bainbridge, 1983).

It is therefore evident that to solve these issues the human driver should be aware at all times of the limitations, capabilities and intentions of the automated system. A continuous communication between both human and system should be present, where this information is continuously provided in both directions. This communication can be attained by using haptic shared control (HSC), a control strategy which uses the interaction on a physical surface – such as a gas pedal or steering wheel – to determine the input to the controlled system (Mulder et al., 2012).

Since haptic shared control is a rather broad term, multiple implementation methods exist which differ in their control architecture. This section discusses two methods previously implemented at the Delft University of Technology: the Meshed Controller and the Four-Design-Choice-Architecture. Both controllers use the steering wheel as haptic surface. To ensure a neutral perspective, some other steering wheel implementation strategies by other researchers are also investigated as starting point in this research.

2.1.1. Meshed Controller

The Meshed Controller – depicted in Figure 2.1 – is an older version of a haptic shared controller (Mulder et al., 2008). It is mainly characterised by the generation of haptic feedback that is lumped to the driver model. This implies that the trajectory generation is inextricably connected to the formation of haptic feedback. As can be seen in Figure 2.1, the controller is programmed to follow the road centerline as trajectory reference and uses both position $(X_{car}(t), Y_{car}(t))$ and heading $\Psi_{car}(t)$ at a look-ahead time t_{LH} to estimate a feedback torque $T_M(t)$. A common value for t_{LH} is 0.7 seconds (Mulder et al., 2008). Note that this approach assumes that the driver will not change the steering angle in the look-ahead time. The exact calculation is made by

36 2. Literature Survey

comparing the predicted position and heading of the car at look-ahead time t_{LH} , $(\hat{X}_{car}(t+t_{LH}), \hat{Y}_{car}(t+t_{LH}))$ and $\hat{\Psi}_{car}(t+t_{LH})$, with the reference position and heading based of the road centerline, $(X_R(t+t_LH), Y_R(t+t_LH))$. At last, the result of the comparison – the error in lateral position Δs_{lat} and heading $\Delta \Psi$ – are multiplied with gains D and P respectively, added together and weighted by the feedback gain K_f to obtain $T_M(t)$.

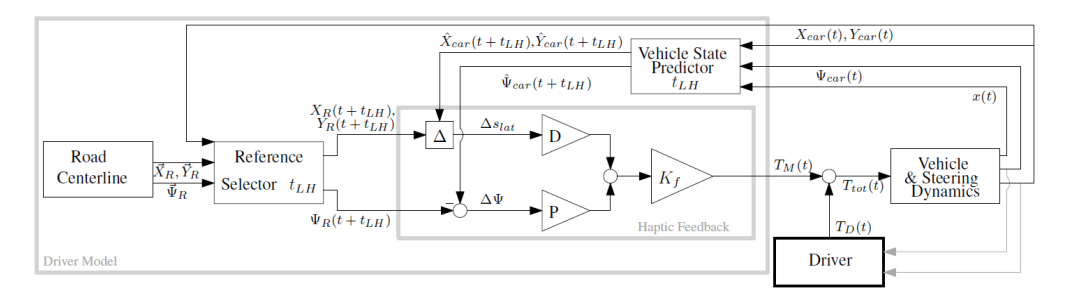


Figure 2.1: The Meshed Haptic Shared Controller (Scholtens et al., 2018).

Earlier research on haptic shared control has shown promising results. It is found that the Meshed Controller boosts curve negotiation performance and reduces control activity for the driver (Mulder et al., 2008). This implies both a lower diversion from the centerline and a reduced standard deviation of steering wheel angle (Mulder et al., 2008, 2012). However, research also shows an increase in control effort, indicating that the driver uses a larger variance of forces to drive through a curve (Mulder et al., 2008). It is theorised that this is the direct results of drivers actively resisting the feedback in case of disagreement, but using smaller forces when they agree with the feedback (Mulder et al., 2012). Furthermore, two major limitations of the Meshed Controller have been identified. First, there is the use of the centerline as reference and secondly, the one-size-fits all implementation (Boink et al., 2014, Mulder et al., 2008, 2012, Scholtens et al., 2018). These limitations are identified since all drivers have an individual driver style and an individual preference on how to drive through a curve. An ideal controller thus incorporates this preference, as a centerline trajectory might not be favoured by everyone.

2.1.2. Four-Design-Choice Architecture

The feedback torques of the Meshed Controller provide the driver with behaviour correcting torques. If the driver deviates from the intended path of the automation, the driver will feel an increasing force, making it harder to follow his/her desired trajectory. The Four-Design-Choice Architecture (FDCA) on the other hand also includes these feedback torques, but also adds feedforward torques. This control architecture – proposed by van Paassen et al. (2017) – not only corrects deviations from the reference trajectory, but also guides the driver through curves. It anticipates the upcoming curve based on a modelled reference trajectory, while the Meshed Controller does this using predicted states. The Four-Design-Choice (FDC) controller is depicted in Figure 2.2. It becomes immediately clear that in contrast to the Meshed Controller, all feedback and feedforward loops are separated from the driver model, making the model easier to control and the results easier to examine. However a big parallel can be seen in the similar feedback blocks of the FDCA and the Meshed Controller, where the only difference is that the FDCA feedback acts on the current error t and the Meshed Controller acts on predicted error $t + t_{LH}$.

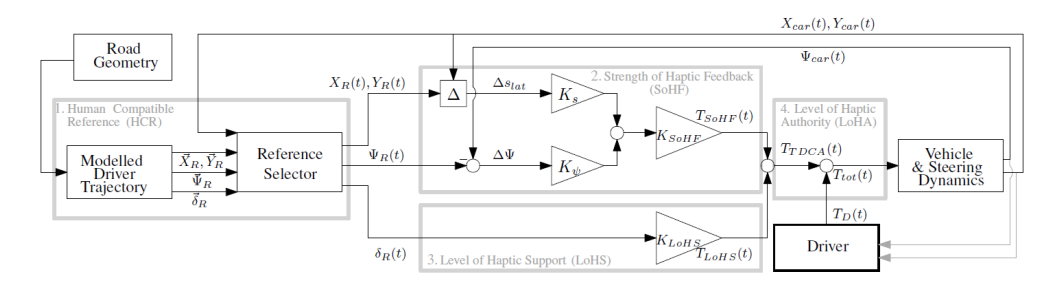


Figure 2.2: The Four-Design-Choice Haptic Shared Controller (Scholtens et al., 2018).

The FDCA roughly consists of four parts:

1. Human Compatible Reference (HCR): The HCR is comparable to the centerline of the Meshed Controller; It represents the path the controller intends to follow. However, the HCR is able to take on many forms and is therefore not limited to only the centerline trajectory (van Paassen et al., 2017). The HCR is thus an important element in the personalisation of the control system as either a One-Size-Fits-All trajectory can be followed – such as the centerline trajectory – or complete individualisation can be reached by choosing an individual's preferred trajectory as reference path (van Paassen et al., 2017). The HCR can either be implemented in the form of a driver model or either by averaging manual trajectories and using the averaged data over the curve. A more in-depth discussion on the personalisation of the HCR is provided in Section 2.2. Often this implementation of the HCR is realised offline (Scholtens et al., 2018).

The output of the Modelled Driver Trajectory block equals the trajectory $(\overrightarrow{X_R}, \overrightarrow{Y_R})$, heading $\overrightarrow{\Psi_R}$ and steering angles $\overrightarrow{\delta_R}$ of the reference trajectory the HSC intends to follow. The Reference Selector block then selects the index of the point in the reference trajectory that is currently closest in distance to the car's position $(X_{car}(t), Y_{car}(t))$ and outputs the corresponding position $(X_R(t), Y_R(t))$ and heading $\Psi_R(t)$ to the feedback loop and the steering angle $\delta_R(t)$ to the feedforward loop (Scholtens et al., 2018).

2. Strength of Haptic Feedback (SoHF): The SoHF determines the strength by which the control system corrects the driver if the vehicle is deviating from the reference path (van Paassen et al., 2017). The SoHF uses the HCR position ($X_R(t)$, $Y_R(t)$) and heading $\Psi_R(t)$ as input and compares them to the car's current position ($X_{car}(t)$, $Y_{car}(t)$) and heading $\Psi_{car}(t)$. This comparison consists of calculating the Euclidean distance, Δ , between the HCR's desired position and the vehicle's current position, which results in the error in lateral position Δs_{lat} (Scholtens et al., 2018). The exact calculation of Euclidean distance is given by Equation (2.1) (Scholtens et al., 2018).

$$\Delta s_{lat} = \sqrt{(X_R(t) - X_{car}(t))^2 + (Y_R(t) - Y_{car}(t))^2}$$
 (2.1)

The difference between the desired and actual heading is also computed, resulting in $\Delta\Psi$. Both Δs_{lat} and $\Delta\Psi$ are subsequently weighted by K_s and K_{Ψ} , respectively, after which they are added together and multiplied by gain K_{SoHF} to obtain the output of the SoHF block, the feedback torque $T_{SoHF}(t)$.

3. Level of Haptic Support (LoHS): The LoHS regulates how much the control system steers the vehicle in the reference direction (van Paassen et al., 2017). Even when the car follows the reference trajectory and the feedback torque $T_{SoHF}(t)$ becomes zero, the feedforward torque $T_{LoHS}(t)$ is still giving guidance to the driver due to its open loop properties (Scholtens et al., 2018). It is important to note that the balance between SoHF and LoHS greatly influences the driver's experience of the FDCA and must thus also be tuned (van Paassen et al., 2017).

The LoHS uses the steering angle $\delta_R(t)$ of the HCR as input and multiplies this variable with gain K_{LoHS} to obtain the feedforward torque $T_{LoHS}(t)$. Furthermore it must be noted that the multiplication of a steering wheel angle with a gain to achieve a torque is a simplification that is only valid for low-frequency angles. For correct approximations at both low and high frequencies, the steering torque must be computed using a rotational mass-spring-damper system.

4. Level of Haptic Authority (LoHA): The LoHA regulates the balance between the steering wheel input of the human and the steering wheel input of the automation (van Paassen et al., 2017). If the LoHA is high, it means that the haptic support is more difficult to override for the driver which is felt by the driver as a stiffness around the optimal steering angle.

The Four-Design-Choice-Architecture has been analysed and compared to the Meshed Controller in an experiment conducted by Scholtens et al. (2018). The experiment – performed by sixteen younger adults, ages ranging from 23 to 28 – consisted of driving with a fixed speed of 24 m/s and taking 5 left and 5 right turns. The test drive is repeated three times: once with manual driving, once using the Meshed Controller and once using the new Four-Design-Choice Controller. For each participant the HCR of the FDCA was personalised by adapting a driver model to fit the driver based on previously obtained manual driving data of that specific test subject (Scholtens et al., 2018).

38 2. Literature Survey

The results of the experiment show that the FDC controller reduces conflicts – events in which the driver must fight the automation as he/she does not agree (Scholtens et al., 2018) – by a factor 2.3 compared to the Meshed Controller. A reduction of conflicts indicates an increase of acceptance for the Four-Design-Choice-Architecture. Furthermore, the FDC controller also reduces driver torque by a factor 3.2 for left curves and by a factor 2.8 for right curves. This difference between directions might be clarified by the initial offset before a left turn, which builds trust and causes the driver to follow the HCR trajectory (Scholtens et al., 2018). Despite it was being hypothesised, the subjective usefulness and satisfaction showed no significant difference between manual driving, Meshed Controller and Four-Design-Choice Controller (Scholtens et al., 2018).

Scholtens et al. (2018) conclude that the reduced amount of conflicts and the reduced driver torque induced by the FDCA originate from an increased acceptance. Since the feedback torques of the FDC Controller closely resembles the feedback torques of the Meshed Controller, it is concluded that the feedforward torque causes the raise in acceptance.

2.1.3. Other Control Strategies

Needless to say, there exist more strategies for the implementation of a haptic shared controller than the two control methods described previously. An example of a different control strategy is realised by Saleh et al. (2013). In this research an H2-preview control system is implemented that uses the road curvature – assumed to be represented by coloured noise – as system input. The controller calculates both an anticipation and pre-compensation term. The anticipation term reacts on the previewed curvature up to the preview horizon, while the pre-compensation term handles the predicted road curvature after the preview horizon. An experiment has shown that the controller improves lane-keeping performance, but was only tested by one participant.

A second example is the controller designed by Pano et al. (2019). This control strategy is to a high degree similar to the Four-Design-Choice-Architecture, since it also utilises a feedback and feedforward loop to aid the driver. However, some differences exist between both controllers, of which the two following are the most apparent: the first main difference includes the reference trajectory, which in this case also covers a steering torque. This steering torque is then multiplied with the level of sharing – similar to the FDCA's LoHA – before being added with the feedback torque. The second main difference is to be found in the feedback loop. An H_2/H_∞ feedback controller is designed which calculates and acts on the difference between the real vehicle state and the reference state. Again, this feedback is separately combined with a level of sharing (Pano et al., 2019) This controller has thus far only been tested in simulations. Results from experiments are still missing.

2.1.4. Conclusion

The implementation and control strategy behind the haptic shared control is crucial to achieve good cooperation between human and automation. While multiple types of controllers exist, earlier types only apply feedback torques to correct the driver, while the newer controllers combine these torques with feedforward torques. This gives the driver a more positive sense of guidance. In particular the Four-Design-Choice-Architecture stands out due to its ability to adapt to the driver with the personalisation of the reference trajectory and the guiding haptic support that increases acceptance of the automation (Scholtens et al., 2018). It is therefore decided to exclusively use the FDCA in this research. Consequently, the next step consists of investigating personalisation possibilities.

2.2. Personalisation Types

The Four-Design-Choice-Architecture allows for several types of personalisation. The options include changing the Level of Haptic Authority, the ratio between the Haptic Feedback and the Haptic Support and the reference trajectory included in the Human Compatible Reference. For a better perspective on how these adjustments change the controller, Figure 2.3 is provided.

2.2.1. Level of Haptic Authority

The higher the LoHA of an FDC controller is, the more authority the automation has over the output torque of the HSC system on the vehicle compared to the driver (van Paassen et al., 2017). Nevertheless, a high LoHA does not equal an autonomous system. Abbink et al. (2012) argue that LoHA illustrates the persuasiveness of the automation as the system is designed to keep the driver in charge at all times. High LoHA might thus

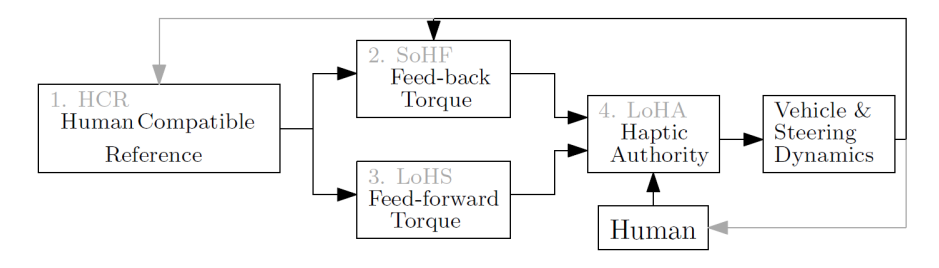


Figure 2.3: A simplified representation of the FDCA (Scholtens et al., 2018).

lead to confusion to the driver about who is actually in charge. Drivers actually prefer to remain in charge of the vehicle and therefore prefer a low LoHA over a high one (Mars et al., 2014). This despite a higher LoHA being more inherently safe (Mulder et al., 2012). In addition, increased authority does not necessarily lead to a better overall performance of the HSC system. The best interaction between human and automation is found for relatively low values of LoHA, since from a certain threshold onwards no additional significant benefit can be found (Boink et al., 2014).

2.2.2. Ratio Haptic Feedback & Haptic Support

The ratio between Haptic Feedback and Haptic Support greatly affects how the driver perceives the haptic shared control (Scholtens et al., 2018). If only feedback is present, the driver will only feel correcting torques, continuously pushing the driver back to the reference trajectory. If only support is present, the driver will sense a guidance, but if he/she decides to not follow this guidance, no correcting torques are present (Scholtens et al., 2018). The gains K_{SoHF} and K_{LoHS} , respectively, determine the importance of the Haptic Feedback and Haptic Support.

2.2.3. Human Compatible Reference

The Human Compatible Reference definitely allows for the greatest degree of personalisation as it defines which trajectory the automation will attempt to follow. Using the road geometry as input, the HCR outputs a reference position, heading and steering angle (van Paassen et al., 2017). There roughly exist two approaches to model the reference trajectory of the HCR: using a driver model or using a generic reference.

· Driver Model:

A driver model tries to represent and thus explicably mimic the driving task as if it is performed by a human driver. A good example of a driver model that focuses on lane keeping control is developed by Saleh et al. (2011). The model – depicted in Figure 2.4 – includes the three functional abilities drivers use when driving: cognitive, perceptual and motor skills.

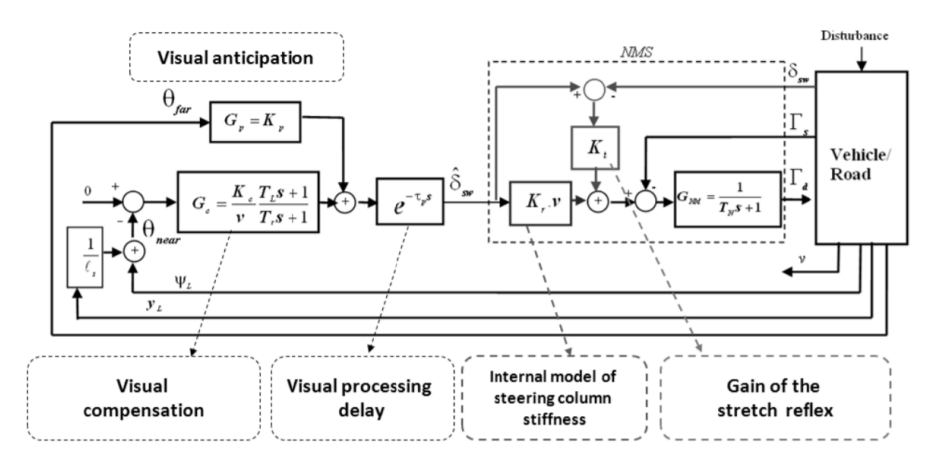


Figure 2.4: Driver model designed by Saleh et al. (2011).

The model in Figure 2.4 consists of "compensation" and "anticipation" blocks. The compensatory part compares the desired vehicle state to the predicted state the vehicle would achieve if the current steer-

40 2. Literature Survey

ing activity would continue. The anticipatory part determines how the driver steers the car depending on the road curvature. In order to make these two parts work, the driver uses both a near and far point on the road for guidance. First, the near point θ_{near} is used by the driver to follow the centerline of the road, while the far angle is used to negotiate the upcoming road curvature (Saleh et al., 2011). The far angle acts upon the angle between the car heading and the tangent point. The angles and points are shown in Figure 2.5.

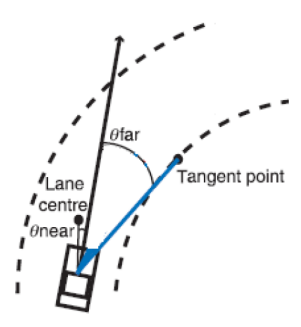


Figure 2.5: Depiction of the near and far angles together with the tangent point (Saleh et al., 2011).

Then, as the human driver's actions are nonlinear, a time delay is included in the driver model. This time delay mimics the delayed reaction to stimuli by the driver. At last, the desired steering wheel angle $\hat{\delta}_{sw}$ is passed on to the neuromuscular system (NMS) and translated into the desired steering torque Γ_d that is subsequently applied to the steering wheel (Saleh et al., 2011). Table 2.1 gives a more complete overview on all used parameters in the driver model and includes the most common values.

Element	Parameter	Value	Function
$G_p = K_p$	K_p	$K_p = 3.4$ (default) $K_p \in [2,5]$	Anticipation gain
	$\frac{K_c}{v}$	$K_c = 15$ (default) $K_p \in [5,30]$	Compensation gain
$G_c = \frac{K_c}{v} \frac{T_L s + 1}{T_l s + 1}$ v = vehicle speed	T_l	$T_l = 1$ (default) $T_l \in [0.5,2]$	Compensation frequency band
	T_L	$T_L = 3$ (default) $T_L \in [2,5]$	Compensation rate
$e^{-\tau_p s} = \frac{1 - 0.5\tau_p s}{1 + 0.5\tau_p s}$	τ_p	$\tau_p = 0.04 \text{ (default)}$ $\tau_p \in [0,0.1]$	Time delay
$K_r \cdot v$	K_r	$K_r = 1$ (default) $K_r \in [0.5, 1.5]$	Angle to torque coefficient
K_t	K_t	$K_t = 12$ (default) $K_t \in [0,\infty]$	Driver steering wheel holding stiffness
$G_{NM} = \frac{1}{T_N s + 1}$	T_N	$T_N = 0.1$ (default)	Neuromuscular time constant

Table 2.1: Overview of all parameters and their value ranges, based on Saleh et al. (2011).

Driver models offer a good mathematical method to imitate human behaviour and are therefore a suitable choice for the generation of the HCR. Driver models are to a great extent customisable, indicating that every driver can be approximated by a certain set of parameters. Each individual can be estimated by a driver model. It is decided that for all further use of a driver model in this research, the model designed by Saleh et al. (2011) will be used.

It is important, however, to also recognise the drawbacks and limitations of this specific choice. The first major drawback of this driver model is finding the correct set of parameters for each individual. This is often computationally extensive and might lead to some difficulties. A second weakness of the

driver model is that it is not generalisable to all situations. These models often mimic a certain situation or behaviour rather well, which in this case is negotiating a curve, but behave poorly outside these constraints. The last drawback is related to the driver model not including preview. The far angle uses current curvature as input and therefore, when a curve is detected, the input goes through the second order vehicle dynamics, resulting in a 180 degree lag. This is further elaborated on by Equation (4.4), where the implementation of this model is explained.

• Generic Reference:

The second method of HCR generation is by the creation of a generic reference. This method is less computationally expensive, but it calls for more available knowledge of the designated situation. These manual trials are then averaged. The average is taken to be the HCR (Vreugdenhil et al., 2019). An example of the generation of the generic reference is depicted in Figure 2.6. The study by Vreugdenhil et al. (2019) seeks a generic reference for both critical and non-critical avoidance situations. The car in this example is supposed to swerve around an object located on the road. The mean of multiple manual trials is then taken as the generic reference.

Not only are generic references computationally preferable, they are also able to capture the prepositioning of the car before a curve starts. This prepositioning phase is vital for an increased acceptance of the automation by the driver (Scholtens et al., 2018) and cannot be captured with the presented driver model by Saleh et al. (2011).

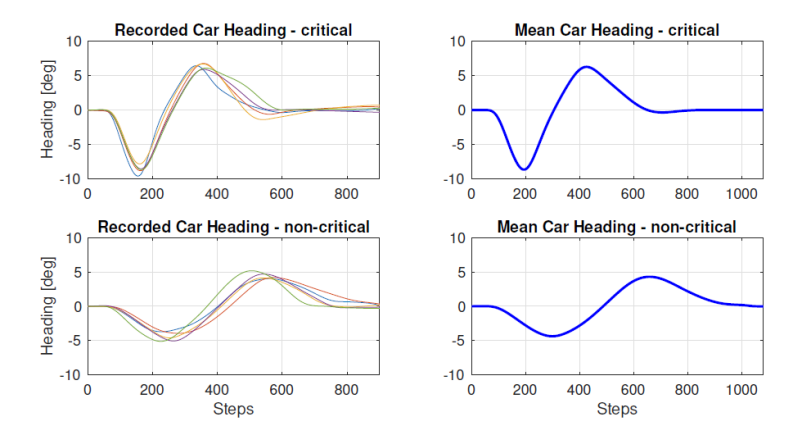


Figure 2.6: Example of manual trials and the resulting generic reference based on the mean, taken from Vreugdenhil et al. (2019).

2.2.4. Conclusion

As the Human Compatible Reference has the most direct influence on the personalisation of the haptic shared controller, it is decided that for this research only the HCR path will be varied, while keeping both the LoHA and SoHF/LoHS-ratio constant. In terms of the exact implementation of the HCR, both the driver model and the generic reference make convincing options. It is therefore chosen to focus on the generic reference for the experiment that follows from this research. This mainly due to the importance of the prepositioning. Prepositioning cannot be captured by current driver models, but is believed to be important for acceptance of the haptic shared control and the classification of driving patterns, such as researched by Barendswaard et al. (2019a). However, for preliminary simulations, it might be favourable to use a driver model as HCR implementation since no experimental data are needed, yet it helps to understand the control system better.

2.3. Driving Behaviour Classification

To reach the goal of increased personalisation, it must be investigated what shape to give the driver model or generic reference. As the HCR represents a predefined path, it must be investigated what path classification suits this research best. Previous research proves that several methods have already been developed. All strategies consist of classifying driver behaviour and matching each driver to a class. The approach behind these methods differ and each one has its own advantages and drawbacks.

42 2. Literature Survey

2.3.1. Normal vs. Aggressive Behaviour

Sundbom et al. (2013) distinguish two different driving styles: normal and aggressive behaviour. Aggressive behaviour is characterised by having higher accelerations in curves and a higher lateral movement compared to normal behaviour. A hybrid model – a model built on the assumption that drivers switch between driving styles – is used to online classify the driver into one of both modes based on the measurements of vehicle sensors. The paper concludes that the model manages to appropriately distinguish between both categories, however, the online prediction of class is only based on measured steering angle, which has been proven to not be suitable in capturing different driver steering behaviours (Barendswaard et al., 2018).

2.3.2. Track Path Classification

Another study, conducted by Spacek (2005), attempts at differentiating between six types of track paths along curves. These paths include among other ideal behaviour (following a centerline), drifting behaviour (an asymmetrical path where the driver starts out with a left inclination, but drifts towards the right side of the curve), and curve cutting behaviour. The intention to classify drivers based on trajectory shows a more objective approach than the normal/aggressive classification as drivers might show normal or aggressive behaviour depending on the traffic situation and this behaviour might thus not be inherent to a person. However this paper lacks quantifiers.

2.3.3. Trajectory Type Classification

Trajectory type classification aims at dividing drivers into one of seven classes based on their personal style of negotiating a curve. The seven classes are depicted in Figure 2.7. It can be seen that for each class the variation in lateral position s_{lat} is plotted over the length of the curve. To identify in which class a certain driver falls, a rule-based classifier is used. This classifier analyses the lateral position of the vehicle at curve-entry and the number of crossings over the road centerline band and places a driver into a class based on this information. Note that the centerline band is defined as being the centerline \pm 0.1 m. To illustrate the classifier, at curve-entry the vehicle is either on the inner or outer part of the curve and during the negotiation either 0, 1 or 2 transitions over the centerline band can be found (Barendswaard et al., 2019a). Table 2.2 gives a more in-depth overview on how all classes are identified.

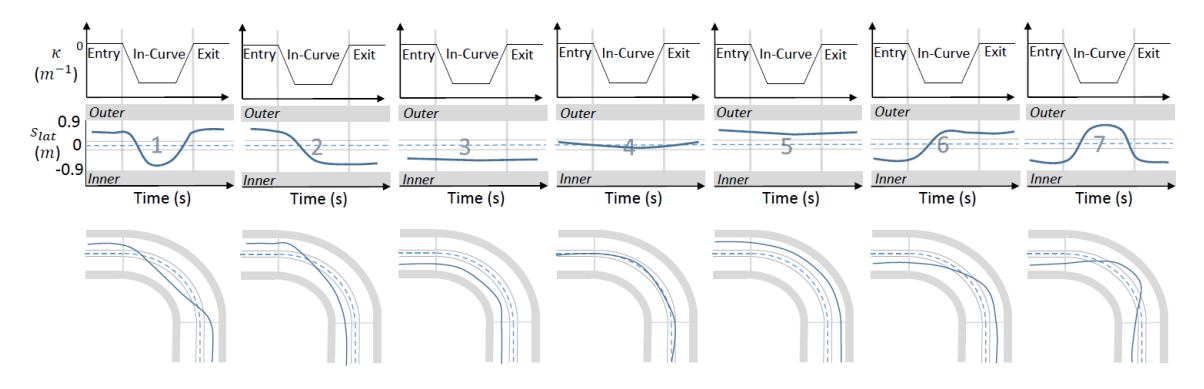


Figure 2.7: The seven identified rule-based classes, taken from Barendswaard et al. (2019a).

This trajectory type classification is based on a study conducted by Barendswaard et al. (2019a). A manual driving experiment was performed on 45 test subjects to determine the plausibility of these classes. It was found that drivers adapt their behaviour for left and right curves, most probably because of a right roadside bias due to the European driving convention. The results show that curve cutting (class 2) and biased inner curve negotiation (class 3) together are employed by 86% of the drivers in right curves, making them the most common classes. For left curves, biased outer curve negotiation (class 5) and curve cutting (class 2) are most prevailing, accounting for 69% of used classes. High levels of consistency were found over three different curve radii. 93% of drivers were found to be consistent for at least two out of three right curves, while 84% are consistent for at least two out of three left curves (Barendswaard et al., 2019a). This implies a high generalisability of the classes and a possible extrapolation to other research and other scenarios. Astonishingly, no drivers fit inside the fourth category, centerline driving. This is surprising as previous research is often based on the assumption that drivers follow the centerline (Aksjonov et al., 2018, Barendswaard et al., 2019a, Mars

2.4. Driver Grouping 43

Class	Description	Curve-Entry	In-Curve Transitions
1	Severe curve cutting	Outer	2
2	Curve cutting	Outer	1
3	Biased inner curve negotiation	Inner	0
4	Centerline driving	Centerline ± 0.1 m	0
5	Biased outer curve negotiation	Outer	0
6	Counter curve cutting	Inner	1
7	Severe counter curve cutting	Inner	2

Table 2.2: Overview of rule-based classes and identifiers, based on Barendswaard et al. (2019a).

et al., 2011, van der El et al., 2019). An example is the meshed controller, which makes the driver follow the centerline as reference trajectory.

2.3.4. Conclusion

Due to the promising results of the well-substantiated trajectory classification, it is decided to continue with this approach for the personalisation of the HCR. It should be remarked that the study by Barendswaard et al. (2019a) only encompasses a manual driving experiment. These trajectories have not served purpose before as Human Compatible Reference. To fit the classes into the HCR, generic references should be used as these are able to easily capture the prepositioning of some of the classes.

2.4. Driver Grouping

When designing an experiment, it is important to select a suitable representative sample of the population of interest. There is an interaction between the topic at investigation and the selection of participants, especially if the research question has not been defined yet. Most research on haptic shared control up to now has investigated the relation between automation and younger people. Examples include the experiments by Boink et al. (2014), Scholtens et al. (2018) and Barendswaard et al. (2019a). Younger people are easily accessible and have a larger mobility and thus make easy participants in an experiment. However, society is ageing. It is estimated that the percentage of people older than 65 in Europe will have risen from 18% currently to 24% by 2040 (Polders et al., 2015). Worldwide this proportion is predicted to increase from 7% currently to 14% by 2030 (Newman and Cauley, 2012). It has been extensively documented that elderly drivers suffer from the deterioration of their sensory, cognitive and psychomotor abilities (Eby et al., 1998, Furlan et al., 2018, Molnar et al., 2013) and are therefore more prone to being involved in car crashes, which raised the question if they should be more involved in experiments on driving.

2.4.1. Driving Habits of the Elderly

Older adults face many age-related changes that affect their driving behaviour. First, there is sensory degradation. Sensory degradation includes amongst other things the decline of visual perception, caused by anatomical changes of the eye, worse visual acuity and the shrinkage of the visual field (Eby et al., 1998). Secondly, there is the decline in cognitive abilities, which comprises of a reduced attention span, decreased ability to problem solving and weakened spatial cognition (Eby et al., 1998). Thirdly, the decrease of psychomotor abilites leads to slower reaction times (Eby et al., 1998) and a poorer eye-hand coordination (Büskens et al., 2012). Often these disadvantages are accompanied by the use of medications and other medical conditions such as heart problems or dementia. This results in elderly drivers being accountable for the highest rate of crashes per distance driven (Eby et al., 1998).

Despite all these deficiencies, older adults can still be found driving cars in large numbers. This as driving provides people with a sense of freedom and no one enjoys being restricted. It is therefore surprising that despite having the highest rate of crashes per distance driven, elderly drivers are less involved in crashes in absolute numbers and commit less violations than any other age group (Eby et al., 1998). This is the direct result of the elderly – being fully aware of their limitations – modifying and adjusting their driving behaviour

44 2. Literature Survey

and patterns in order to be more safe. In this process, often referred to as self-regulation, drivers will try to drive less or avoid situations which they acknowledge to be demanding (Molnar et al., 2013). Examples include maintaining a greater following distance (Molnar et al., 2013, Strayer and Drews, 2004), having larger decision times (Middleton et al., 2005, Molnar et al., 2013) and avoiding driving during rush hour traffic, at night or in bad weather conditions. Note that having driving preferences does not equal self-regulation as these can be found for younger drivers as well (Molnar et al., 2013).

Despite the self-regulation, elderly drivers still pose a threat to others and themselves on the road. As Advanced Driver Assistance Systems (ADAS) are becoming increasingly meaningful and intelligent, they have the potential to counteract the performance limitations inherent to older adults. However, these systems will only be beneficial if the elderly are willing to use them.

2.4.2. Different Effects of ADAS

Advanced Driving Assistance Systems are assistance systems capable of increasing safety and comfort for the driver. Needless to say, the use and trust in ADAS highly depend on the acceptance of the system by the driver. The acceptance of assistance systems is an essential requirement for its use and is defined by Adell (2009) as "the degree to which an individual intends to use a system and, when available, to incorporate the system in his/her driving" (p. 31). It is assumed that older drivers have a lower initial acceptance towards ADAS than younger adults as they are less likely to use technology in general (Czaja et al., 2006). It has, however, not yet been researched how acceptance of ADAS varies over age and how to optimise this acceptance for different age categories.

It is evident that young adults are aware of the existence of assistance systems and are willing to use them. More surprising is the relatively high level of awareness about ADAS by the elderly. They mostly learn about the systems through acquaintances or the press. Despite the high level of awareness, the level of practice or ownership is still low. This can be attributed to the perceived lack of usefulness of assistance systems by older adults. They feel like either their driving skills are good enough manually or they do not see a situation in which ADAS would be helpful (Trübswetter and Bengler, 2013). This might also further indicate a lack of acceptance of ADAS, a problem less likely to be found in younger adults.

2.4.3. Gender And Age

Since not only age, but also gender is a variable which might influence the outcome of an experiment, some information is gathered on the topic and two hypotheses are formed.

Most research on haptic shared control does not seem to differentiate between men and women. Examples of such studies where both men and women participate, but no distinction is made between the respective outcomes of the experiment include experiments by Mulder and Abbink (2010) and Vreugdenhil et al. (2019). Therefore, it is not immediately clear if differences in gender are present when using haptic shared control. Nevertheless, a recent study by Pano et al. (2019) tests a new haptic shared controller by having one man and one woman using the system. They note clear differences between the male and female participant, however, these results do not seem to be representative as these differences could also be attributed to different individual driving styles. As only two people partake in the experiment, these results are inconclusive on gender differences.

In terms of manual driving, risky driving styles are linked to increased masculinity, while safety skills are linked to increased femininity. Masculinity and femininity, however, are gender roles which show no significant relation with biological gender or sex (Özkan and Lajunen, 2006), indicating that both sexes have both masculine and feminine characteristics. This demonstrates that no noticeable difference in driving behaviour is found for men or women. This, however, only holds true for young people (Özkan and Lajunen, 2006). The elderly do show differences in driving patterns based on gender. Men older than 65 years old tend to drive longer than they are safely able to, while women limit their driving and rely on others much earlier, even when they are still healthy (Barrett et al., 2018). This means the influence of haptic shared control systems on older men and women can be significant and may help both oin a different way. The driving safety of men will greatly incease and women on the other hand will regain some of their freedom.

Previous research by Delft University of Technology on haptic shared control on both young and old drivers did not show any large differences between both age groups (Mulder and Abbink, 2010, Mulder et al., 2008), however, the mean age of the older test group was only 58 years old. For a better understanding of agerelated changes, it is more beneficial to use people who are at least older than 65 as this age group is growing

2.5. Method Trade-off 45

very fast (Newman and Cauley, 2012, Polders et al., 2015) and the effects of ageing are more obvious in them. Their reaction to haptic shared control will differ from 58 year olds as HSC will more influence their lives.

2.4.4. Conclusion

In conclusion, ADAS are capable of helping both younger and elderly adults in increasing safety and comfort in their driving experience as long as their acceptance of the system is optimised. This optimisation might differ between both age groups as they have different needs and deficiencies, however for ADAS this has not been examined yet.

In terms of experiment variables, it is firstly hypothesised that for young people, gender does not matter as gender does not seem to be related to gender roles. For older people, however, both genders should be considered as the effect of haptic shared control on their driving behaviour and patterns could be larger. Secondly, it is hypothesised that people from different age groups will have different preferences and distinctive levels of acceptance for haptic shared control. Due to their self-regulating behaviour, it can be assumed that older people drive slower in curves. This reduces their need to lower lateral acceleration and thus to cut curves. It is thus hypothesised that older people will often fall into one of the middle classes: class 3, 4 or 5. To add to this, assuming that they are more cautious, they would want to decrease their perceived risk when negotiating a curve, which is possible by minimising the lateral displacement s_{lat} .

The outcome of this section suggests that including age in the experiment also means including gender to guarantee a complete picture of society.

2.5. Method Trade-off

This section summarises the findings of the past chapter. All information gathered is crucial in making the correct design choices for an experiment concerning haptic shared control. Table 2.3 presents all possible design choices discussed earlier and argues which design choice is most optimal.

			Τ
Table 2.3: Conclu	ısion and summary of all design o	choices made, resulting from	n the antecedent chapter.

Design Choice	Positive argument	Negative argument
Meshed Controller	Simple implementation	Centerline as reference trajectory One-size-fits-all approach Lumped components
Four-Design-Choice-Architecture	Personalisation possible Components not lumped	Complex implementation
Driver Model by Saleh et al. (2011)	Individualisable	Not generalisable for all scenarios Multiple parameters No preview
Generic Reference	Prepositioning possible	Manual experiments needed
Normal/Aggressive Behaviour	Easy classification	Based on steering angle Behaviour might change by circumstances
Rule-Based Trajectory Classification	Objective rule-based classification with numerical quantification	No previous experiments on haptic shared control
Young participants	Limited amount of experiment parameters Never researched before in relation to trajectory types	Does not give a full picture of society
Young and older participants	Never researched before in relation to HSC	Too many experiment variables

At last, two remarks must be made. Firstly, the trajectory followed by drivers when negotiating a curve is either conscious or unconscious. Curve cutting is an example of a conscious trajectory, as the driver has a clear intention when entering the curve. An unconscious trajectory occurs due to a lack of information,

2. Literature Survey

which forces the driver to act different than intended (Yuan-Yuan et al., 2012). Since these unconscious trajectories could greatly influence the results of the experiment, it should be ensured that all information is clearly available to the driver. This can be achieved by providing clear, bright graphics to the driver, to ensure that the entire curve is clearly visible. Secondly, the experiment will be performed in a simulator. Simulators lack the ability to replicate a physical sense of lateral acceleration, so the operator's vestibular senses will not be affected while driving (Boer, 1996). It is expected that this influences the results and reduces realism.

Research Objective and Questions

From the literature survey it is concluded that in order to maximise the usage and trust in driver assistance systems – of which haptic shared control is an example – the objective and subjective acceptance of the driver in the system must be optimised as well. The latest developments concerning haptic shared control introduce the Four-Design-Choice-Architecture and trajectory-type classification. Both show great promise to increase the acceptance of the human driver, however, both alternatives have never been combined before and their absolute potential is unknown. Each driver's manual driving style is assumed to fall into one of the seven predefined classes, nonetheless, it has never been researched before how such a driver reacts if the Human Compatible Reference of the FDCA falls into the same class. Or, how a driver with a certain manual driving style class reacts to a HCR of a different class. Therefore, the current research objective is defined as follows:

To understand what level of individualisation in trajectory-driven haptic shared control results in the highest acceptance by comparing both the objective and subjective responses of different types of drivers to the different reference trajectories.

This research objective leads to a series of research questions that need to be investigated. The main research question is defined as:

How does trajectory type affect driver's acceptance in trajectory-driven haptic shared control?

Answering such a broad research question is never easy. Therefore some sub-questions are presented, which should be answered first in order to help answering the main research question. These sub-questions come in five different categories. Also, per sub-question an indication is given on which evaluation criteria to use.

- 1. Regarding manual driving style:
 - (a) What is the consistency of driving classes within each driver?
 - (b) What is the correlation between left and right curve negotiation classes per driver?
- 2. Regarding collaborative driving performance:
 - (a) How accurately does the driver follow the guidance of the Human Compatible Reference?

 <u>Criteria to check:</u> Error to HCR, lateral position and lateral acceleration. To understand how accurately the driver follows the trajectory of the HSC, the lateral error and closed loop steering wheel error must be considered. To gain more insight in the collaboration between HCR and driver, the lateral position measured from the centerline to the center of the car and lateral acceleration must be recorded. These two variables also allow for tracking of changes in driving behaviour over the changing conditions.
 - (b) How safe is the trajectory followed by the driver combined with the Human Compatible Reference?
 - <u>Criterion to check:</u> Time-to-Lane Crossing (TLC). TLC indicates the time before the vehicle reaches the road boundaries in case a constant steering angle is maintained (Godthelp et al., 1984) and is perceived by the driver as a measure of risk (van Winsum et al., 2000). The larger the TLC, the more safe a trajectory is perceived.

- 3. Regarding the workload for the human driver:
 - (a) For which trajectory class is the workload minimised?

 <u>Criteria to check:</u> Steering Reversal Rate (SRR) and Absolute Driver Torque. Both variables allow for an objective measure of workload. SRR is defined as being the amount of times the steering wheel direction is reversed by more than 2° (Macdonald and Hoffmann, 1980). The Absolute Driver Torque represents the total torque on the steering wheel applied by the driver. It represents the driver's physical effort (Scholtens et al., 2018).
- 4. Regarding objective and subjective acceptance of the haptic shared control:
 - (a) For what type of curve negotiating trajectory is the amount of conflicts minimised?

 <u>Criterion to check:</u> Number of Conflicting Torques. A conflict is said to occur when the driver and automation exert torques in opposite directions. No conflicts are present when driver and automation exert torques in the same direction.
 - (b) When is the subjective satisfaction of the haptic shared control optimised?
 <u>Criterion to check:</u> Van der Laan questionnaire. Subjective usefulness and satisfaction can be measured using a Van der Laan questionnaire, which needs to be filled out by all participants (van der Laan et al., 1997).
- 5. Regarding consistency over the different experiment trials:
 - (a) Is the reaction of an individual driver to the different types of curve negotiating trajectories consistent over the different trials?
 - (b) Is there a generalisable relation noticeable between manual driving styles and curve negotiating trajectory preferences?

Preliminary Simulations

In order to gain a deeper understanding of the human driver and the Four-Design-Choice-Architecture, some preliminary computer simulations were performed. These simulations help gain some insight in the torques the drivers will express when driving with haptic shared control in a simulator. These torques could either be agreeing with the guidance or could be opposing, indicating a difference in intention. This chapter covers the structure and control systems behind the simulations, the results of the simulations, but also the verification, validation and discussion.

4.1. Simulation Setup

The simulations consist of two main parts that need to be programmed: the driver and the haptic shared controller. In Section 2.2, it has already been mentioned that a driver can be approximated using either a driver model or a generic reference. For the experiment, it has been opted to use a generic reference, mainly due to its capabilities of recreating the natural pre-positioning of the driver before a curve. However, to simplify the simulations and gain more insight in the information a driver uses to negotiate a curve, the simulations will run using a driver represented by a driver model. The setup of the haptic shared controller is kept identical to the setup that will be used in experiments, namely using the Four-Design-Choice-Architecture.

4.1.1. Driver Model

The driver model used in the simulations is based on the model developed by Saleh et al. (2013). This model combines a driver model directly with vehicle dynamics and eliminates the need for coordinate system transformations during calculations. The model is slightly altered before implementation as to not include the auto-aligning feedback loops, which include torque and steering wheel angle feedback (Saleh et al., 2013). These loops are a part of the haptic shared controller designed by Saleh et al. (2013) and are thus not purely driver model elements. The resulting model can be seen in Figure 4.1.

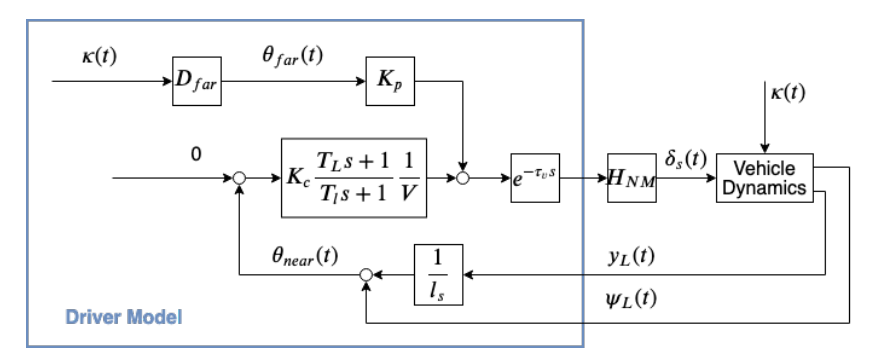
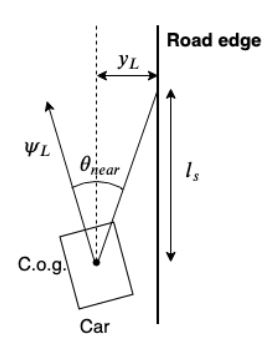


Figure 4.1: The simplified model that combines the driver and vehicle dynamics, based on Saleh et al. (2013).

The workings of the driver model are mainly based on the differentiation between an anticipatory and compensatory part. As explained in Section 2.2, the compensatory, closed loop is designed to follow the center of the road, while the anticipatory – or open loop – part determines how the driver steers based on current

road curvature $\kappa(t)$. In order to calculate the resulting steering angles of the compensatory and anticipatory parts, respectively, the near angle, $\theta_{near}(t)$, and far angle, $\theta_{far}(t)$, must be computed first. These calculations are simplified by making two assumptions: first of all, constant curvature is assumed throughout the curves. This does make the driver model less realistic for real roads, where curves are irregular and unpredictable. However, in case of a simulation, curves are often much simpler. Additionally, constant curvature leads to more precise conclusions as the data can be interpreted much easier. This in contrast to highly irregular curves. Second, small angles are assumed, meaning that all computations can be simplified. Note that this also implies that the simulations are only valid for very small angles, close to zero degrees. Putting these assumptions together, $\theta_{near}(t)$ is calculated from Figure 4.2. See Equation (4.1) for the full derivation.

$$\theta_{near} = \tan\left(\frac{y_L}{l_s}\right) + \psi_L = \frac{y_L}{l_s} + \psi_L \tag{4.1}$$



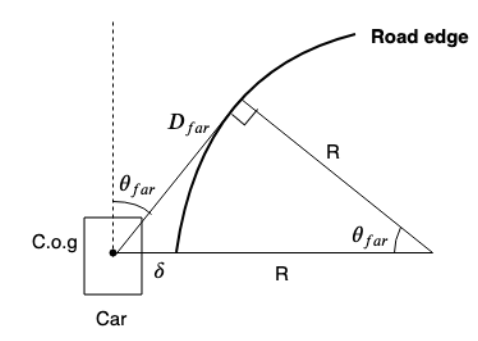


Figure 4.2: The calculation of the compensatory near angle, based Figure 4.3: The calculation of the anticipatory, tangent far angle, on Saleh et al. (2013).

Note that in both Figure 4.2 and 4.3, C.o.g. is the centre of gravity, R is the radius of the curve and δ equals the road width. This is followed by the computation of the far angle, which is a bit more complex. As can be found from Figure 4.3, the calculation of D_{far} is as follows:

$$(\delta + R)^2 = R^2 + D_{far}^2 (4.2)$$

$$D_{far} = \sqrt{\delta^2 + 2\delta R} \tag{4.3}$$

This then leads to Equation (4.4), which calculates θ_{far} .

$$\theta_{far} = \tan\left(\frac{D_{far}}{R}\right) = \kappa(t) \cdot D_{far}$$
 (4.4)

More information on the near and far angle and other variables from the driver model can be found in Section 2.2. Table 2.1 gives a description of all parameters and their feasible value interval. In the simulations, the default values are used for all parameters.

The ' H_{nm} '-block in Figure 4.1 represents the neuromuscular dynamics of the driver and is given by Equation (4.5) (Saleh et al., 2013). The near angle projection distance l_s , needed for the calculation of $\theta_{near}(t)$, has been given a constant value of 5 m, based on Saleh et al. (2013).

$$H_{nm} = \frac{1}{T_N s + 1} \tag{4.5}$$

At last, the 'Vehicle Dynamics' block contains a Linear Bicycle Model, which is again a simplification of the dynamics presented by Saleh et al. (2013). The model is represented using the state space system presented in Equations (4.6)–(4.12). The input to the system is the steering angle δ_s and curvature κ . The state vector consists of side slip angle β , yaw rate r, heading angle ψ_L and offset from the centerline γ_L (Saleh et al., 2013).

$$\begin{bmatrix} \beta \\ \dot{r} \\ \dot{\psi}_L \\ \dot{y}_L \end{bmatrix} = \begin{bmatrix} a_{11c} & a_{12c} & 0 & 0 \\ a_{21c} & a_{22c} & 0 & 0 \\ 0 & 1 & 0 & 0 \\ V_x & l_s & V_x & 0 \end{bmatrix} \begin{bmatrix} \beta \\ r \\ \psi_L \\ y_L \end{bmatrix} + \begin{bmatrix} 0 \\ 0 \\ -V_x \\ -l_s V_x \end{bmatrix} \kappa + \begin{bmatrix} a_{15c} \\ a_{25c} \\ 0 \\ 0 \end{bmatrix} \delta_s$$
 (4.6)

4.1. Simulation Setup 51

$$a_{11c} = -\frac{2(c_j + c_r)}{MV_x}$$
 (4.7)
$$a_{12c} = \frac{2(c_r l_r + c_f l_f)}{MV_x^2} - 1$$
 (4.8)
$$a_{15c} = \frac{2c_f}{MV_x R_s}$$
 (4.9)

$$a_{21c} = \frac{2(c_r l_r + c_f l_f)}{I}$$
 (4.10)
$$a_{22c} = \frac{2(c_r l_r^2 + c_f l_f^2)}{IV_x}$$
 (4.11)
$$a_{25c} = \frac{2c_f l_f}{IR_s}$$
 (4.12)

The parameters used in Equations (4.7)–(4.12) are explained in Table 4.1. Note that V_x represents the longitudinal velocity. This parameter has no fixed value and varies depending on trajectory, curve radius and objective of the simulation. Velocity is always expressed in m/s.

Parameter	Description	Value, dimension
$\overline{}_{l_f}$	Distance from center of gravity to front axle	1.127 m
l_r	Distance from center of gravity to rear axle	1.485 m
M	Total mass	1476 kg
J	Vehicle yaw moment of inertia	$1810 \ kg \cdot m^2$
c_f	Front cornering stiffness	$65000\ N/rad$
c_r	Rear cornering stiffness	57000 N/rad
R_s	Steering gear ratio	16

Table 4.1: Parameters used in the bicycle model, taken from Saleh et al. (2011).

It is important to repeat the major disadvantage of this driver model, which is the lack of preview. There is a look-ahead distance present in the model, but this one acts on current curvature information as shown by Equation (4.4). This means that before the curve starts, the model assumes an infinite straight road ahead. This clashes with reality in the sense that people preposition the car at around seven seconds before the curve and turn into the curve at 1 second to the curve (Barendswaard et al., 2019b). When the curve is finally detected by the model, the curvature input first goes through vehicle dynamics, which is a second order system and leads to a lag of 180 degrees.

4.1.2. Trajectory tuning

As the simulations should help understand the outcome of an experiment, it is essential that both simulations and experiment include the same – or similar – conditions. For the experiment, it has been decided to only implement one condition, namely a constant velocity of 80 km/h with a constant curve radius of 204 m (Barendswaard et al., 2019a). Therefore, the simulations use the same fixed speed and same clothoidal curves. More information about the reasoning behind this condition is given in Chapter 5.

Trajectory-type classification puts drivers into one of seven categories. The implemented driver model, however, has only limited capabilities to mimic these. It is therefore decided to design three variants of the driver model, each variant representing one of the seven classes. Despite the driver model lacking the ability to simulate pre-positioning behaviour before curves, the simulations do demonstrate how similar or opposing HCR-driver trajectories influence each other. The three variants of the driver model to be tested are: centerline driving (class 4), curve cutting (class 2) and counter curve cutting (class 6). In order to do so, the influence of K_p and K_c is investigated.

 K_p is the anticipation gain and thus influences the steering angle in relation to the curvature of the road. K_c on the other hand is the compensation gain, which is responsible for the following of the centerline of the road. In other words, a high K_p gives importance to following the curvature and will result in an extreme curve cutting trajectory, while a high K_c results in centerline driving behaviour. The effect of changing K_p can be seen in Figure 4.4, where a right curve is simulated. The lines in the lateral position s_{lat} -plot represent the trajectories of the centres of gravity of the vehicles when driving through the curve. The plot shows the entire width of the road (3.6 m) where the dashed line represents the centerline and the dotted lines indicates

the centerlineband, which equals the centerline \pm 0.1 m. The grey area in the figure represents the effective road boundaries, indicating that if the COG of the vehicle is located here, the vehicle (partially) leaves the road. From Figure 4.4, it can be noted that an increase in K_p increases the curve cutting behaviour of the driver, until the driver crosses the effective road boundary. The overshoot in steering angle that happens at the beginning of the curve is caused by the sudden increase of the far angle. Because of the rather short length of the curve, a steady-state solution is not reached and oscillations endure. The oscillations in the system actually worsen as K_p increases in value, which will lead to an unstable system in case K_p increases even more.

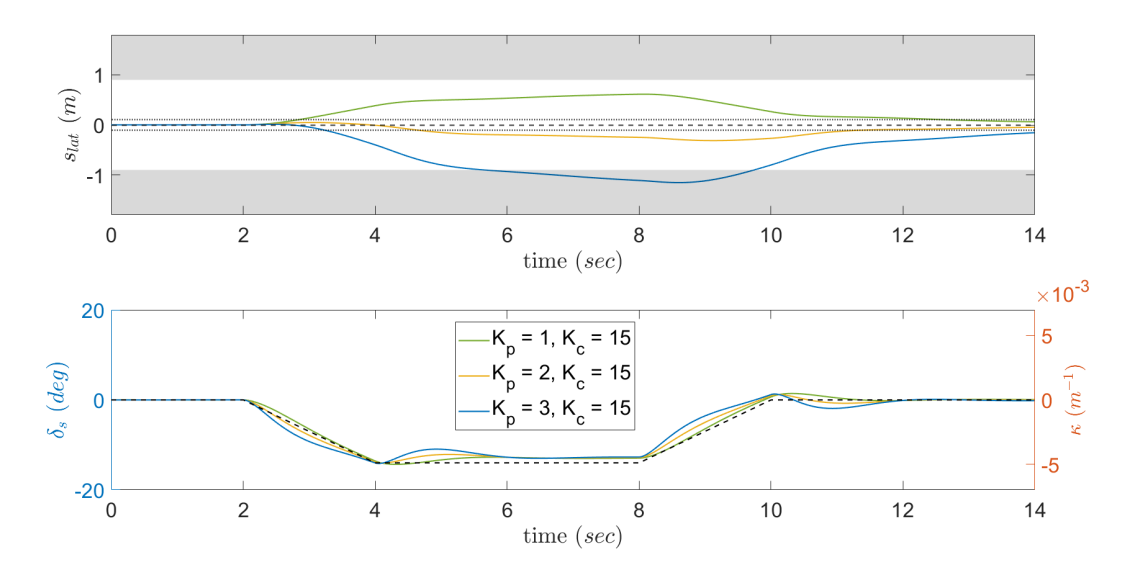


Figure 4.4: The effects of changing K_p on both lateral position and steering wheel angle.

On the other hand, the effects of changing K_c are different. Figure 4.5 shows how the lateral displacement of the vehicle continuously gets closer to the centerline as K_c increases. Despite the oscillations of high K_c being less than the oscillations caused by high K_p , they are visibly present. Once again, they are caused by the high gain value.

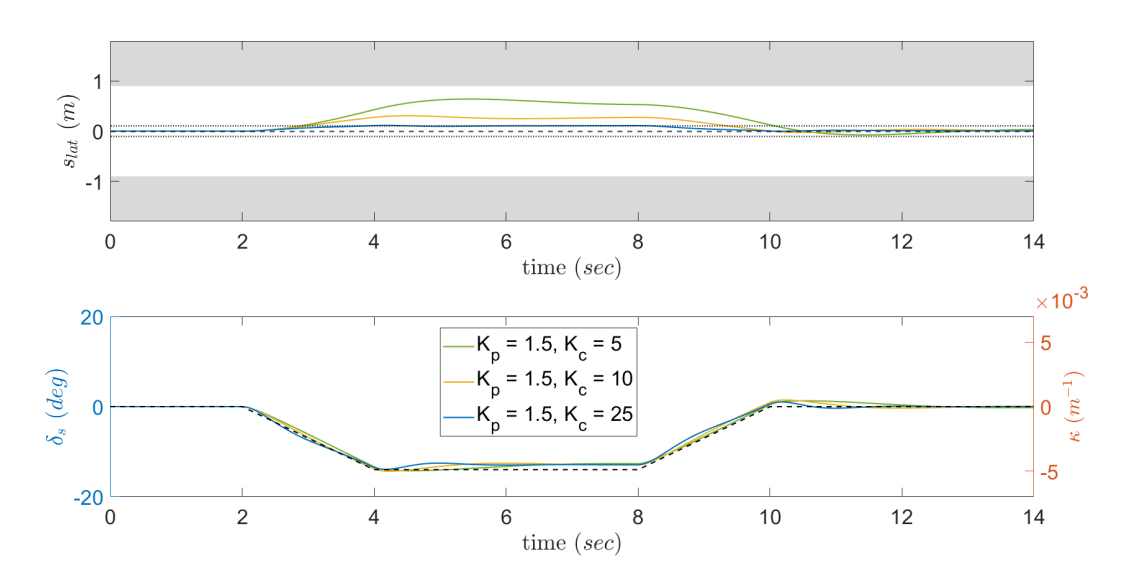


Figure 4.5: The effects of changing K_c on both lateral position and steering wheel angle.

At last, the correct combination of anticipation K_p and compensation K_c gains must be found for the three

4.1. Simulation Setup 53

defined scenarios: centerline driving, curve cutting and counter curve cutting. Based on the above described findings about the influence of increasing and/or decreasing K_p and K_c , the three optimal combinations are found. The results are presented in Table 4.2.

	K_p	K_c
Centerline driving (class 4)	1.7	28
Curve cutting (class 2)	2.7	15
Counter curve cutting (class 6)	1.4	5

Table 4.2: Different K_p and K_c combinations to reach the desired trajectory type.

The resulting behaviour of these combinations is shown in Figure 4.6.

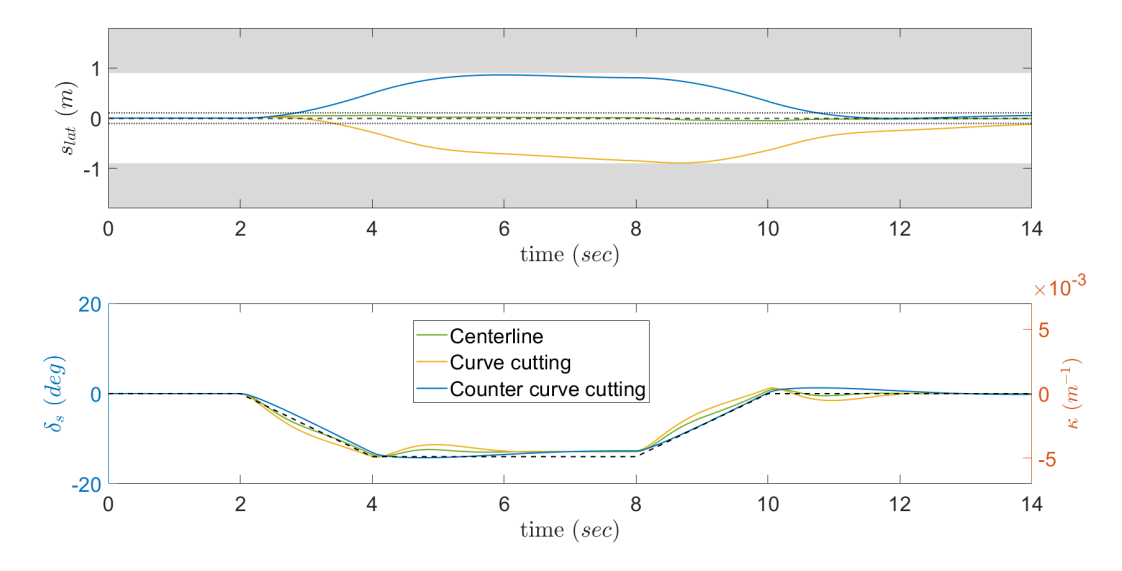


Figure 4.6: The three simulated trajectory types, resulting from the K_p - K_c combinations in Table 4.2.

Having the three trajectory types ready for simulation, the next step is evidently simulating the Four-Design-Choice-Architecture as haptic shared controller.

4.1.3. Four-Design-Choice-Architecture

The details on the Four-Design-Choice-Architecture have mostly been covered in Section 2.1 and its implementation is thus rather straightforward. The most important differences between the FDCA used in simulation and the FDCA used for experiments are the HCR- and Driver-blocks. In the simulations, both blocks are replaced by the driver model from Section 4.1.1, although the implementation of the model differs for both applications. The HCR in the simulations is generated using the driver model before the vehicle starts driving, which results in a ready-to-use input to the Reference Selector-block. This block determines which data point from the HCR is closest to the current vehicle position and is thus used at that certain time step for the calculation of the FDCA torque. Also represented by a driver model is the driver itself. In this case, the driver model is included in the simulation loop and the driver torques are updated for every time instant, depending on the cooperation with the FDCA. A visualisation on how the FDCA structure is added to the existing driver model and vehicle dynamics is presented in Figure 4.7. Note that the driver and vehicle dynamics blocks are taken from the already existing simulation, but the torques of the FDCA are added in the loop. Since the driver model is able to take on three forms, nine scenarios are to be simulated. Some scenarios include the HCR and driver pursuing the same trajectory, while in other scenarios their desired path is highly different.

The most crucial part in the implementation of the Four-Design-Choice controller is the tuning of the gains. These gains are shown in Figure 2.2 and consist of the feedforward gain K_{LoHS} and the feedback gains

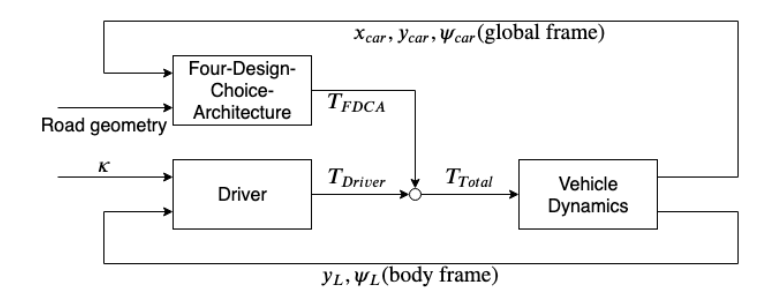


Figure 4.7: The interaction philosophy for the driver model and FDCA.

 K_s , K_ψ and K_{SoHF} . Note that all these gains and this tuning solely takes place in the "Four-Design-Choice-Architecture" block of Figure 4.7 as the "Driver" and "Vehicle Dynamics" are already established at this point. The tuning of these FDCA gains is necessary as together they ensure that the produced FDCA torque T_{FDCA} is able to steer the vehicle according to the reference path. To ensure proper gain tuning, a parameter identification problem is created which optimises these four gains by minimising the cost function provided in Equation (4.13). This function compares the desired lateral position on the road, $s_{lat_{HCR}}$, to the lateral position based on the current combination of gains, $s_{lat_{total}}$.

$$J_{cost} = \frac{1}{2m} \sum_{i=0}^{m} \left[s_{lat_{total}}(i) - s_{lat_{HCR}}(i) \right]^{2}$$
 (4.13)

In Equation (4.13), J_{cost} is the cost to be minimised in order to find the optimal combination of gains. Additionally, m are the total number of data points along the curve and $s_{lat_{total}}(i)$ represents the lateral displacement of the combined (collaboration between HCR and driver) trajectory along the curve. At last, $s_{lat_{HCR}}(i)$ is the lateral displacement of the Human Compatible Reference trajectory. To correctly calculate these gains, the driver torque must be reduced to zero, implying that there can be no intervention from the driver. This approach relies on the characteristic that the controller should always be able to follow the HCR perfectly if the driver does not give any inputs. The result of the parameter identification can be found in Table 4.3.

Table 4.3: Gain tuning of K_S , K_{ψ} , K_SoHF and K_{LoHS} by parameter identification.

	K_s	K_{ψ}	K_{SoHF}	K_{LoHS}
Radius 204 m, Velocity 80 km/u	0.05	0.03	1.5	1

Once the gains are tuned to follow the HCR in case of no driver input, the driver contribution is added to the system to complete the simulations.

4.1.4. Joining of driver and controller

The joining of the driver with the FDCA structure seems simple, but has proven to be surprisingly complex. The simplified representation of the simulation in Figure 4.7 shows that the output of both the FDCA- and driver-block is a torque, that are added together to form the total torque as input to the vehicle dynamics. In the simulations however, the output of the driver model is a steering wheel angle, not a torque. Moreover, the input to the vehicle dynamics is also a steering wheel angle and not a torque as presented in Figure 4.7. This indicates that a conversion from steering wheel angle to steering wheel torque and vice versa is necessary to complete the simulations. See Figure 4.8 for a detailed picture of the FDCA and Driver outputs and the Vehicle Dynamics input. The figure includes the needed conversion that needs to take place to ensure the proper working of the entire system.

The steering wheel angle and torque of the vehicle are related to each other by a rotational mass-spring-damper system. Their exact relationship is presented in Figure 4.9, where a steering wheel is represented by a simple mass-spring-damper system. From the figure, a second-order differential equation is deducted that further illustrates the conversion between both properties. This conversion can be found in Equation (4.14). θ represents the steering wheel angle and τ the steering wheel torque. Furthermore, the steering wheel's moment of inertia is symbolised by J_w , its friction coefficient by B_w and its spring constant by K_w .

4.1. Simulation Setup 55

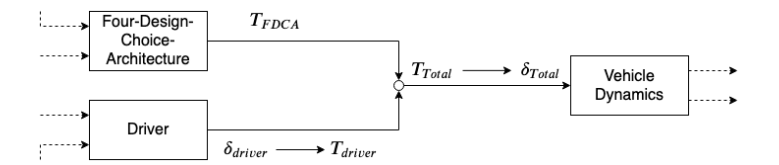


Figure 4.8: A clarification of the needed conversions to complete the simulations.

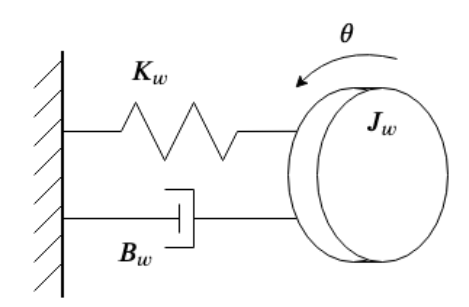


Figure 4.9: The rotational mass-spring-damper system representing the steering wheel.

$$J_w \ddot{\theta} + B_w \dot{\theta} + K_w \theta = \tau \tag{4.14}$$

Often, when faced with slow steering rotations, it is decided to omit the higher order derivatives of Equation (4.14), resulting in a simple linear relationship:

$$\tau = K_w \theta \tag{4.15}$$

Equation (4.15) leads to the steering wheel angle and torque being related by a simple gain. Surely, omitting the higher order derivatives of the steering wheel angle means assuming that all steering wheel angles are of low frequency. If all angles on the steering wheel are of low frequency, the first and second order derivatives of the steering wheel angle are comparatively small, making the relationship between angle and torque more or less linear and thus leading to the discarding of the derivatives. The best example of this application is the LoHS – or feedforward – part of the FDCA controller. The reference steering wheel angle $\delta_R(t)$ is related to the output of the LoHS-block – T_{LoHS} – via the following relation:

$$T_{LoHS}(t) = \delta_R(t) \cdot K_{LoHS} \tag{4.16}$$

This is a simplification of the rotational mass-spring-damper system and shows that the feedforward component of the FDCA assumes low-frequency steering angles following from the HCR. However, for the simulations such an assumption cannot be made as it is unknown how driver and FDCA react to each other. Another approach is thus required.

The first attempt at establishing a conversion method consists of a mathematical approach. The conversion of steering angle to steering torque is given by Equation (4.14), where the first and second derivatives of θ are computed by calculating the change of θ and dividing this by the change in time. Hence the opposing conversion – steering torque to angle – is computed using the state space system given in Equation (4.17) and Equation (4.18).

$$\dot{\boldsymbol{\theta}} = \begin{bmatrix} \dot{\boldsymbol{\theta}} \\ \ddot{\boldsymbol{\theta}} \end{bmatrix} = \begin{bmatrix} 0 & 1 \\ -\frac{K_w}{J_w} & -\frac{B_w}{J_w} \end{bmatrix} \begin{bmatrix} \boldsymbol{\theta} \\ \dot{\boldsymbol{\theta}} \end{bmatrix} + \begin{bmatrix} 0 \\ \frac{1}{J_w} \end{bmatrix} \boldsymbol{\tau} \tag{4.17}$$

$$\mathbf{y} = \begin{bmatrix} 1 & 0 \end{bmatrix} \begin{bmatrix} \theta \\ \dot{\theta} \end{bmatrix} \tag{4.18}$$

To complete both equations, the values of the steering wheel inertia, friction coefficient and spring constant must be determined as well. Saleh et al. (2013) suggests values for J_w , B_w and K_w that are compatible

with the rest of their driver model, but it is preferred to use the steering wheel values of the simulator in the Human-Machine Interaction (HMI) Laboratory, at the Faculty of Aerospace Engineering of the Delft University of Technology. This makes the simulations more realistic and usable for this particular experiment. The simulator values can be found in Table 4.4.

Table 4.4: Simulator values of J_w , B_w and K_w .

	Inertia J_w	Friction coefficient B_w	Spring constant K_w
Simulator value	0.005	0.03	1

The resulting conversion is shown in Figure 4.10. The original and converted steering wheel angle overlap entirely and as expected, the torque takes a shape similar to the steering wheel angle. The torque however has a lead on the steering wheel angle – due to the positive phase of the inverse second order dynamics – and is plagued by some irregularities. As these irregularities occur at changes in curvature, it is assumed they are caused by the higher order derivatives of the steering wheel angle. It is reasoned that this second-order system becomes unstable for large frequencies as the output magnitude keeps increasing past the corner frequency.

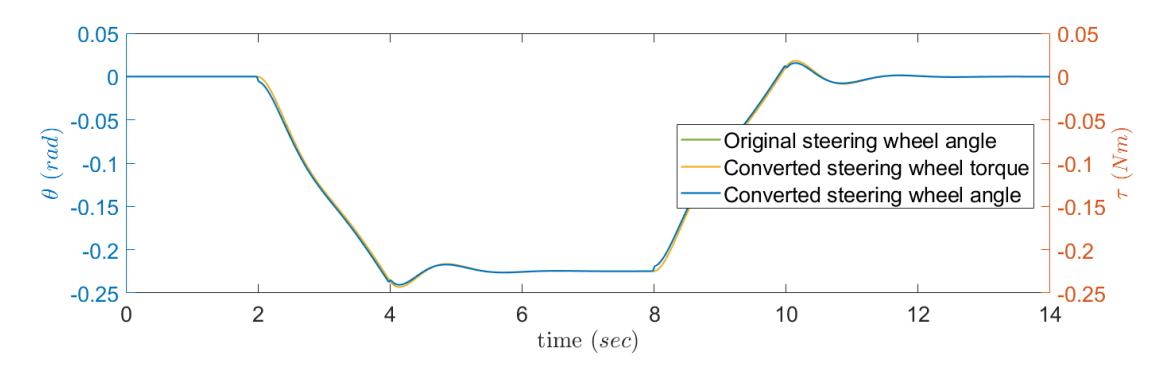


Figure 4.10: Conversion of steering wheel angle to torque and vice versa.

To smoothen the converted torque, it is decided to change the angle to torque conversion method to a procedure that is sure to guarantee stability. The steering wheel torque is still calculated using Equation (4.14), however the individual derivatives are calculated differently. First of all, the calculation now takes place in the Laplace domain, where deriving a variable equals multiplying the variable by 's'. Second, to ensure stability a low pass filter is added, which limits the impact of the higher frequency inputs. The transfer function to calculate the derivative of θ is then given by Equation (4.19). Note that it is decided to put the crossover frequency at 20 rad/s as this should allow all natural inputs to pass.

$$\frac{\dot{\theta}(s)}{\theta(s)} = s \cdot \frac{1}{\frac{s}{20} + 1} \tag{4.19}$$

Figure 4.11 shows the intention of this approach more clearly. Equation (4.14) represents a second-order lead term that becomes unstable for large frequencies, therefore it has been decided to limit the calculation of the first and second order derivative of θ as can be seen in Equation (4.19). The differentiator term 's' results in a steadily increasing magnitude plot of 20 dB/decade and a constant lead of +90°. The second term, a low pass filter, then adds a constant zero-magnitude until the crossover frequency of 20 rad/s is reached, after which the magnitude plot decreases by 20 dB/decade. The phase plot of the low pass filter on the other hand makes the lag shift from 0° to -90°. This multiplication between the differentiator and the low pass filter equals an addition in the Bode plot, resulting in Figure 4.11. As the magnitude plot stagnates after 20 rad/s, it is evident that outliers in input frequencies do not disrupt the system anymore as their magnitude is limited.

On the other hand, the method behind the other side of the conversion is sustained, but is now also solved in the Laplace domain for transparency. The torque-angle conversion is thus achieved using the transfer function from Equation (4.20).

4.1. Simulation Setup 57

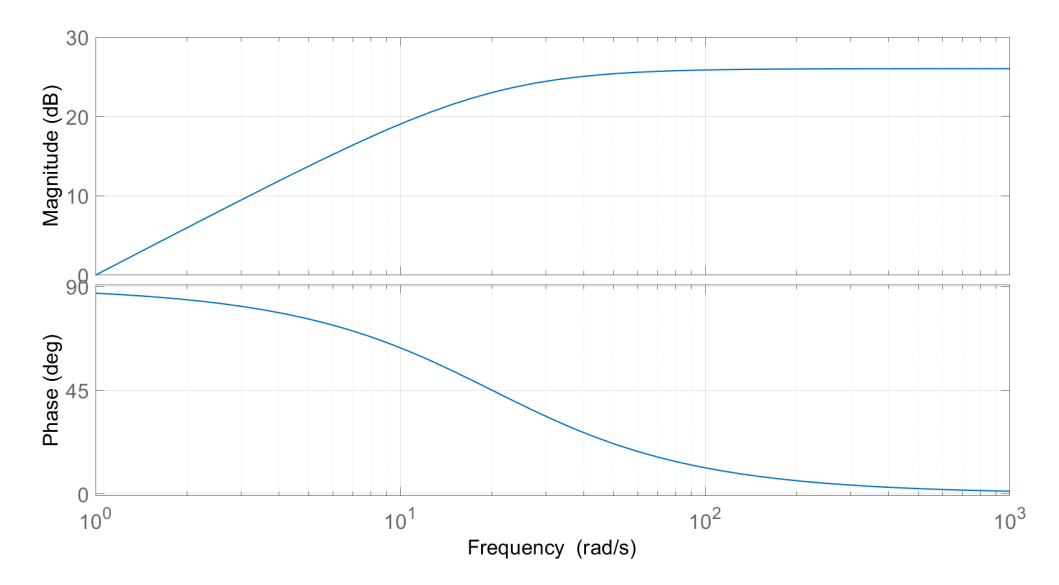


Figure 4.11: Bode plot of transfer function to compute derivative of θ .

$$\frac{\theta(s)}{\tau(s)} = \frac{1}{I_s s^2 + B_s s + K_m} \tag{4.20}$$

The resulting conversion is shown in Figure 4.12. It is apparent that this conversion is more smooth and does not cause problems in the FDCA-driver loop. At last, the steering wheel angle to steering wheel torque conversion is applied to the output of the Driver block, which is then in turn added to the output of the FDCA block and then converted back to steering wheel angle to serve as input to the Vehicle Dynamics. The last step before the simulations are finished is then to understand how the driver and Four-Design-Choice-Architecture work together in terms of torques on the steering wheel.

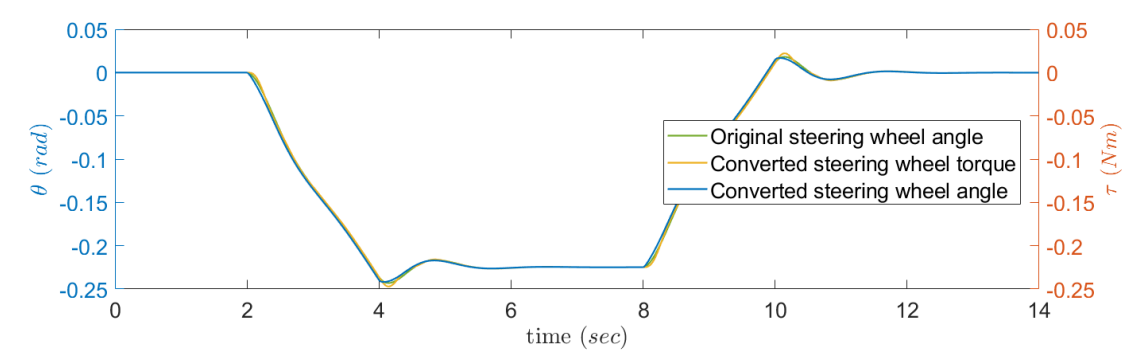


Figure 4.12: New conversion of steering wheel angle to torque and vice versa.

4.1.5. Collaboration between parties

It is important that the simulations also take into account the torque division between the driver and the FDCA. When adding the driver model and FDCA together in a loop, it is possible that the combination of torques makes that the desired trajectory is not reached due to an overshoot in torque. The perfect example to illustrate the issue is provided in Figure 4.13. Both the HCR of the FDCA and the driver model are programmed to follow the centerline trajectory. However due to both of them exerting the same torques to follow this trajectory, they overshoot the centerline and end up in a trajectory that closely resembles curve cutting. Of course in reality this never occurs since the driver and controller feel each others torques and therefore modify their behaviour.

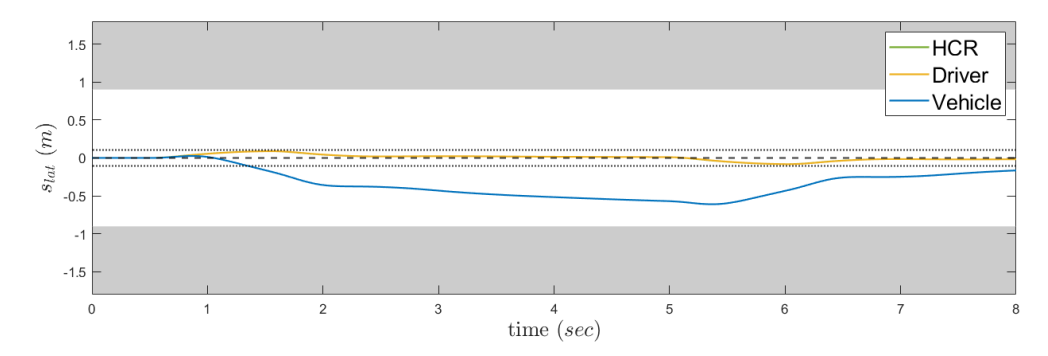


Figure 4.13: An illustration of the collaboration issue. Note that the "Vehicle" line corresponds to the resulting, combined trajectory of the HCR and driver. Curve starts at 1 second and ends at 7 seconds.

To understand the resolution to this issue, Figure 4.14 is provided. It shows a zoomed-in illustration of the core of the simulation and is an updated version of Figure 4.8. In comparison to Figure 4.8, the functions representing the angle to torque and torque to angle conversions are included. Additionally, two new gains are added, K_{co-fdc} and K_{co-dr} . These help balancing the system to avoid situations such as in Figure 4.13 and mimic the FDCA and driver reacting to each other. To ensure correct torques, it is important that:

$$K_{co-fdc} + K_{co-dr} = 1 (4.21)$$

If Equation (4.21) is satisfied – with any combination of K_{co-fdc} and K_{co-dr} – then the vehicle from Figure 4.13 will follow the centerline. This is because the percentage of the FDCA torque and Driver torque will together equal the amount of torque needed to follow the desired trajectory.

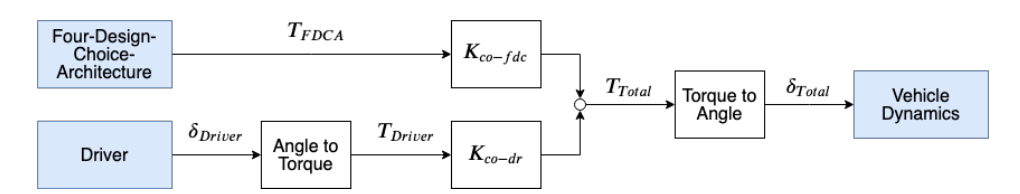


Figure 4.14: Concentrated illustration of part of the simulation loop.

The correct values of K_{co-fdc} and K_{co-dr} thus depend on previous experiments where a driver and FDC controller cooperate. The best case for reference is the experiment performed by Scholtens et al. (2018). This experiment was performed recently and included the complete FDCA. Figure 4.15 shows a plot taken from Scholtens et al. (2018). It shows the absolute driver and HSC torque for Manual driving (D), FDCA with individualised HCR (iFDCA), FDCA with averaged HCR (mFDCA) and the Meshed controller (Referred to as Two-Level Controller TwL).

To estimate the collaboration between driver and HSC, Figure 4.15 is used. From the iFDCA and mFDCA, the different driver and total HSC torques are read and rescaled to fit Equation (4.21). The end result of this averaging and calibrating culminates in Table 4.5, where the final K_{co-fdc} and K_{co-dr} are presented.

Table 4.5: Collaboration gain values for simulations.

	K_{co-dr}	K_{co-fdc}
Collaboration gain value	0.37	0.63

Having determined the collaboration gains, the setup of the simulations is now finished. The last step, which is unrelated to the setup of the simulations, but is necessary for the analysis, is the calculation of conflict torques between driver and FDCA.

4.2. Results 59

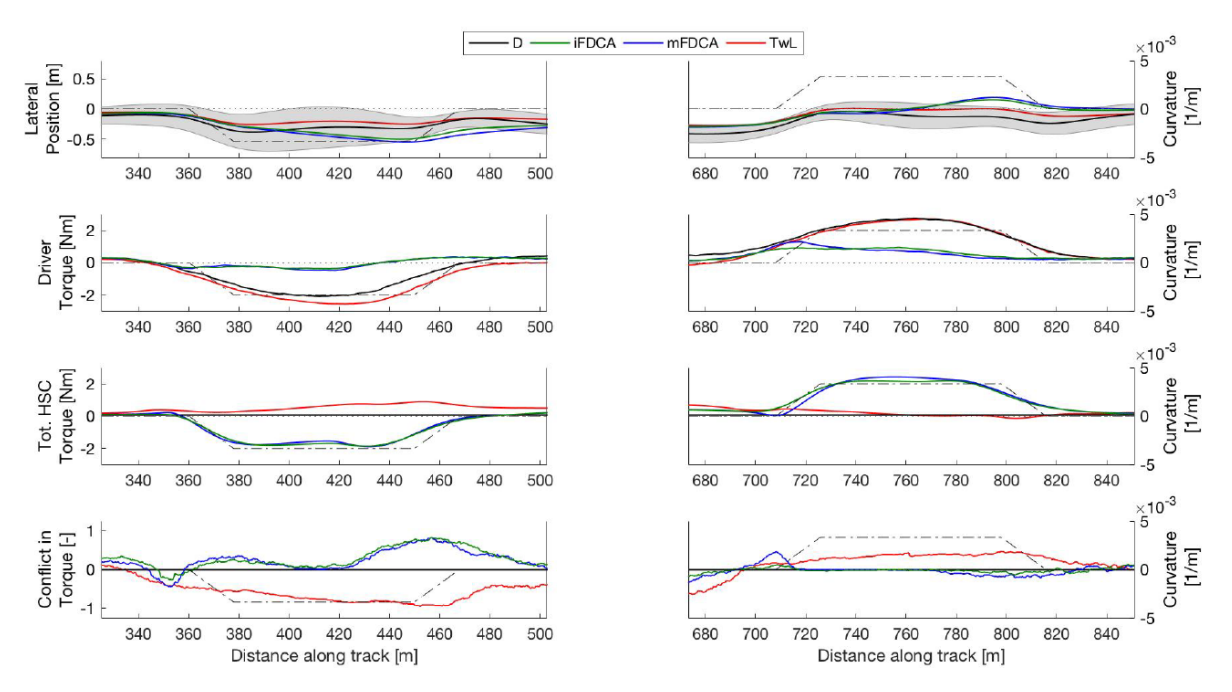


Figure 4.15: Driver and HSC torques, adapted from Scholtens et al. (2018).

4.1.6. Conflict torques

The results of the simulations mainly contain plots of lateral position, steering wheel angle and steering wheel torque. It is also decided to calculate both the conflict torque between the FDCA and the driver and also their relative time of being in conflict with each other during the simulation interval. These two parameters should add information on how the driver and FDCA react to each other, whether their interaction is positive or negative. Before any calculations can be made, a consensus must be reached on what a conflict actually is and therefore the following definition is created:

$$O_{conflict} = \begin{cases} 1, & \text{if } T_{driver} \cdot T_{FDCA} < 0 \\ 0, & \text{otherwise} \end{cases}$$

Basically this definition entails that if the torque exerted by the driver on the steering wheel and the torque by the controller are in opposite direction, the driver and controller are in conflict. If their torques are aimed in the same direction, then there is no conflict present. At the end of each simulation, it will be determined for every time step whether or not the driver and controller are in conflict. For each time step in conflict, the absolute conflict torque is calculated by taking the absolute value of the difference between the FDCA torque and driver torque. Also, the time percentage of being in conflict is calculated.

4.2. Results

In total, nine scenarios are simulated. These are all combinations of the driver and HCR either exhibiting centerline, curve cutting or counter curve cutting behaviour. Within those nine scenarios, several levels of disagreement become apparent. In some scenarios the driver and HCR are programmed to drive identical trajectories, leading to low conflict simulations. An example is provided in Figure 4.16, where both the HCR of the FDCA and the driver follow a counter curve cutting trajectory. The figure shows that – as expected – when both agents intend to follow the same path, then the individual steering wheel angles overlap. It is important to note that the HCR and driver steering wheel angles in this figure represent the ideal steering wheel angles needed to follow the HCR's and driver's intended path. The result of their cooperation is an almost identical total steering wheel angle, i.e., the total vehicle steering wheel angle in the figure. As a result of this total (vehicle) steering wheel angle, the vehicle nicely follows the same counter curve cutting trajectory as both the HCR and driver intended.

A more extreme scenario is where the HCR and driver both follow different trajectories. An example of such a scenario is provided in Figure 4.17. The HCR is pre-programmed to follow a curve cutting trajectory,

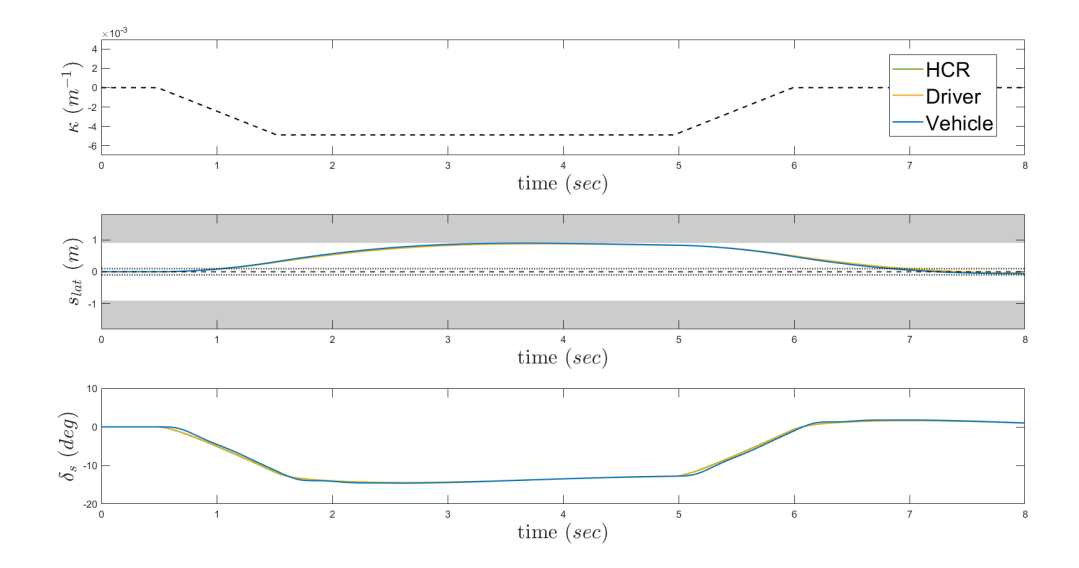


Figure 4.16: Simulation result of both HCR and driver following a counter curve cutting path. Note that the "Vehicle" line corresponds to the combined, total result of the HCR and driver.

while the driver follows the centerline path. The resulting vehicle trajectory falls somewhere in between the HCR and driver trajectory, although it lies much closer to the driver's centerline path. In terms of steering wheel angles, the total vehicle steering wheel angle nicely fluctuates between the driver and HCR steering angles.

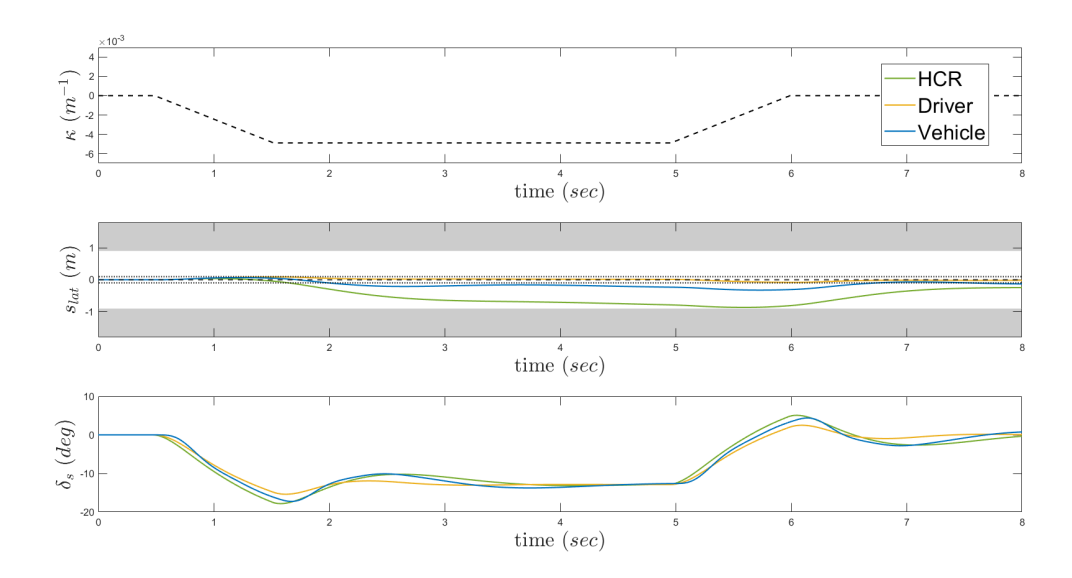


Figure 4.17: Simulation result of HCR driving curve cutting and driver following a centerline trajectory. Note that the "Vehicle" line corresponds to the combined, total result of the HCR and driver.

4.2. Results 61

At last, some extreme scenarios are presented as well. Figure 4.18 presents the scenario where the HCR is programmed to follow a counter curve cutting trajectory, while the driver aims to do the opposite and thus performs a curve cutting path. The other extreme scenario is presented in Figure 4.19. In this scenario the HCR follows a curve cutting trajectory, while the driver carries out counter curve cutting. At first, one would expect the resulting vehicle trajectories from both these scenarios to be similar and lie somewhere in the middle between the HCR and driver paths. The outcome of the simulations, however, shows some interesting differences between both. In the first scenario the driver performs curve cutting. Curve cutting is one of the more optimal trajectories as this leads to a lower average lateral acceleration and heightened TLC. The HCR in this case performs counter curve cutting, which is a more inefficient trajectory. It seems that due to the collaboration between both, the resulting vehicle path initially inclines toward the HCR path, following the guidance, but then slightly steers back towards the more efficient driver's trajectory. In the end, the resulting vehicle path more or less resembles a centerline scenario.

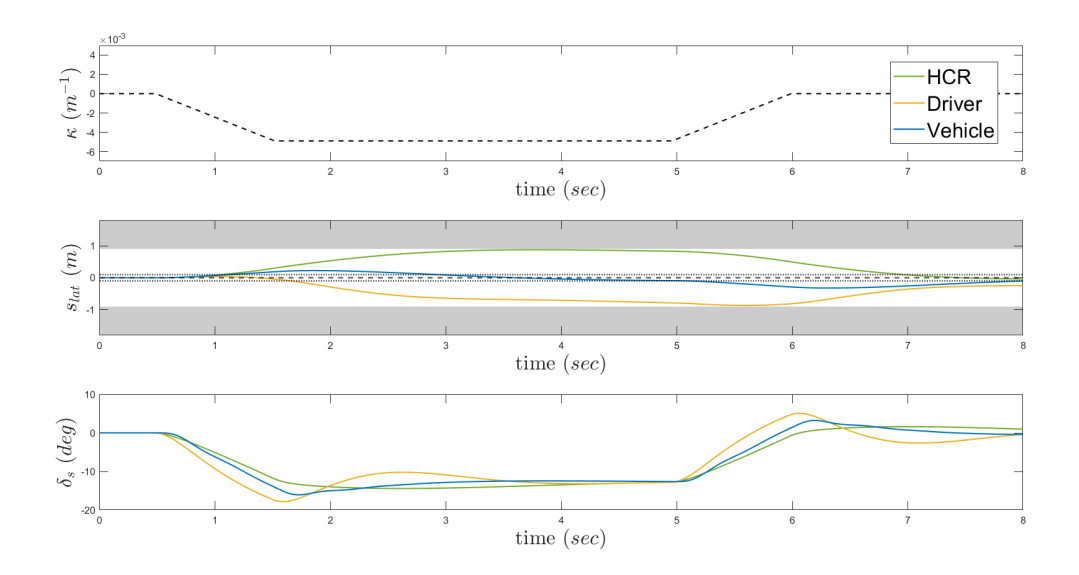


Figure 4.18: Simulation result of HCR counter curve cutting and driver following a curve cutting path. Note that the "Vehicle" line corresponds to the combined, total result of the HCR and driver.

The opposite scenario – presented in Figure 4.19 – shows a very efficient HCR and a less efficient driver. Also here, the resulting trajectory inclines towards the HCR at the beginning and keeps following the HCR to a high degree throughout the curve. This is contrary to the previous case, where the vehicle path lies closer to the driver's performed trajectory. It appears that the resulting trajectory always initially tends towards following the HCR trajectory, but over time more tends towards the more efficient trajectory. To further understand what exactly is happening, the conflict torques must be analysed. Note that all other results of the simulations are presented in Appendix A.

4.2.1. Conflict Torque Analysis

For each of the nine scenarios both the conflict torque and time percentage of being in conflict is determined. The results of this analysis are shown in Table 4.6. At first glance, one can immediately see that the earlier referred to low-conflictual scenarios indeed show the lowest amount of absolute conflict torque and also the lowest percentages of time in conflict.

For all other scenarios the amount of conflict torque and time of being in conflict is heightened. Note that the resulting vehicle path in the simulations is a representation of the possible behaviour of drivers in a haptic shared control experiment. Therefore, the earlier made assumption that drivers might be more compliant with the HCR if the HCR is following a more efficient trajectory is confirmed with the calculation of the conflict torques. In the example of the highest conflicting scenario, the conflict torque and the time of being in conflict is lower when the driver has a less efficient trajectory than the HCR, indicating that the driver acknowledges this HCR path as being comfortably. In the opposing scenario, when the driver has a more efficient trajectory, the driver seems to fight the guidance more in order to follow his/her own trajectory more.

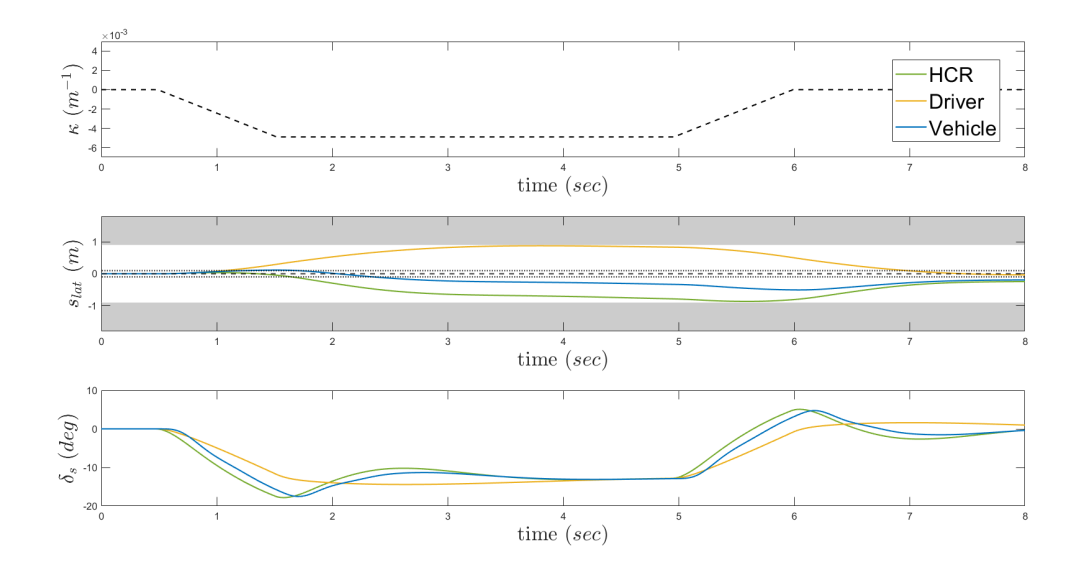


Figure 4.19: Simulation result of HCR curve cutting and driver following a counter curve cutting path. Note that the "Vehicle" line corresponds to the combined, total result of the HCR and driver.

	Driver Centerline	Driver Curve cutting	Driver Counter curve cutting
HCR	0.0958 Nm	0.6716 Nm	0.7157 Nm
Centerline	7.30%	16.00%	17.50%
HCR	3.5788 Nm	0.0384 Nm	0.8596 Nm
Curve cutting	19.60%	1.20%	14.50%
HCR	3.2378 Nm	1.6226 Nm	0.0113 Nm
Counter curve cutting	32.90%	21.60%	0.90%

Table 4.6: Outcome of conflict torque analysis for all nine scenarios.

Furthermore, there seems to be a mismatch in the exact amount of conflict. See, for example, the scenario where the driver follows the centerline, but the HCR is programmed to cut the curves, in Table 4.6. The conflict torque then equals about 3.58 Nm and the time of being in conflict equals 19.60%. One would expect more or less similar values for the opposite scenario – where the driver cuts curves, but the HCR follows a centerline trajectory – however, that does not seem to be the case. The time in conflict is with 16.00% rather similar to the opposing scenario, but the biggest difference is noticeable in the absolute conflict torque with equals 0.67 Nm and is thus about a factor 5 smaller.

It appears that especially the scenarios in which the driver follows the centerline trajectory show excessive absolute conflict torque values and sometimes also large time percentages. Even the scenario where both the HCR and driver perform centerline driving, the conflict torque and time percentage are higher than the other two scenarios where the driver and HCR follow the same driving path. To investigate this issue further, it is decided to check the internal torques of the simulation. Figure 4.20 provides the internal torques – T_{FDCA} and T_{Driver} – after scaling of two scenarios: HCR curve cutting, driver centerline driving and HCR curve cutting, driver counter curve cutting. Both scenarios show that the behaviour of T_{FDCA} is really similar and thus is not the cause of the extra conflicts. The T_{Driver} plot on the other hand clearly shows why the centerline trajectories cause higher conflict torques. The internal T_{Driver} for centerline fluctuates much more than the other torques.

It was explained in Section 4.1 that high K_c values might cause oscillations in steering wheel angles. This behaviour was not yet completely visible in the individual trajectories, but now – in combination with another party – becomes clearly visible. To see if this behaviour can be prevented, a new centerline trajectory was generated.

4.2. Results 63

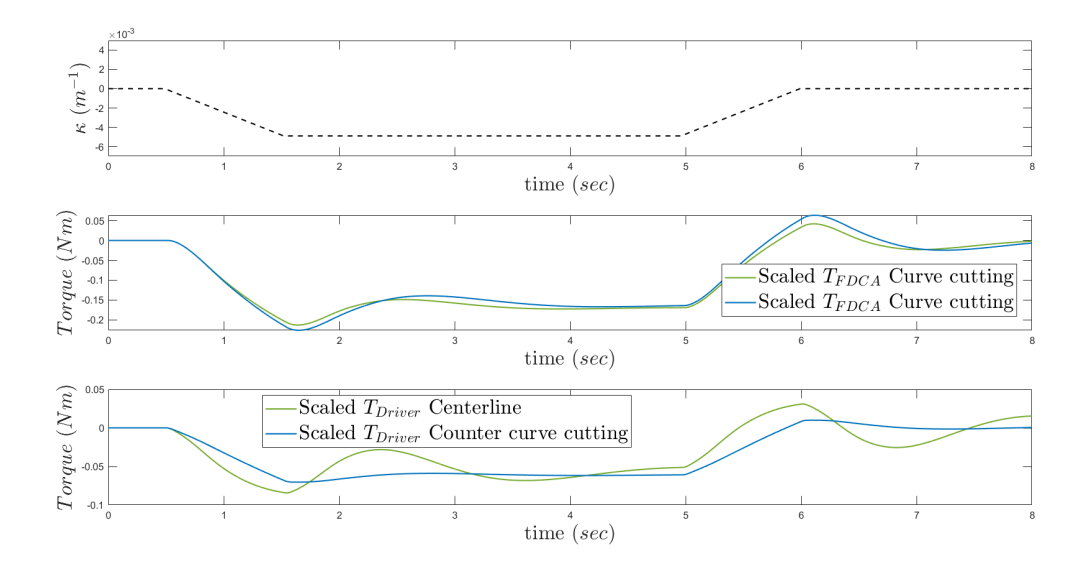


Figure 4.20: Internal torque of simulation where HCR is programmed to follow a curve cutting trajectory and the driver follows either a centerline path (green) or a counter curve cutting path (blue).

4.2.2. New Centerline Trajectory

In an attempt to eliminate all oscillations, it is decided to lower the K_c value as much is possible, while still maintaining a centerline trajectory. The result of this analysis is presented in Table 4.7.

Table 4.7: Original and new K_p and K_c tuning for centerline driving.

	K_p	K_c
Original centerline driving	1.7	28
New centerline driving	1.5	18

This re-tuning of the trajectory parameters also leads to a slightly different centerline path, as is shown in Figure 4.21. The original centerline shows a small overshoot of the centerline at the beginning of the curve and a small undershoot at the end of the curve. This is caused by the driver model that is used for the simulations. This model only takes into account current curvature, so when an actual curve appears, the model's response is lagged. The new centerline trajectory does not satisfy the centerline path constraints in a strict matter of speaking. The trajectory lies outside the centerline band, but remains constant at a deviation of 0.15m from the centerline.

The same simulations as presented in Figure 4.20 are now repeated in Figure 4.22, but the results from all internal torques originating from the new centerline trajectory are added. Reducing the K_c value by 10 clearly reduces the fluctuations, nevertheless they are still visibly present. As this is the lowest the K_c is able to go and still have centerline driving behaviour, it is decided to recalculate all conflict torques with the new centerline configuration.

4.2.3. Updated Simulations

Table 4.8 is an extension of Table 4.6, where the blue values represent the new conflict torques and time percentages due to the new centerline trajectory. Immediately it shows that overall the absolute conflict torque and the percentage of being in conflict has decreased. As a reference, it appears that the conflict values for the "HCR centerline" - "driver centerline" case are much more in line with the other low conflictual scenarios. Also for the other scenarios, the conflicts have decreased in size and occurrence, but are in some cases still higher than normal. It is at this point that the situation becomes very questionable.

The original centerline trajectory causes the driver to exhibit extreme oscillatory behaviour, which an everyday driver does not express. This is an artifact of the driver model used for the simulations. It represents

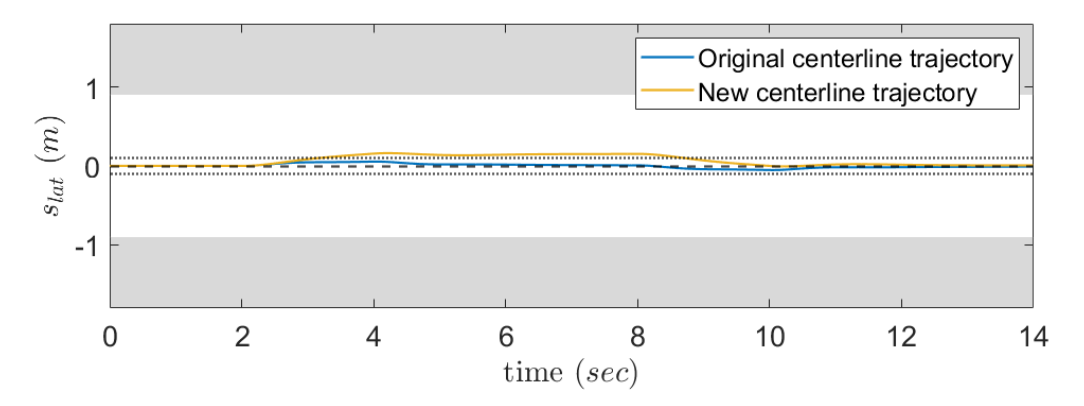


Figure 4.21: Internal torque of simulation where HCR is programmed to follow a curve cutting trajectory and the driver follows either a centerline path (green) or a counter curve cutting path (blue).

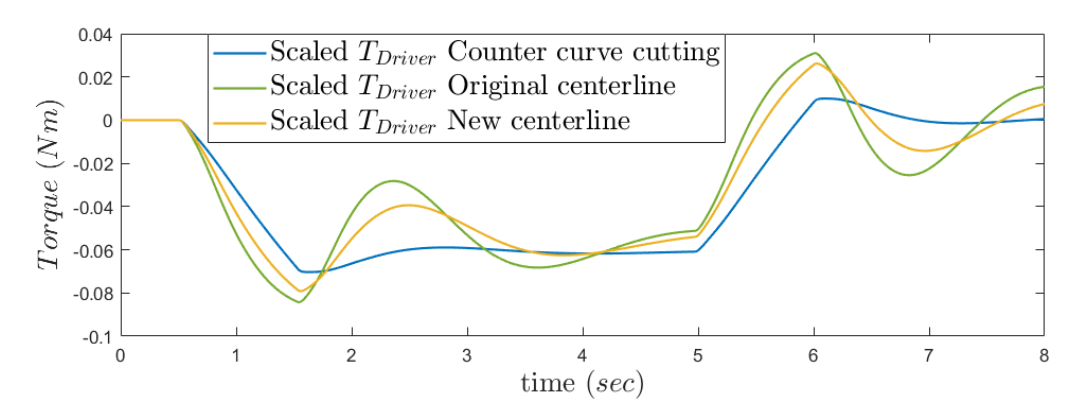


Figure 4.22: Internal torque of simulation where HCR is programmed to follow a curve cutting trajectory and the driver follows either a counter curve cutting path (blue), the original centerline path (green) or the new centerline path (yellow).

a situation which takes place in the simulations, but does not occur in real life. The new centerline trajectory on the other hand, reduces the oscillations, but does not take them away completely. Moreover, the new centerline trajectory creates a path that does not completely lie within the centerline band. The newly formed trajectory has an offset of 0.15 m to the outside of the curve, thus favouring counter curve cutting behaviour. This offset therefore reduces conflicts with a counter curve cutting HCR or driver extensively.

Table 4.8: Outcome of conflict torque analysis for all nine scenarios, with all values changed by the new centerline trajectory indicated in blue.

	Driver	Driver	Driver
	Centerline	Curve cutting	Counter curve cutting
HCR	0.0957 Nm - 7.30%	0.6716 Nm - 16.00%	0.7157 Nm - 17.50%
Centerline	0.0530 Nm - 2.70%	0.7774 Nm - 18.00%	0.5102 Nm - 12.70%
HCR	3.5788 Nm - 19.60%	0.0384 Nm	0.8596 Nm
Curve cutting	1.3821 Nm - 14.50%	1.20%	14.50%
HCR	3.2378 Nm - 32.90%	1.6226 Nm	0.0113 Nm
Counter curve cutting	1.2311 Nm - 23.00%	21.60%	0.90%

4.3. Verification 65

4.3. Verification

Both verification and validation are essential elements in each simulation process. First of all, verification tries answering the question 'Are we building the product right?', by checking whether the computational model correctly represents the mathematical model and its solution. Verification consists in this case of two parts: a code verification and a calculation verification.

4.3.1. Code Verification

Code verification encompasses all finding and fixing of errors in the code. Most of these errors can be fixed with the help of the compiler. The compiler gives an error message when something is wrong in the structure of the code, such as a forgotten semicolon or typing mistake. However, code verification also includes mistakes that cannot be found by the compiler, such as a wrongly coded 'if-statement' or 'for-loop'. The code verification process for this simulation entirely takes place during the writing of the code and therefore mainly consists of unit tests. Each block of code is individually checked by using the compiler and by confirming the proper functioning of all statements.

4.3.2. Calculation Verification

After the code verification, it is concluded that the code has been programmed correctly, however, this does not indicate that the computational model is also correct or sufficiently representative. Calculation verification checks if the computational model is able to replicate the behaviour of the real world. To perform this type of verification, it is useful to start with some unit tests and if these tests are successful, to expand to a complete system test.

The best method to verify the implemented Four-Design-Choice-Architecture is to select some simplified scenarios of which the outcome is known or can easily be calculated and compare these results to the outcome of the programmed system. This leads to the first verification test, in which the influence of the FDCA is switched off, and the vehicle thus – evidently – should follow the driver's desired trajectory. Figure 4.23 shows once again how the FDCA and driver are connected to each other and to the Vehicle dynamics. The FDCA-block is grey to illustrate the working of this verification test. Without the influence of the FDCA, the output trajectory of the vehicle dynamics should be the same as the driver's intended path.

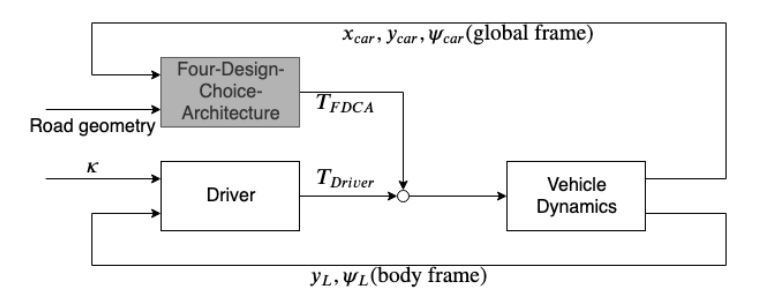


Figure 4.23: Simplification of simulation setup with the FDCA deactivated, based on Figure 4.7.

In total this results in three different simulations to be run for this part of the calculation verification: a centerline driving, curve cutting and counter curve cutting driver. Figure 4.24 shows the output of one of those scenarios, specifically the curve cutting example, and shows that the vehicle indeed properly follows the driver's intentions. There are some slight differences noticeable between the driver and vehicle steering wheel angles, δ_s , but these are due to the transformation between steering wheel angle and torque (and vice versa) in the simulation loop. The curve cutting output of Figure 4.24 is very representative for the other two scenarios as the vehicle follows the driver perfectly in all cases.

Another unit test to consider is the opposite of the test described above. The system should be programmed in such a way that the vehicle also follows the FDCA's intentions if the driver does not give any input on the steering wheel. The simulation loop then resembles Figure 4.25, where the driver-block is grey, representing the lack of steering wheel input. Once again this verification test is performed for all three trajectory types.

To explain the results of this verification test, the curve cutting scenario is provided. Figure 4.26 shows that the FDCA and vehicle trajectories nicely overlap, but show some more differences than in the verification test

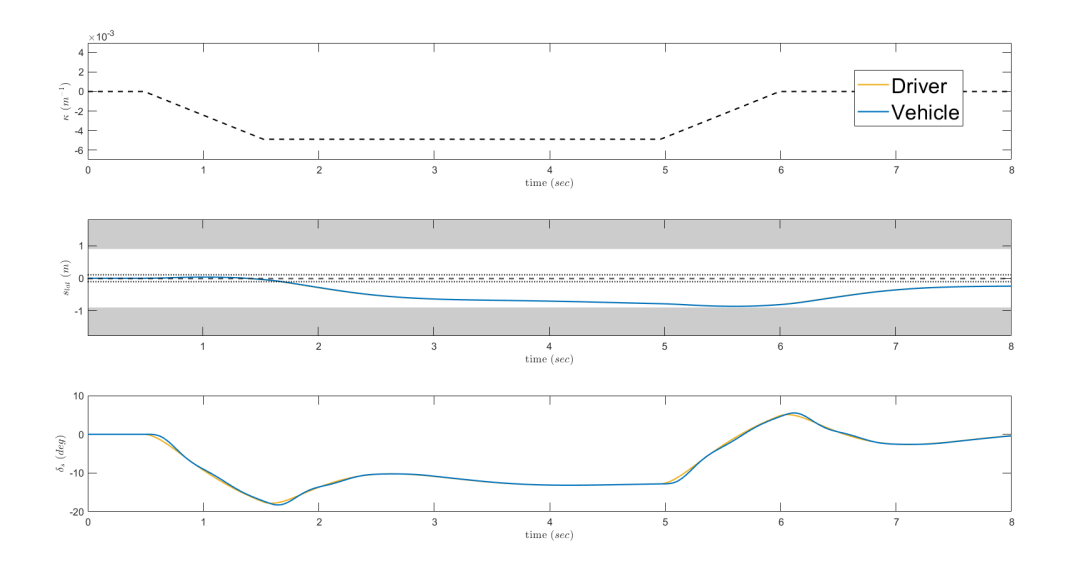


Figure 4.24: Outcome of curve cutting driver calculation verification.

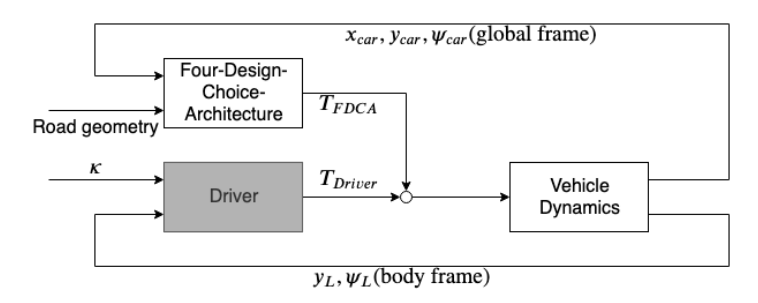


Figure 4.25: Simplification of simulation setup with the driver deactivated, based on Figure 4.7.

of the driver. This is due to the imperfect tuning of the FDCA gains, K_s , K_ψ , K_{SoHF} and K_{LoHS} . Despite being optimised for following the FDCA trajectory by minimising a cost function, the resulting gains are rounded off for simplicity. The same difference is visible in the steering wheel angles, alongside the discrepancies caused by the angle-torque conversion. The same holds for the other scenarios as well.

After some successful unit tests, the verification process proceeds to the execution of system tests. System tests are in a way harder to complete than unit tests, as their outcome is harder to predict. It is opted to conduct two system tests. The first one considers the lowest conflictual scenario, while the second one examines the highest conflictual case. The lowest conflictual scenario occurs when both driver and FDCA intend to follow the same trajectory. In reality, one would assume that in case both driver and FDCA prefer to follow the same path, the consequent vehicle trajectory is identical. Therefore this scenario is tested as the first system test. Figure 4.27 shows the result of this verification in case of a counter curve cutting trajectory. It is concluded that in this case the simulation works as is expected. It should be added that this conclusion repeats itself for all three low conflictual scenarios and also for all combinations of K_{co-dr} and K_{co-fdc} as long as their sum equals one. The presented result in Figure 4.27 shows an example when K_{co-dr} and K_{co-fdc} are both 0.5, giving the driver and FDCA thus an equal share in the output trajectory. The previously presented result in Figure 4.16 can also be used for system verification as it shows the same solution for counter curve cutting, but with the final combination of K_{co-dr} and K_{co-fdc} , where K_{co-dr} equals 0.29 and K_{co-fdc} equals 0.71. This part of the simulation code is therefore verified.

The second system verification test is an evaluation of the highest conflictual scenario's in the simulations. The highest conflictual scenario's consists of the driver and FDCA preferring opposing trajectories. It has already been shown in the unit tests that in a scenario where the driver prefers counter curve cutting and the FDCA is programmed to follow a curve cutting path, the code is able to follow either of them depending on

4.4. Validation 67

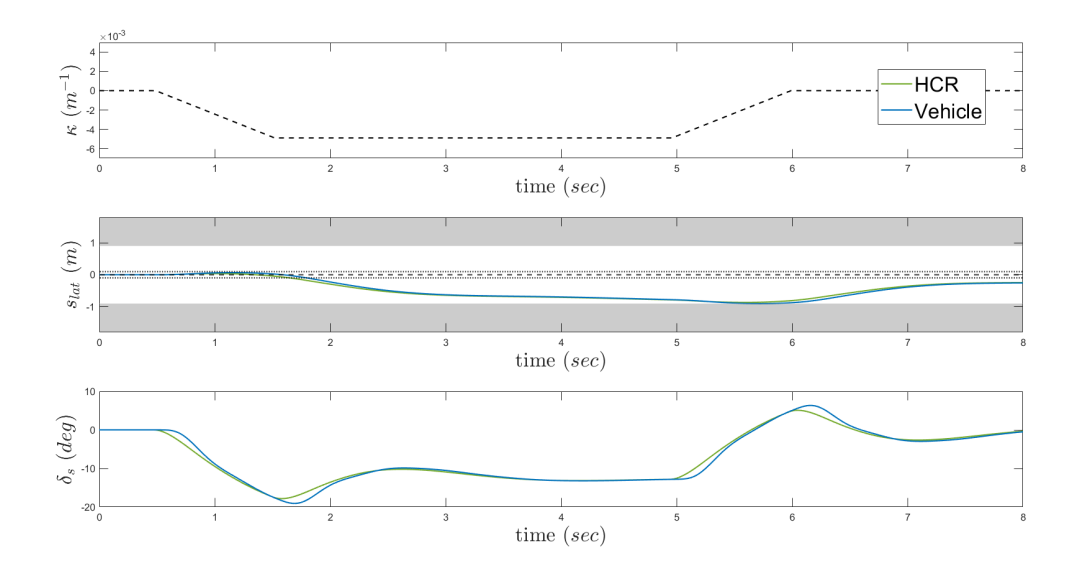


Figure 4.26: Outcome of simulations if driver does not give input on the steering wheel, curve cutting scenario.

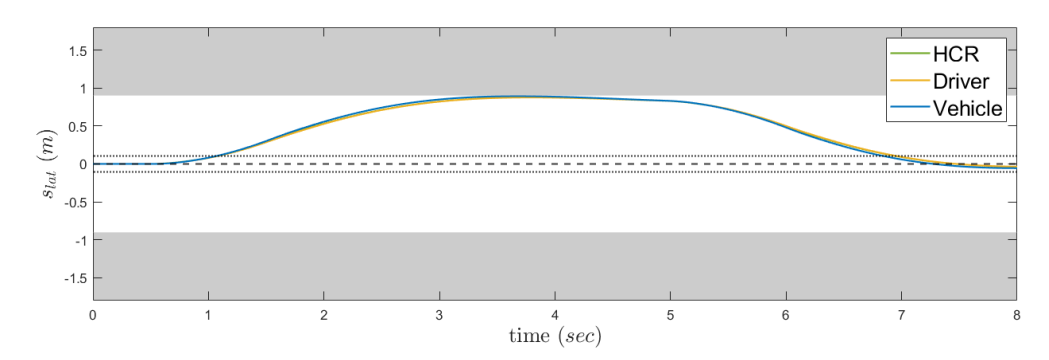


Figure 4.27: System test of the lowest conflictual case, illustration of counter curve cutting trajectory.

which block is activated and which is deactivated. In the event that both are activated – such as in the regular simulations – the code should be able to combine both inputs to reach a final vehicle state. It is therefore expected that the vehicle trajectory lies in the middle between both HCR and driver trajectory in case both have an equal share of influence (K_{co-dr} and K_{co-fdc} are both 0.5). The result of this test is depicted in Figure 4.28. The figure – as was foreseen – shows the vehicle trajectory to be more or less in the middle between both opposing trajectories. This test can also be expanded to other combinations of K_{co-dr} and K_{co-fdc} , to see if the collaboration between driver and FDCA develops correctly.

Two more scenarios are analysed to complete this verification. The first scenario is where K_{co-dr} and K_{co-fdc} respectively correspond to 0.75 and 0.25. It is expected that changing the equal share of influence to a greater influence for the driver results in the vehicle following a trajectory that lies closer to counter curve cutting than the trajectory presented in Figure 4.28. The result of this verification test is shown in Figure 4.29 and demonstrates that the simulations react accordingly to a change in collaboration ratio.

At last, the second scenario is tested to verify once more the proper functioning of the simulation code and the collaboration ratios. The opposite scenario of the previous test is generated. This means a K_{co-dr} of value 0.25 and a K_{co-fdc} that equals 0.75. Figure 4.30 shows a resulting vehicle trajectory that lies closely to the FDCA's preferred trajectory, as was expected from a simulation with this specific set of parameters.

4.4. Validation

Validation is equally necessary as verification and aims at answering the question 'Are we building the right product?', by questioning whether the model is an accurate representation of reality. In order to start valida-

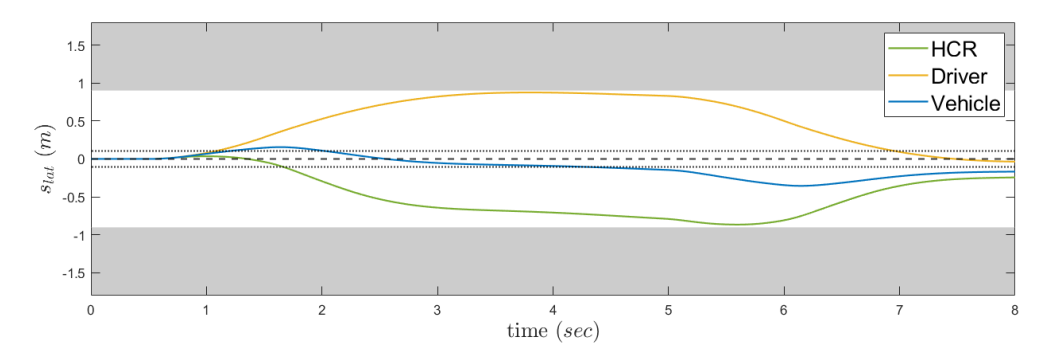


Figure 4.28: System test of the highest conflictual scenario, where the collaboration between driver and FDCA is $K_{co-dr} = K_{co-fdc} = 0.5$. Note that the "Vehicle" line corresponds to the combined, total result of the HCR and driver.

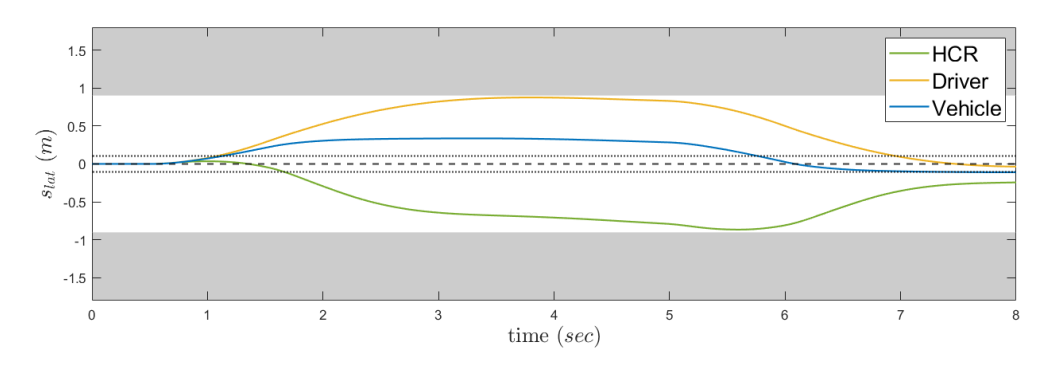


Figure 4.29: System test of the highest conflictual scenario, where K_{co-dr} and K_{co-fdc} respectively correspond to 0.75 and 0.25. Note that the "Vehicle" line corresponds to the combined, total result of the HCR and driver.

tion, verification must already have taken place. The best practise to validate a simulation code is to check the simulation output against real world or experiment output data. This real world and experiment data are, however, not yet available and thus validation is currently not possible. In later stages of this research, once the experiment data are available, the model can finally be validated.

Of course, it could be argued that because of the presence of an artifact of simulation, the simulations can never fully pass a validation test. Validation means comparing the simulation output to real-life data and checking if their behaviour corresponds. An artifact of simulation already indicates that this behaviour is very unlikely or even impossible to occur in reality, but that does not mean trends between cases cannot be accurately predicted.

4.5. Discussion

The simulation results presented in this chapter have shown that some of the outcomes are debatable. An artifact of simulation is present in the centerline behaviour of the driver model. An artifact of simulation indicates a certain type of behaviour showing in the simulations that does not occur in reality. In this particular case, the centerline driving model causes unrealistic oscillations in the internal torque of the system, leading to high and improbable conflict torque results. The proposed solution to this issue is the changing of the centerline gains, which in turn results in a trajectory with offset towards the counter curve cutting trajectory. Hence, this solution does not guarantee a realistic conflict torque analysis either. The largest cause of this behaviour is the selected driver model. Beforehand it was already known that the driver model had its limitations in the capturing of accurate driving behaviour since it lacks the capability to pre-position the vehicle ahead of a curve. It was decided to use the driver model from Saleh et al. (2013) as this is a rather well-know model, that has been used in combination with Haptic Shared Controllers before. However, due to the many shortcomings of the model, the validity of the conflict torques analysis is questioned.

Originally, the intention of the simulations was to gain a deeper understanding of the mechanics behind the Four-Design-Choice-Architecture and to construct some hypotheses for the experiment. Unfortunately

4.6. Conclusion 69

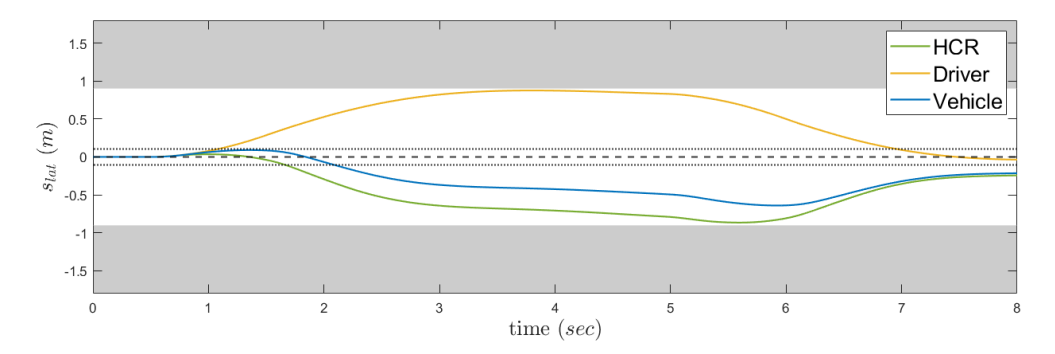


Figure 4.30: System test of the highest conflictual scenario, where K_{co-dr} and K_{co-fdc} respectively correspond to 0.25 and 0.75. Note that the "Vehicle" line corresponds to the combined, total result of the HCR and driver.

due to the nature of the driver model, only a few hypotheses can be deduced from the simulations. Mostly about the scenarios where the centerline is not involved. These simulations were a first attempt at implementing the driver model from Saleh et al. (2013) in the FDCA as both a replacement for the Driver and the HCR and it has been proven that this model is unsuited for any further simulations. It is recommended for future research to replace the driver model by a different model, preferably one that is able to capture prepositioning.

At last, a remark should be made about one of the biggest differences between the simulation and the experiment that will take place in the simulator. Whereas the simulations need a steering wheel angle to torque conversion (and vice versa) to close the loop, this conversion does not happen during the experiment in the simulator. The simulator measures the driver torque from the steering wheel directly and immediately uses this as input to the vehicle dynamics without any conversions. This might allow for the output of the experiment to differ from the simulations in some scenarios.

4.6. Conclusion

The goal of this chapter is to accurately recreate certain types of driver trajectories and to understand how these drivers react to different trajectory types of a Four-Design-Choice Controller. It is decided to use the driver model created by Saleh et al. (2013) and recreate three different types of drivers: a centerline driver, a curve cutting driver and a counter curve cutting driver. After these behaviours are fixed, the model is used both as Human Compatible Reference in the Four-Design-Choice-Architecture and as substitute for the driver himself/herself. In order to correctly join the driver and FDCA together, a correct method to convert steering wheel angle to torque and vice versa is found using a rotational mass-spring-damper system. At last, to optimise the reality of the system the previously compiled collaboration ratio's of driver and FDCA are included in the simulation.

The lateral position plots show vehicle trajectories resulting from the collaboration between driver and FDCA in line with the anticipated results from literature. If both parties prefer the same trajectory type, then the resulting vehicle trajectory is identical to their preferred type. If both driver and FDCA prefer a different type of trajectory, then both sides compromise which results in a vehicle trajectory that lies in between both respective trajectories. This compromised trajectory shows an inclination from the driver to follow the HCR more closely if the HCR is driving a more efficient trajectory. During an analysis of the conflict torques – where a conflict is defined as an occurrence of the driver and FDCA torque having opposing torques – this prediction is supported by a lower conflict torque and a lower conflict time. In case the driver inherently prefers a more efficient trajectory than the HCR, then the driver will fight the controller more intensely to raise the efficiency of the developing vehicle path.

During the analysis of conflict torques and conflict time percentages, it is remarked that all scenarios where the centerline is involved are afflicted with disproportionate amounts of conflict. It is found that this phenomenon is caused by the highly oscillating internal torques that arise when the centerline trajectory is being pursued. After a lowering of the centerline gains in an attempt to lower the oscillatory behaviour, the conflict torques and conflict time percentages are indeed lowered, however, the new centerline trajectory has a counter curve cutting inclination, which produces a bias in the conflict analysis. It is therefore concluded

to limit the use of the conflict analysis for the design of hypotheses.

As it should be in any simulation project, the code is subjected to verification and validation tests. After a set of unit and system tests, it is concluded that the system passes all requirements and is therefore verified. The validation of the code is more difficult as no data from reality or experiments are available. One could argue that because of the artifact of simulation present in the centerline trajectory, the simulation lacks the needed realism and therefore is not yet validated.

Proposal Final Experiment

In order to continue with the research and eventually answer the research question formulated in Chapter 3, an experiment must be conducted. This experiment will also further validate the simulations from Chapter 4. This chapter drafts a proposal for this experiment and aims at eliminating all possible confounding factors from the experiment and the subsequent results. The chapter discusses the used apparatus, the chosen subjects, the control task, the experiment design and the hypotheses to be tested.

5.1. Apparatus

The experiment will take place in the fixed-base driving simulation in the Human-Machine Interaction (HMI) Laboratory at the faculty of Aerospace Engineering at the Delft University of Technology. The experiment room – as the lab is split up in an experiment and observation room – consists of an aircraft and car side. For this experiment only the car side of the simulator will be used. The car side of the simulator consists of a control-loaded steering wheel, a 12" LCD instrument panel, an accelerator and brake pedal and an adjustable driver seat (Section Control & Simulation, 2020). Note that the accelerator and brake pedal will not be used in the experiment as the velocity of the vehicle is constant and fixed. A MOOG FCS Ecol18000S Actuator is used for generating haptic torques on the steering wheel and runs at a rate of 2500 Hz (Scholtens et al., 2018). Its stiffness is fixed at 1 Nm/rad, its damping coefficient at 0.03 Nms/rad and its inertia at 0.005 Nm/rad.

The road and scenery is projected using three projectors. Together these projectors have an 800×600 pixel resolution (Section Control & Simulation, 2020) and cover a Field of View (FoV) of $180^{\circ} \times 40^{\circ}$. The image generation delay of these projectors is 10 ms and they have an update rate of 50 Hz. The simulation itself has an update rate of 100 Hz (Vreugdenhil et al., 2019).

The scenery of the simulation shows a single lane road surrounded by a few trees. The road boundaries are marked with clear, visible lines to aid the participants of the experiment. The road itself consists of some straight sections and some curves both to the left and right. The vehicle simulated is a sedan of 1.8 m width with NISSAN vehicle dynamics that have already been used in previous experiments (Vreugdenhil et al., 2019). Note that to improve immersion also car sounds are added in the experiment.

5.2. Control Task

To optimise the amount of data gathered – as this will help generalise the outcome of the experiment – the experiment is split up in two large studies. In the first part, participants will be asked to drive manually over a certain trajectory, while for the second part, the haptic shared controller will assist them. Both the manual and Haptic Shared Control supported experiment consists of the same trajectory with identical conditions. The vehicle will have a fixed speed of 80 km/h and the drivers will be asked to follow a trajectory consisting of five left and five right clothoidal turns. These turns all have a radius of 204 m. In between the curves, straight stretches of road will be present to reset the drivers' positions on the road before curves.

The decision to keep the vehicle velocity constant at 80 km/h and the curve radius fixed at 204 m originated from previous research performed at the Delft University of Technology. Barendswaard et al. (2019a) also uses this combination of velocity and radius as it ensures a maximum centerline lateral acceleration

equal to $2.41 \ ms^{-2}$, which is the upper limit of allowed lateral acceleration for road design rules (Schofield, 2001). Surely other combinations of velocity and curve radius exist, however, this scenario is chosen as it most closely resembles a highway scenario. The velocity of the car is fixed in all experiments, which is not very realistic as people often brake in curves. However, at higher speeds and wider curves, driver may choose to use cruise control which fixes their speed as well. In other words, the fixing of the speed makes the experiments lose realism, but by selecting this combination of velocity and curve radius the realism factor is a bit heightened since drivers are more inclined to use cruise control in this setting.

5.3. Subjects and Instructions

To avoid procedural confounds, it is of major importance to select a homogeneous target group. From the Literature Survey in Chapter 2 follows that it is best to focus on one specific age group. Since elderly people suffer from the deterioration of their sensory, cognitive and psychomotor abilities – all factors which might influence their driving behaviour – it is opted to exclusively use younger people for participation in the experiment, preferably between the ages of 20 and 35. Limiting the subject group to younger drivers also eliminates the need to investigate gender differences as is concluded in Chapter 2. In other words, both men and women are allowed to participate in the experiment as gender is conjectured to cause no differences. At last, the level of expertise must be considered for the test subjects. Inexperience might lead to confounded results. Therefore it is desired that all test subjects have been in possession of a drivers license for at least one years. This period of time was decided based on Dutch regulations (ANWB). All participants will be instructed to operate the vehicle as they normally would and to maintain their hands on a "ten to two" position on the steering wheel.

5.4. Experiment Design

To optimally explain the experiment design, the manual and HSC experiment are explained separately. First, the manual experiment will take place in which drivers will be asked to drive the trajectory manually. There is only one experiment condition in this case, which is manual driving. This is a within-subjects design in which anyone in possession of a drivers license for over a year is allowed to partake. All drivers are asked to drive the same trajectory three times. All three times are completely identical. The first trial, however, is a training for the driver to avoid training and learning effects in the resulting data. Since the learning curve for this type of experiment is rather low, one trial run suffices to avoid confounds. Afterwards, the remaining two trials are completed. The data collected during these trials is the data that will be used for further analysis.

For each participant in this experiment, it is then determined to which trajectory type their curve negotiating performance matches. This analysis is performed for right and left curves separately as drivers might prefer a different negotiating class depending on the direction of the curve. This classification is accomplished with the help of a Matlab script that implements the rule-based classifier from Barendswaard et al. (2019a) to understand for each curve how many centerline transitions occur and how the vehicle is positioned at curve-entry. With this method each curve of each driver is fitted into one of the seven trajectory types. Each driver's final right and left classes are then determined by totalling which class is most prevalent per driver.

In order to reach a meaningful conclusion, it is decided to limit the amount of experiment conditions for the second part of the experiment. In this part, the drivers will become subjected to several different trajectory classes that try to guide them through the curves. To optimise the utility of the results, it is important to include drivers that match the classes in the HCR and drivers that do not match these. The exact experiment conditions are decided with the help of Figure 5.1. This figure shows the classification results of the research by Barendswaard et al. (2019a), which was also conducted in the HMI Lab at the faculty of Aerospace Engineering, in the form of a heatmap. The map shows the distribution of the drivers over the different classes. It is clearly visible that most drivers do not favour the same path in left and right curves. Moreover, for right curves most drivers follow rather efficient trajectories – such as class 2 and 3 – while the results for left curves are a bit more divided. In total 45 drivers participated in the experiment and it seems that most of those (16 drivers, so 36%) prefer class 3 for right curves and class 5 for left curves. Also a notable trend is present in the more optimal regions, as many driver prefer class 2 for right curves combined with class 1, 2 or 3 for their left curves.

With the help of Figure 5.1, it is decided that both right class 3, left class 5, or R3L5, and right class 2, left class 1, or R2L1 are the two most meaningful class combinations to use in any further experiments. R3L5 is meaningful as most drivers fall into this combined class, while R2L1 is meaningful due to it being the most

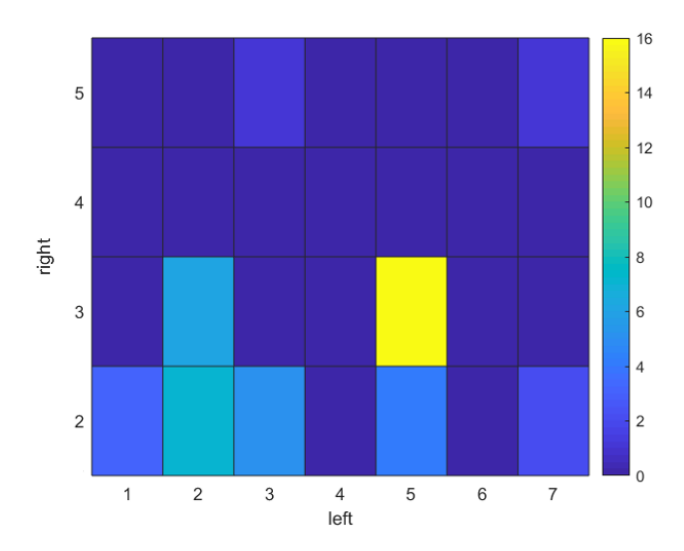


Figure 5.1: Classification results of manual driving behaviour, research by Barendswaard et al. (2019a).

"optimal" driving combination that occurs. This as the R1L1 combination is completely empty. In the simulations it was found that drivers more willingly follow optimal trajectories and fight less optimal trajectories, so including an optimal trajectory helps validating this finding. It is therefore decided to only continue to the second part of the experiment with driver that either fall into the R3L5 or R2L1 category. Finding drivers that fit into the R3L5 category should not pose any problems, as they seem to make up about 36% of all drivers. Finding R2L1 drivers on the other hand might turn out to be a bit trickier as only 7% of drivers fits this class. In terms of experiment conditions, it is decided to test only four conditions: an HCR with R3L5 behaviour, an HCR with R2L1 behaviour, a replay of the drivers own trajectory, which represents utmost individualisation and an R4L4 HCR which is the baseline condition as it represents the industry standard. Of course, there is no way to know if drivers actually like their own driving style. This then leads to the experiment matrix as is presented in Table 5.1. Note that this second part of the experiment is also within-subjects.

P1 P2 Р3 **P4** ••• Training R3L5 R4L4 R2L1 own R2L1 R3L5 R4L4 own ... Repetition 1 own R2L1 R3L5 R4L4 ... R4L4 R2L1 R3L5 own ... Break R2L1 own R3L5 R4L4 ... R2L1 R4L4 own R3L5 ... Repetition 2 R3L5 R4L4 own R2L1 ... R2L1 R3L5 R4L4 own ... Break R2L1 R3L5 R4L4 own own R2L1 R3L5 R4L4 ... Repetition 3 R2L1 R3L5 R4L4 own ••• R3L5 R4L4 own R2L1

Table 5.1: Experiment matrix for the second part of the experiment.

Due to the within-subjects design of the experiments, it is preferred to have at least 6 drivers per category. Important to note, the HCR for the R3L5 and R2L1 categories is generated using data from Barendswaard et al. (2019a) and is formed by use of generic references as explained in Chapter 2. The last step before beginning

experiments is to draft some hypotheses to help the analysis of the data.

5.5. Hypotheses

In order to efficiently draw conclusions from the experiment, hypotheses are outlined. The experiment data will either confirm or reject these hypotheses and so help to answer the research question. To ensure a holistic approach and not miss anything of great importance, hypotheses should be established for both experiments and preferable even for each experiment condition. It was the original intention of this preliminary research to base most of the hypotheses on the outcome of the simulations from Chapter 4. However due to the artifact of simulation present in the simulations, this now seems much more complicated and sometimes even inaccurate. Therefore it is decided to only use the simulation outcomes when no centerline is involved and further rely on literature to complete the hypotheses.

In total three hypotheses have been derived. All of them are listed below along with their respective reasoning:

1. The averaged class HCR of the natural driving class of the driver and the replay of the own trajectory will lead to equal values of subjective usefulness and satisfaction scores from the Van Der Laan Questionnaire, indicating an equal subjective acceptance.

This hypothesis is based on the research by Griesche et al. (2016), which concluded that drivers like their own trajectory as reference trajectory of a semi-automated system equally much as a similar trajectory. That is why the second part of the experiment should include an HCR which is an exact replay of the drivers natural driving and an HCR based on a generic reference of the class the driver falls in. As the own trajectory should in theory be very similar to the class average, it is assumed that they will be liked equally much. Indeed this would also ease the individualisation issue as complete individualisation would not be necessary. Then it would be sufficient to only provide the seven trajectory classes defined by Barendswaard et al. (2019a).

2. When the HCR has a more optimal trajectory in terms of TLC than the driver's natural driving, then the conflict torque will be less and the acceptance increased.

The analysis of the conflict torques in the simulations from Chapter 4 has shown that a driver is likely to resist the controller less if the controller is driving a more efficient trajectory than the driver normally would. The opposite also holds true, the conflict torques will increase if the driver normally drives an efficient trajectory, but the HCR is programmed to follow a less optimal trajectory. Since the driver will fight the automation, the conflict torques rise. Note that efficiency is defined by a lower lateral acceleration and larger TLC.

3. The centerline HCR will cause the largest amounts of driver torque compared to all other conditions and lead to a low acceptance rate.

The centerline HCR is the most simple one. It is also the industry favourite implementation when designing an automated system and many controllers still use the centerline trajectory as a baseline (Mulder et al., 2008). However as literature shows, centerline driving does not come natural to drivers (Barendswaard et al., 2019a) and drivers do prefer similar driving styles in their controllers (Griesche et al., 2016). In all likelihood, drivers will thus fight the centerline guidance in order to avoid following this trajectory. This might lead to high driver torques. It should also be noted that the centerline trajectory is not efficient in terms of lateral acceleration or TLC, which might be an extra cause of driver torques.

6

Conclusion

This report contains a research proposal for a master thesis on the personalisation of trajectory-driven haptic shared control. The literature survey has showed that semi-automated systems in cars are becoming increasingly popular. Since haptic shared control offers a solution in which both driver and controller communicate to each other through the steering wheel, a lot of research is currently being performed in this area. The most optimal structure and working of the controller has been already found by (Scholtens et al., 2018), however, the question remains if haptic shared control can be made more accessible to the drivers. The main problem is that is has not been researched yet how drivers react to individualisation in the haptic shared controllers, especially in the tuning of the controller's reference trajectory. The main question therefore asks how different reference trajectories of the controller lead to different levels of acceptance with different types of drivers.

This master thesis aims at answering this question by means of a realistic simulation and an experiment. The intent behind the simulations is to deepen the understanding of the Four-Design-Choice-Architecture and to set expectations for the experiment. However, due to an unforeseen artifact of simulation in the centerline trajectory of the driver model, the simulations are less relevant than hoped. The report continues to the proposal of an experiment in which different types of drivers will be subjected to different programmed reference trajectories. Both the subjective and objective reactions of the drivers will be measured to understand what level of personalisation results in the highest level of acceptance.

- D.A. Abbink, M. Mulder, and E.R. Boer. Haptic shared control: smoothly shifting control authority? *Cognition, Technology Work*, 14(1):19–28, 2012. doi: https://doi.org/10.1007/s10111-011-0192-5.
- E. Adell. *Driver Experience and Acceptance of Driver Support Systems A Case of Speed Adaptation*. PhD thesis, Department of Technology and Society, Lund University, 2009. URL http://lup.lub.lu.se/record/1504012.
- A. Aksjonov, P. Nedoma, V. Vodovozov, E. Petlenkov, and M. Herrmann. A novel driver performance model based on machine learning. *15th IFAC Symposium on Control in Transportaion Systems*, 51(9):267–272, 2018. doi: 10.1016/j.ifacol.2018.07.044.
- Algemene Nederlandse Wielrijdersbond (ANWB). Beginnend bestuurder, 2019. URL https://www.anwb.nl/auto/rijbewijs/het-rijbewijs/beginnend-bestuurder.
- L. Bainbridge. Ironies of automation. *Automatica*, 19(6):775–779, 1983. doi: https://doi.org/10.1016/0005-1098(83)90046-8.
- S. Barendswaard, D.M. Pool, and D.A. Abbink. A method to assess individualized driver models: Descriptiveness, identifiability and realism. *Transportation Research Part F*, 61:16–29, 2018. doi: https://doi.org/10.1016/j.trf.2018.02.014.
- S. Barendswaard, D.M. Pool, E.R. Boer, and D.A. Abbink. A classification method for driver trajectories during curve-negotiation. *2019 IEEE International Conference on Systems, Man, and Cybernetics (SMC)*, pages 3729–3734, 2019a. doi: 10.1109/SMC.2019.8914301.
- S. Barendswaard, L. van Breugel, B. Schelfaut, J. Sluijter, L. Zuiker, D.M. Pool, E.R. Boer, and D.A. Abbink. Effect of velocity and curve radius on driver steering behaviour before curve entry. *2019 IEEE International Conference on Systems, Man and Cybernetics (SMC)*, pages 3866–3871, 2019b. doi: 10.1109/SMC.2019.8914263.
- A.E. Barrett, C. Gumber, and R. Dougles. Explaining gender differences in selfregulated driving: what roles do health limitations and driving alternatives play? *Ageing & Society*, 38(10):2122–2145, 2018. doi: https://doi.org/10.1017/S0144686X17000538.
- E.R. Boer. Tangent point oriented curve negotiation. *Proceedings of the 1996 IEEE Intelligent Vehicles Symposium*, pages 7–12, 1996. doi: https://doi.org/10.1109/IVS.1996.566341.
- R. Boink, M.M. van Paassen, M. Mulder, and D.A. Abbink. Understanding and reducing conflicts between driver and haptic shared control. *IEEE International Conference on Systems, Man, and Cybernetics (SMC)*, pages 1510–1515, 2014. doi: https://doi.org/10.1109/SMC.2014.6974130.
- J. Büskens, D.M. Pool, J.J.M. Pel, and M. Mulder. Quantifying ageing effect on gaze dynamics using an eye-only and an eye-hand tracking pursuit task. Master's thesis, Control & Simulation, Department Control and Operations, Faculty of Aerospace Engineering, Delft University of Technology and Erasmus MC department of Neuroscience Rotterdam, 2012.
- S.J. Czaja, N. Charness, A.D. Fisk, C. Hertzog, S.N. Nair, W.A. Rogers, and J.Sharit. Factors predicting the use of technology: Findings from the center for research and education on aging and technology enhancement (create). *Psychology and Aging*, 21(2):333–352, 2006. doi: https://doi.org/10.1037/0882-7974.21.2.333.
- D.W. Eby, D.A. Trombley, L.J. Molnar, and J.T. Shope. The assessment of older drivers' capabilities: A review of the literature. Technical report, The University of Michigan Transportation Research Institute, http://hdl.handle.net/2027.42/1245, 1998.

A. Furlan, B. Vrkljan, H.H. Abbas, J. Babineau, J. Campos, S. Haghzare, T. Kajaks, M. Tiong, M. Vo, and M. Lavalliere. The impact of advanced vehicle technologies on older driver safety: A scoping review of subjective outcomes, 2018.

- H. Godthelp, P. Milgram, and G.J. Blaauw. The development of a time-related measure to describe driving strategy. *Human Factors The Journal of the Human Factors and Ergonomics Society*, 26(3):257–268, 1984. doi: https://doi.org/10.1177/001872088402600302.
- S. Griesche, E. Nicolay, D. Assmann, M. Dotzauer, and D. Kätner. Should my car drive as i do? what kind of driving style do drivers prefer for the design of automated driving functions? In *Braunscheiger Symposium Automatisieringssysteme*, *Assistenzsysteme und eingebettete Systeme für Transportmittel (AAET)*, pages 185–204. Deutches Zentrum für Luft- und Raumfahrt e.V., February 2016. ISBN 978-3-937655-37-6.
- P.G. Griffiths and R.B. Gillespie. Sharing control between humans and automation using haptic interface: Primary and secondary task performance benefits. *Human Factors: The Journal of the Human Factors and Ergonomics Society*, 47(3):574–590, 2005. doi: 10.1518/001872005774859944.
- F. Hartwich, M. Beggiato, and J.F. Krems. Driving comfort, enjoyment and acceptance of automated driving effects of drivers' age and driving style familiarity. *Ergonomics*, 61(8):1017–1032, 2018. doi: https://doi.org/10.1080/00140139.2018.1441448.
- M. Kyriakidis, J. C. F. de Winter, N. Stanton, T. Bellet, B. van Arem, K. Brookhuis, M. H. Martens, K. Bengler, J. Andersson, N. Merat, N. Reed, M. Flament, M. Hagenzieker, and R. Happee. A human factors perspective on automated driving. *Theoretical Issues in Ergonomics Science*, 20(3):223–249, 2019. doi: https://doi.org/10.1080/1463922X.2017.1293187.
- W.A. Macdonald and E.R. Hoffmann. Review of relationships between steering wheel reversal rate and driving task demand. *Human Factors*, 22(6):733–739, 1980. doi: https://doi.org/10.1177/001872088002200609.
- E Mars, L. Saleh, F. Chevrel, F. Claveau, and J. Lafay. Modeling the visual and motor control of steering with an eye to shared-control automation. *Human Factors and Ergonomics Society, 55th Annual Meeting*, 55(1): 1422–1426, 2011. doi: 10.1177/1071181311551296.
- F. Mars, M. Deroo, and J. Hoc. Analysis of human-machine cooperation when driving with different degrees of haptic shared control. *IEEE Transactions on Haptics*, 7(3):324–333, 2014. doi: https://doi.org/10.1109/TOH.2013.229509.
- H. Middleton, D. Westwood, J. Robson, and D. Kok. Assessment and decision criteria for driving competence in the elderly. In G. Underwood, editor, *Traffic and Transport Psychology: Theory and Application*, chapter 9, pages 101–113. Elsevier, 2005.
- L.J. Molnar, D.W. Eby, J.L. Charlton, J. Langford, S. Koppel, S. Marshall, and M. Man-Son-Hing. Driving avoidance by older adults: Is it always self-regulation? *Accident Analysis and Prevention*, 57:96–104, 2013. doi: https://doi.org/10.1016/j.aap.2013.04.010.
- M. Mulder and D.A. Abbink. Sharing control with elderly drivers: Haptic guidance during curve negotiation. *IFAC Proceedings Volumes*, 2010.
- M. Mulder, D.A. Abbink, and E.R. Boer. The effect of haptic guidance on curve negotiation behavior of young, experienced drivers. *2008 IEEE International Conference on Systems, Man and Cybernetics (SMC 2008)*, pages 804–809, 2008.
- M. Mulder, D.A. Abbink, and E.R. Boer. Sharing control with haptics: Seamless driver support from manual to automatic control. *Human Factors and Ergonomics Society*, 54(5):786–798, 2012. doi: https://doi.org/10.1177/0018720812443984.
- A.B. Newman and J.A. Cauley. The Epidemiology of Aging. Springer, 2012. doi: 10.1007/978-94-007-5061-6.
- B. Pano, Y. Zhao, P. Chevrel, F. Claveau, and F. Mars. Shared control based on an ecological feedforward and a driver model based feedback. *9th IFAC International Symposium on Advances in Automotive Control*, 2019. doi: hal-02110825.

S.M. Petermeijer, D.A. Abbink, M. Mulder, and J.C.F. De Winter. The effect of haptic support systems on driver performance: A literature survey. *IEEE Transactions on Haptics*, 8(4):467–479, 2015. doi: 10.1109/TOH. 2015.2437871.

- E. Polders, T. Brijs, E. Vlahogianni, E. Papadimitriou, G. Yannis, F. Leopold, C. Durso, and K. Diamandouros. Eldersafe risks and countermeasures for road traffic of elderly in europe. Technical report, European Commission Directorate-General for mobility and transport (DG-MOVE), https://uhdspace.uhasselt.be/dspace/handle/1942/21056, 2015.
- L. Saleh, P. Chevrel, F. Mars, J. Lafay, and F. Claveau. Human-like cybernetic driver model for lane keeping. *IFAC Proceedings Volumes*, 44(1):4368–4373, 2011. doi: https://doi.org/10.3182/20110828-6-IT-1002.02349.
- L. Saleh, P. Chevrel, F. Claveau, J. Lafay, and F. Mars. Shared steering control between a driver and an automation: Stability in the presence of driver behavior uncertainty. *IEEE Transactions on Intelligent Transportation Systems*, 14(2):974 983, 2013. doi: https://doi.org/10.1109/TITS.2013.2248363.
- W. Schofield. Engineering surveying theory and examination problems for students, 2001.
- W. Scholtens, S. Barendswaard, D.M. Pool, M.M. van Paassen, and D.A. Abbink. A new haptic shared controller reducint steering conflicts. *2018 IEEE International Conference on Systems, Man, and Cybernetics (SMC)*, pages 2705–2710, 2018. doi: https://doi.org/10.1109/SMC.2018.00462.
- Delft University of Technology Section Control & Simulation, Faculty of Aerospace Engineering. Hmi lab overview, 2020. URL http://cs.lr.tudelft.nl/facilities/hmi-lab/.
- P. Spacek. Track behavior in curve areas: Attempt at typology. *Journal of Transportation Engineering*, 131(9): 669–676, 2005. doi: https://doi.org/10.1061/(ASCE)0733-947X(2005)131:9(669).
- D.L. Strayer and F.A. Drews. Profiles in driver distraction: Effects of cell phone conversations on younger and older drivers. *Human Factors*, 46(4):640–649, 2004. doi: https://doi.org/10.1518/hfes.46.4.640.56806.
- M. Sundbom, P. Falcone, and J. Sjöberg. Online driver behaviour classification using probabilistic arx models. *International IEEE Conference on Intelligent Transportation Systems (ITSC 2013)*, 16:1107–1112, 2013. doi: https://doi.org/10.1109/ITSC.2013.6728380.
- N. Trübswetter and K. Bengler. Why should i use adas? advanced driver assistance systems and the elderly: Knowledge, experience and usage barriers, 2013.
- K. van der El, D.M. Pool, and M. Mulder. Measuring and modeling driver steering behavior: From compensatory tracking to curve driving. *Transportation Research Part F: Traffic Psychology and Behaviour*, 61: 337–346, 2019. doi: 10.1016/j.trf.2017.09.011.
- J. van der Laan, A. Heino, and D. de Waard. A simple procedure for the assessment of acceptance of advance transport telematics. *Transportation Research Part C: Emerging Technologies*, 5(1):1–10, 1997. doi: https://doi.org/10.1016/S0968-090X(96)00025-3.
- M.M. van Paassen. Heidegger versus carthesian dualism or where is my hammer? *Proceedings of the IEEE International Conference on Systems, Man and Cybernetics*, pages 1684–1688, 2010. doi: https://doi.org/10.1109/ICSMC.2010.5642318.
- M.M. van Paassen, R.P. Boink, D.A. Abbink, M. Mulder, and M. Mulder and. Four design choices for haptic shared control. In M.A. Vidulich, P.S. Tsang, and J. Flach, editors, *Advances in Aviation Psychology, Volume* 2 - Using Scientific Methods to Address Practical Human Factors Needs, chapter 12, pages 237–254. Oxford University Press, Routhledge New York, NY, 2017.
- W. van Winsum, K.A. Brookhuis, and D. de Waard. A comparison of different ways to approximate time-to-linecrossing (tlc) during car driving. *Accident Analysis & Prevention*, 32(1):47–56, 2000. doi: https://doi.org/10.1016/S0001-4575(99)00048-2.
- W. Vreugdenhil, S. Barendswaard, S.M. Petermeijer, C. Borst, and D.A. Abbink. Complementing automotive haptic shared control with visual feedback for obstacle avoidance. Master's thesis, Faculty of Mechanical Engineering, Delft University of Technology, 2019.

G.H. Walker, N.A. Stanton, and M.S. Young. Where is computing driving cars. *International Journal of Human-Computer Interaction*, 13(2):203–229, 2001. doi: https://doi.org/10.1207/S15327590IJHC1302_7.

- R. Yuan-Yuan, Z. Hong-Wei, L. Xian-Sheng, and Z. Xue-Lian. Study on vehicle track model in road curved section based on vehicle dynamic characteristics. *Mathematical Problems in Engineering*, 2012:1–17, 2012. doi: https://doi.org/10.1155/2012/818136.
- T. Özkan and T. Lajunen. What causes the differences in driving between young men and women? the effects of gender roles and sex on young drivers' driving behaviour and self-assessment of skills. *Transportation research part F: Traffic psychology and behaviour*, 9(4):269–277, 2006. doi: https://doi.org/10.1016/j.trf. 2006.01.005.



Simulation Results

This Chapter displays the results of the original simulations that were not displayed in Section 4.2.

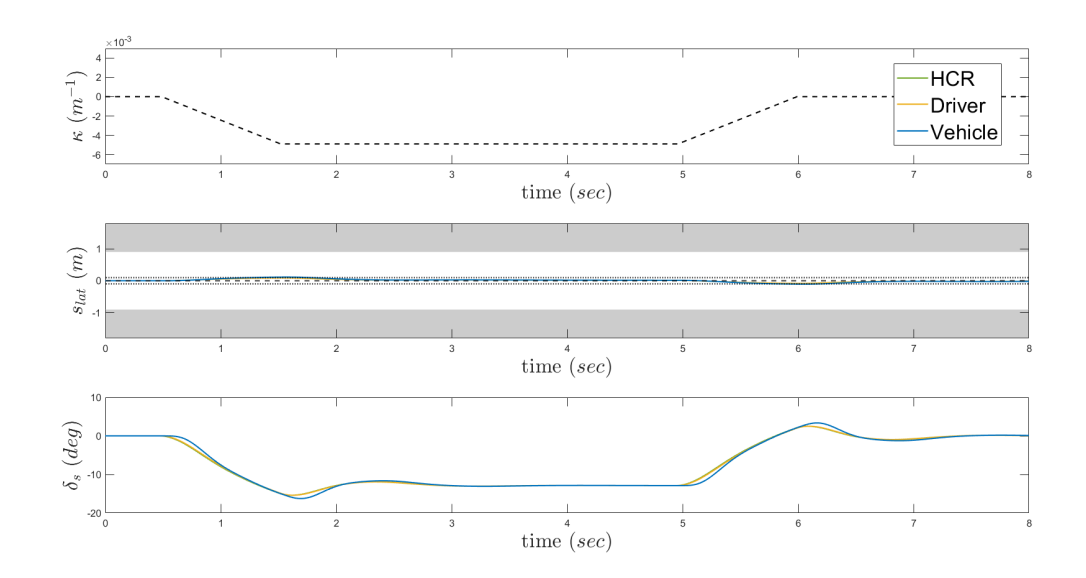


Figure A.1: Simulation result of both HCR and driver following a centerline path.

A. Simulation Results

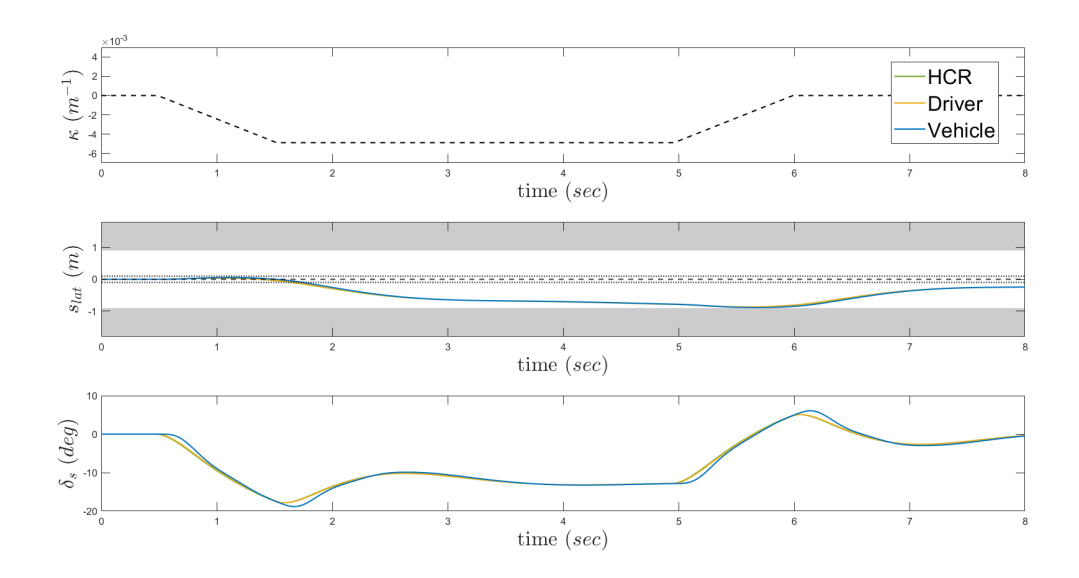


Figure A.2: Simulation result of both HCR and driver following a centerline path.

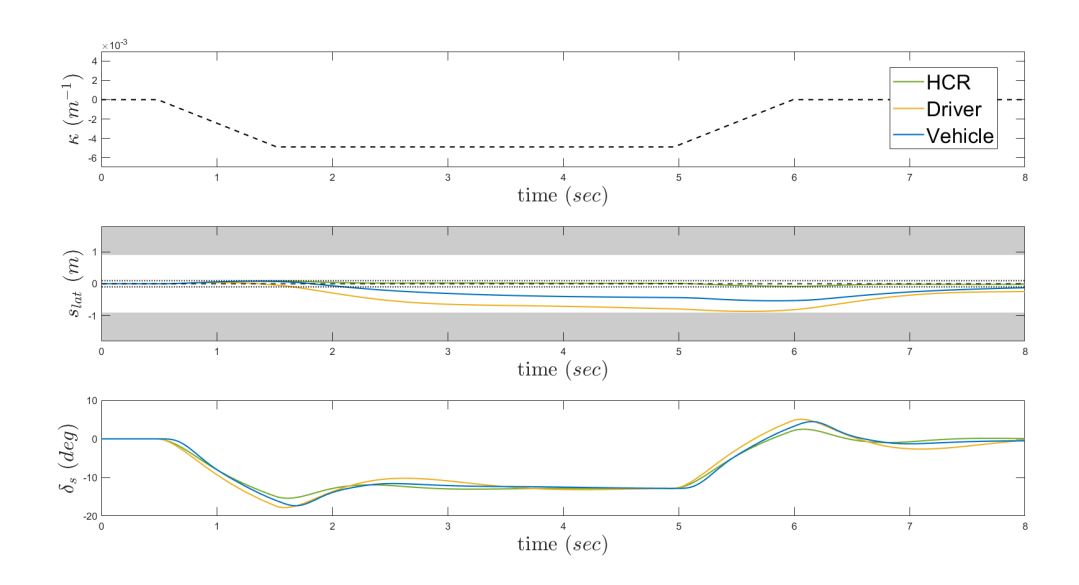


Figure A.3: Simulation result of HCR driving centerline and driver following a curve cutting trajectory.

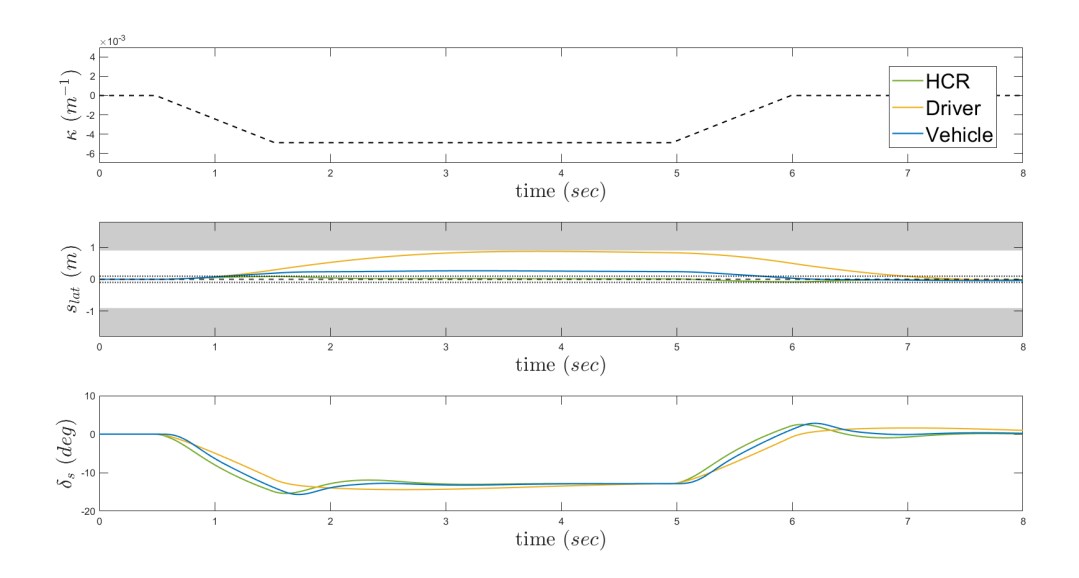


Figure A.4: Simulation result of HCR driving centerline and driver following a counter curve cutting trajectory.

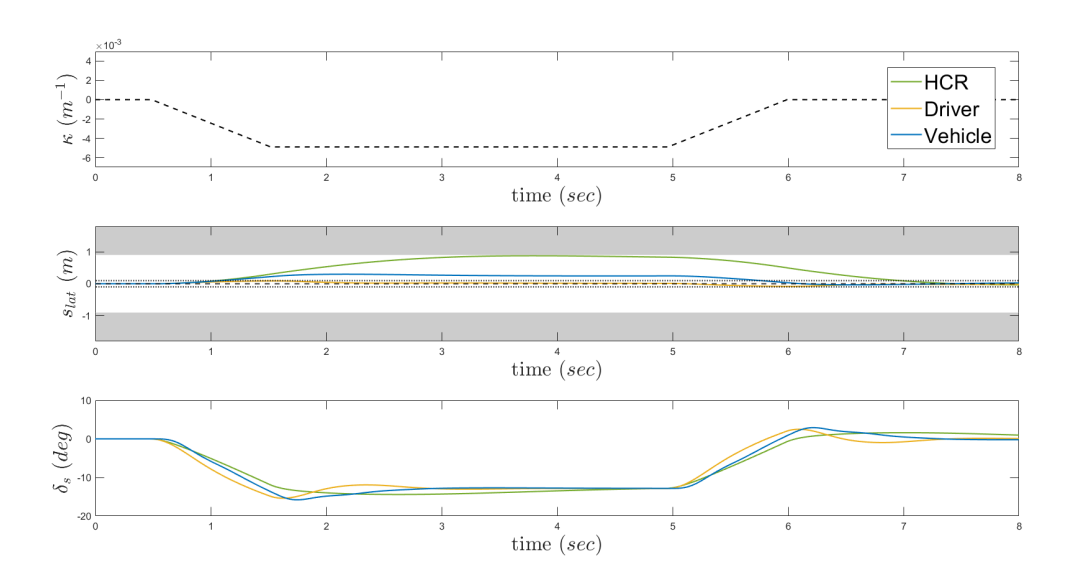


Figure A.5: Simulation result of HCR driving a counter curve cutting trajectory and driver following a centerline trajectory.



Individual Driver Results

This appendix contains the results of the haptic shared control experiment per individual driver.

R2L1 Driver 1 - FF 0.5

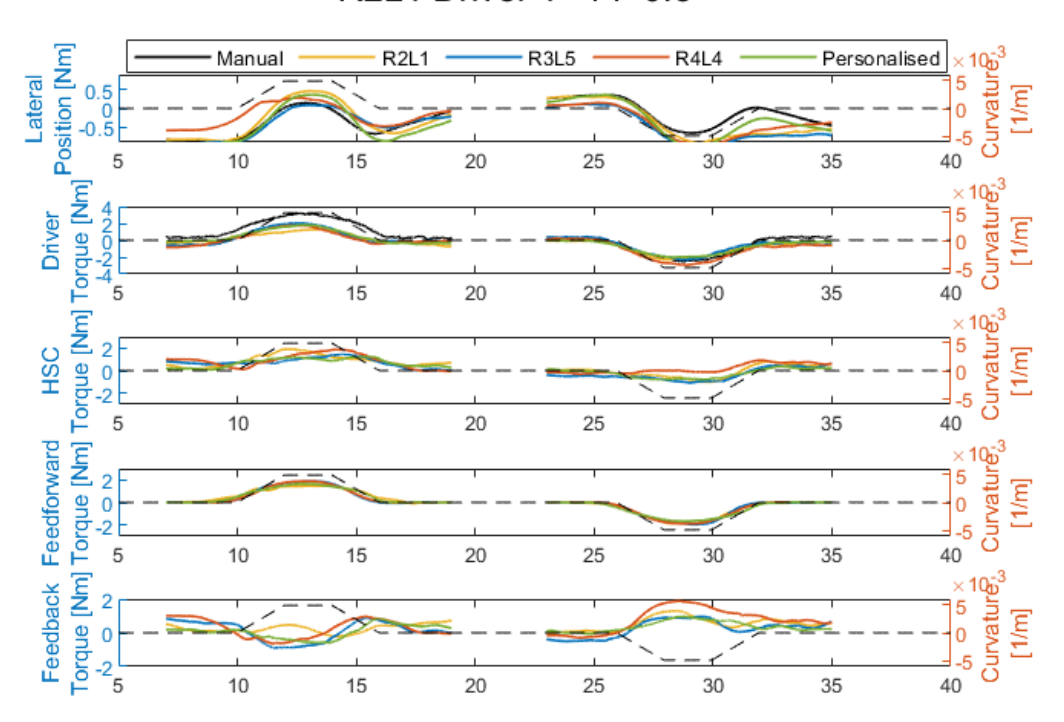


Figure B.1: Timeseries R2L1 driver 1 – FF 0.5

R2L2 Driver 7 - FF 0.5

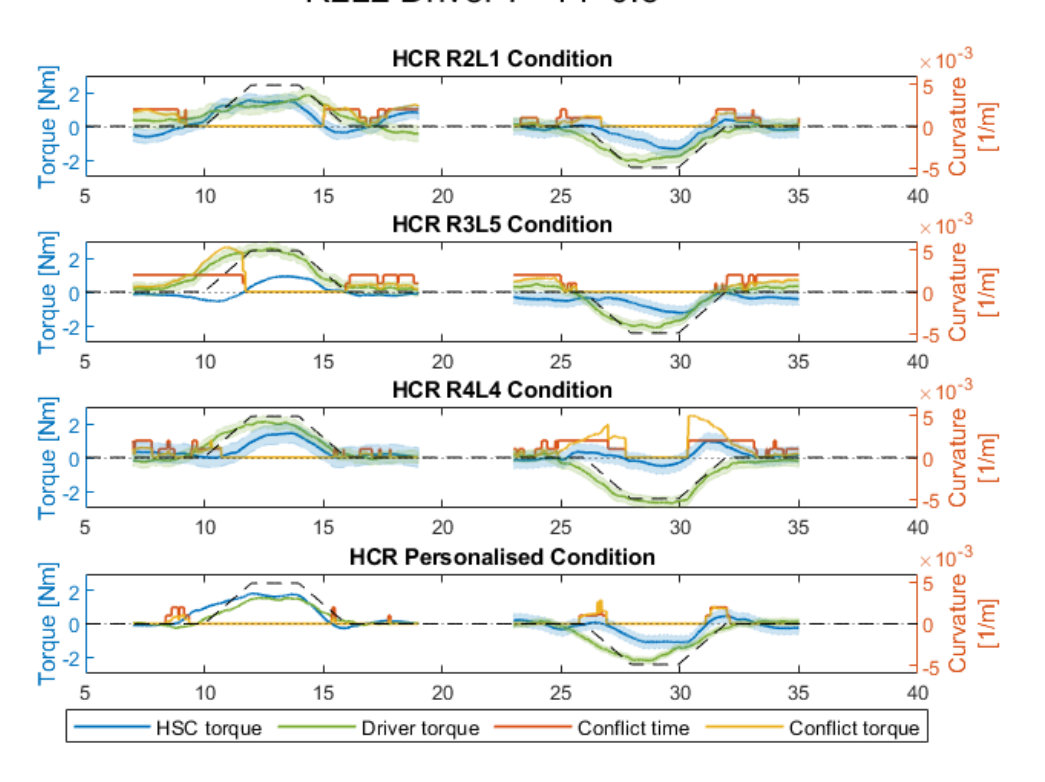


Figure B.54: Timeseries of conflict R2L2 driver 7 – FF 0.5

R2L1 Driver 1 - FF 0.5

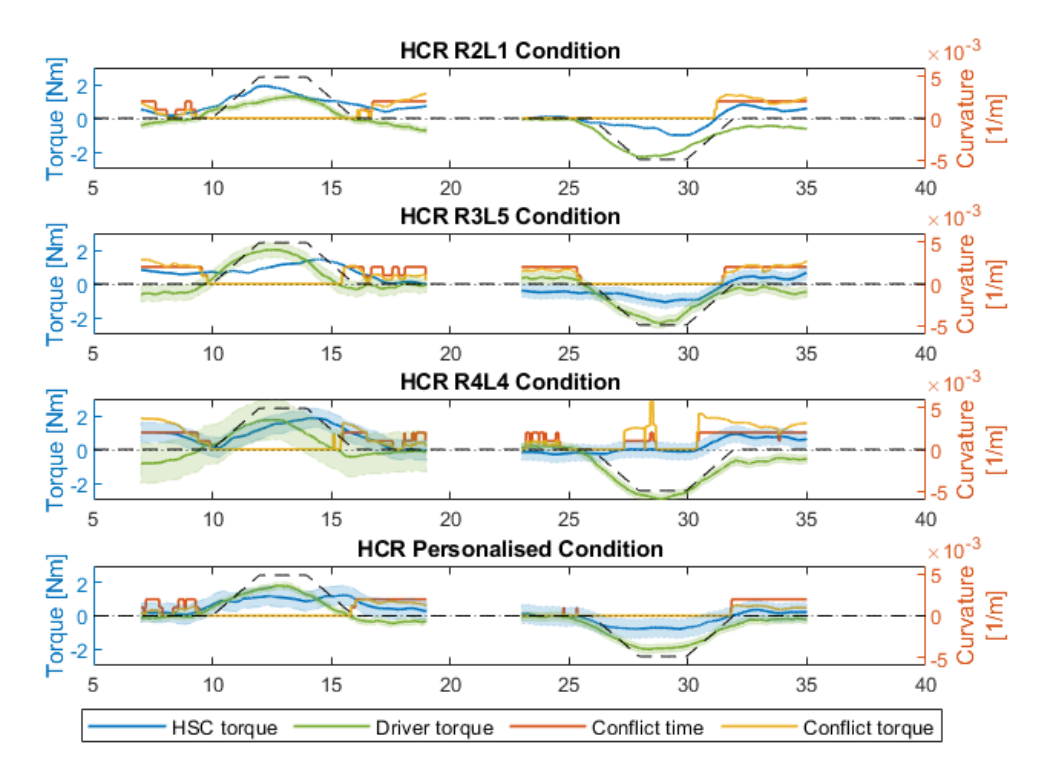


Figure B.2: Timeseries of conflict R2L1 driver 1 - FF 0.5

R2L1 Driver 1 - FF 0.92

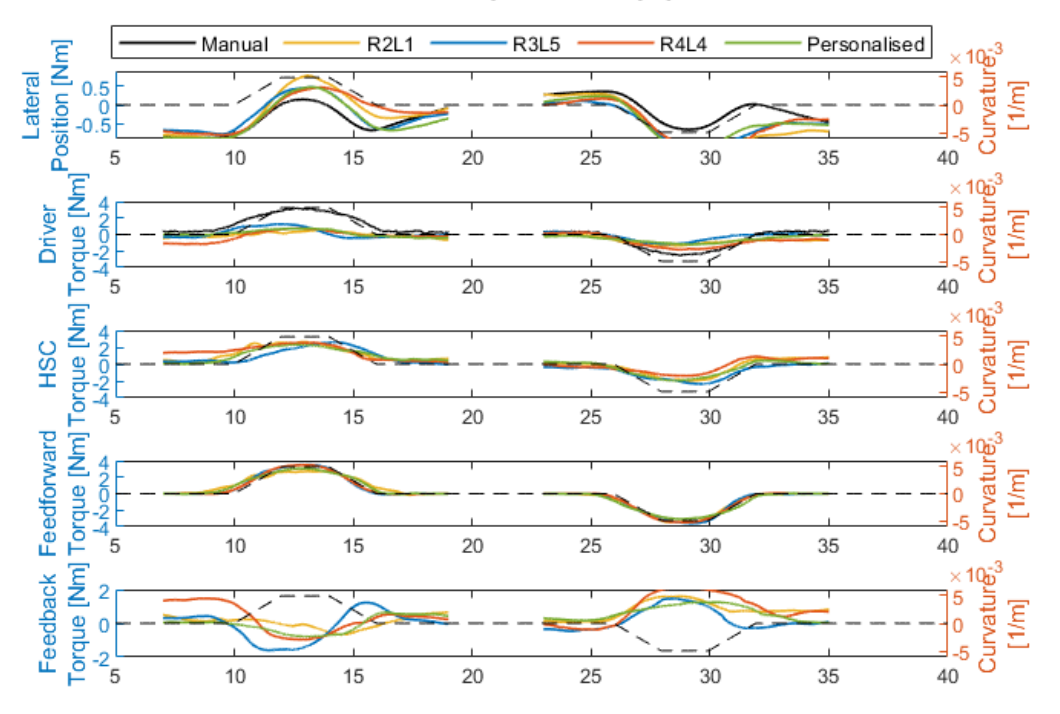


Figure B.3: Timeseries R2L1 driver 1 – FF 0.92

R2L1 Driver 1 - FF 0.92

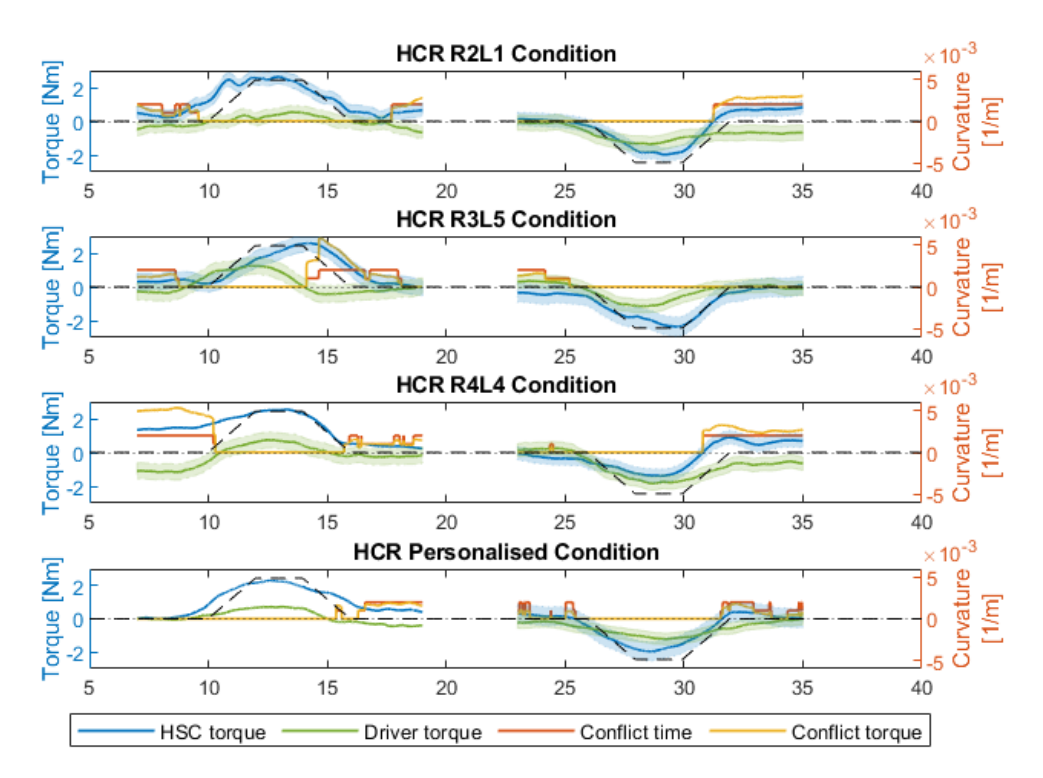


Figure B.4: Timeseries of conflict R2L1 driver $1-FF\ 0.92$

R2L1 Driver 2 - FF 0.5

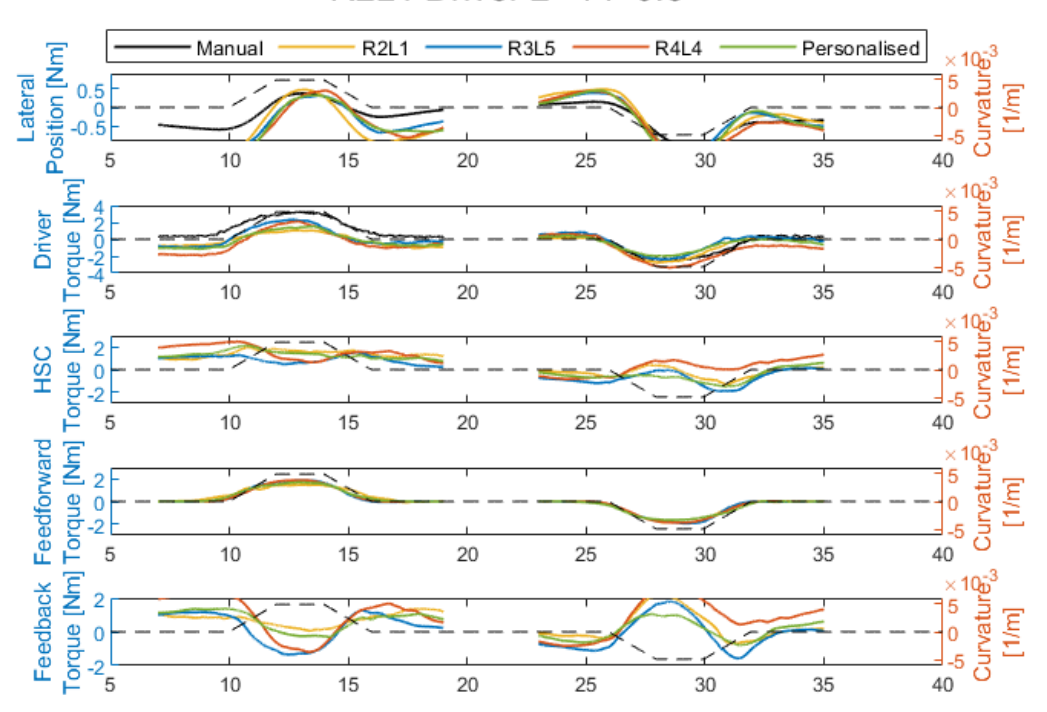


Figure B.5: Timeseries R2L1 driver 2 - FF 0.5

R2L1 Driver 2 - FF 0.5

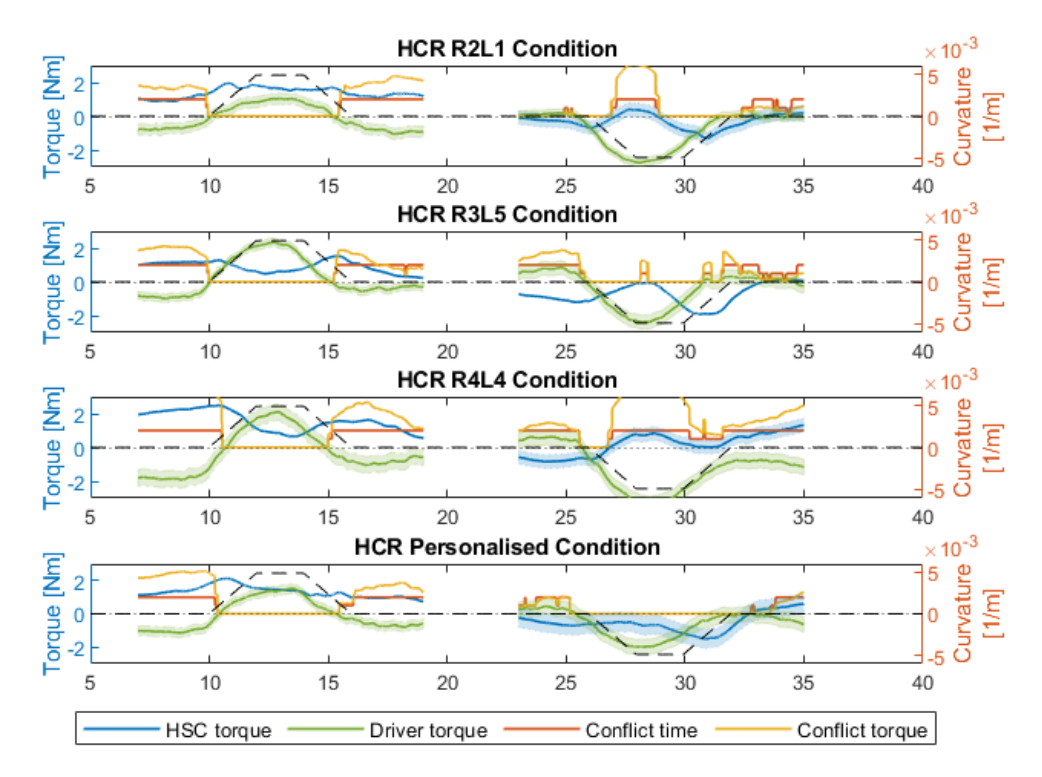


Figure B.6: Timeseries of conflict R2L1 driver 2 – FF 0.5

R2L1 Driver 2 - FF 0.92

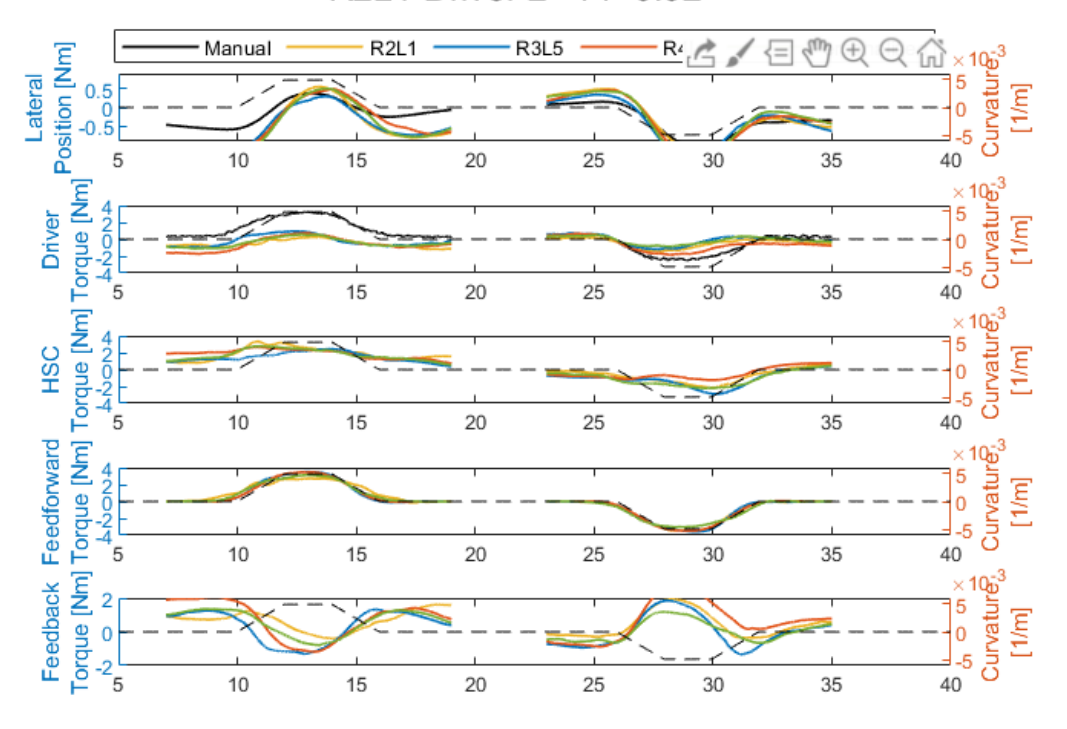


Figure B.7: Timeseries R2L1 driver 2 – FF 0.92

R2L1 Driver 2 - FF 0.92

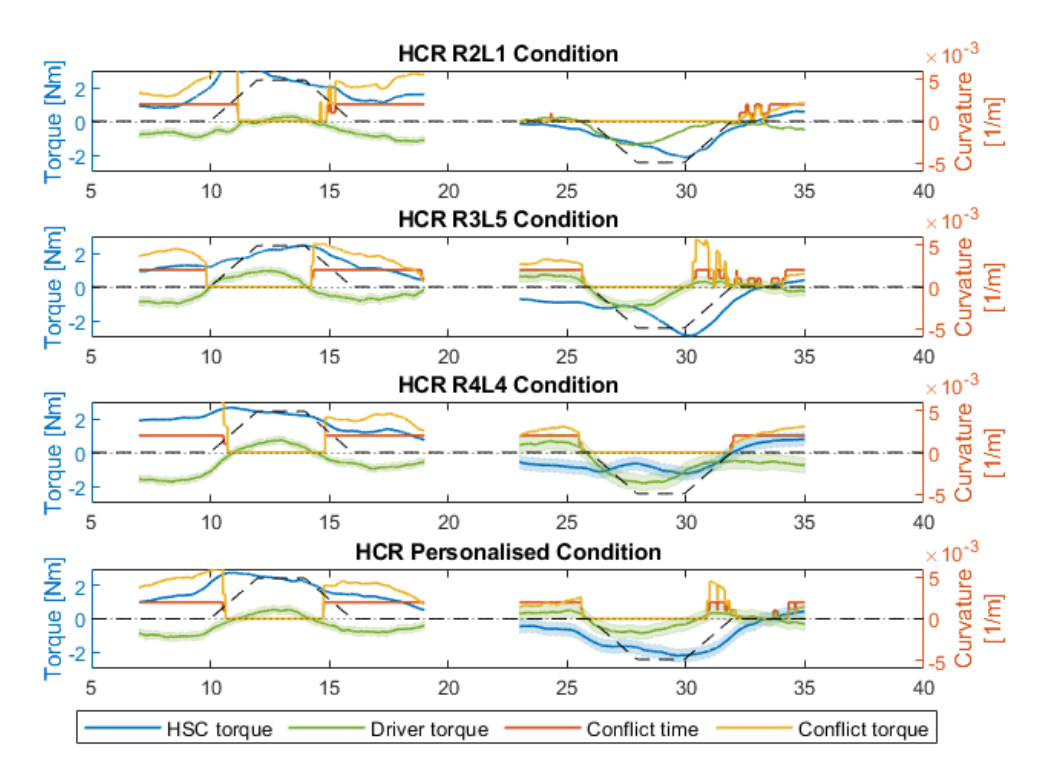


Figure B.8: Timeseries of conflict R2L1 driver $2-FF\ 0.92$

R2L1 Driver 3 - FF 0.5

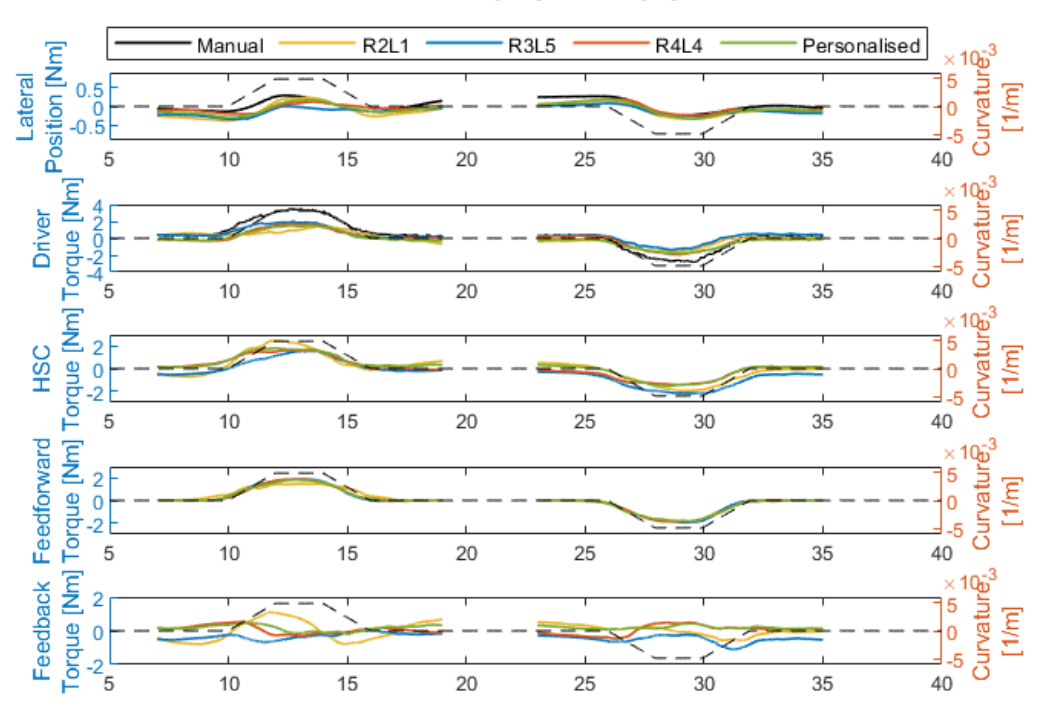


Figure B.9: Timeseries R2L1 driver 3 – FF 0.5

R2L1 Driver 3 - FF 0.5

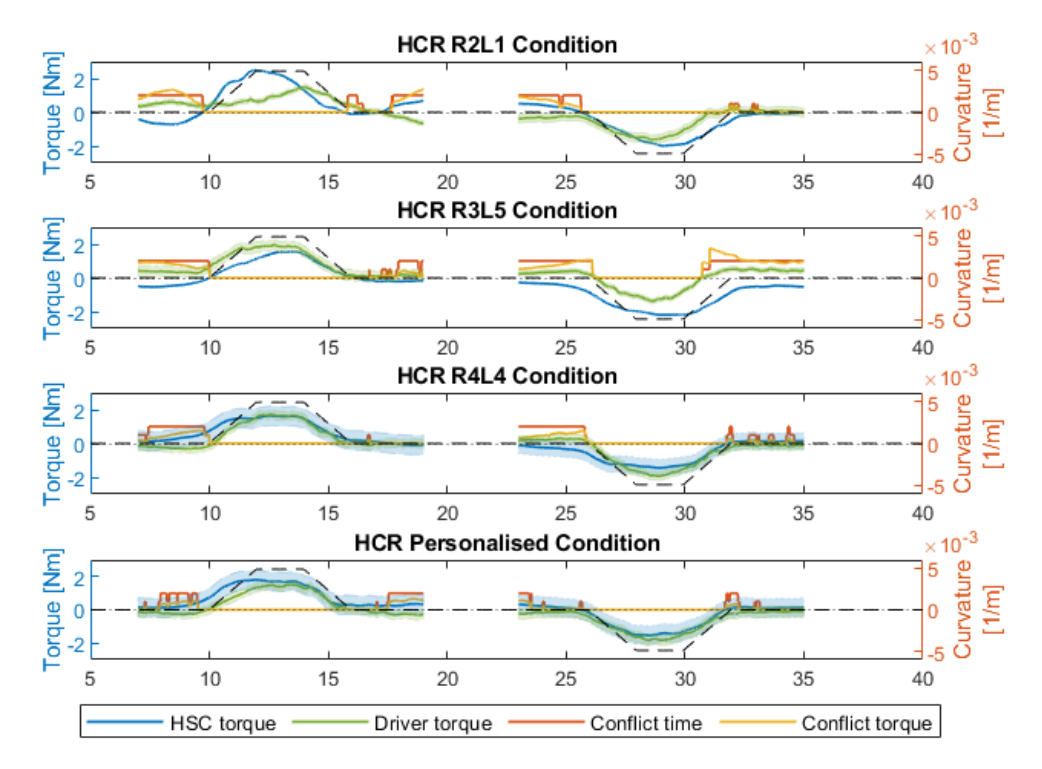


Figure B.10: Timeseries of conflict R2L1 driver $3-FF\ 0.5$

R2L1 Driver 3 - FF 0.92

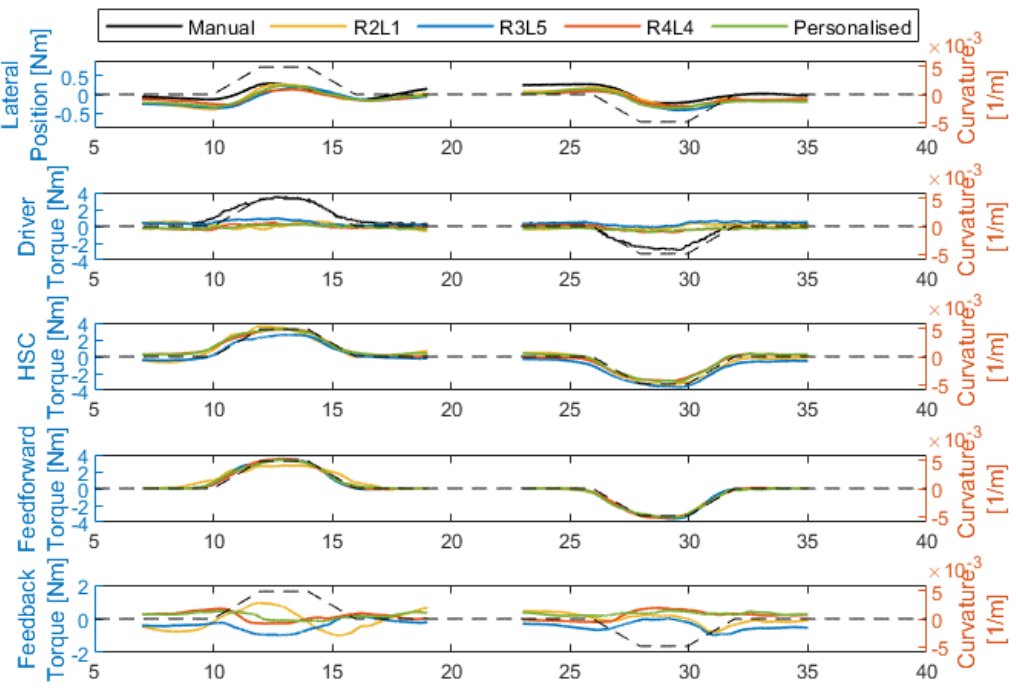


Figure B.11: Timeseries R2L1 driver 3 – FF 0.92

R2L1 Driver 3 - FF 0.92

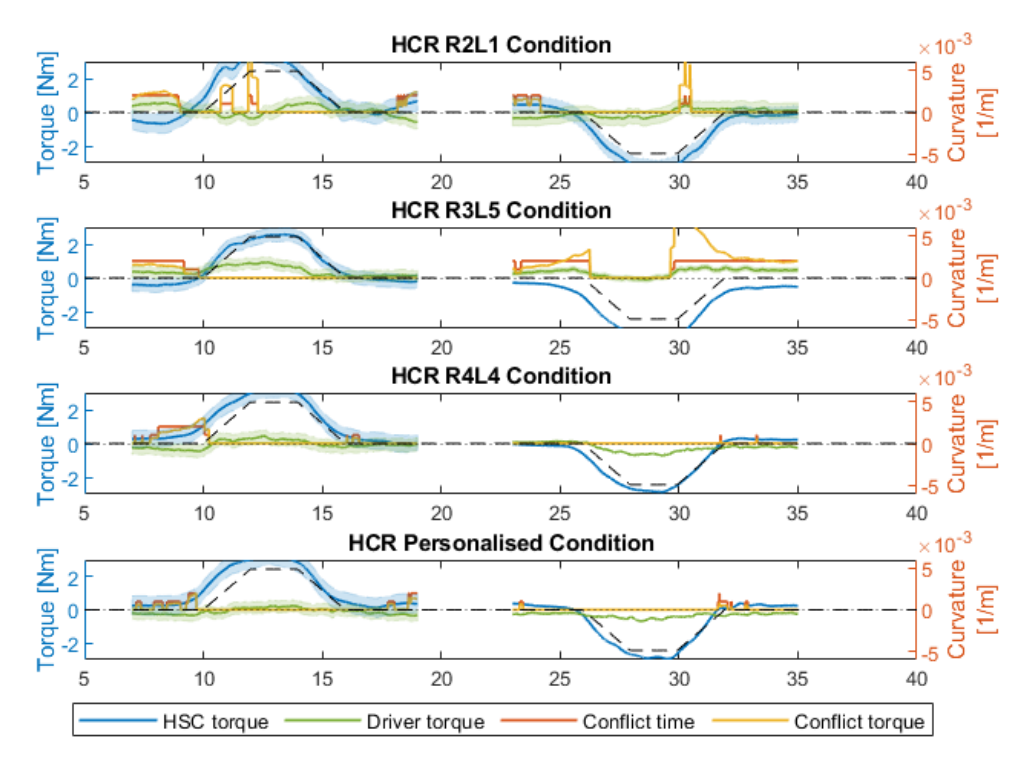


Figure B.12: Timeseries of conflict R2L1 driver $3-FF\ 0.92$

R2L1 Driver 4 - FF 0.5

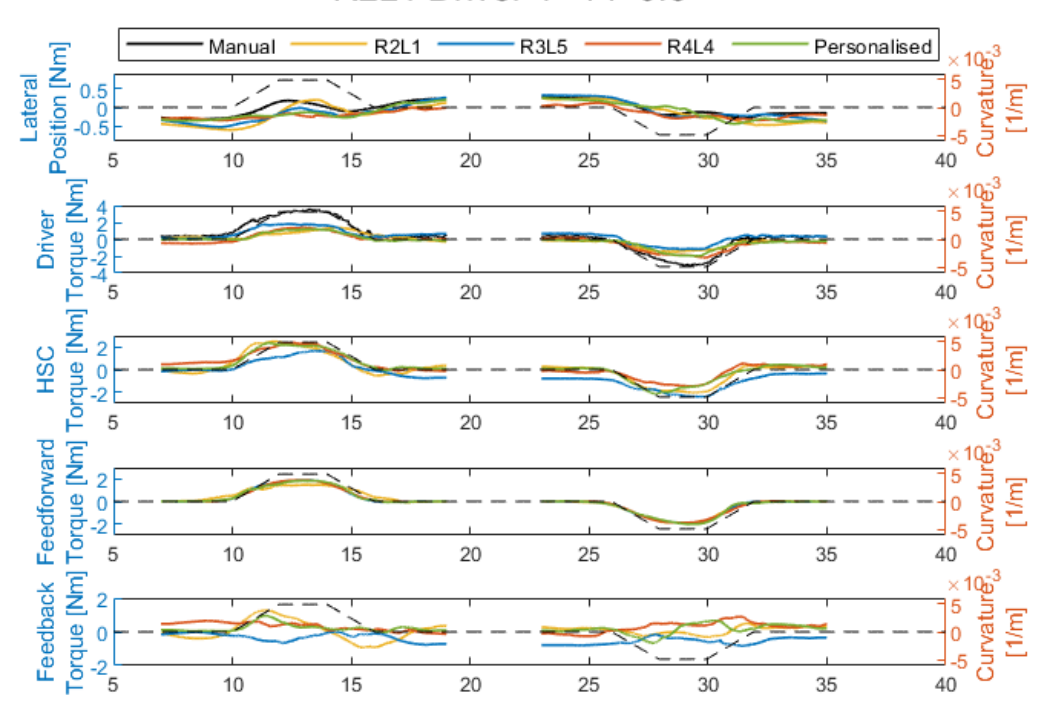


Figure B.13: Timeseries R2L1 driver 4 – FF 0.5

R2L1 Driver 4 - FF 0.5

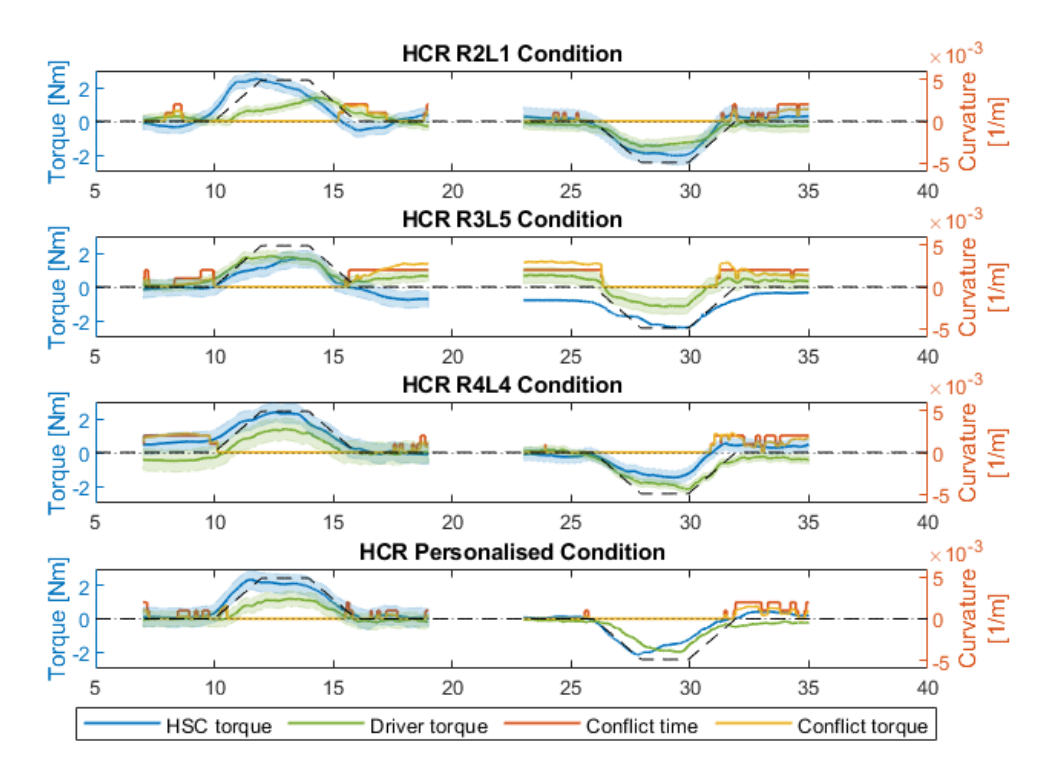


Figure B.14: Timeseries of conflict R2L1 driver $4-FF\ 0.5$

R2L1 Driver 4 - FF 0.92

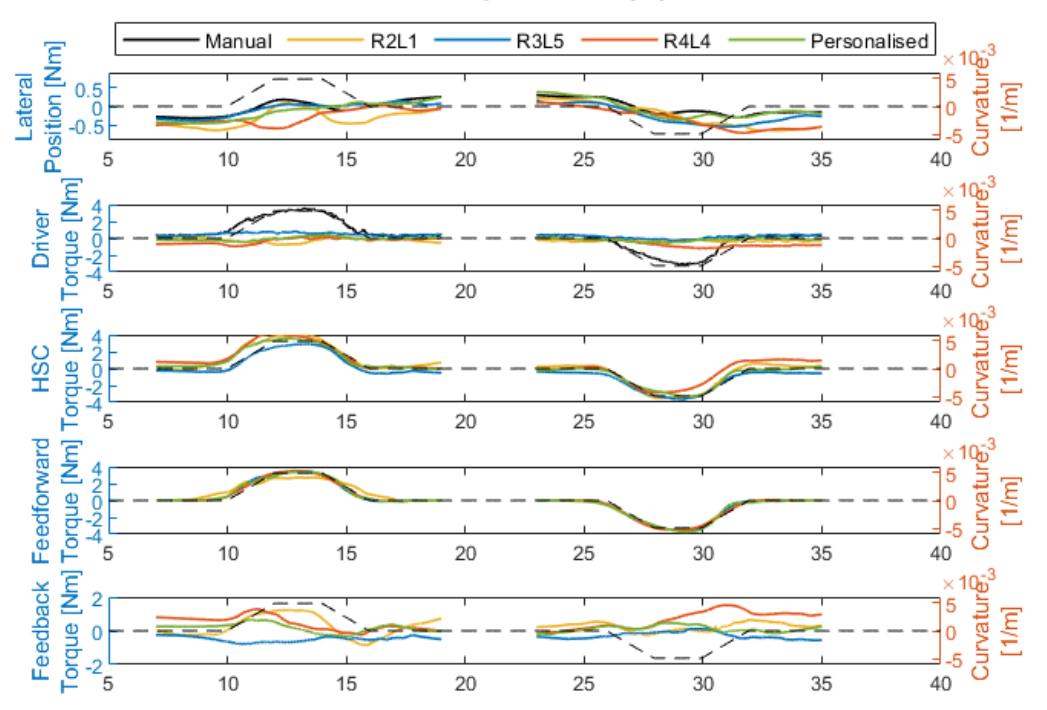


Figure B.15: Timeseries R2L1 driver 4 – FF 0.92

R2L1 Driver 4 - FF 0.92

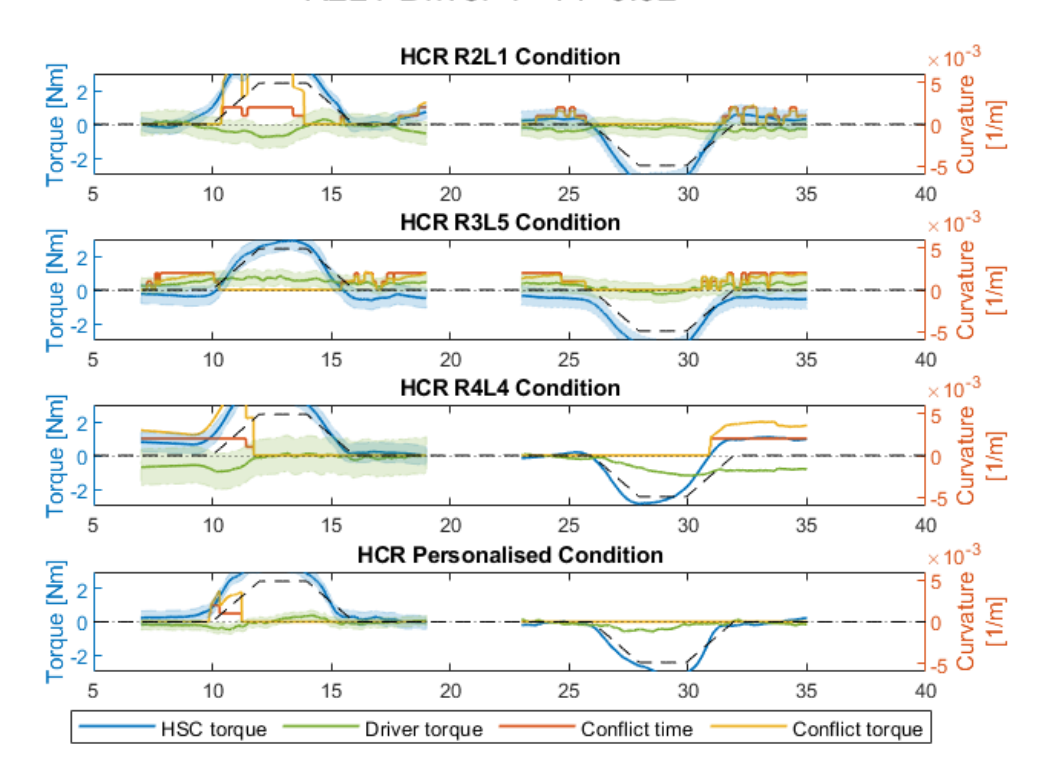


Figure B.16: Timeseries of conflict R2L1 driver 4 – FF 0.92

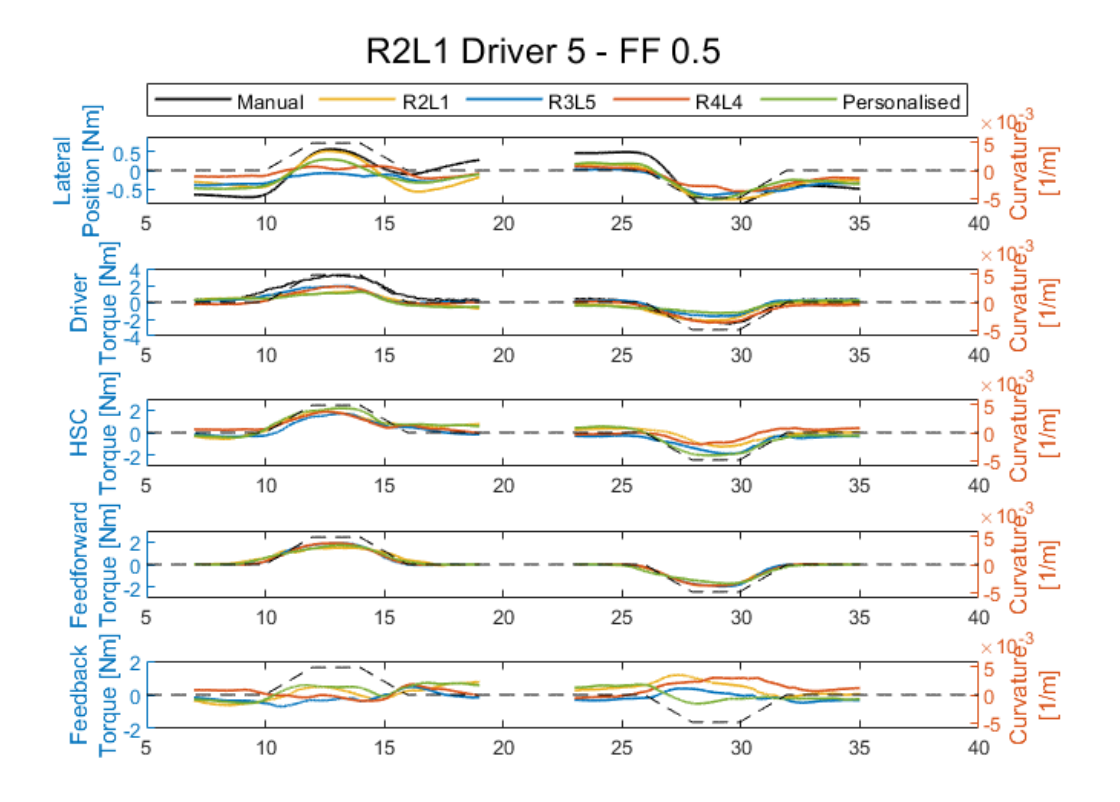


Figure B.17: Timeseries R2L1 driver 5 – FF 0.5

R2L1 Driver 5 - FF 0.5

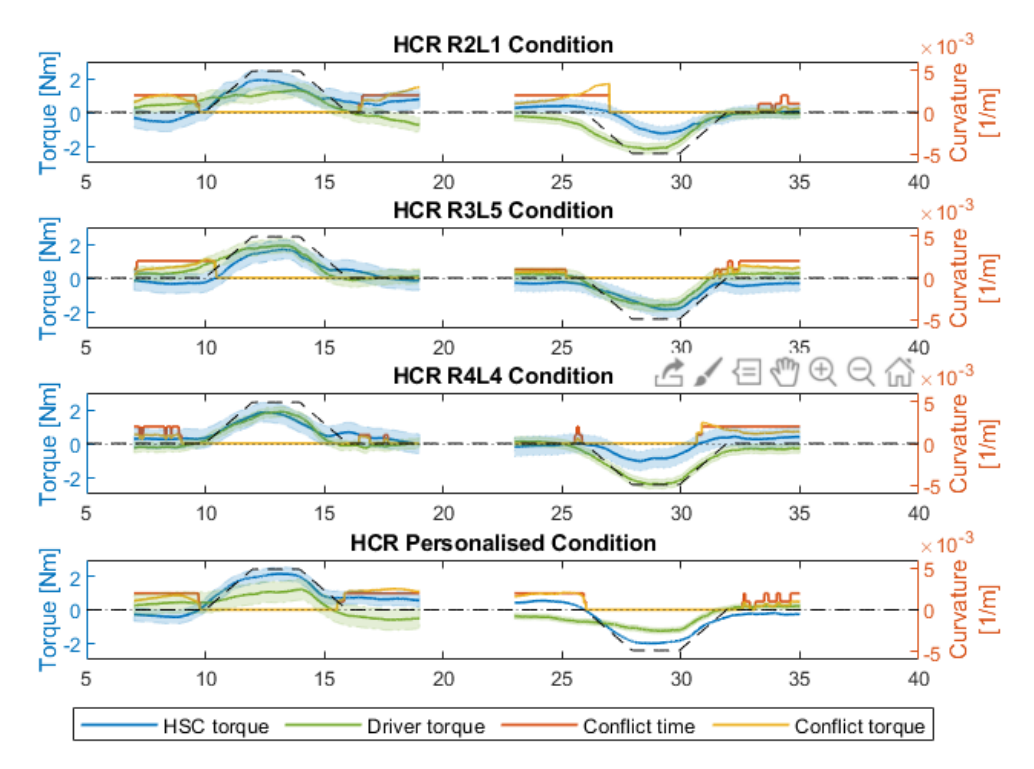


Figure B.18: Timeseries of conflict R2L1 driver $5-FF\ 0.5$

R2L1 Driver 5 - FF 0.92

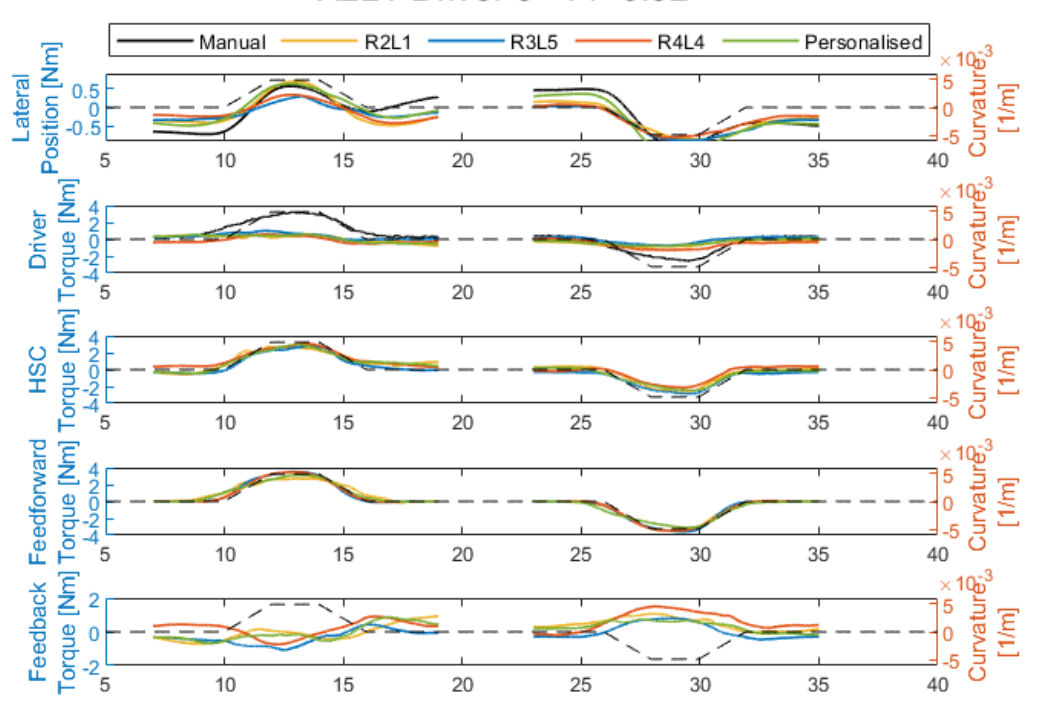


Figure B.19: Timeseries R2L1 driver 5 – FF 0.92

R2L1 Driver 5 - FF 0.92

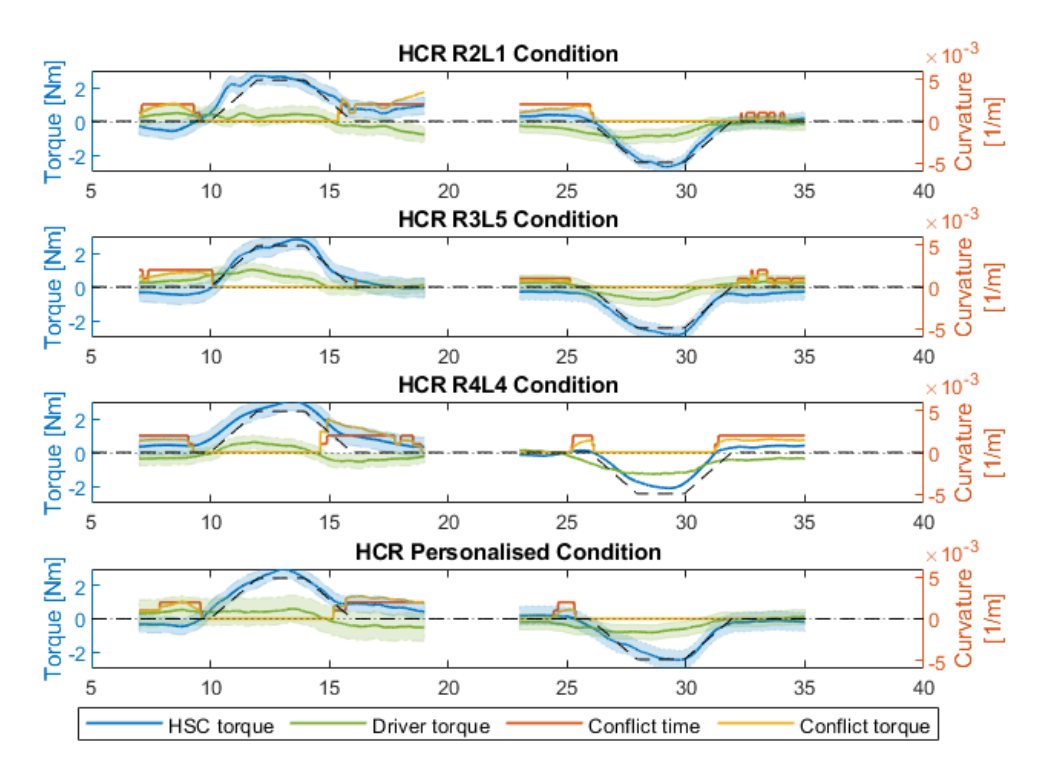


Figure B.20: Timeseries of conflict R2L1 driver 5 - FF 0.92

R2L1 Driver 6 - FF 0.5

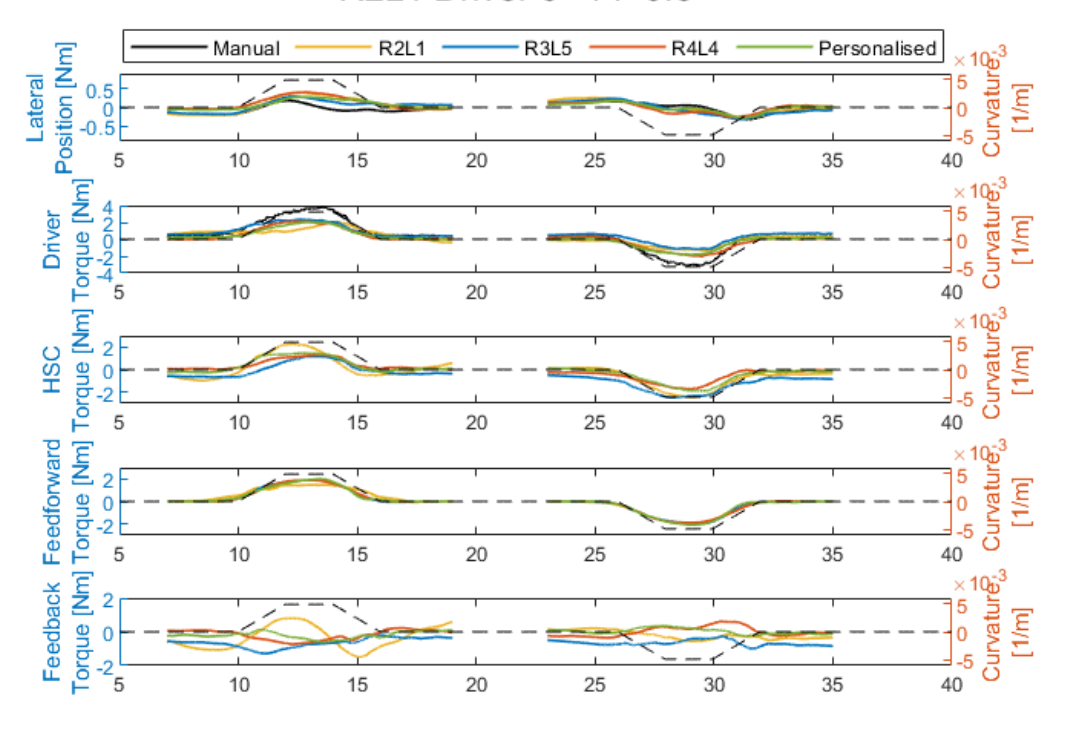


Figure B.21: Timeseries R2L1 driver 6 – FF 0.5

R2L1 Driver 6 - FF 0.5

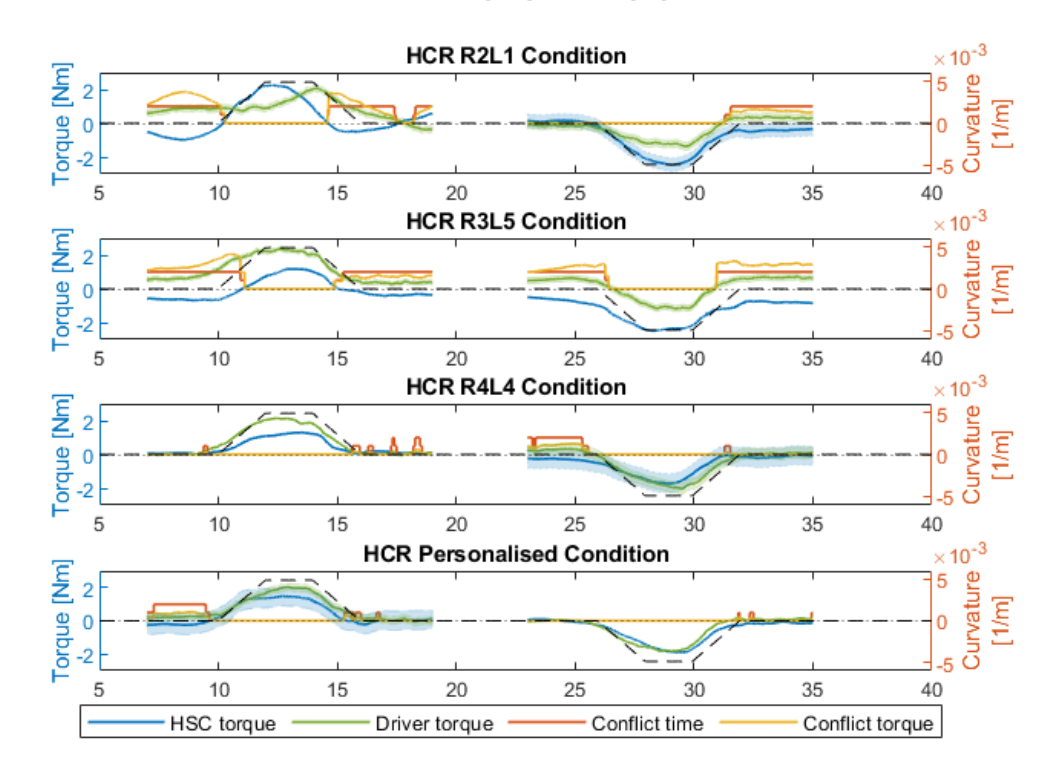


Figure B.22: Timeseries of conflict R2L1 driver 6 – FF 0.5

R2L1 Driver 6 - FF 0.92

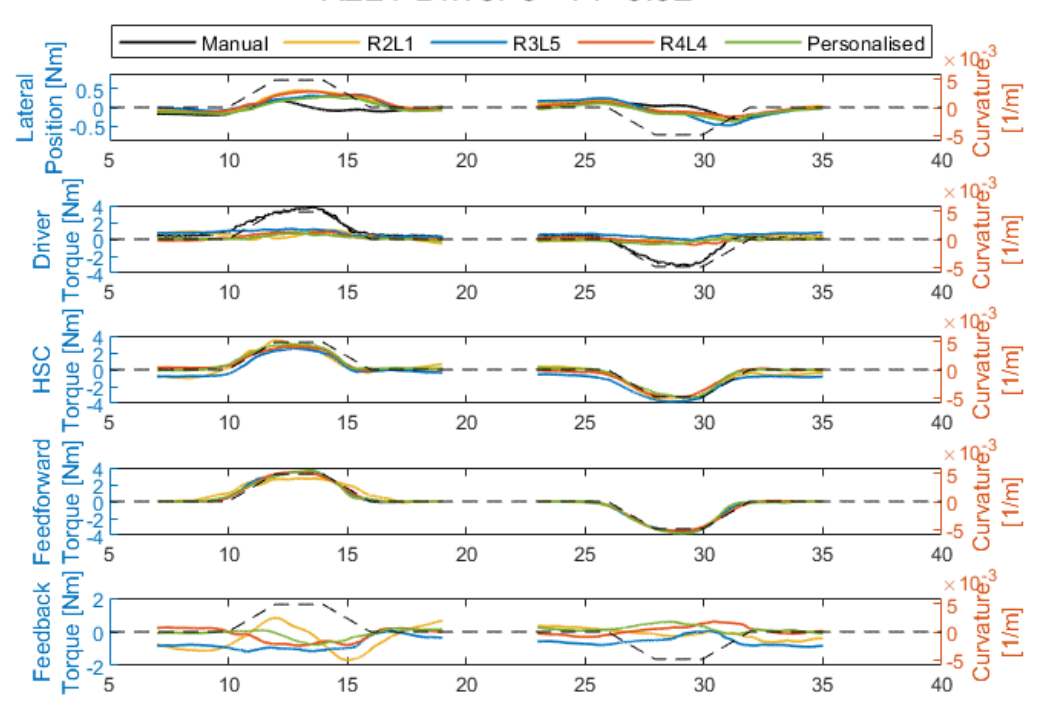


Figure B.23: Timeseries R2L1 driver 6 – FF 0.92

R2L1 Driver 6 - FF 0.92

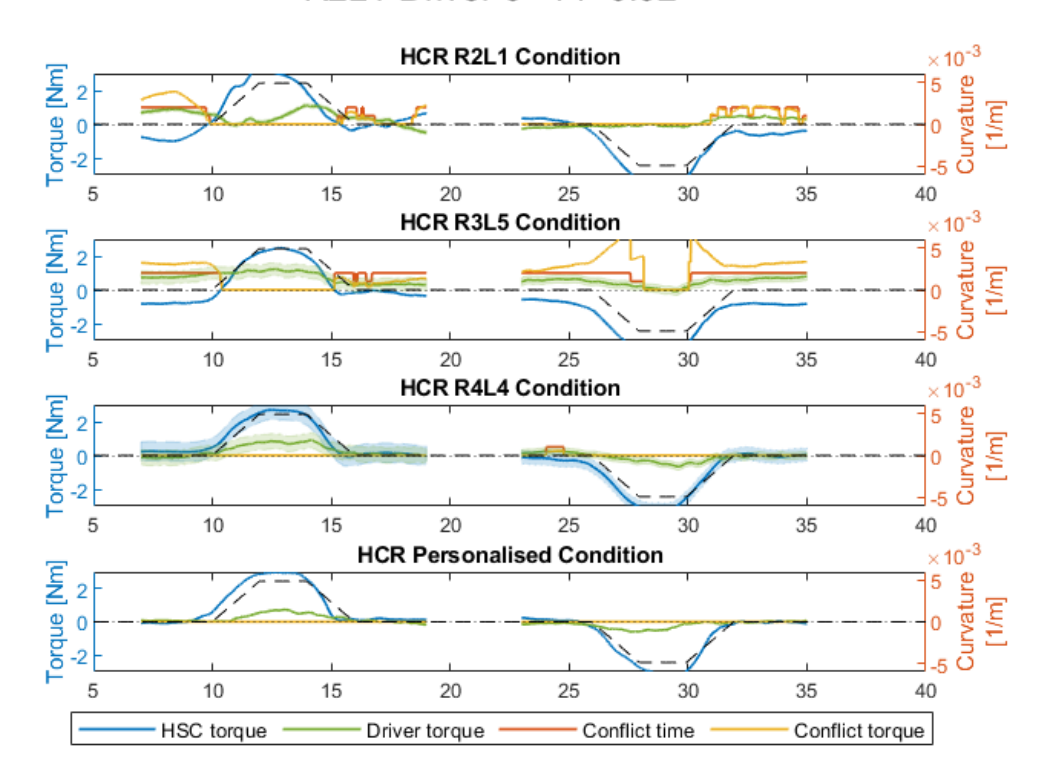


Figure B.24: Timeseries of conflict R2L1 driver 6 - FF 0.92

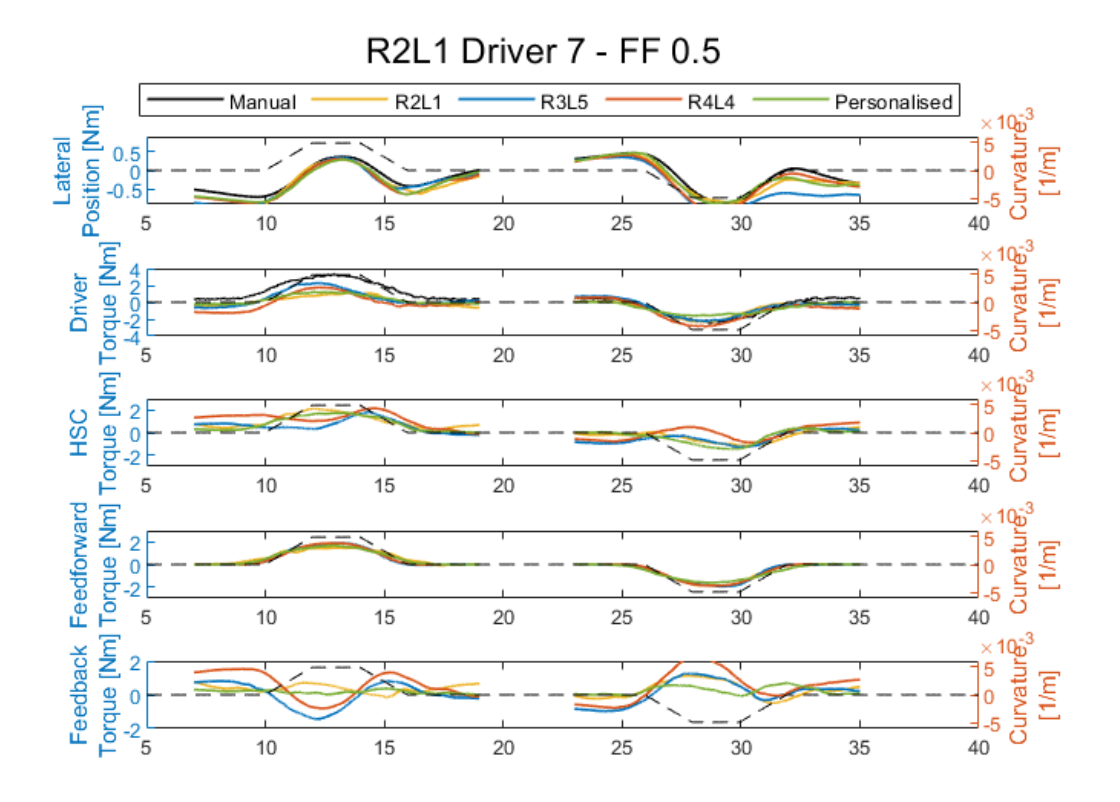


Figure B.25: Timeseries R2L1 driver 7 – FF 0.5

R2L1 Driver 7 - FF 0.5

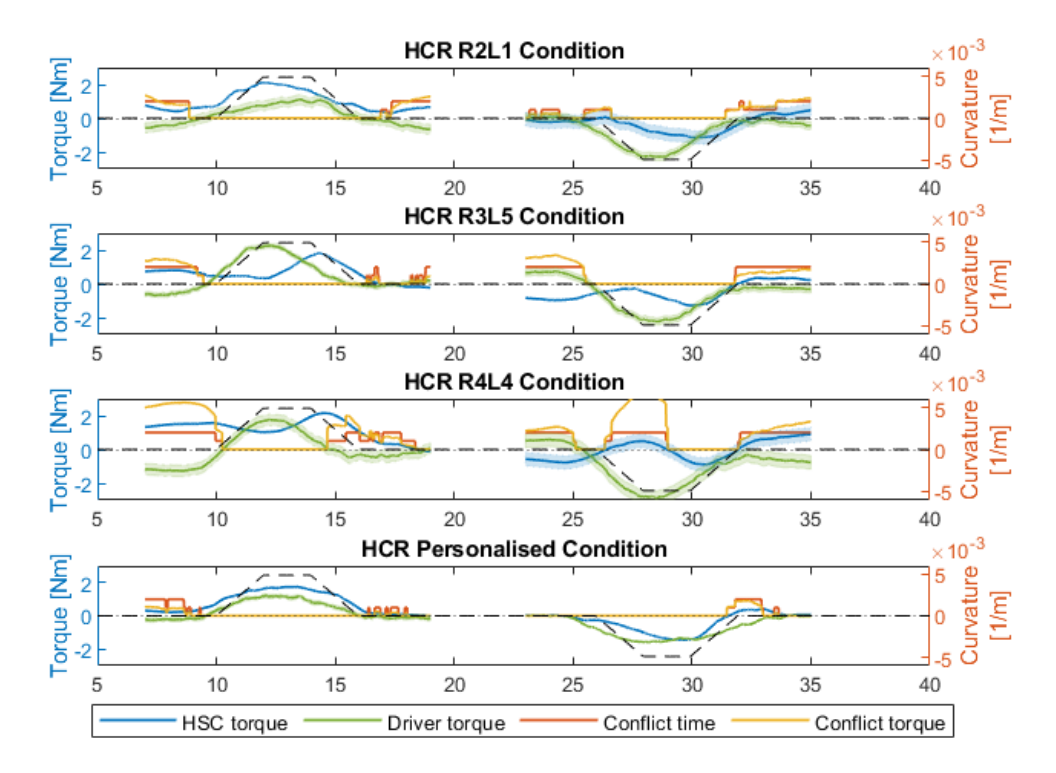


Figure B.26: Timeseries of conflict R2L1 driver $7-FF\ 0.5$

R2L1 Driver 7 - FF 0.92

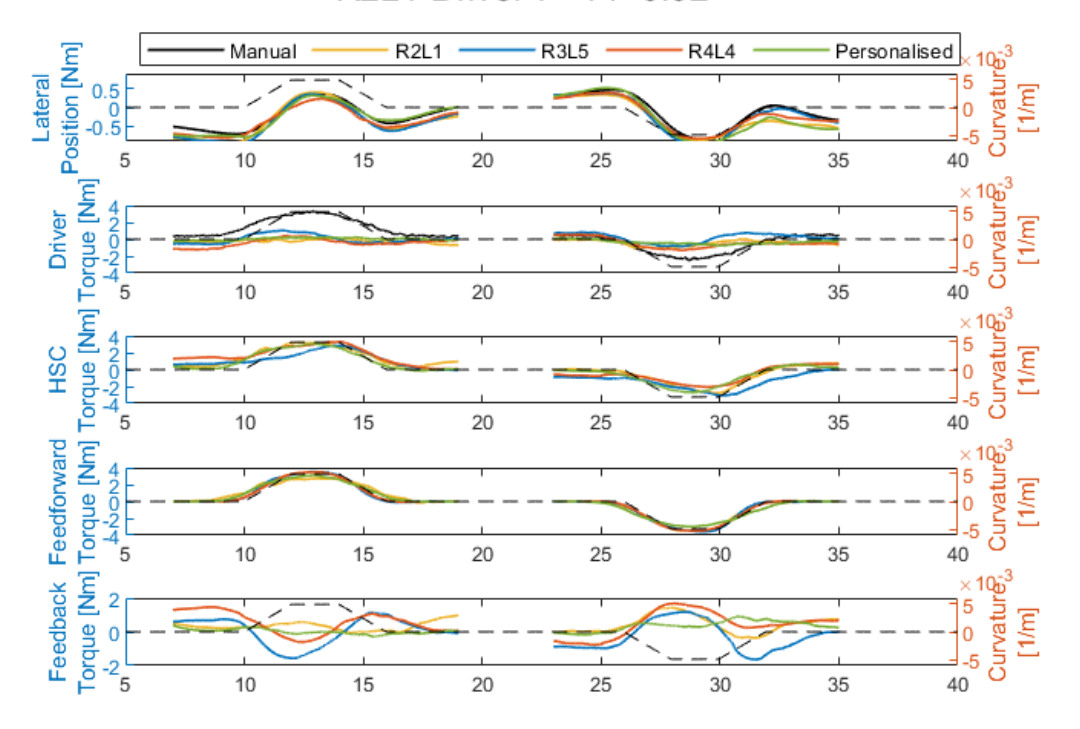


Figure B.27: Timeseries R2L1 driver 7 - FF 0.92

R2L1 Driver 7 - FF 0.92

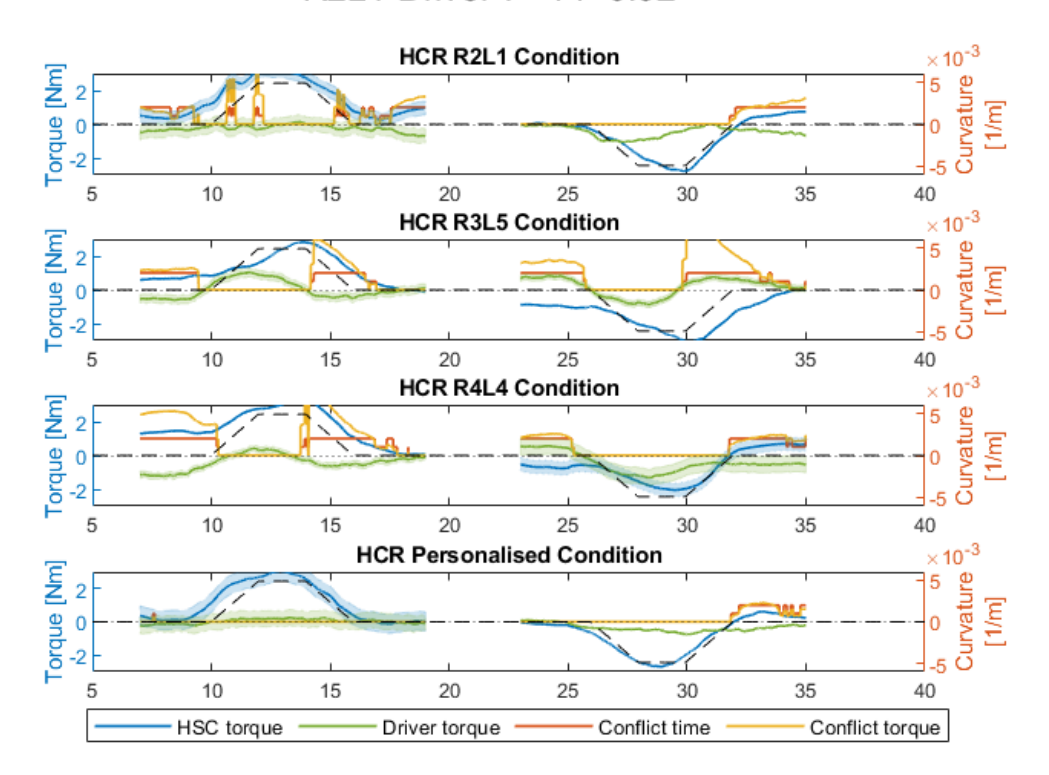


Figure B.28: Timeseries of conflict R2L1 driver 7 - FF 0.92

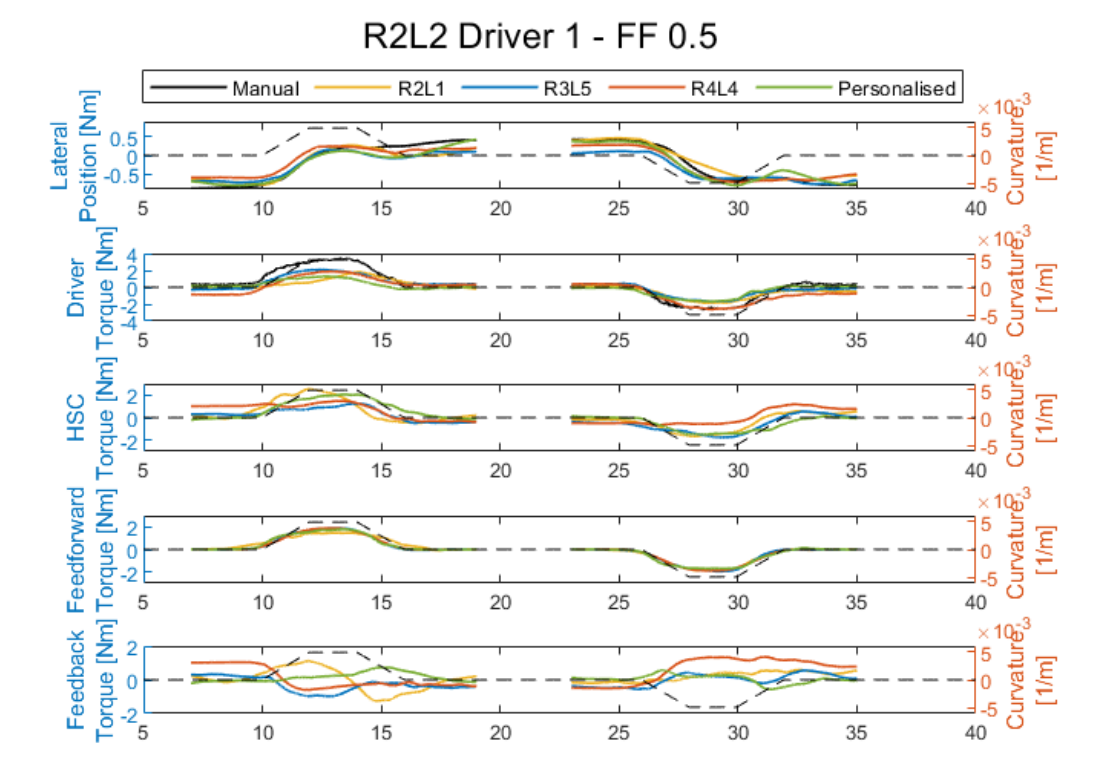


Figure B.29: Timeseries R2L2 driver 1 – FF 0.5

R2L2 Driver 1 - FF 0.5

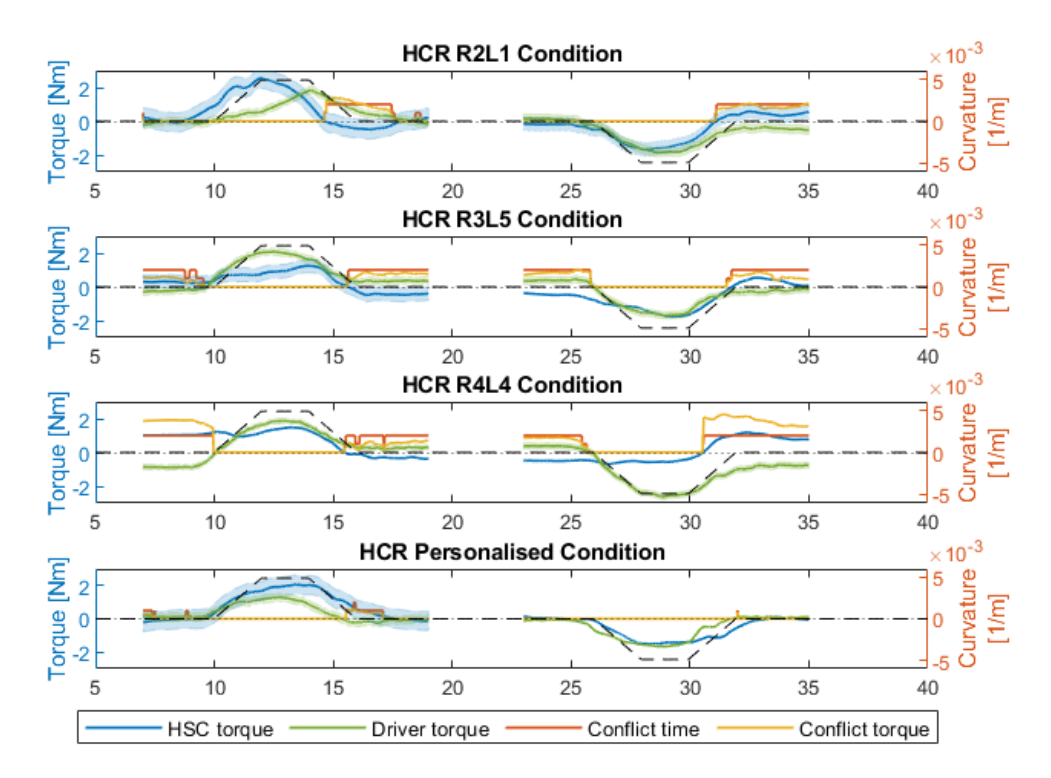


Figure B.30: Timeseries of conflict R2L2 driver $1-\mathrm{FF}\ 0.5$

R2L2 Driver 1 - FF 0.92

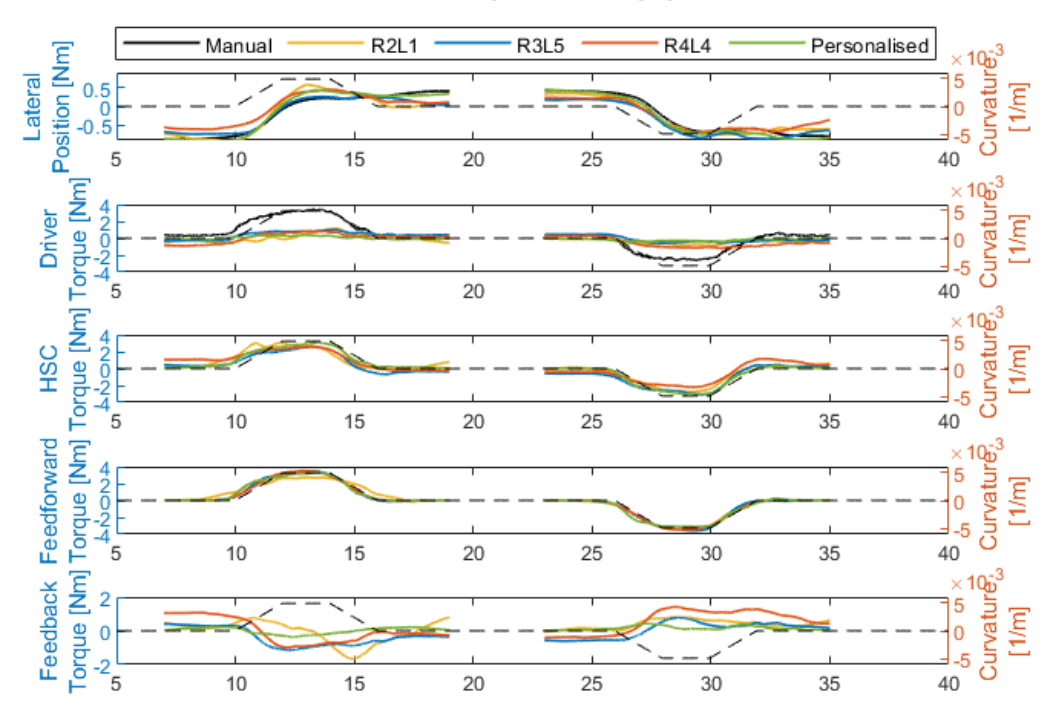


Figure B.31: Timeseries R2L2 driver 1 – FF 0.92

R2L2 Driver 1 - FF 0.92

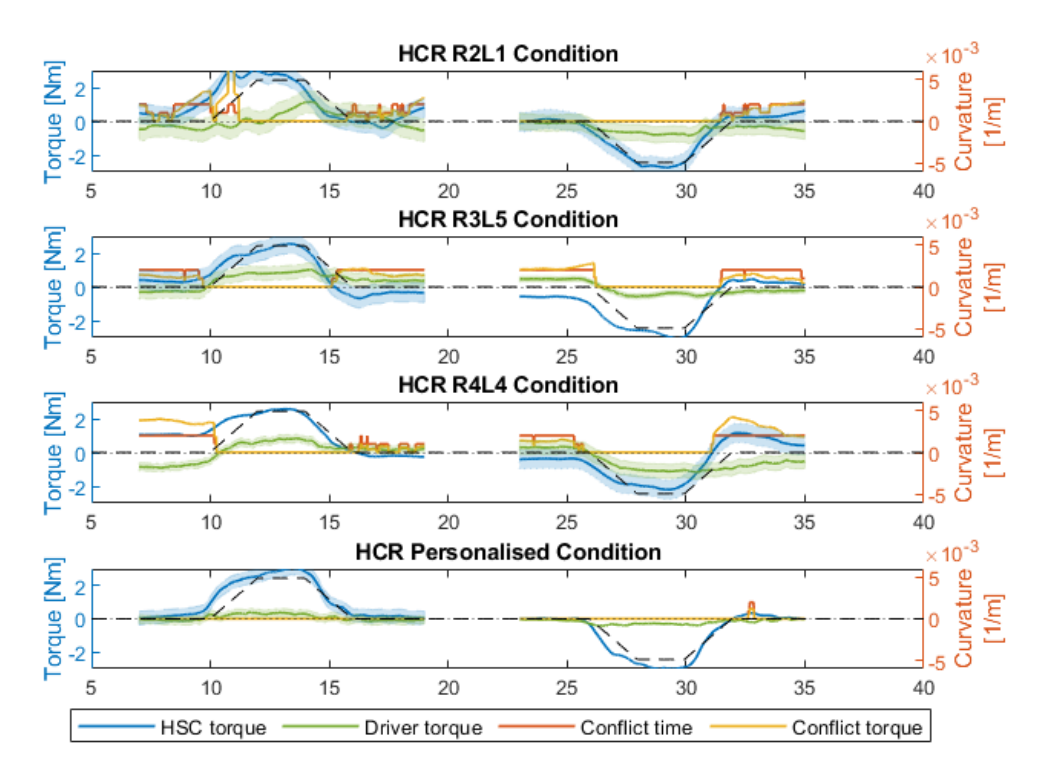


Figure B.32: Timeseries of conflict R2L2 driver $1-{\rm FF}~0.92$

R2L2 Driver 2 - FF 0.5

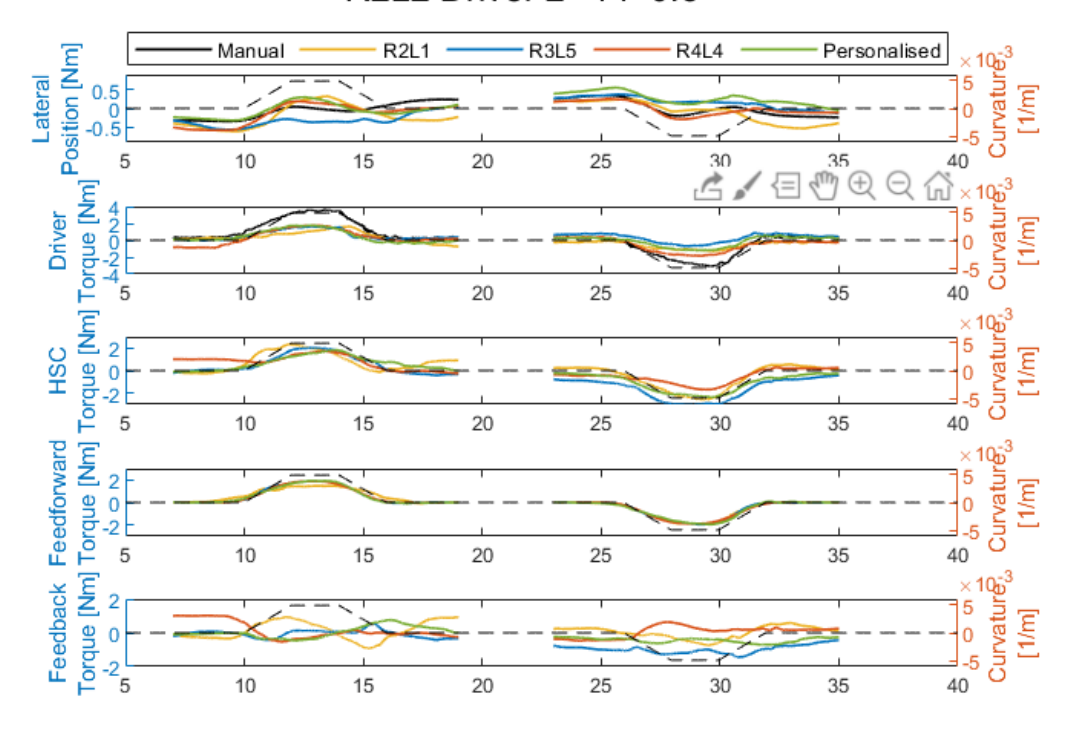


Figure B.33: Timeseries R2L2 driver 2 – FF 0.5

R2L2 Driver 2 - FF 0.5

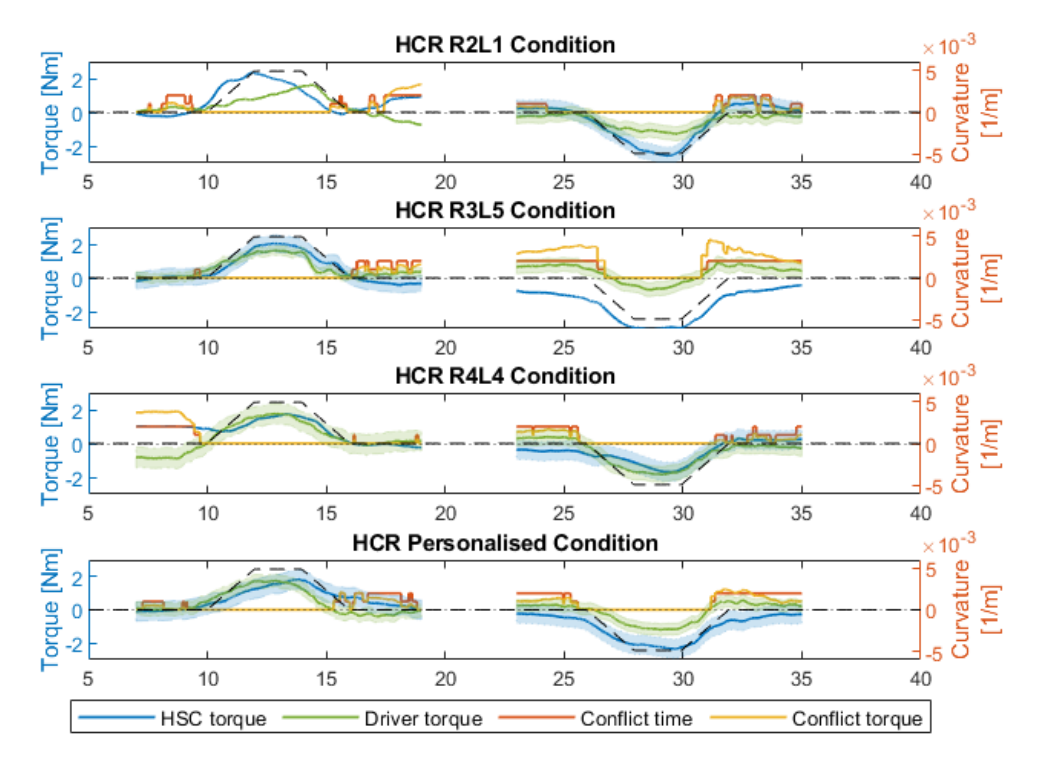


Figure B.34: Timeseries of conflict R2L2 driver $2-FF\ 0.5$

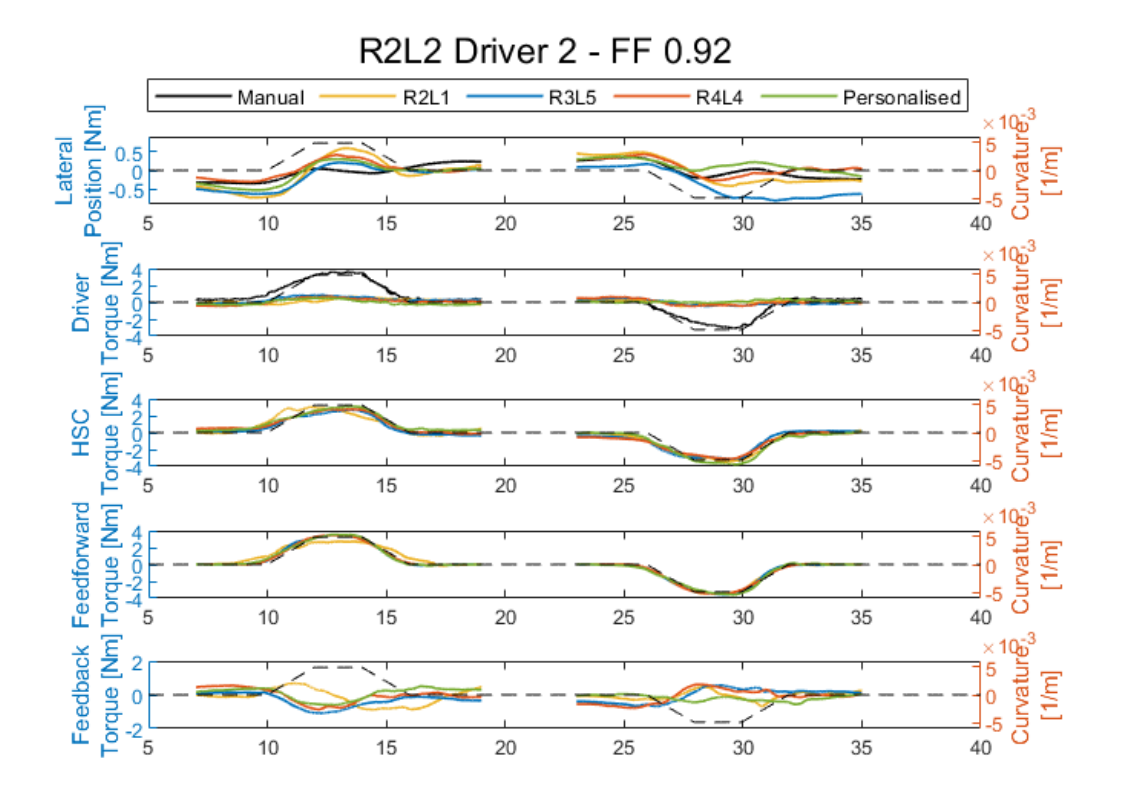


Figure B.35: Timeseries R2L2 driver 2 – FF 0.92

R2L2 Driver 2 - FF 0.92

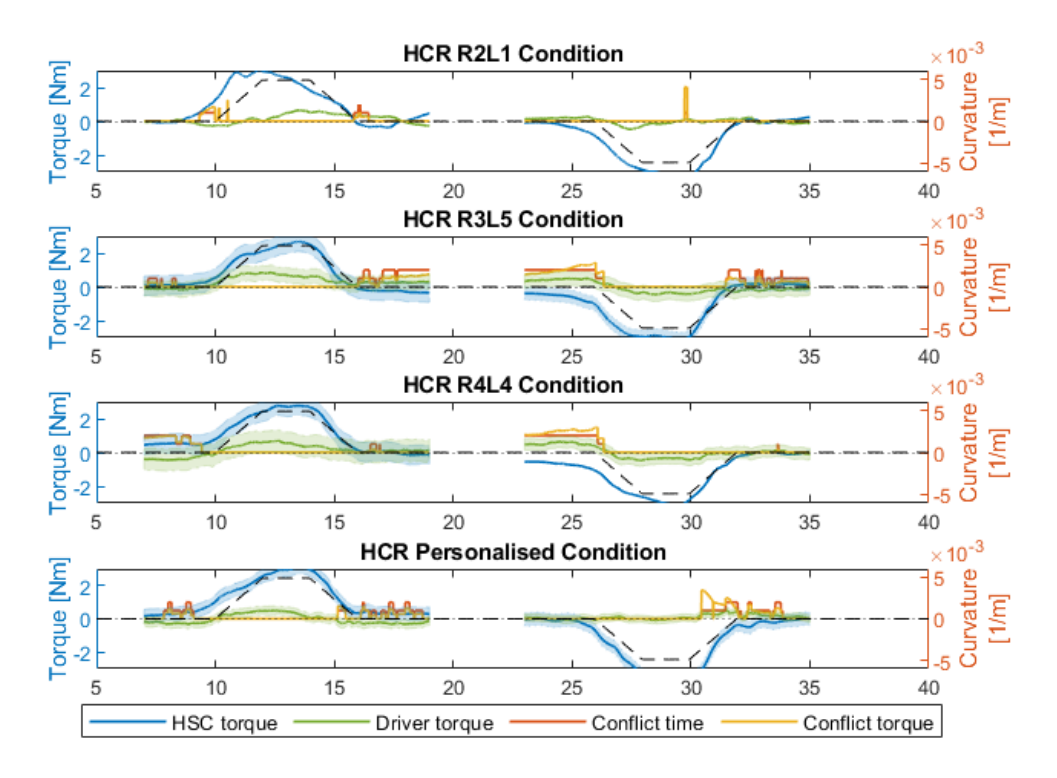


Figure B.36: Timeseries of conflict R2L2 driver 2 - FF 0.92

R2L2 Driver 3 - FF 0.5

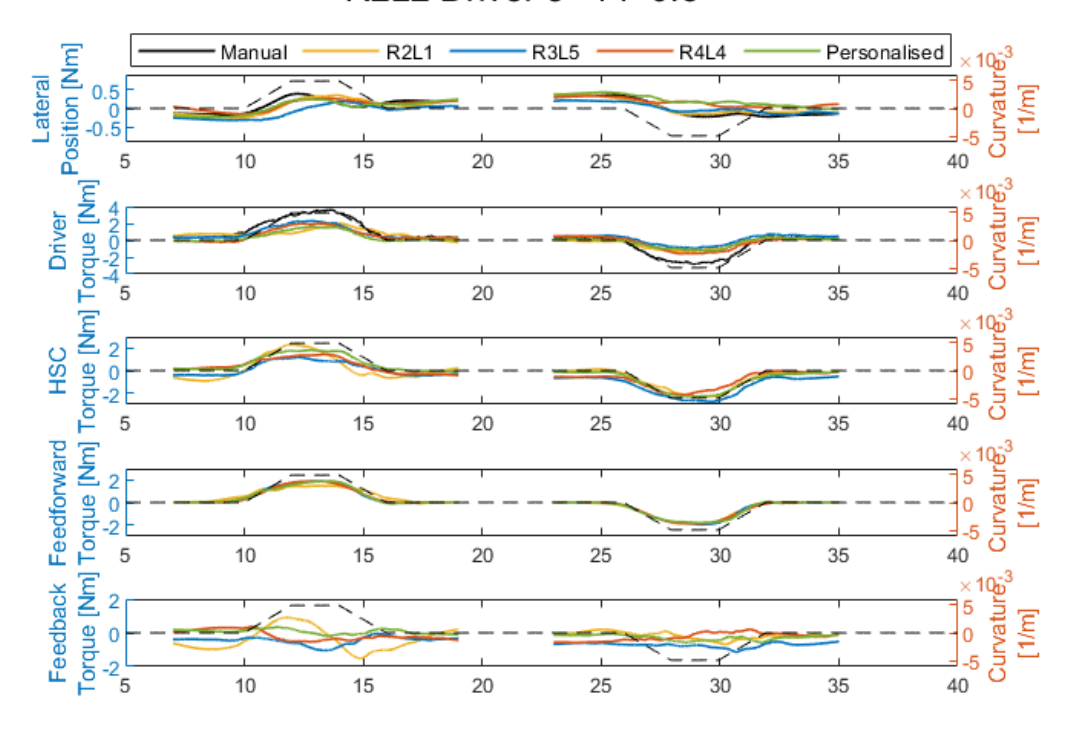


Figure B.37: Timeseries R2L2 driver 3 – FF 0.5

R2L2 Driver 3 - FF 0.5

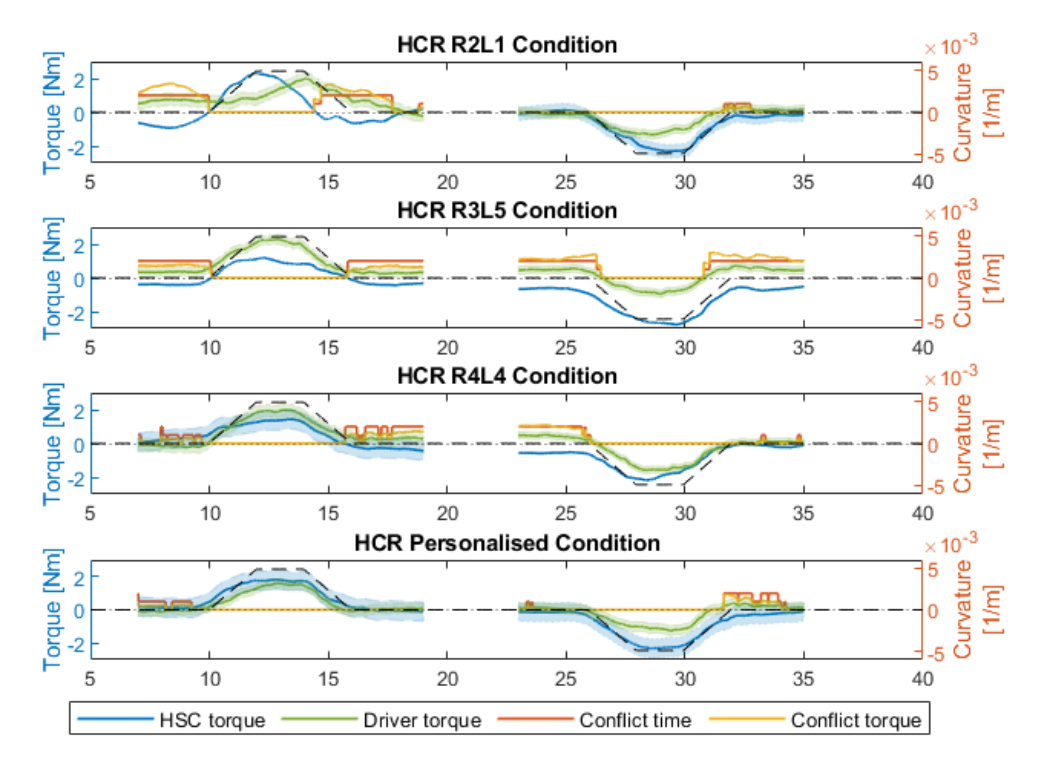


Figure B.38: Timeseries of conflict R2L2 driver $3-FF\ 0.5$

R2L2 Driver 3 - FF 0.92

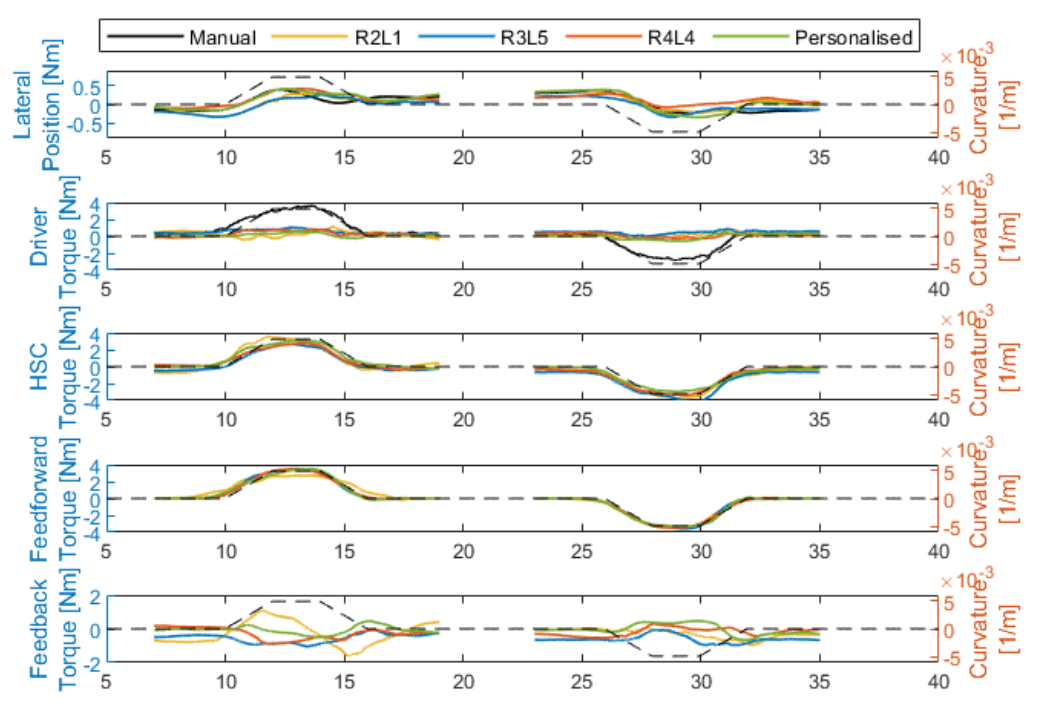


Figure B.39: Timeseries R2L2 driver 3 - FF 0.92

R2L2 Driver 3 - FF 0.92

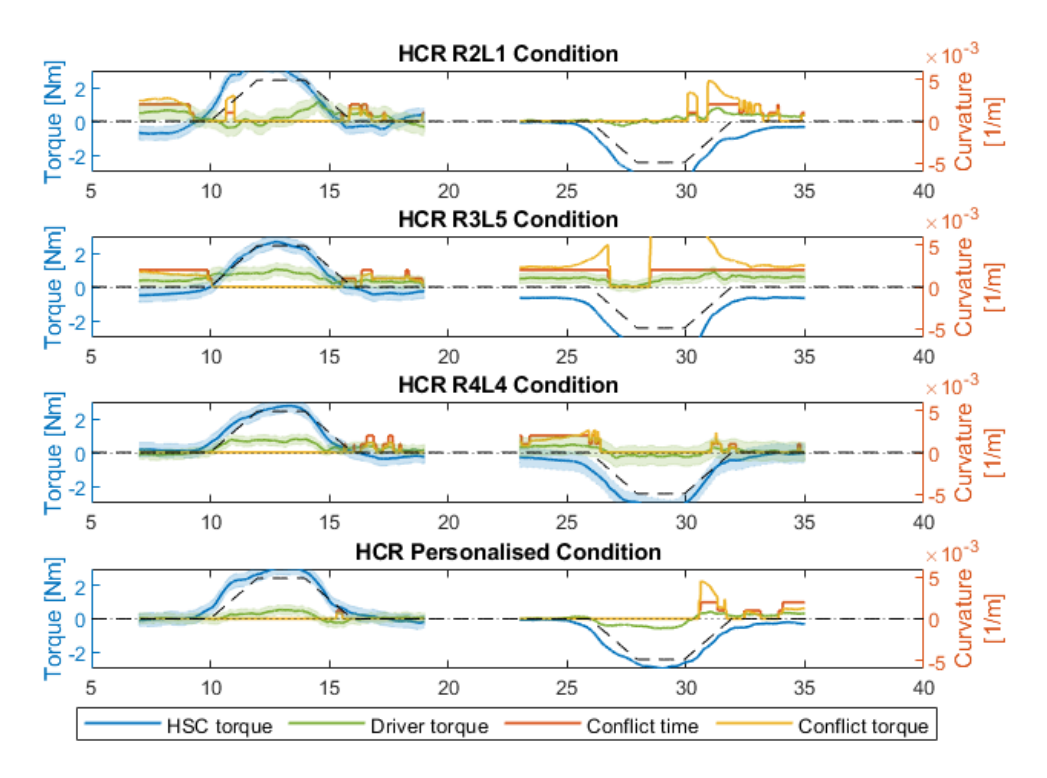


Figure B.40: Timeseries of conflict R2L2 driver $3-FF\ 0.92$

R2L2 Driver 4 - FF 0.5

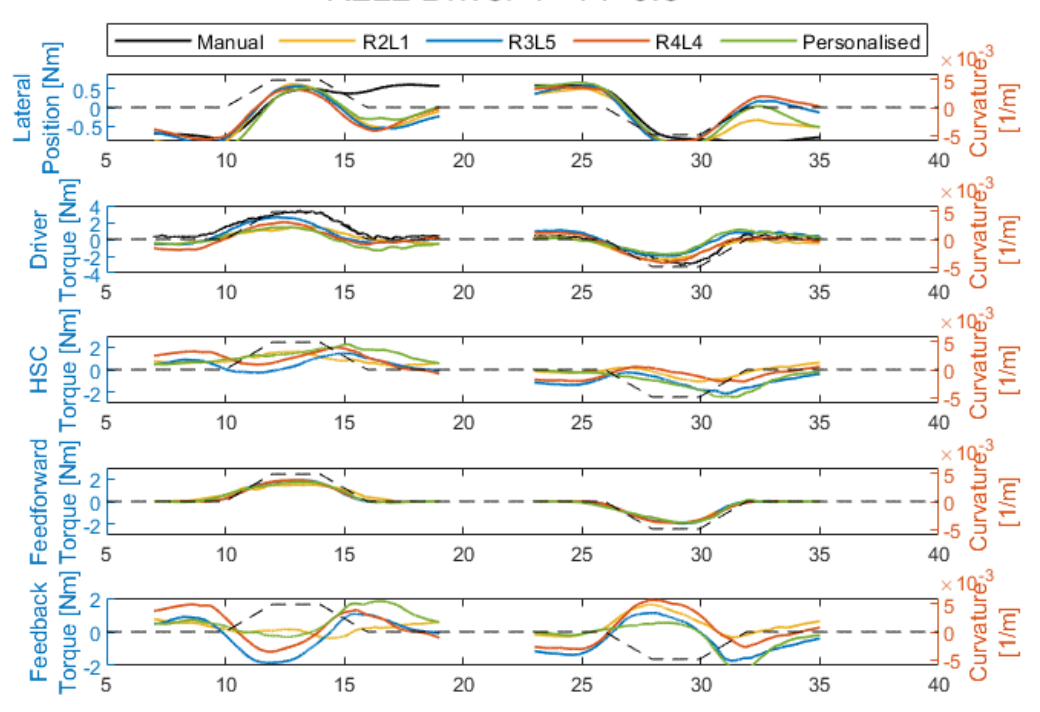


Figure B.41: Timeseries R2L2 driver 4 – FF 0.5

R2L2 Driver 4 - FF 0.5

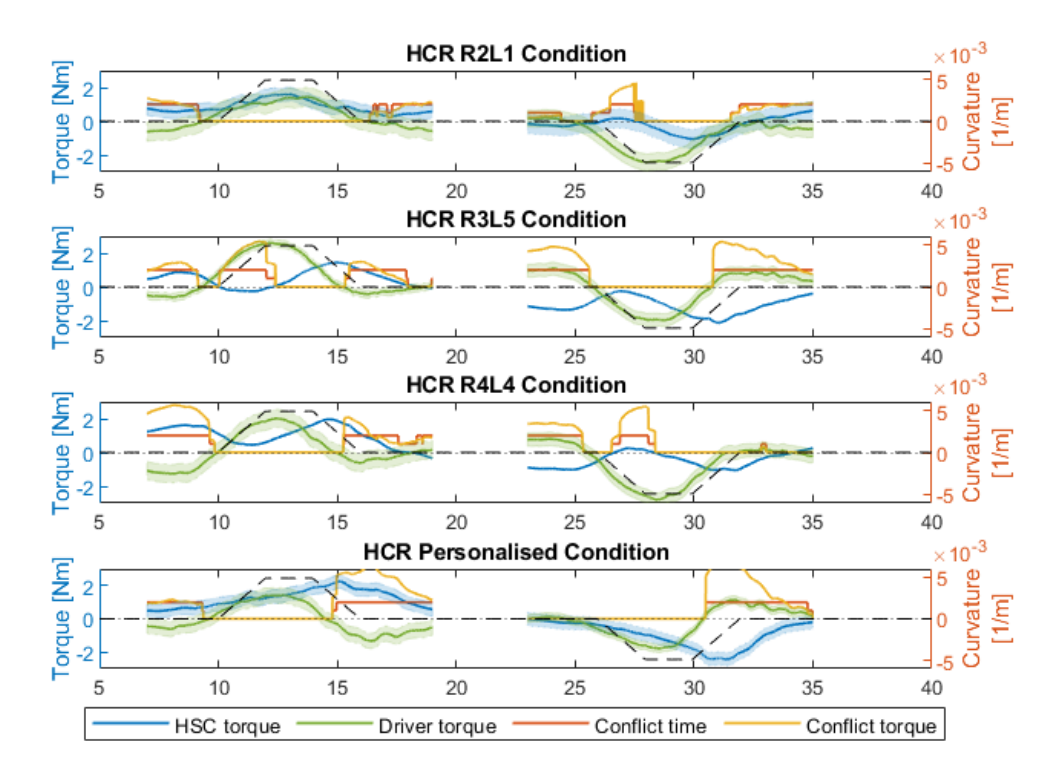


Figure B.42: Timeseries of conflict R2L2 driver $4-FF\ 0.5$

R2L2 Driver 4 - FF 0.92

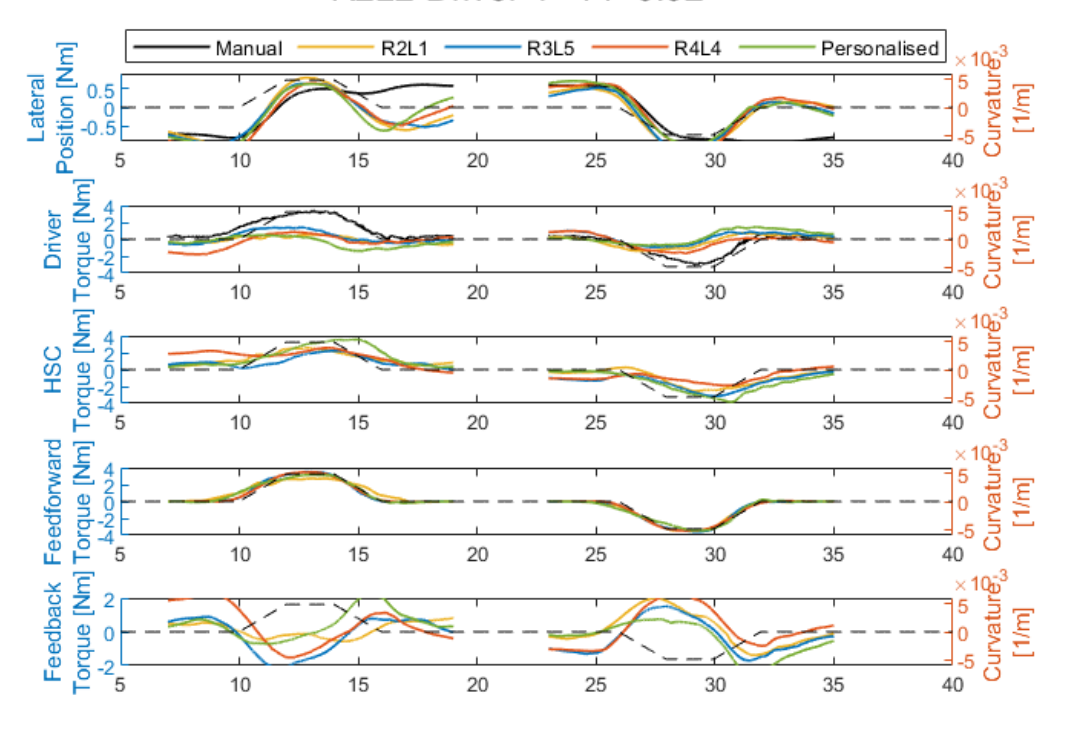


Figure B.43: Timeseries R2L2 driver 4 - FF 0.92

R2L2 Driver 4 - FF 0.92

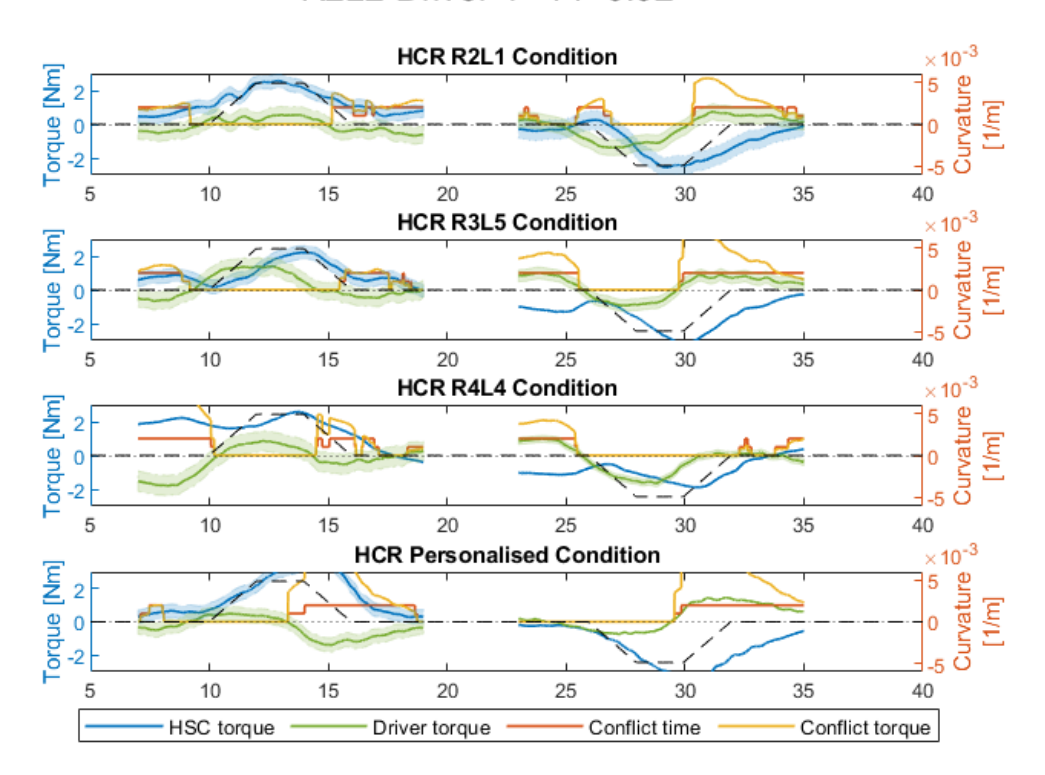


Figure B.44: Timeseries of conflict R2L2 driver 4 – FF 0.92

R2L2 Driver 5 - FF 0.5

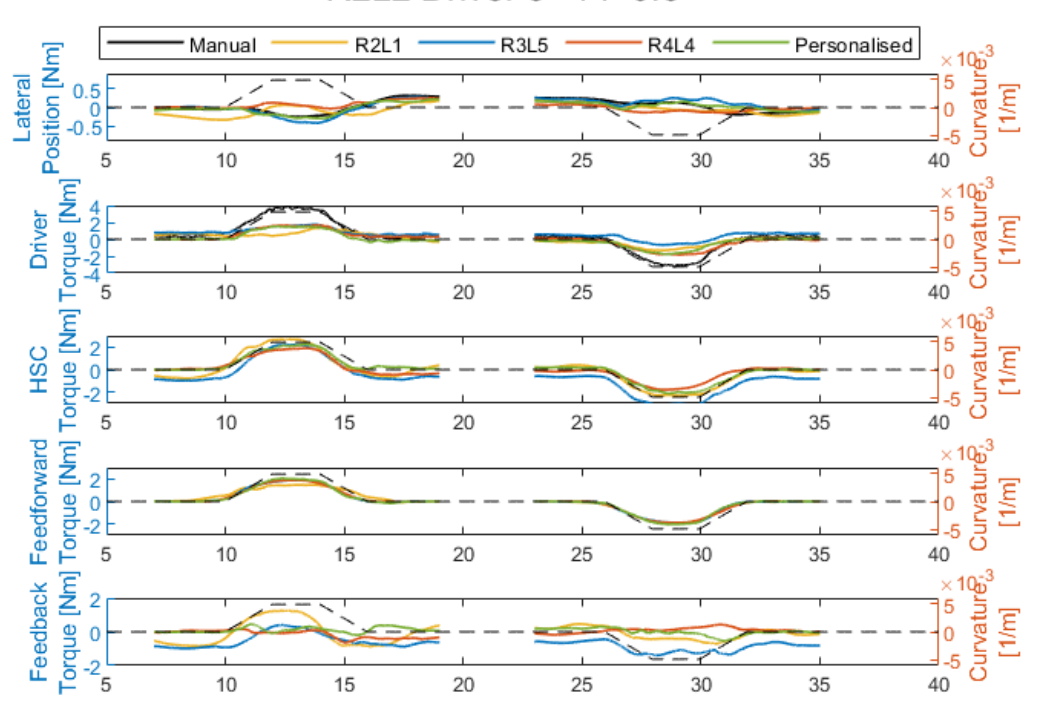


Figure B.45: Timeseries R2L2 driver 5 - FF 0.5

R2L2 Driver 5 - FF 0.5

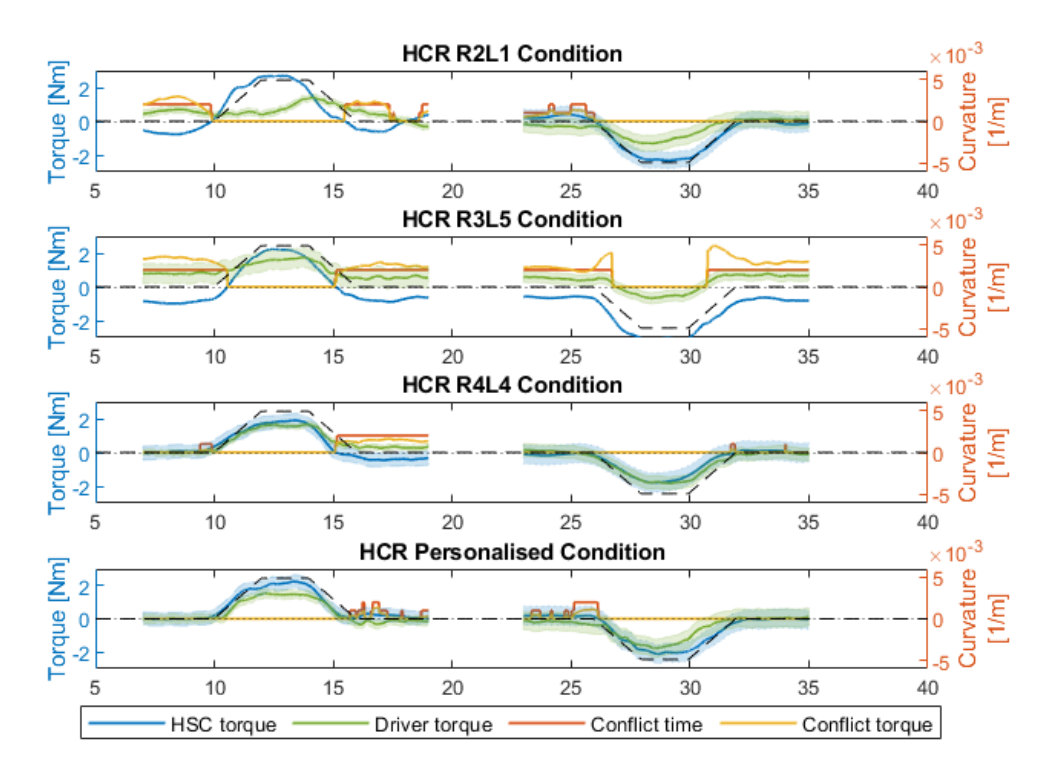


Figure B.46: Timeseries of conflict R2L2 driver $5-FF\ 0.5$

R2L2 Driver 5 - FF 0.92

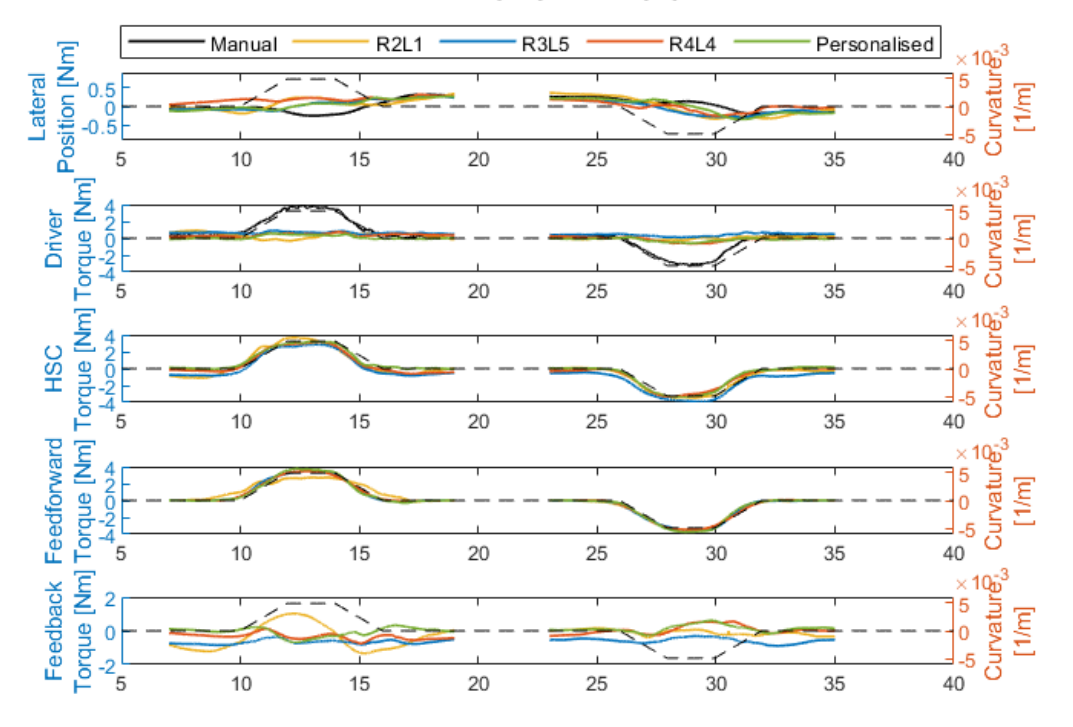


Figure B.47: Timeseries R2L2 driver 5 – FF 0.92

R2L2 Driver 5 - FF 0.92

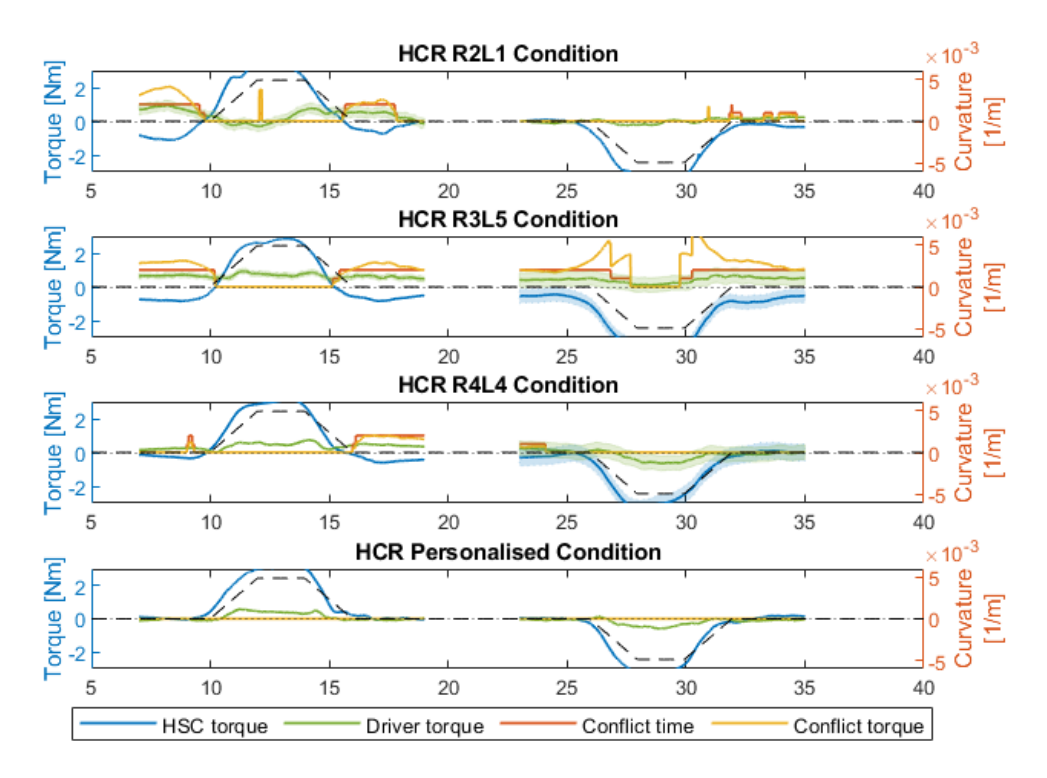


Figure B.48: Timeseries of conflict R2L2 driver 5 - FF 0.92

R2L2 Driver 6 - FF 0.5

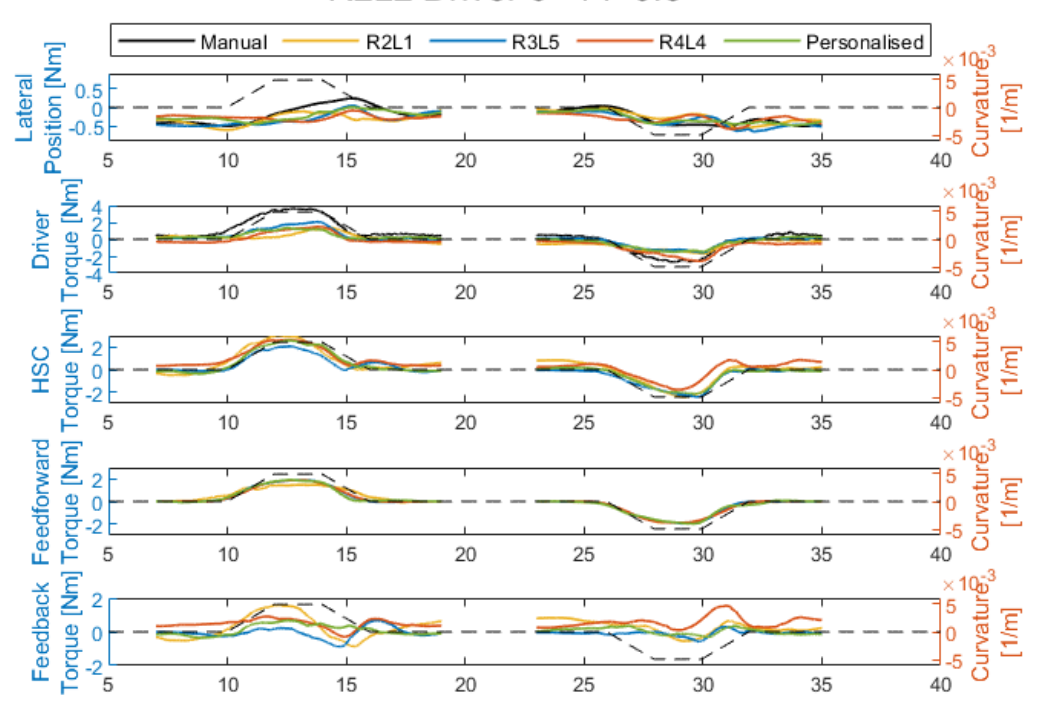


Figure B.49: Timeseries R2L2 driver 6 – FF 0.5

R2L2 Driver 6 - FF 0.5

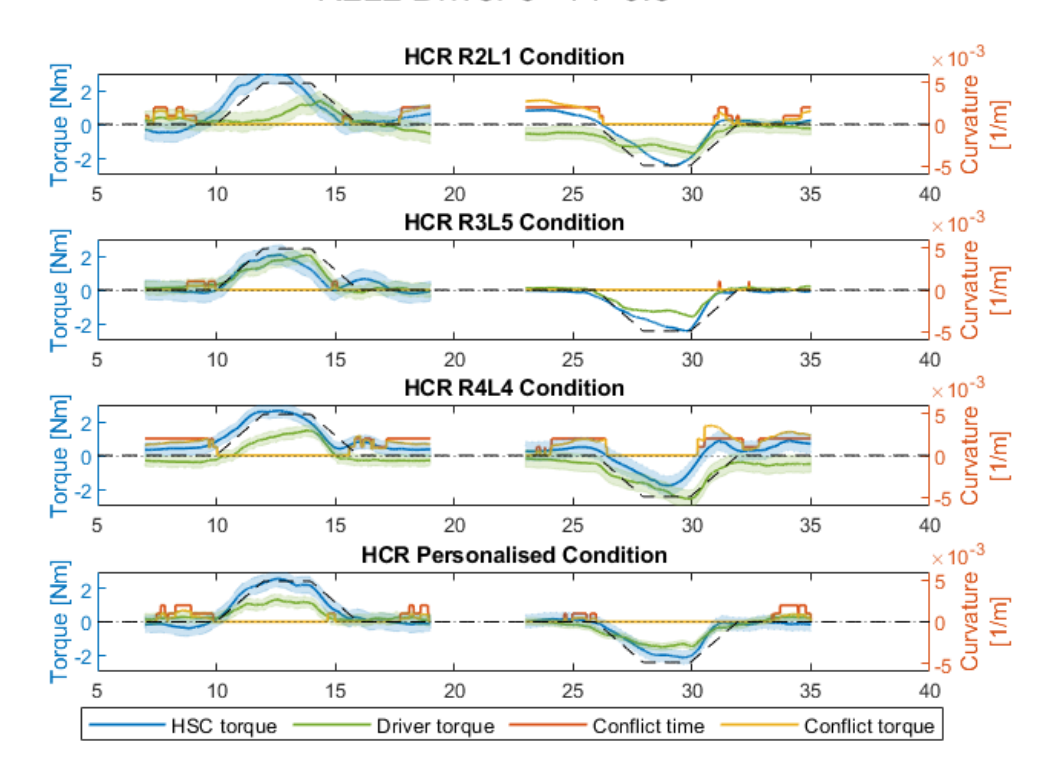


Figure B.50: Timeseries of conflict R2L2 driver $6-\mathrm{FF}~0.5$

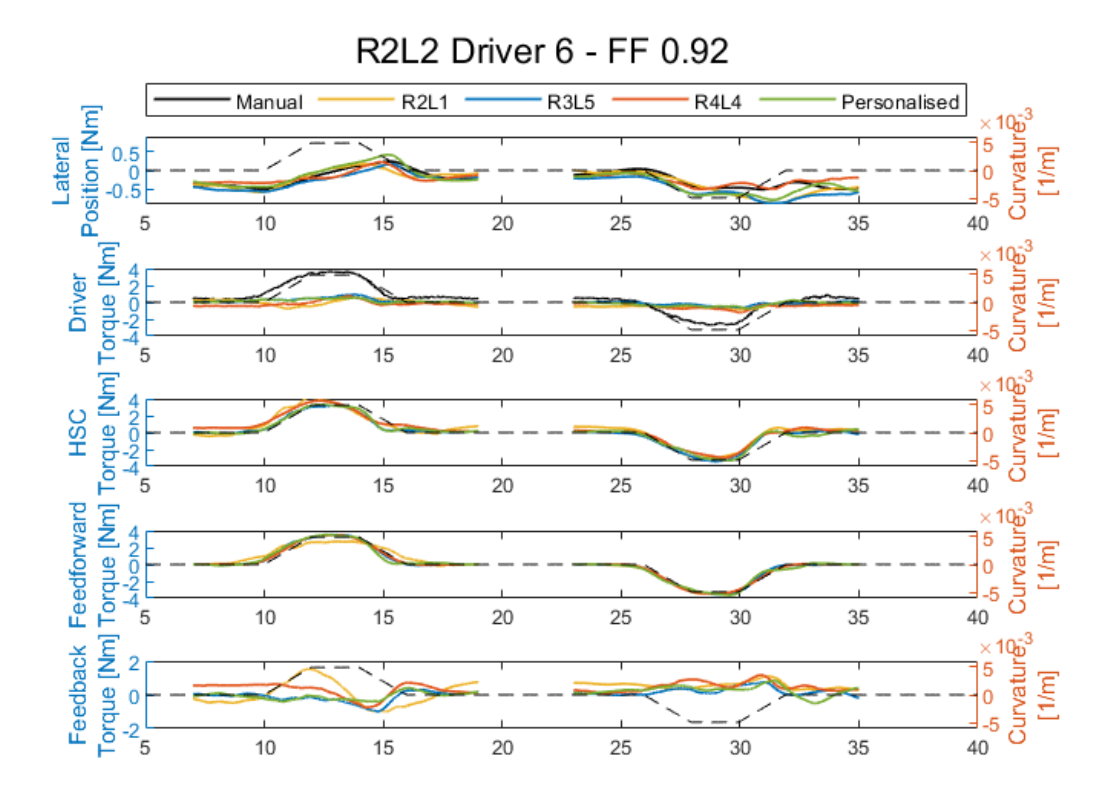


Figure B.51: Timeseries R2L2 driver 6 – FF 0.92

R2L2 Driver 6 - FF 0.92

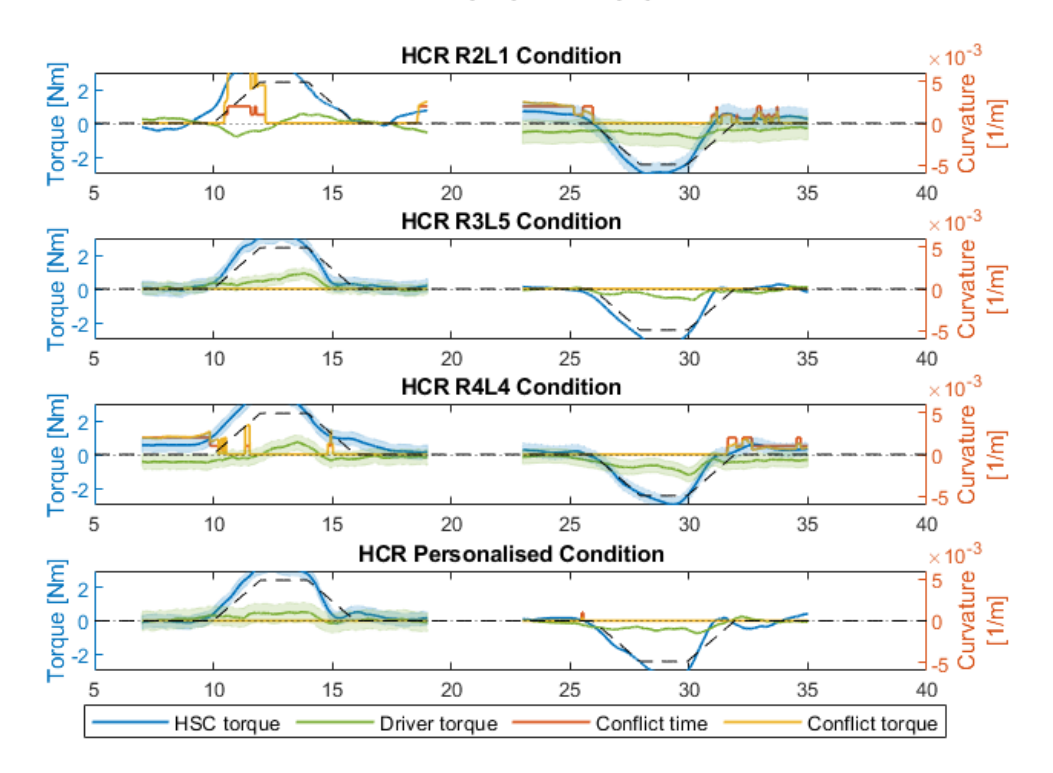


Figure B.52: Timeseries of conflict R2L2 driver $6 - FF\ 0.92$

R2L2 Driver 7 - FF 0.92

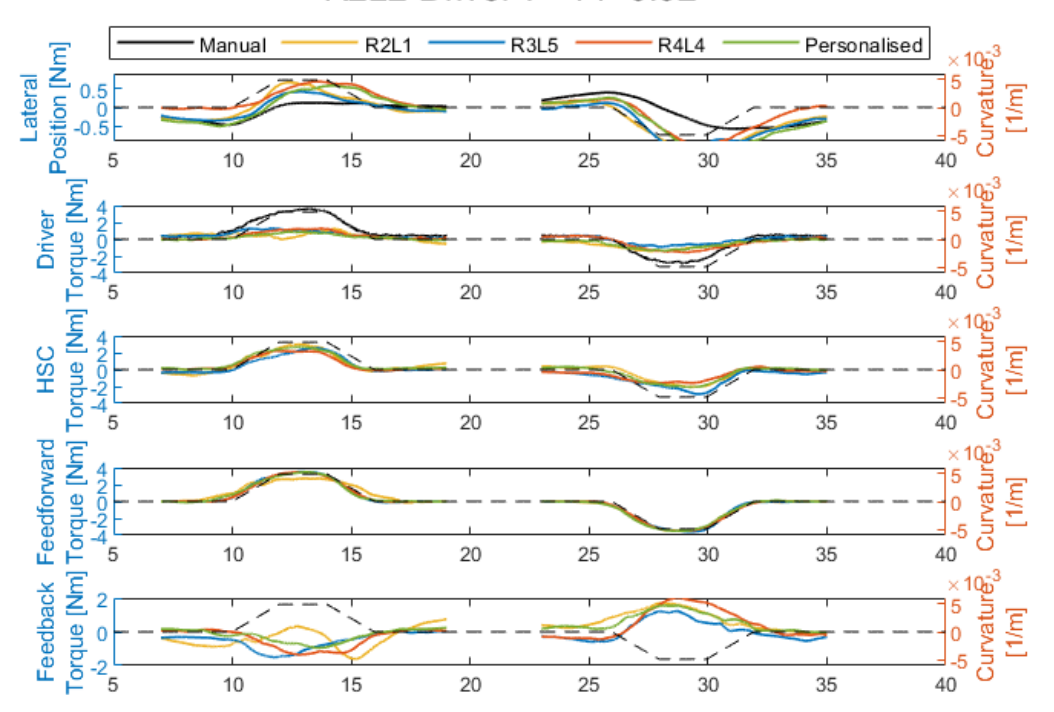


Figure B.55: Timeseries R2L2 driver 7 – FF 0.92

R2L2 Driver 7 - FF 0.92

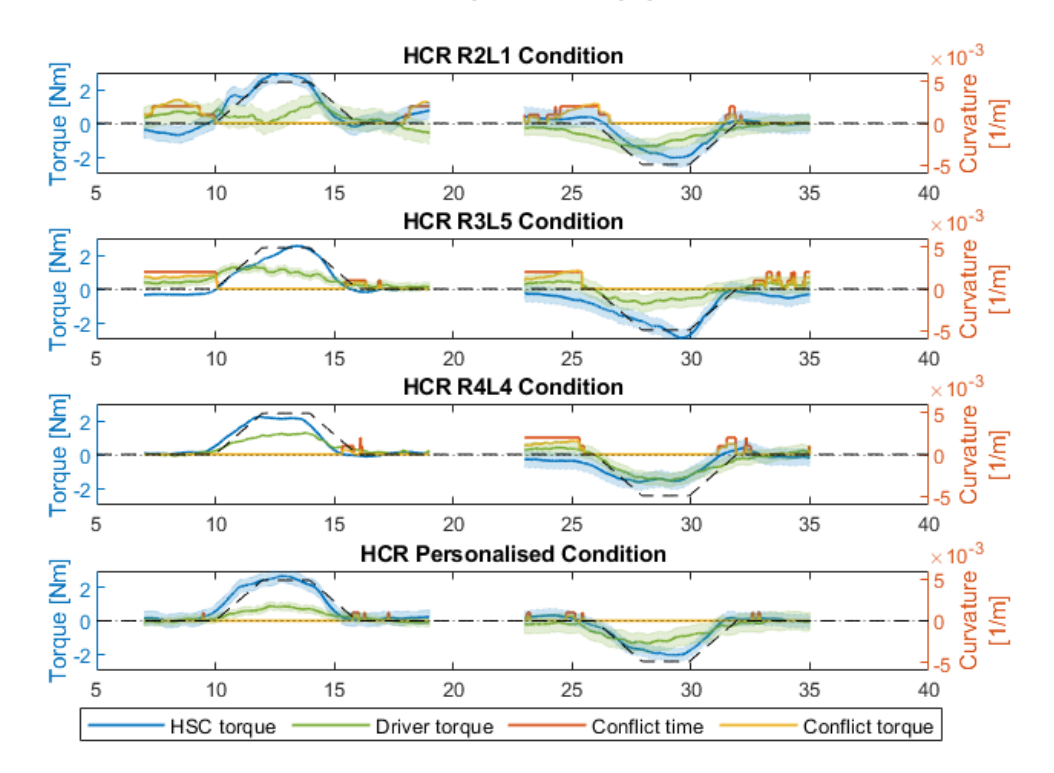


Figure B.56: Timeseries of conflict R2L2 driver 7 - FF 0.92

R2L2 Driver 8 - FF 0.5

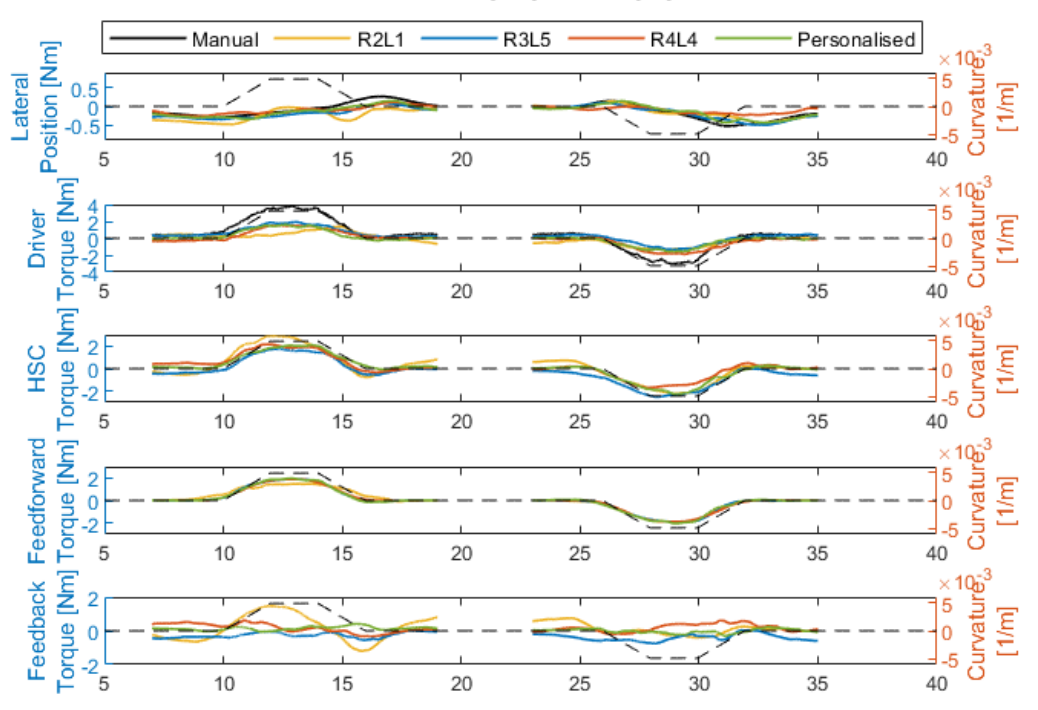


Figure B.57: Timeseries R2L2 driver 8 – FF 0.5

R2L2 Driver 8 - FF 0.5

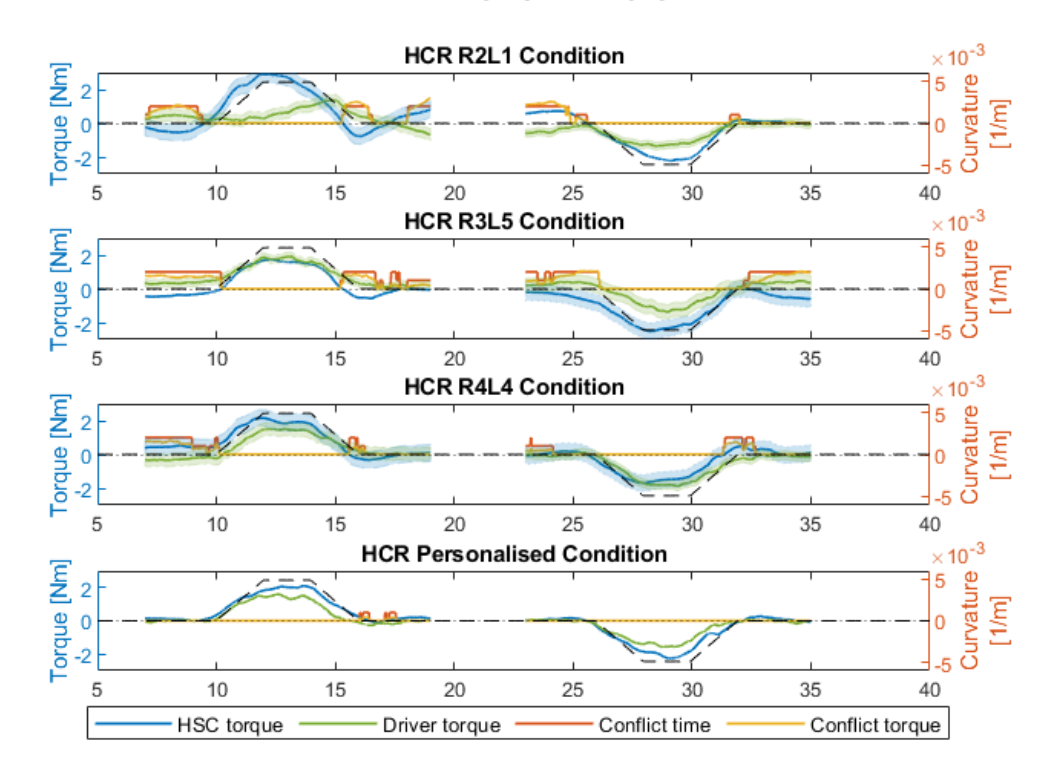


Figure B.58: Timeseries of conflict R2L2 driver $8-{\rm FF}~0.5$

R2L2 Driver 8 - FF 0.92

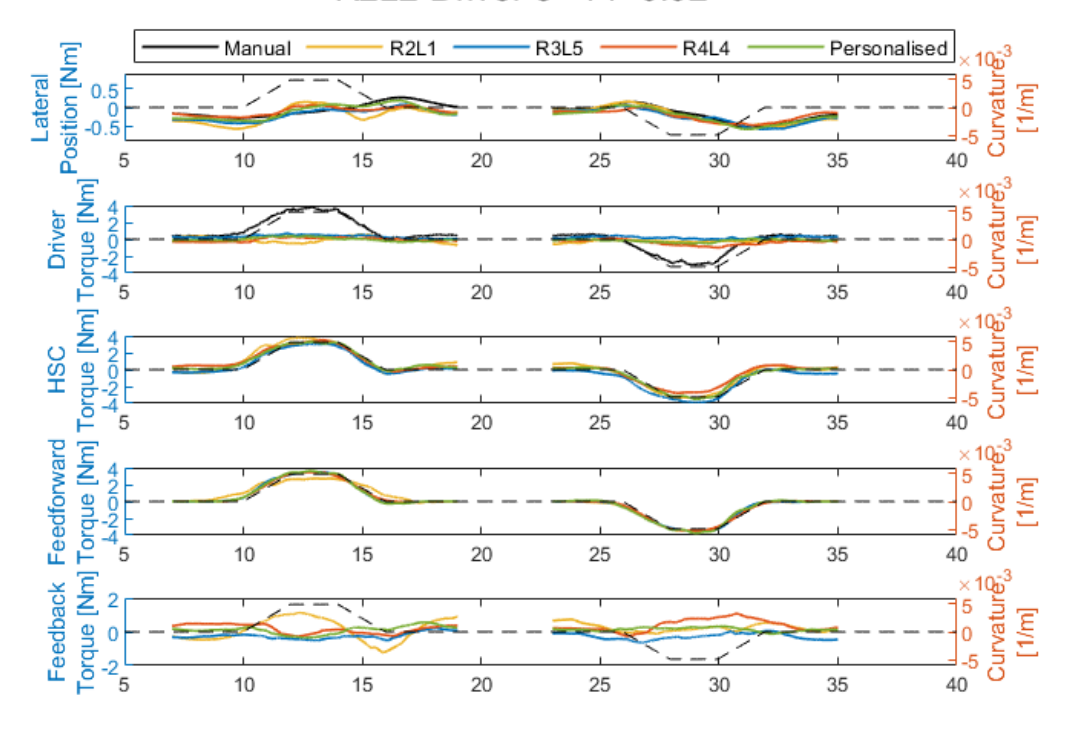


Figure B.59: Timeseries R2L2 driver 8 – FF 0.92

R2L2 Driver 8 - FF 0.92

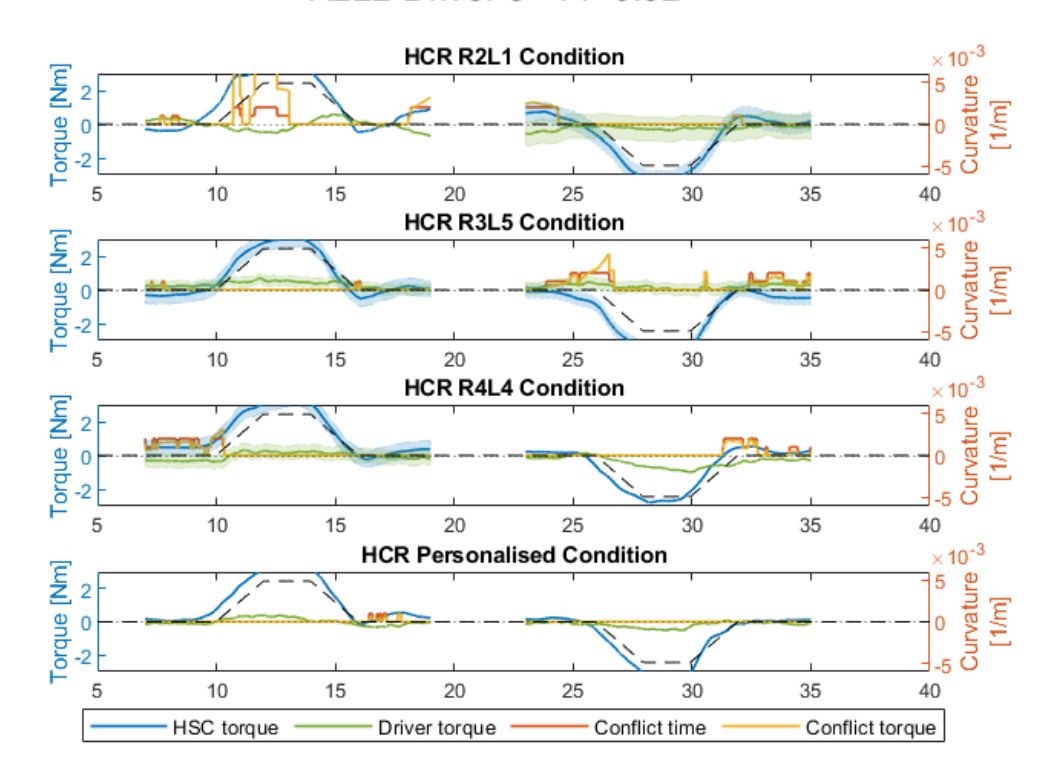


Figure B.60: Timeseries of conflict R2L2 driver $8-{\rm FF}~0.92$

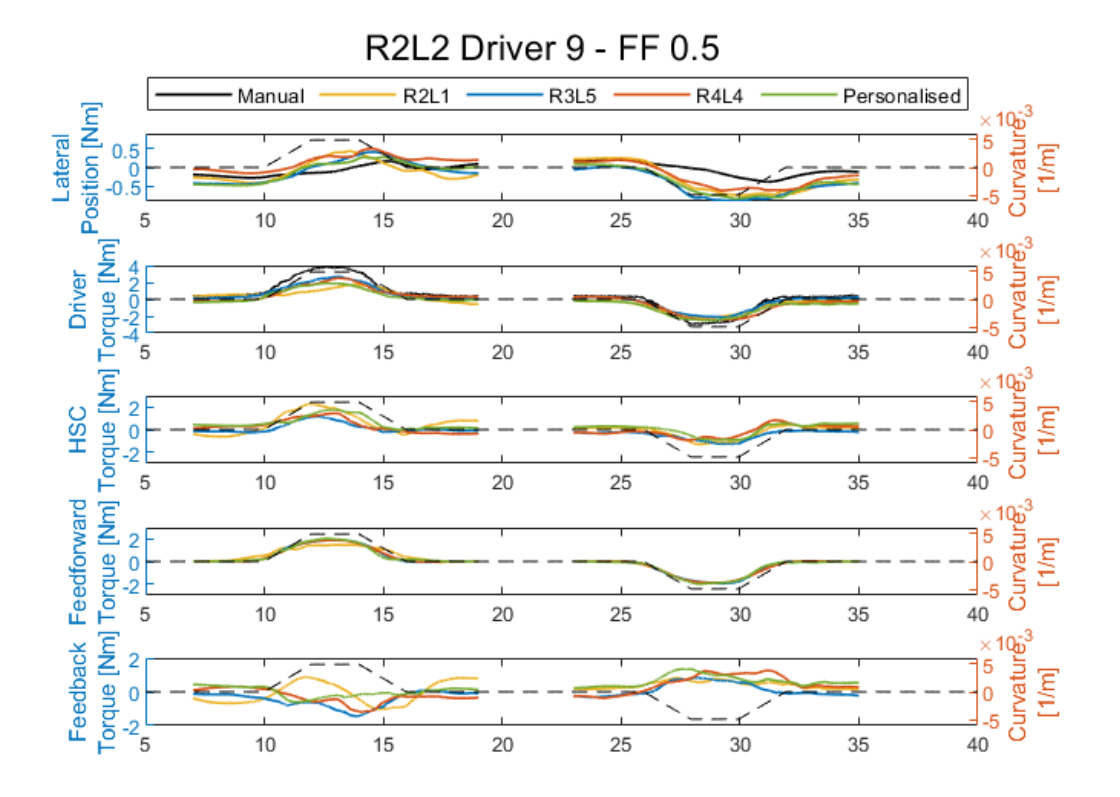


Figure B.61: Timeseries R2L2 driver 9 – FF 0.5

R2L2 Driver 9 - FF 0.5

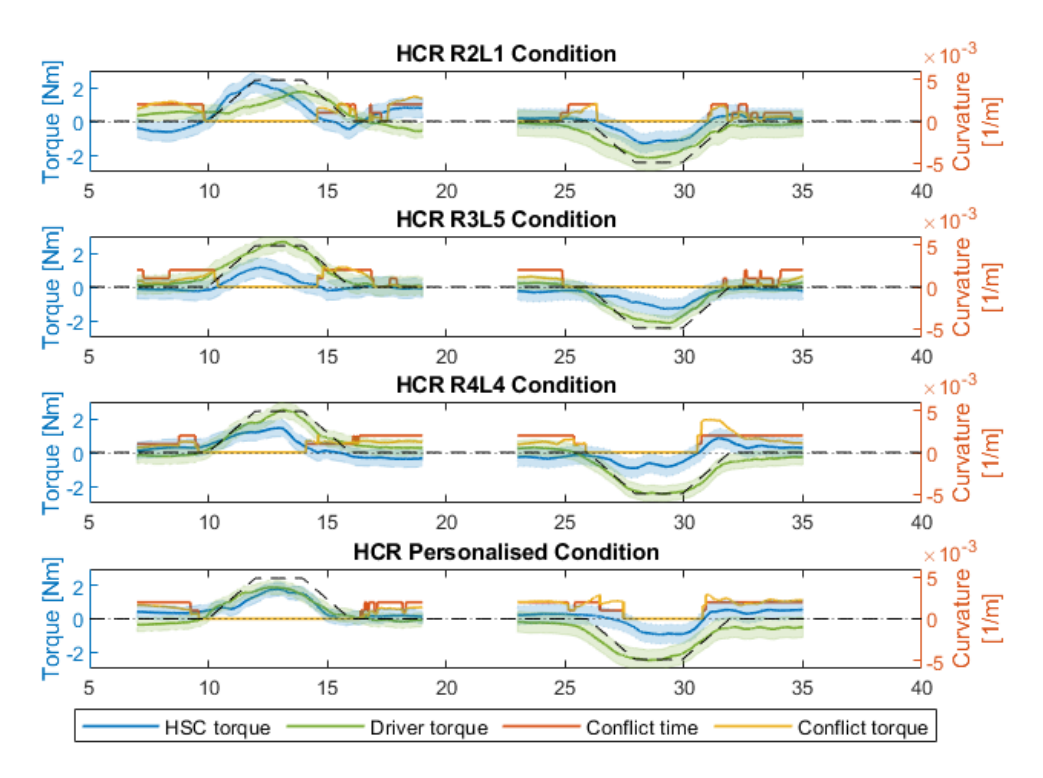


Figure B.62: Timeseries of conflict R2L2 driver 9 - FF 0.5

R2L2 Driver 9 - FF 0.92

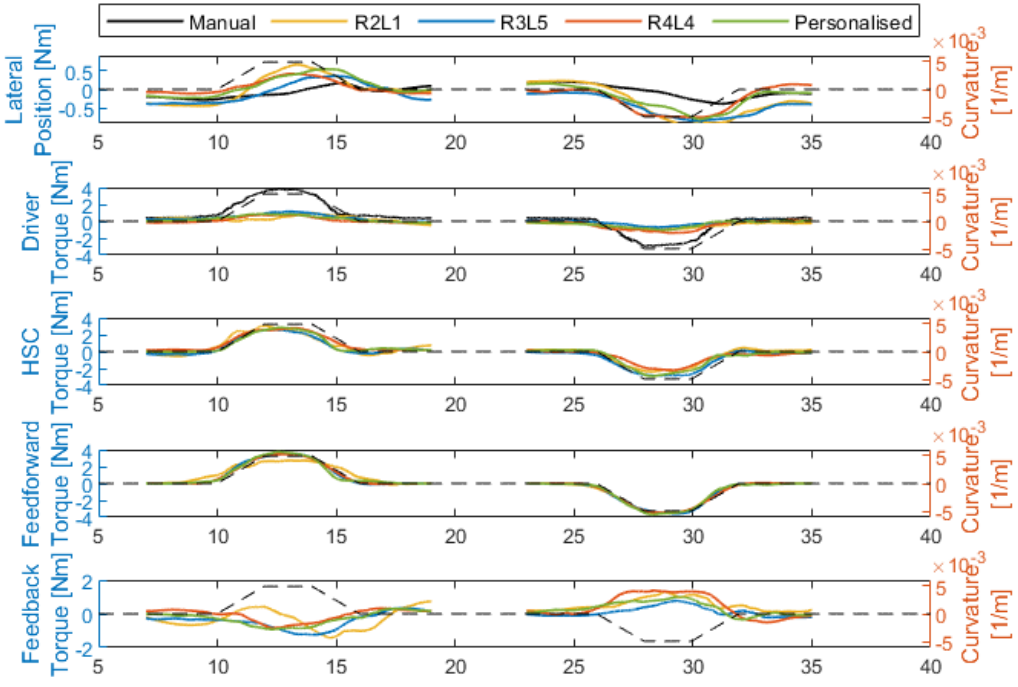


Figure B.63: Timeseries R2L2 driver 9 – FF 0.92

R2L2 Driver 9 - FF 0.92

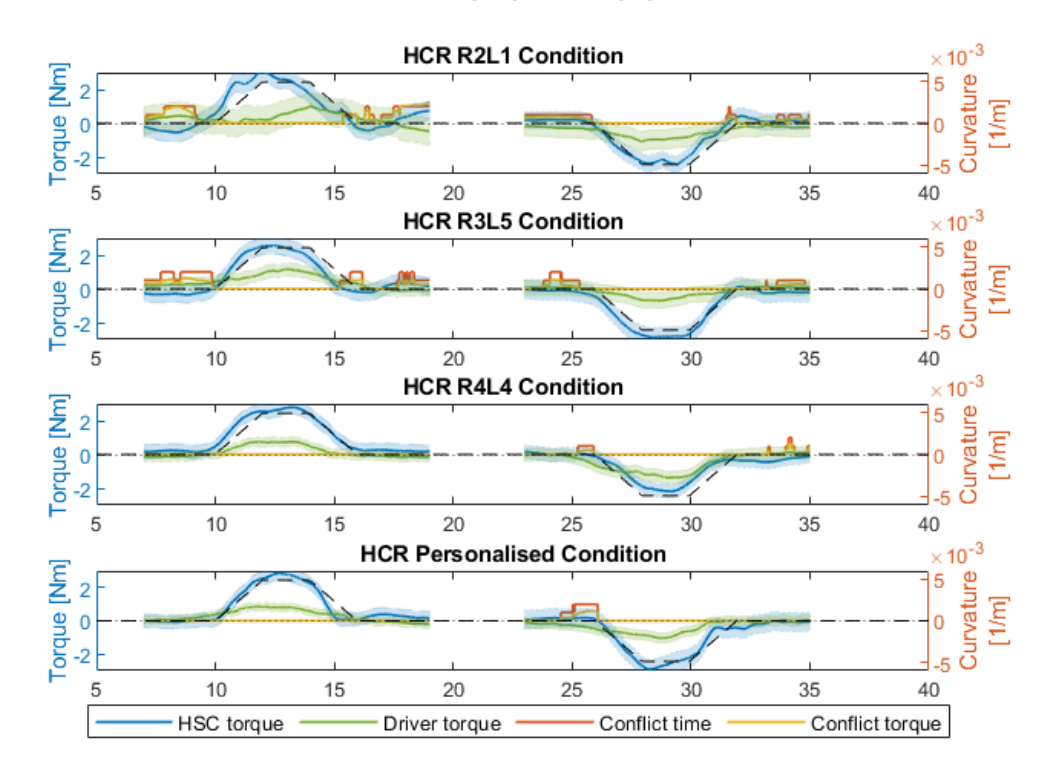


Figure B.64: Timeseries of conflict R2L2 driver 9 - FF 0.92

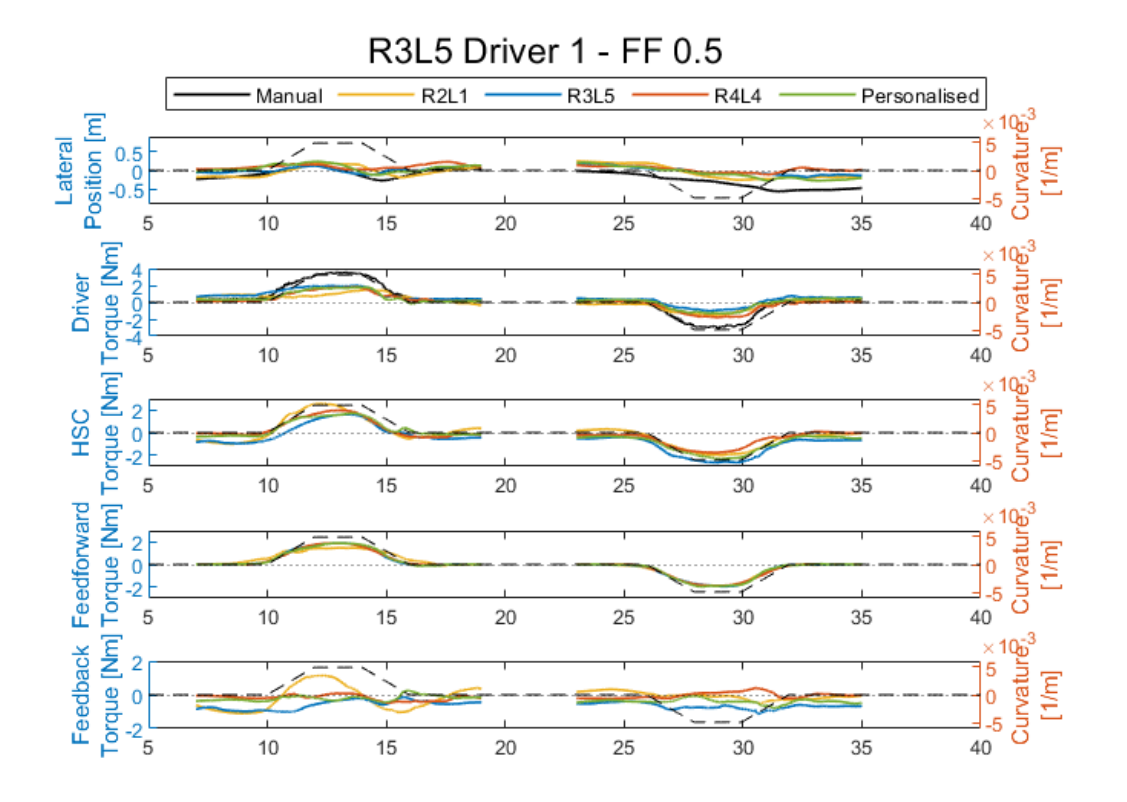


Figure B.65: Timeseries R3L5 driver 1 – FF 0.5

R3L5 Driver 1 - FF 0.5

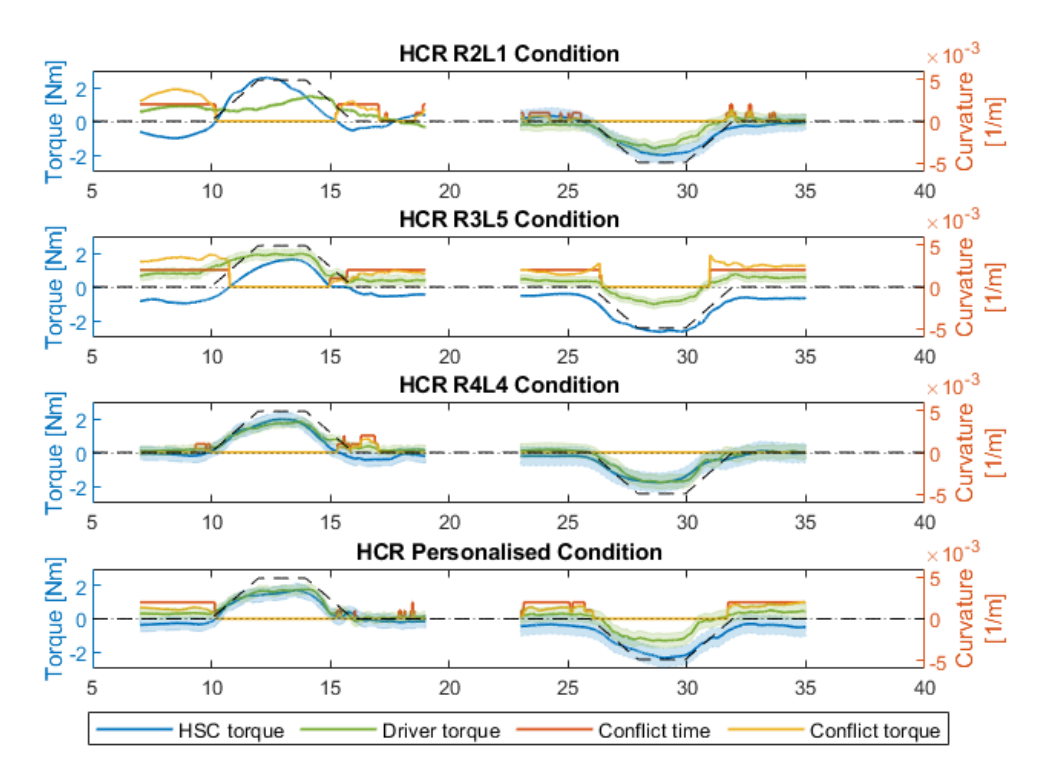


Figure B.66: Timeseries of conflict R3L5 driver $1-FF\ 0.5$

R3L5 Driver 1 - FF 0.92

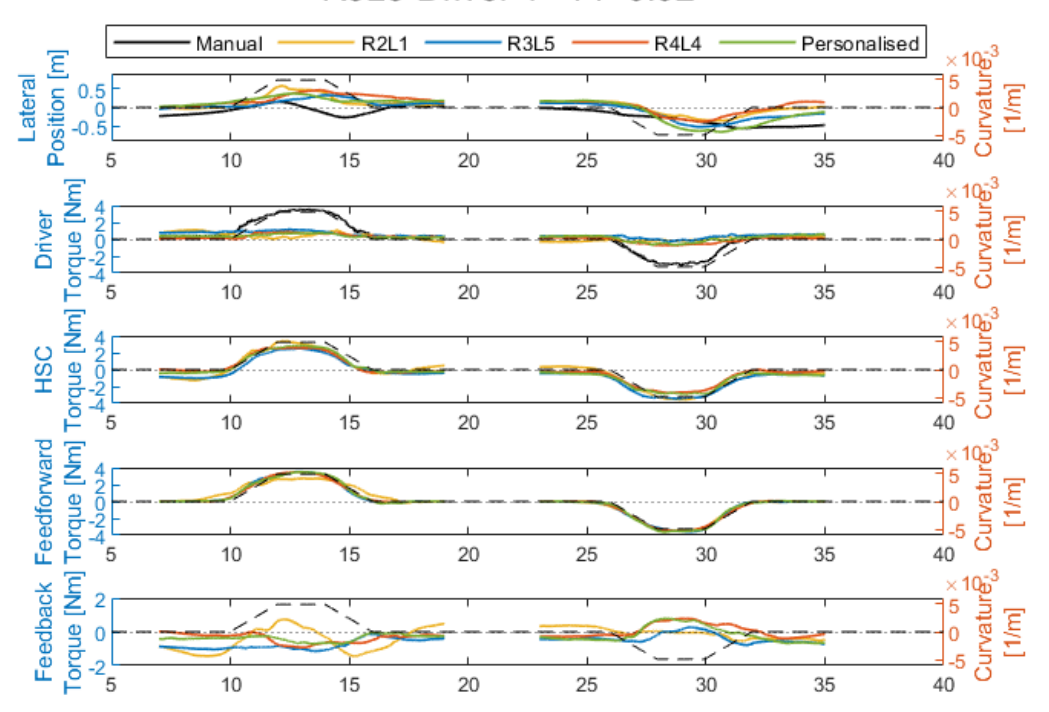


Figure B.67: Timeseries R3L5 driver 1 – FF 0.92

R3L5 Driver 1 - FF 0.92

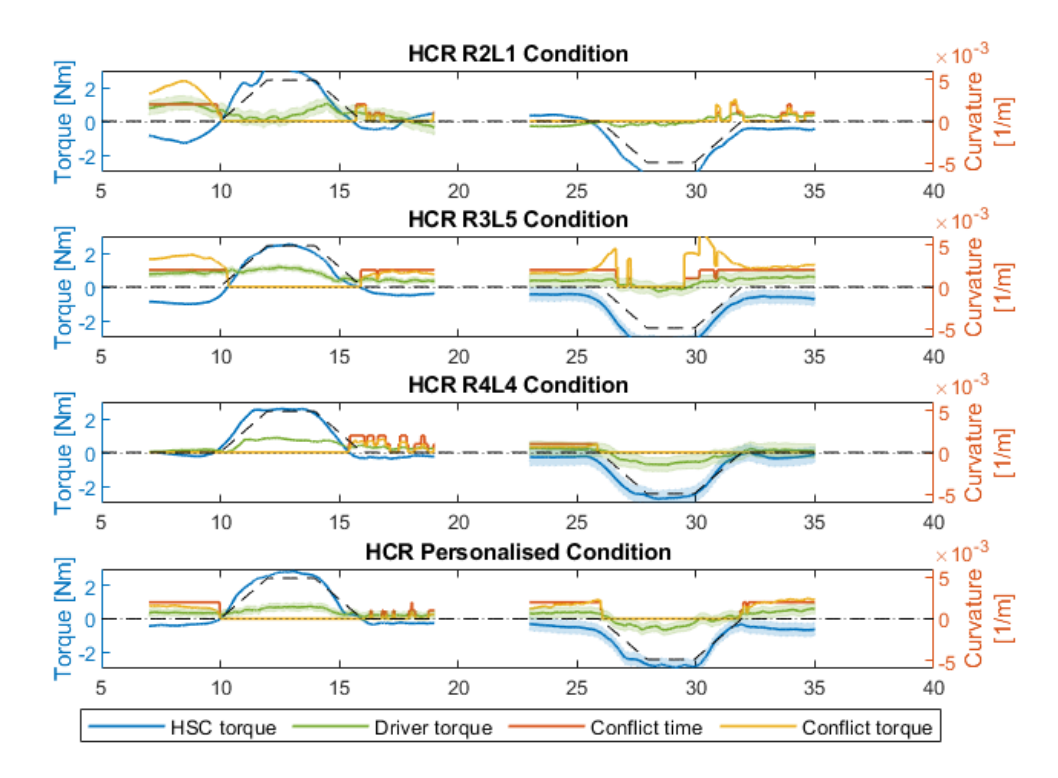


Figure B.68: Timeseries of conflict R3L5 driver $1-{\rm FF}~0.92$

R3L5 Driver 2 - FF 0.5

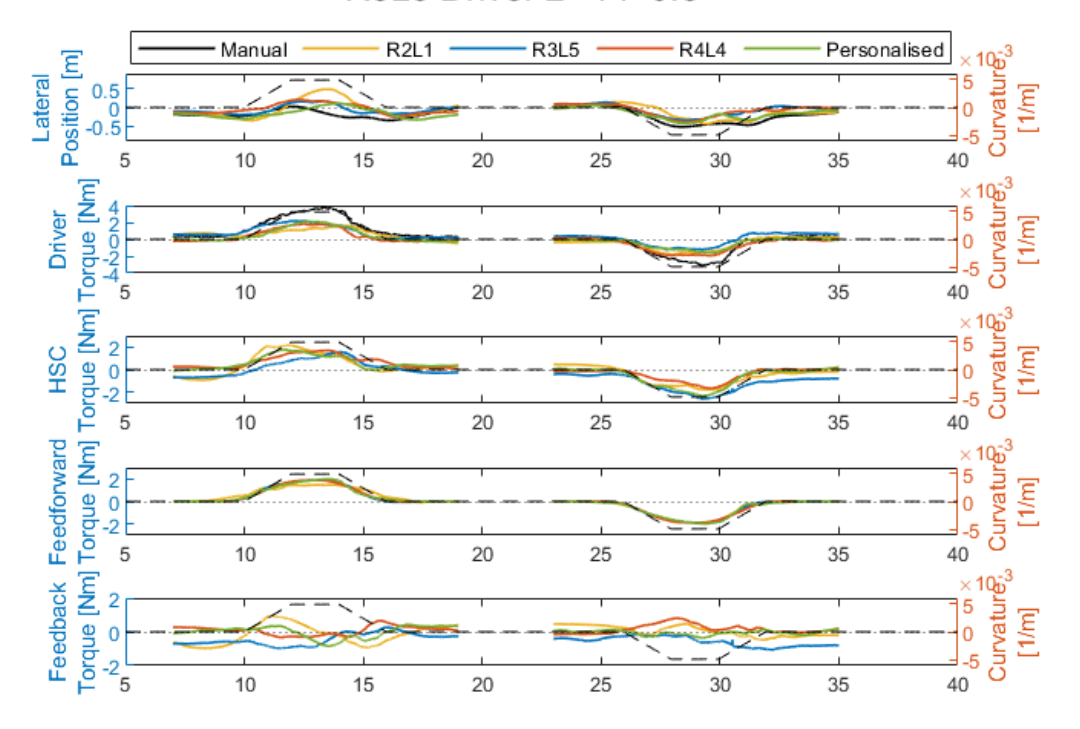


Figure B.69: Timeseries R3L5 driver 2 – FF 0.5

R3L5 Driver 2 - FF 0.5

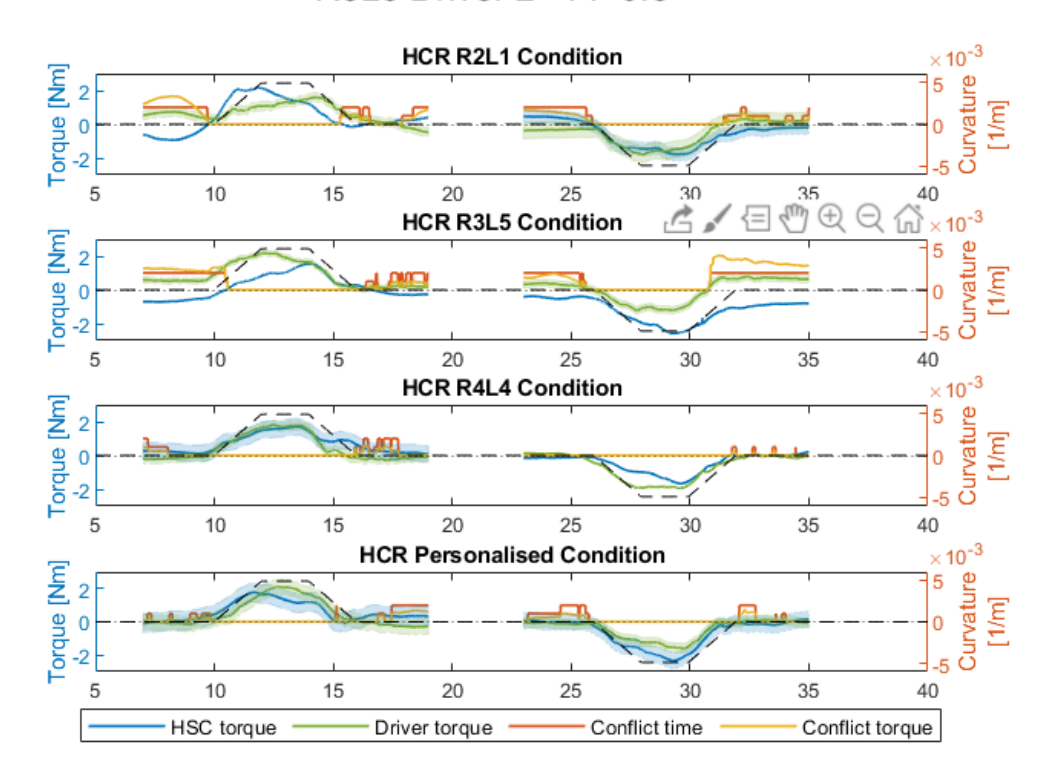


Figure B.70: Timeseries of conflict R3L5 driver $2-FF\ 0.5$

R3L5 Driver 2 - FF 0.92

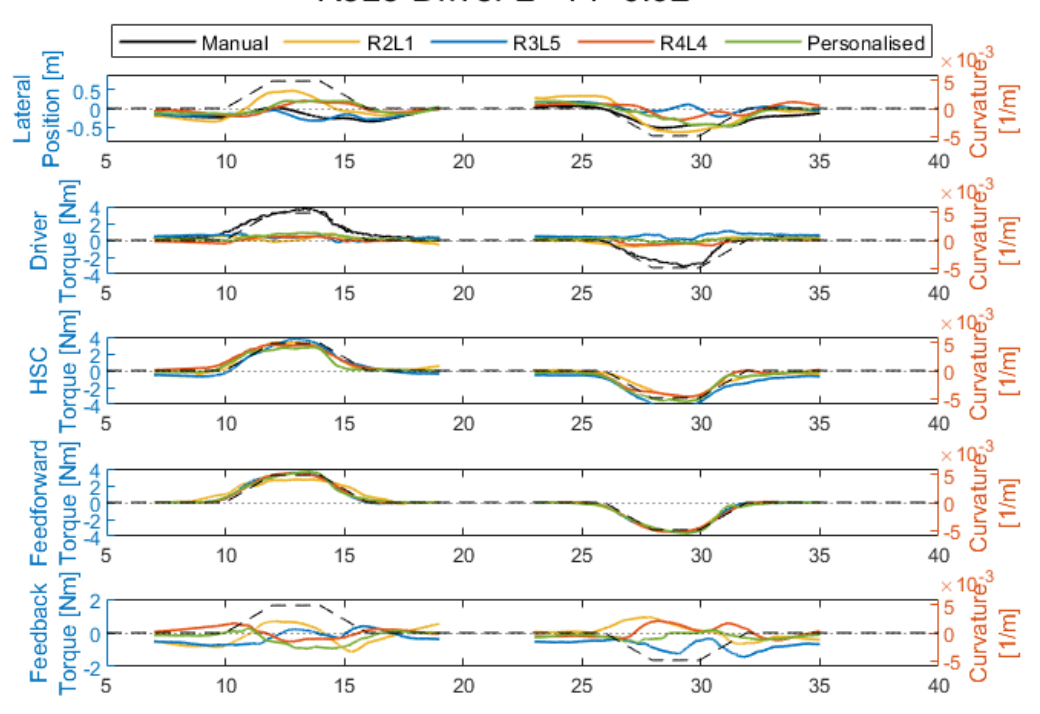


Figure B.71: Timeseries R3L5 driver 2 – FF 0.92

R3L5 Driver 2 - FF 0.92

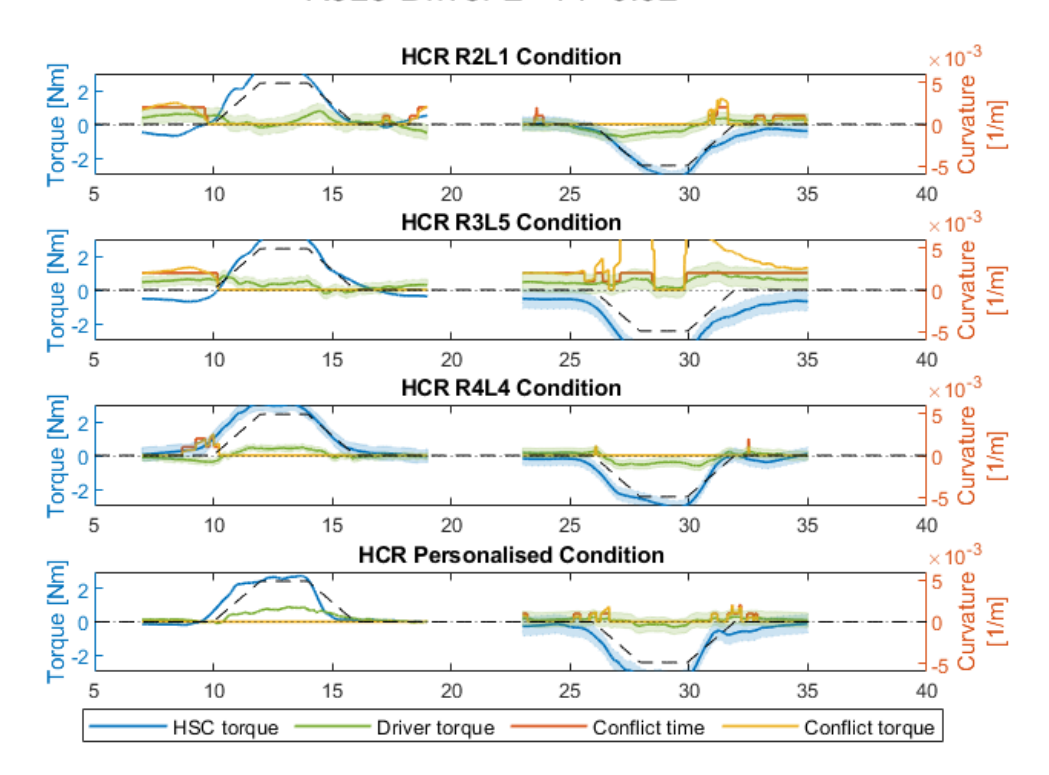


Figure B.72: Timeseries of conflict R3L5 driver 2 - FF 0.92

R3L5 Driver 3 - FF 0.5

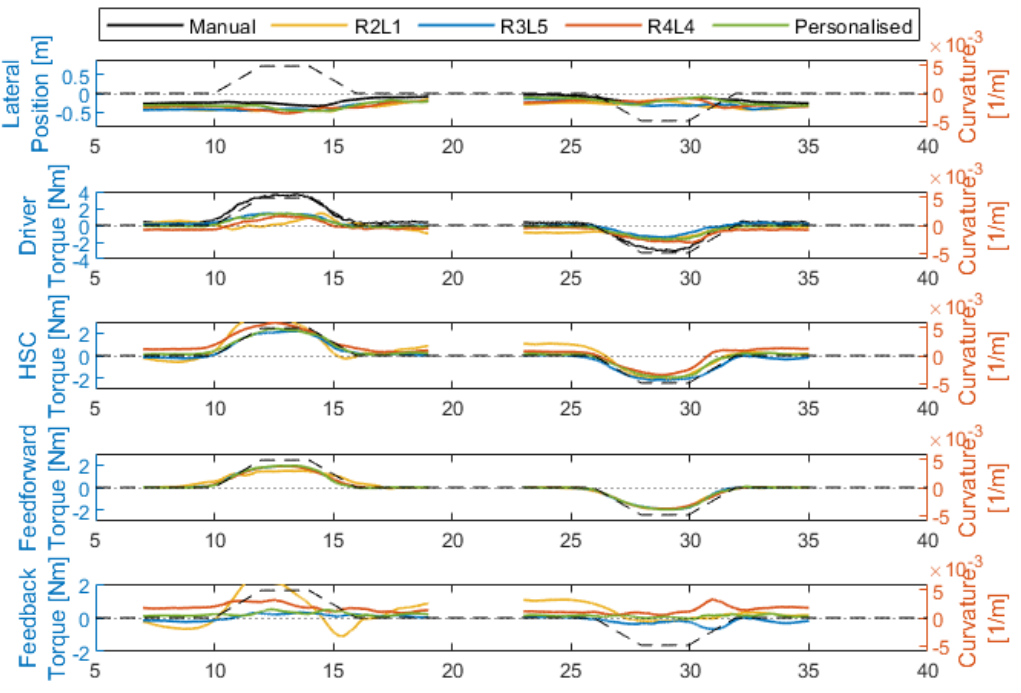


Figure B.73: Timeseries R3L5 driver 3 – FF 0.5

R3L5 Driver 3 - FF 0.5

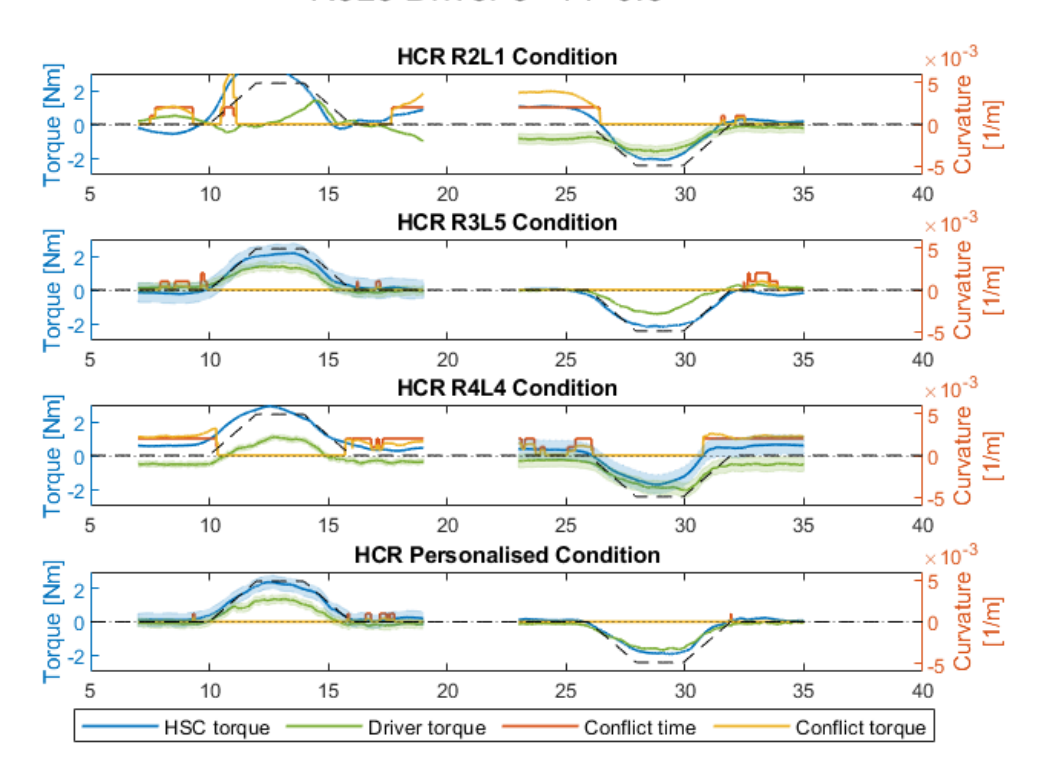


Figure B.74: Timeseries of conflict R3L5 driver $3-FF\ 0.5$

R3L5 Driver 3 - FF 0.92

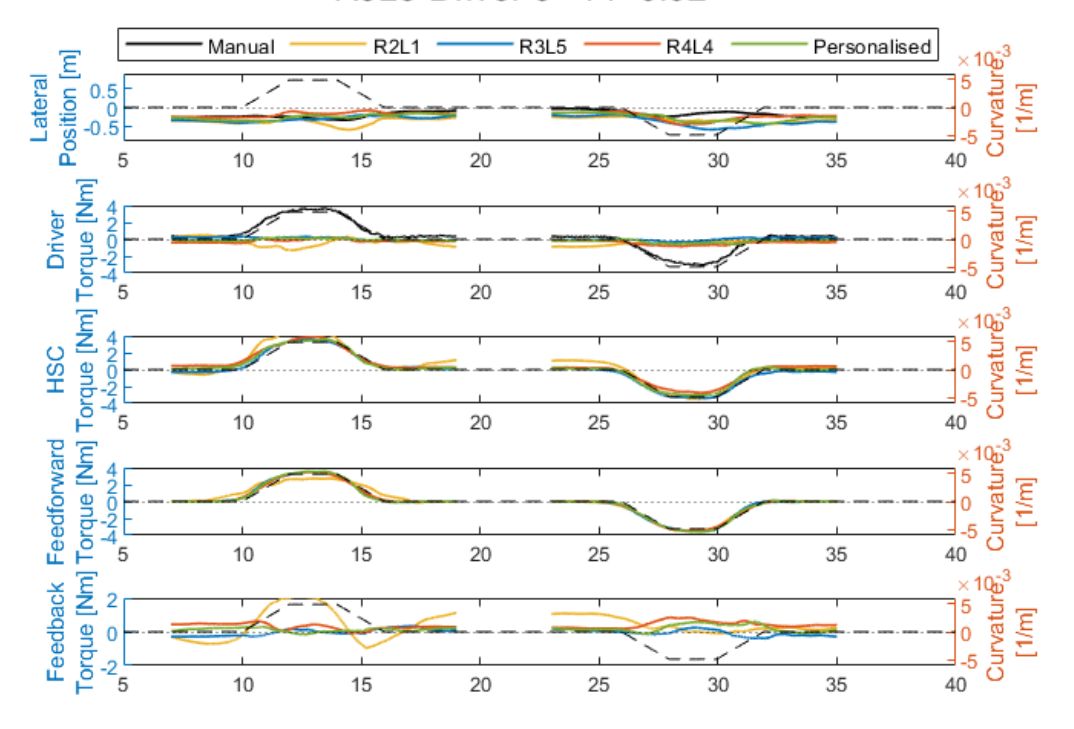


Figure B.75: Timeseries R3L5 driver 3 – FF 0.92

R3L5 Driver 3 - FF 0.92

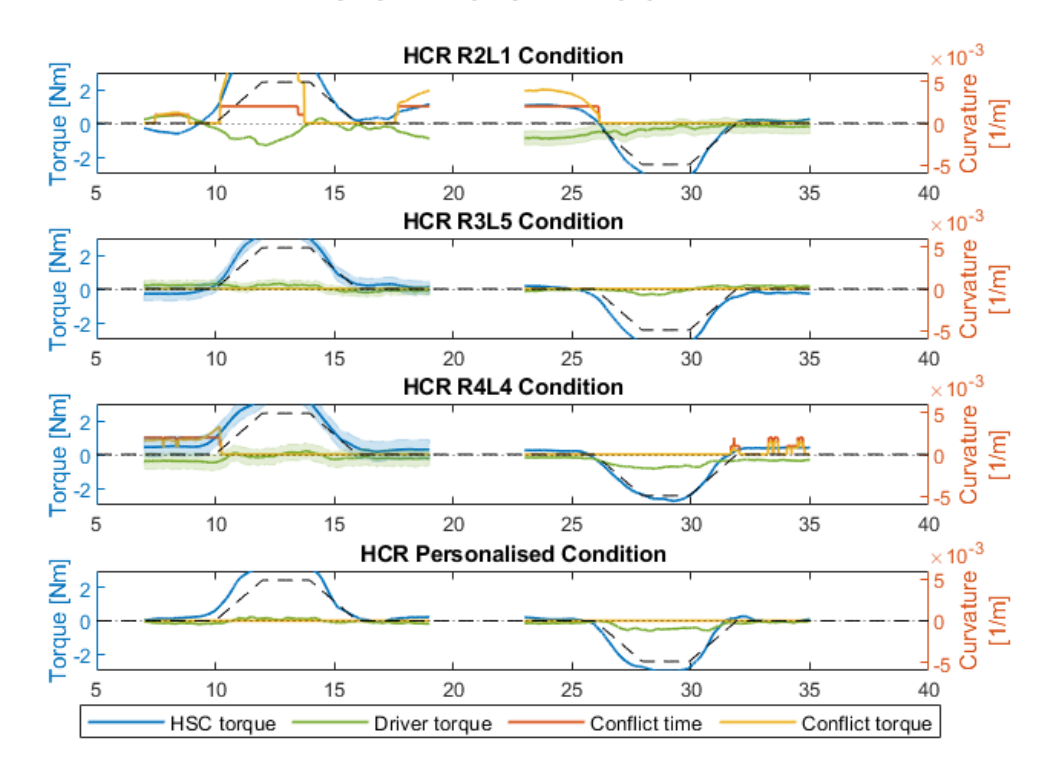


Figure B.76: Timeseries of conflict R3L5 driver $3-FF\ 0.92$

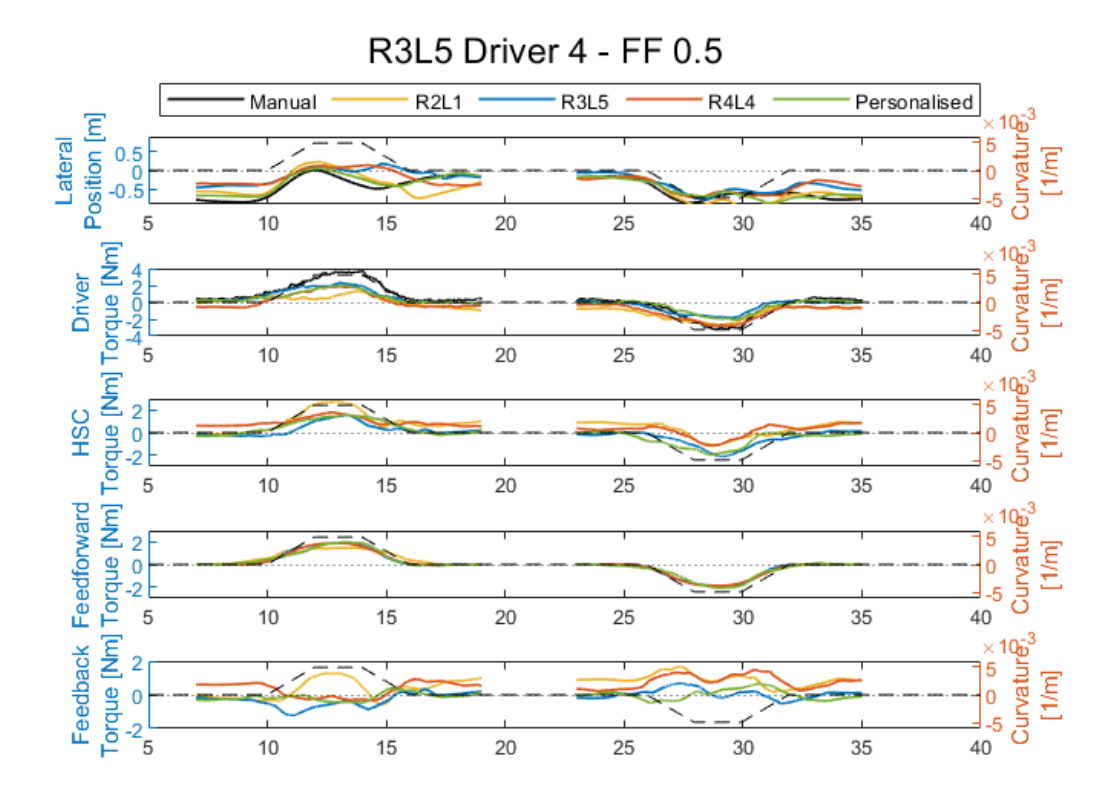


Figure B.77: Timeseries R3L5 driver 4 – FF 0.5

R3L5 Driver 4 - FF 0.5

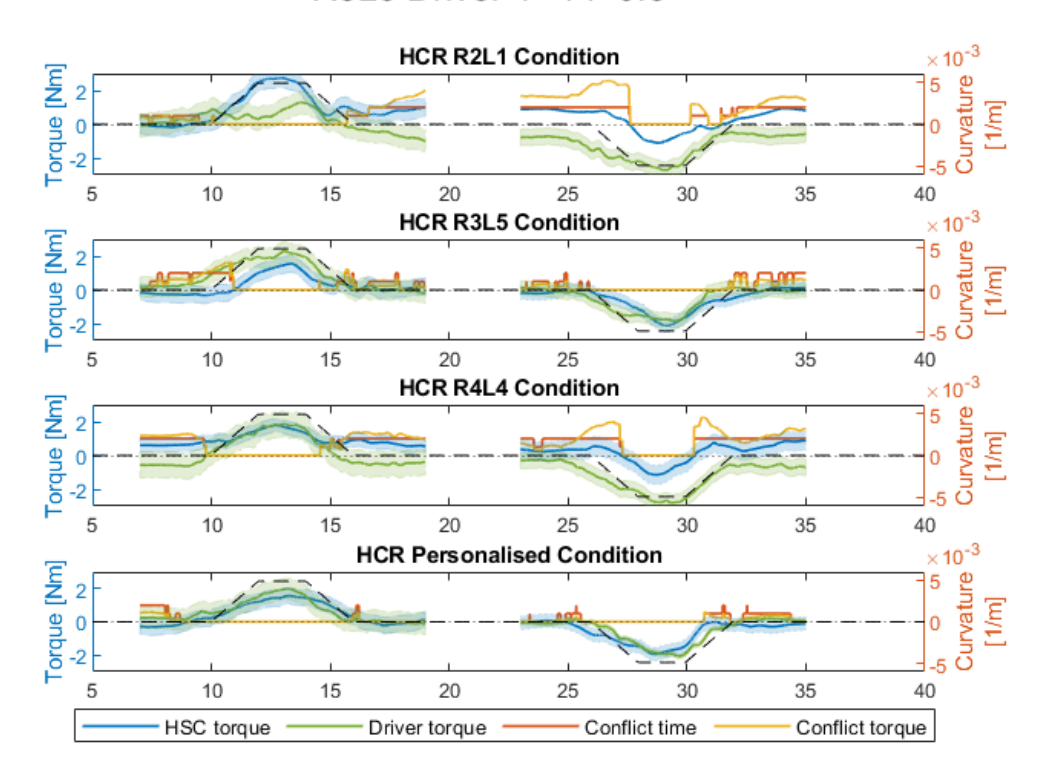


Figure B.78: Timeseries of conflict R3L5 driver 4 - FF 0.5

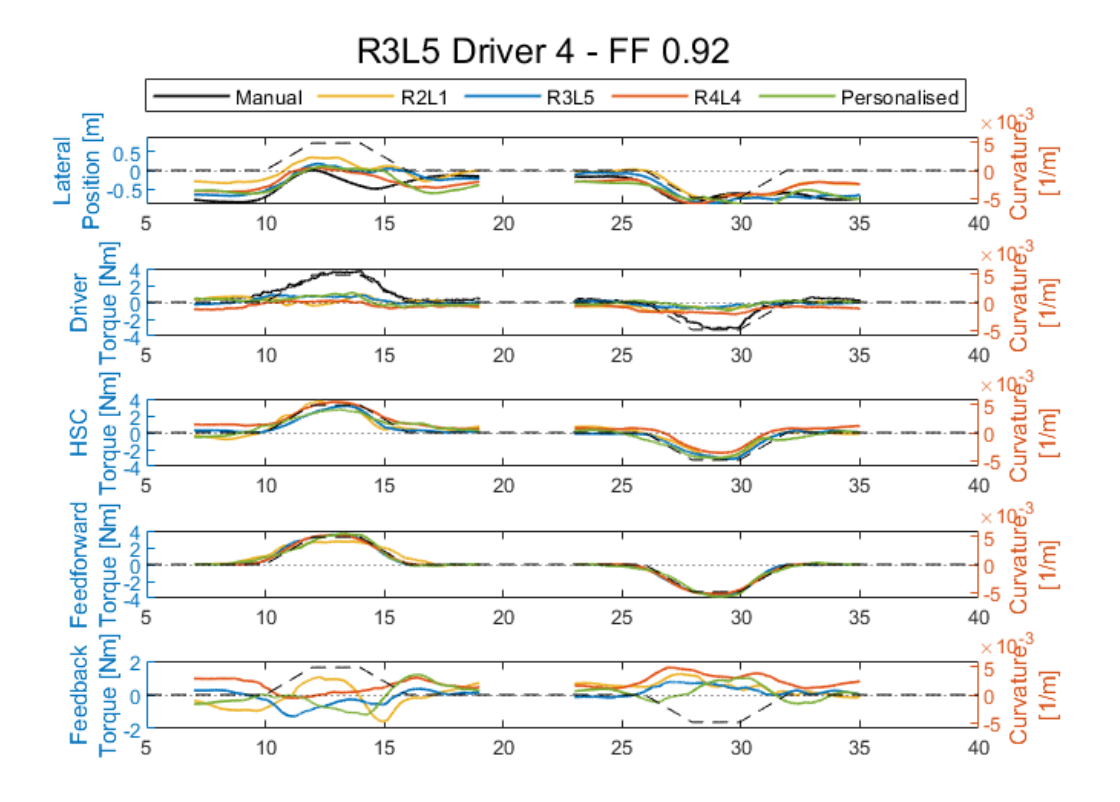


Figure B.79: Timeseries R3L5 driver 4 – FF 0.92

R3L5 Driver 4 - FF 0.92

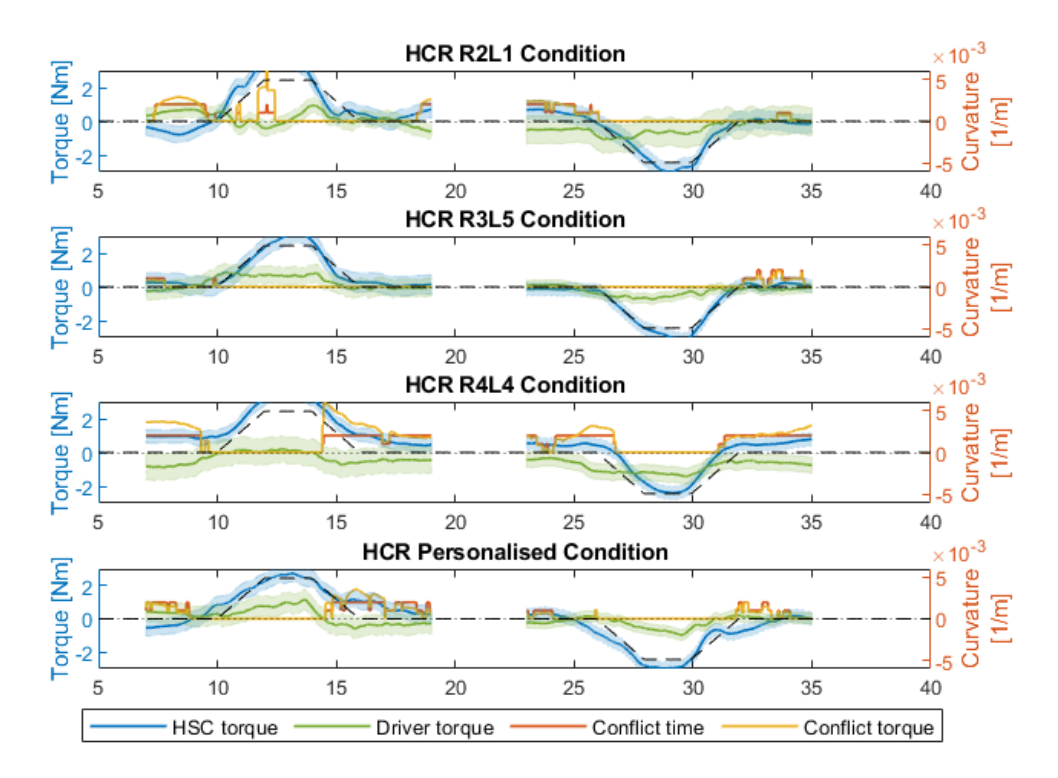


Figure B.80: Timeseries of conflict R3L5 driver $4-FF\ 0.92$

R3L5 Driver 5 - FF 0.5

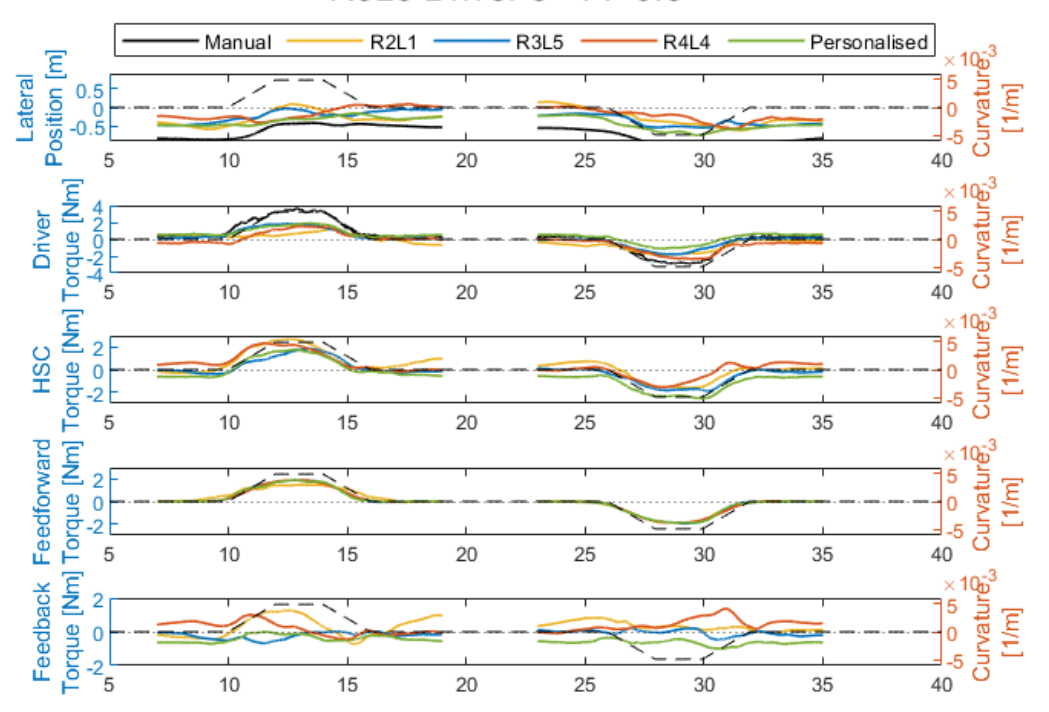


Figure B.81: Timeseries R3L5 driver 5 – FF 0.5

R3L5 Driver 5 - FF 0.5

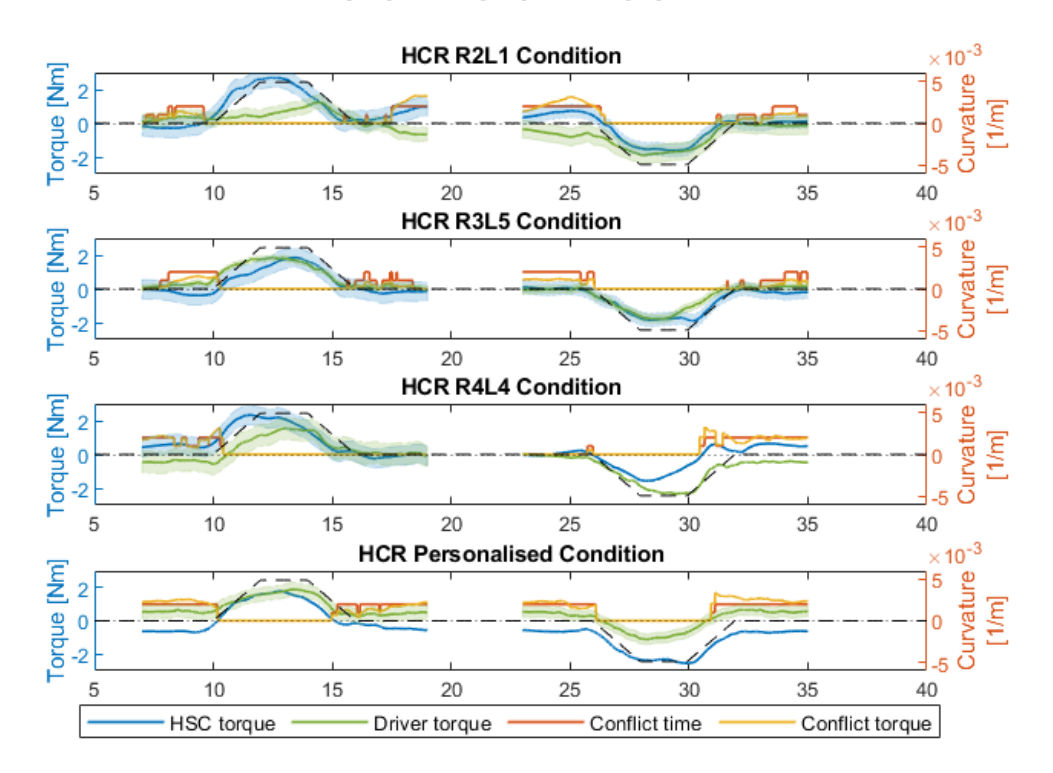


Figure B.82: Timeseries of conflict R3L5 driver 5 - FF 0.5

R3L5 Driver 5 - FF 0.92

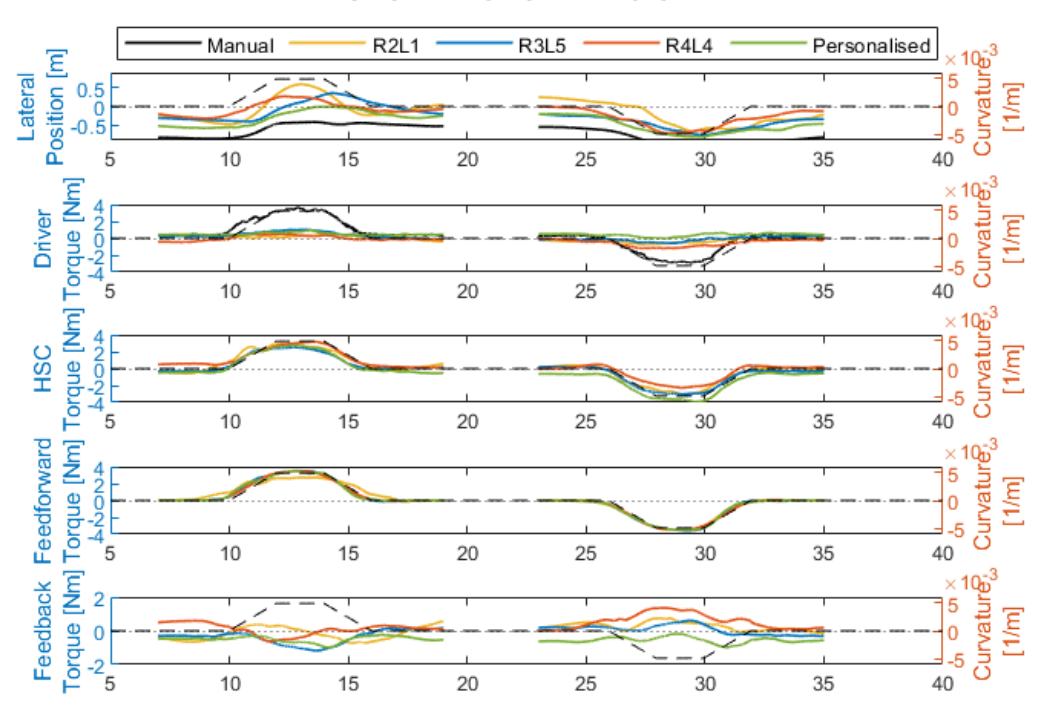


Figure B.83: Timeseries R3L5 driver 5 – FF 0.92

R3L5 Driver 5 - FF 0.92

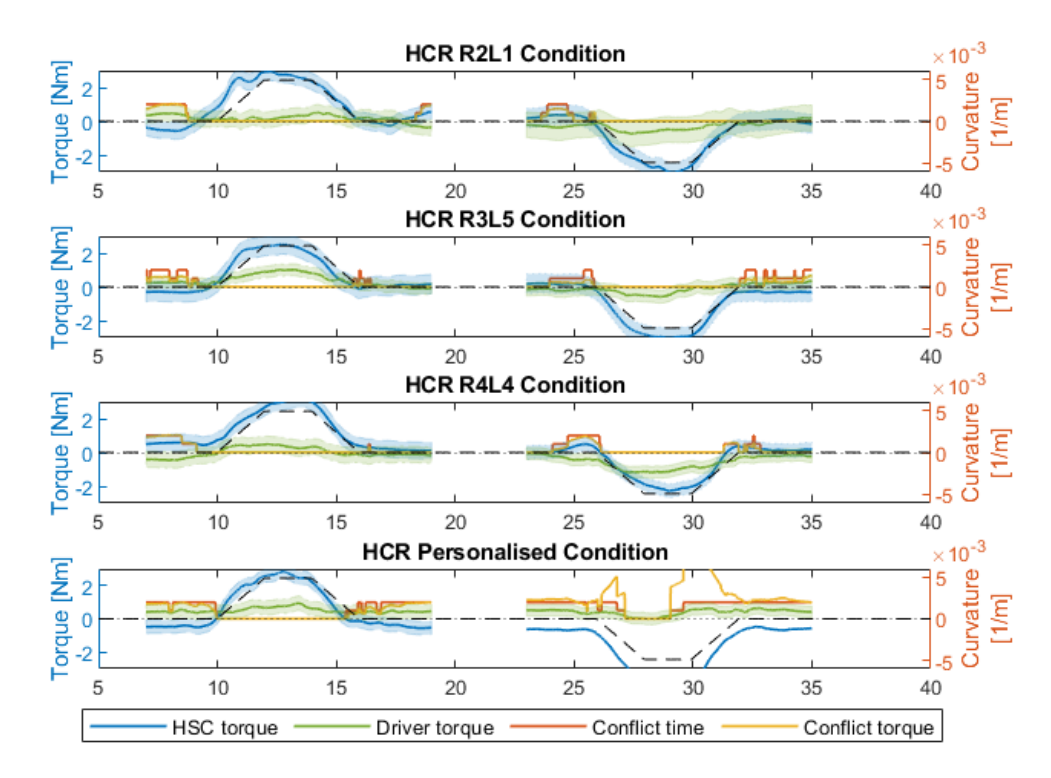


Figure B.84: Timeseries of conflict R3L5 driver 5 - FF 0.92

R3L5 Driver 6 - FF 0.5

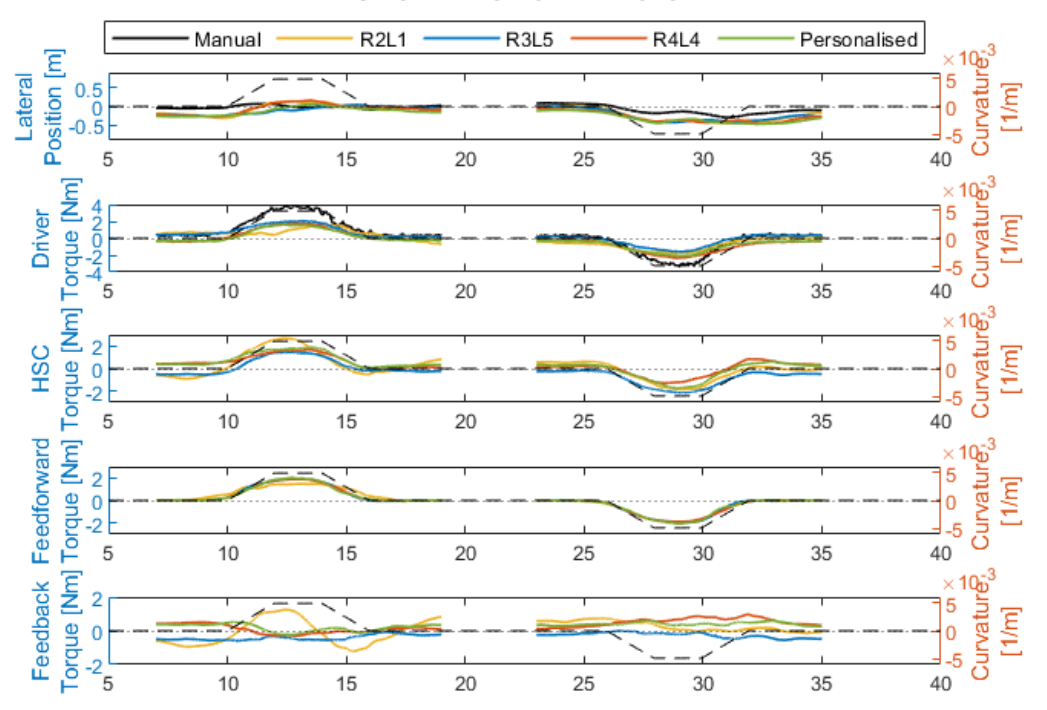


Figure B.85: Timeseries R3L5 driver 6 – FF 0.5

R3L5 Driver 6 - FF 0.5

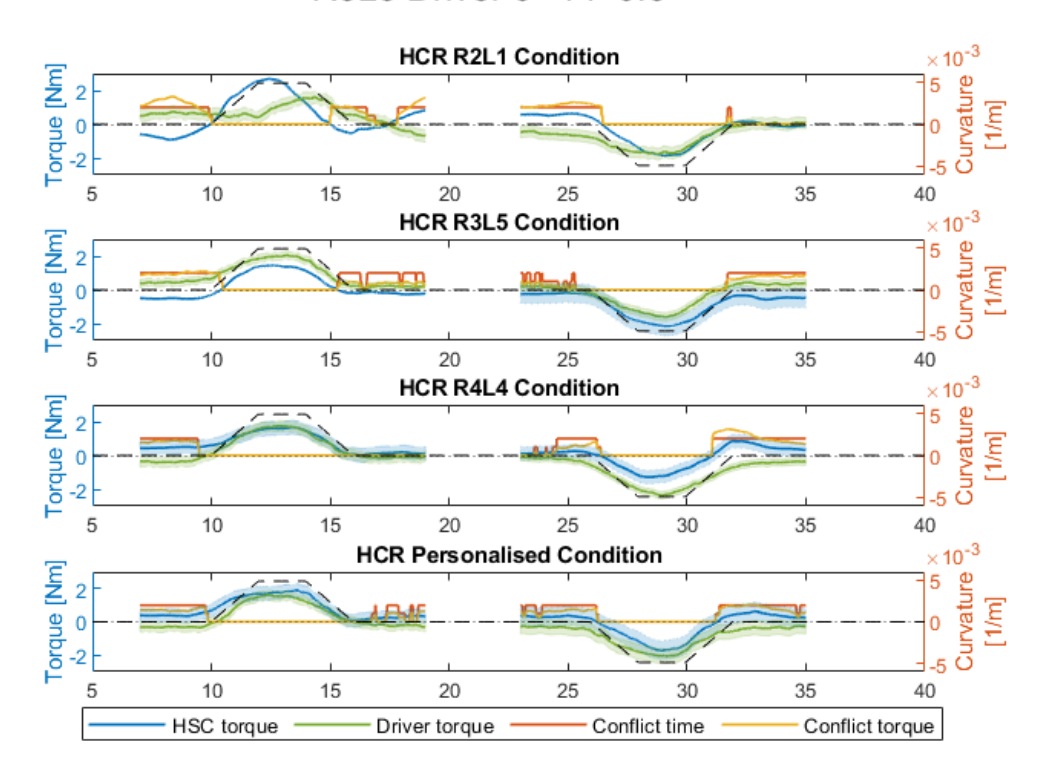


Figure B.86: Timeseries of conflict R3L5 driver 6 - FF 0.5

R3L5 Driver 6 - FF 0.92

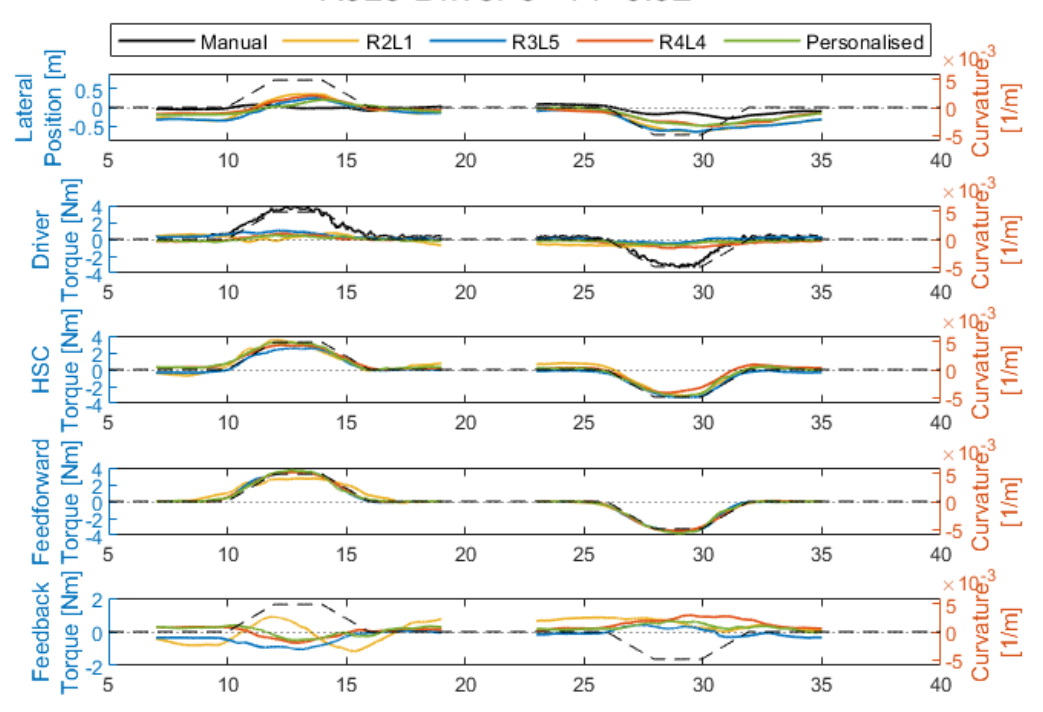


Figure B.87: Timeseries R3L5 driver 6 – FF 0.92

R3L5 Driver 6 - FF 0.92

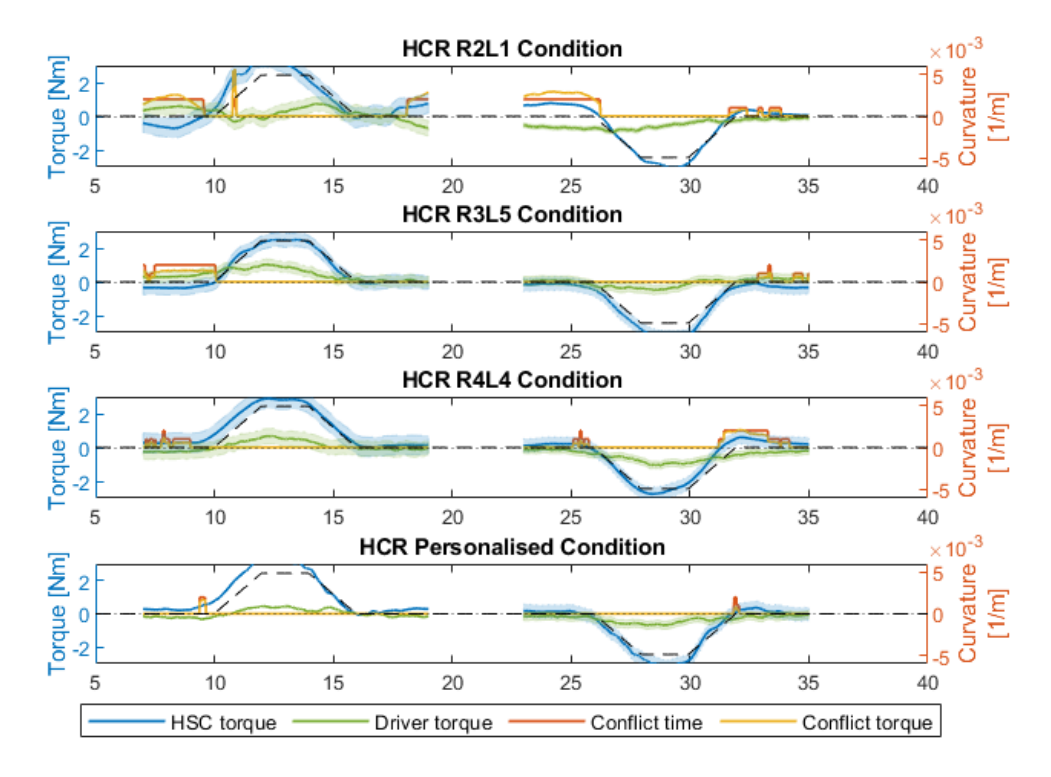


Figure B.88: Timeseries of conflict R3L5 driver 6 - FF 0.92

R3L5 Driver 7 - FF 0.5 R2L1 R3L5 Manual R4L4 Personalised Curvature. Position [m] 0 0.5 0 -0.5 [1/m] -5 × 10-3 5 0 5-7 Curvature 40 Torque [Nm] Torque [Nm] Torque [Nm] Driver Curvature 2 0 -2 HSC -5 Feedback Feedforward 0 -2 Curvature 5 -2 5

Figure B.89: Timeseries R3L5 driver 7 – FF 0.5

R3L5 Driver 7 - FF 0.5

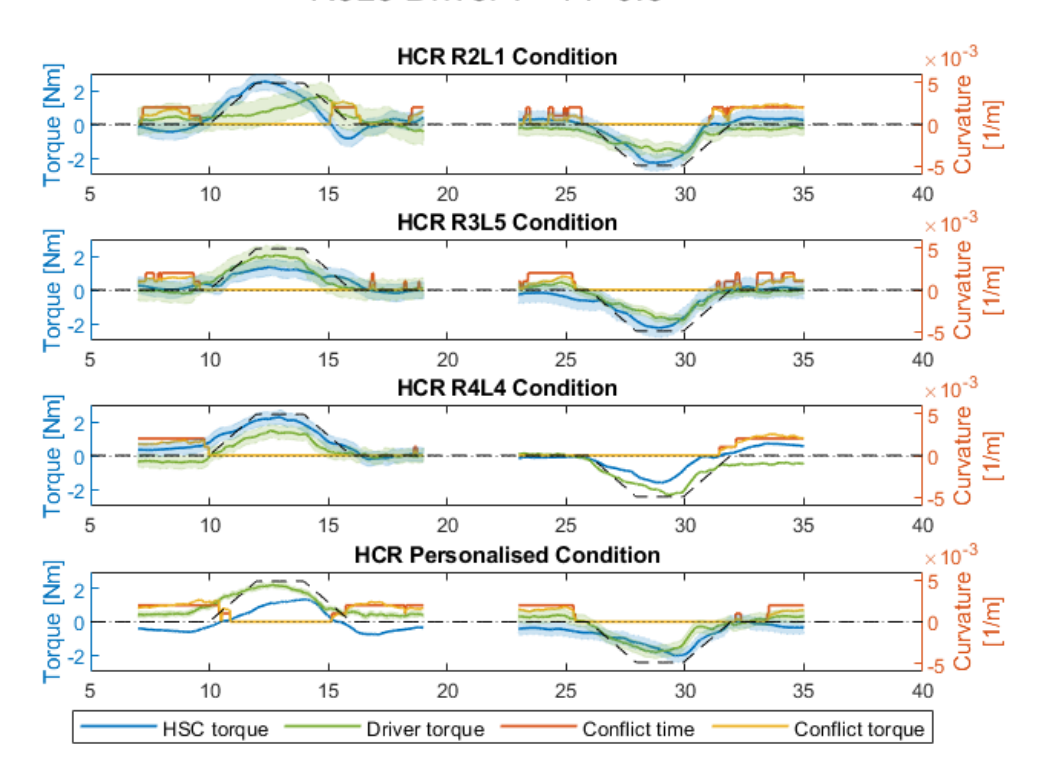


Figure B.90: Timeseries of conflict R3L5 driver 7 - FF 0.5

R3L5 Driver 7 - FF 0.92

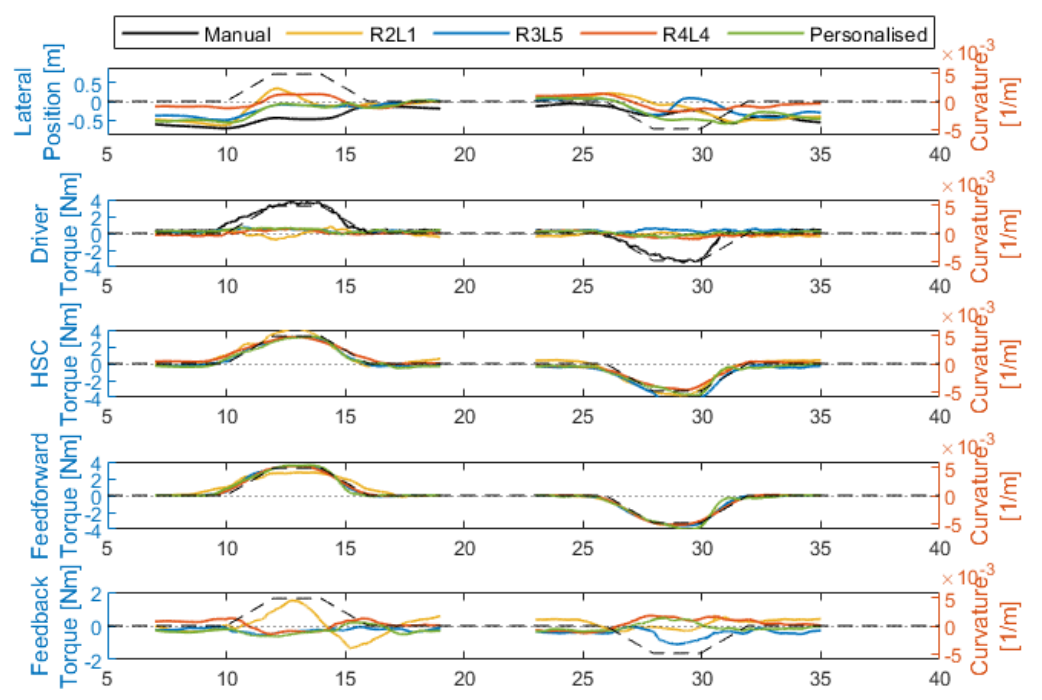


Figure B.91: Timeseries R3L5 driver 7 – FF 0.92

R3L5 Driver 7 - FF 0.92

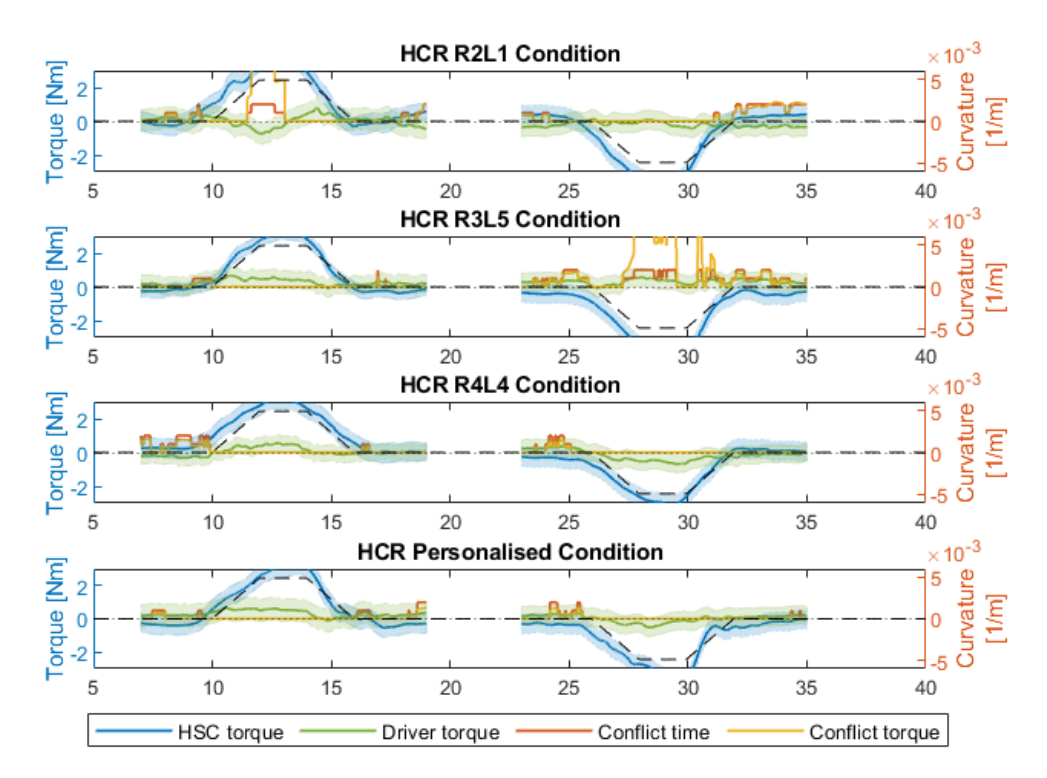


Figure B.92: Timeseries of conflict R3L5 driver 7 - FF 0.92

R3L5 Driver 8 - FF 0.5

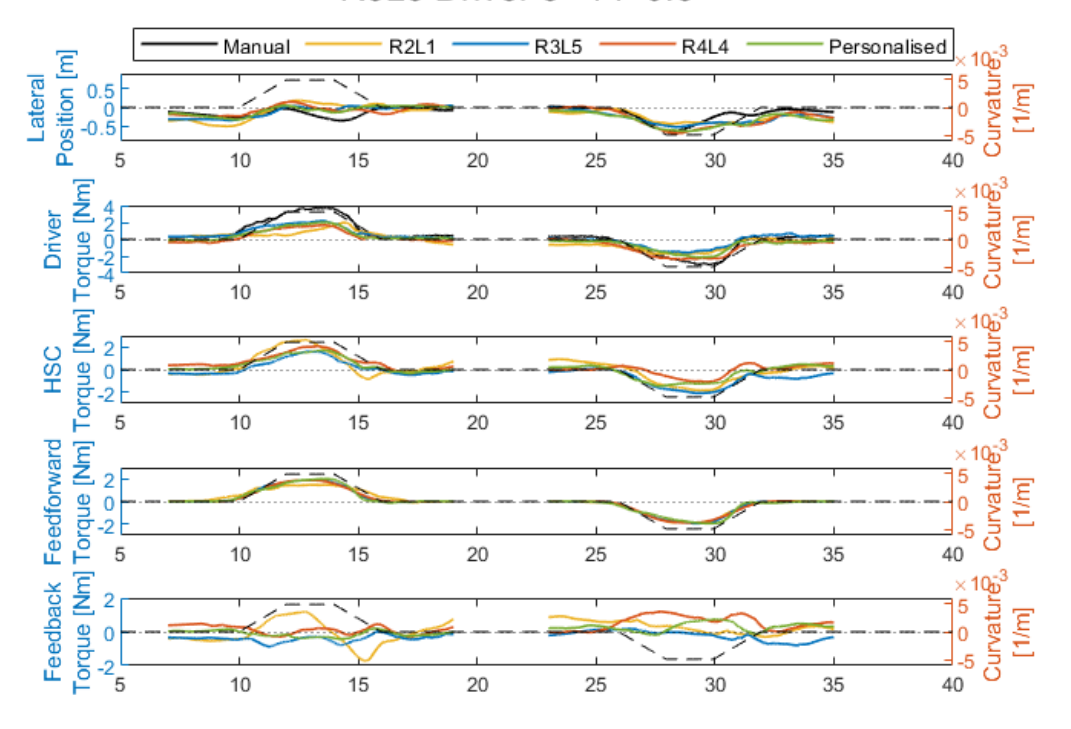


Figure B.93: Timeseries R3L5 driver 8 – FF 0.5

R3L5 Driver 8 - FF 0.5

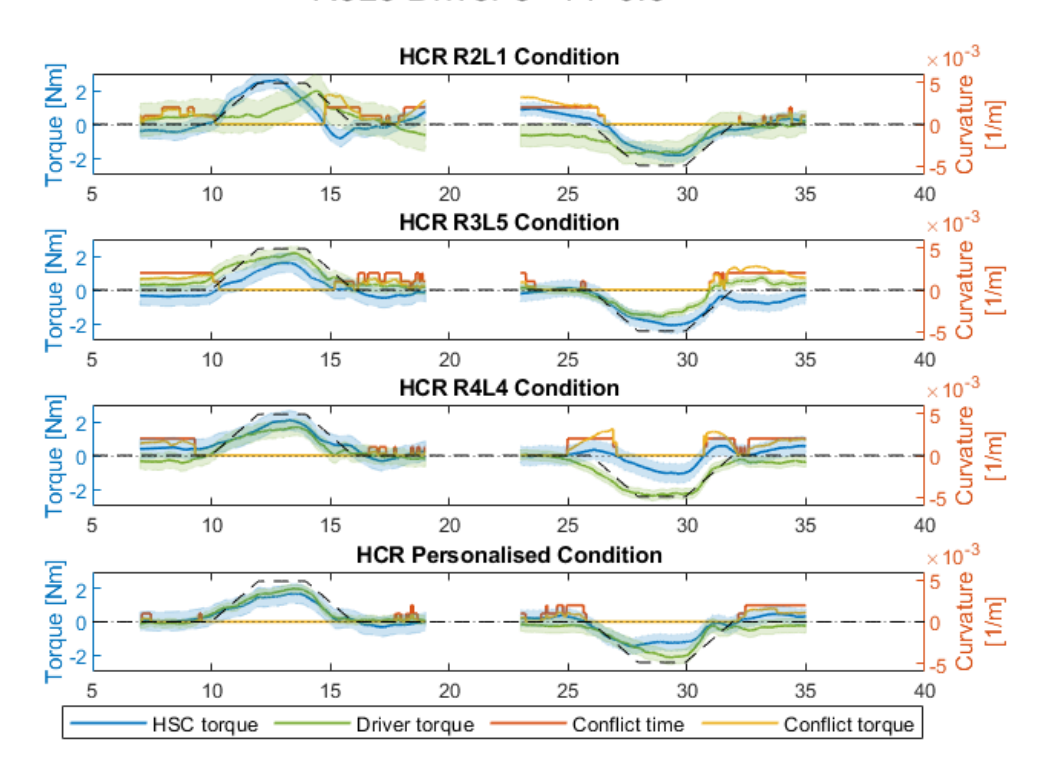


Figure B.94: Timeseries of conflict R3L5 driver 8 – FF 0.5

R3L5 Driver 8 - FF 0.92

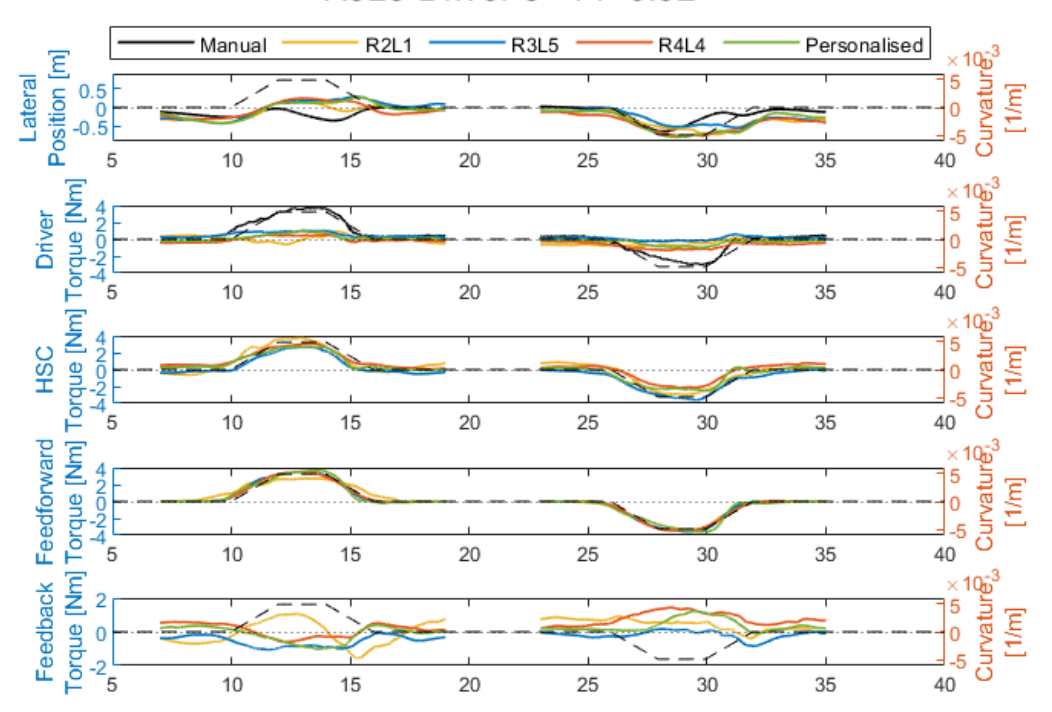


Figure B.95: Timeseries R3L5 driver 8 – FF 0.92

R3L5 Driver 8 - FF 0.92

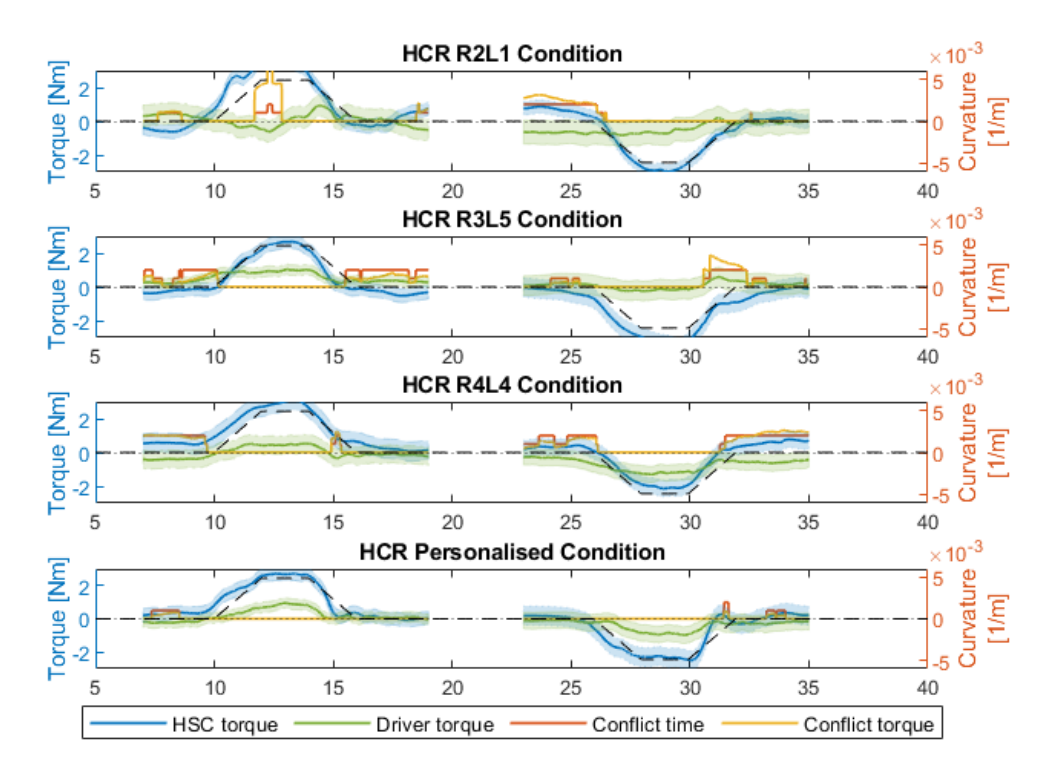


Figure B.96: Timeseries of conflict R3L5 driver $8-FF\ 0.92$

R3L5 Driver 9 - FF 0.5

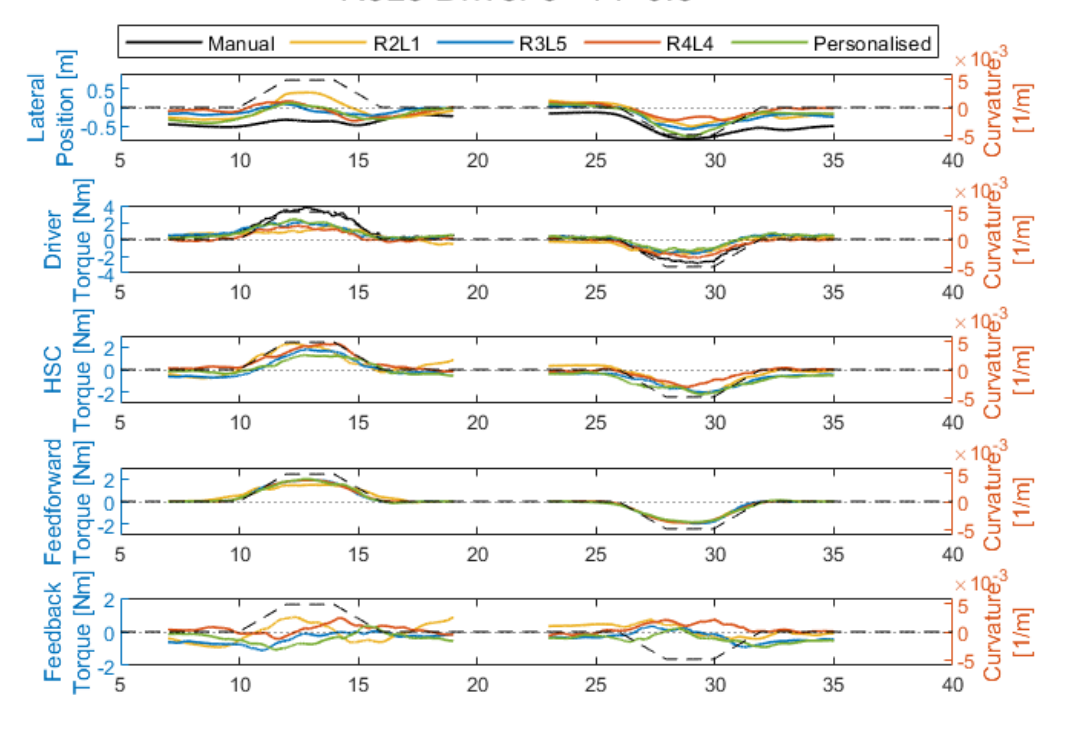


Figure B.97: Timeseries R3L5 driver 9 – FF 0.5

R3L5 Driver 9 - FF 0.5

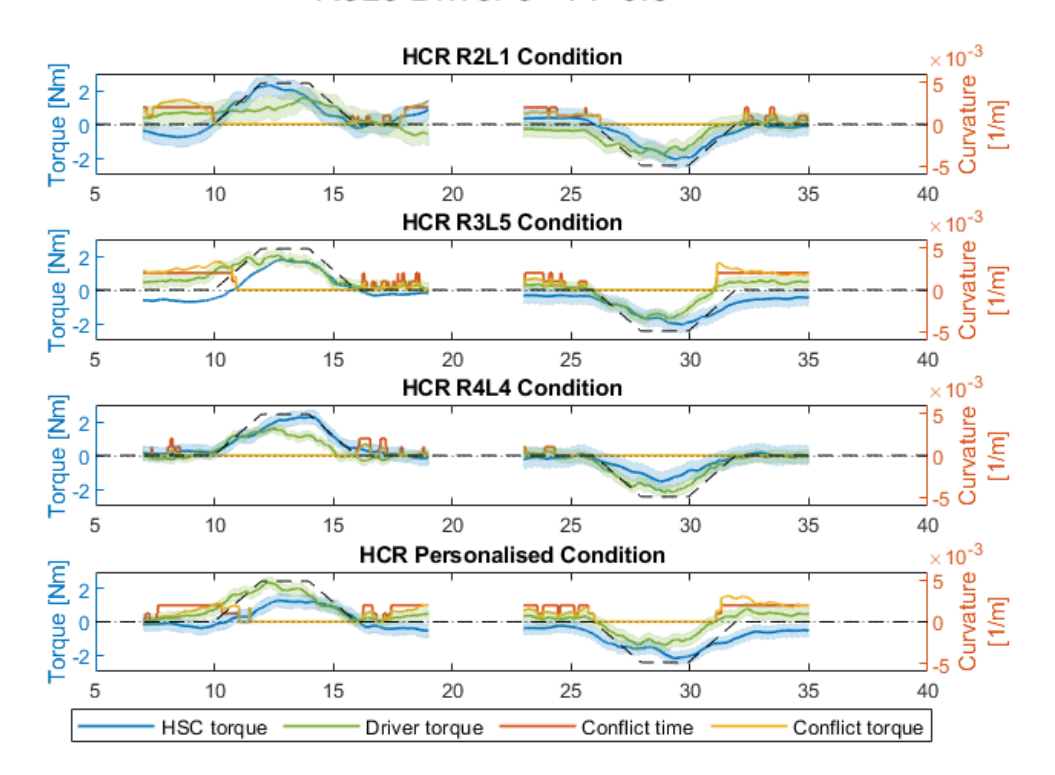


Figure B.98: Timeseries of conflict R3L5 driver 9 - FF 0.5

R3L5 Driver 9 - FF 0.92

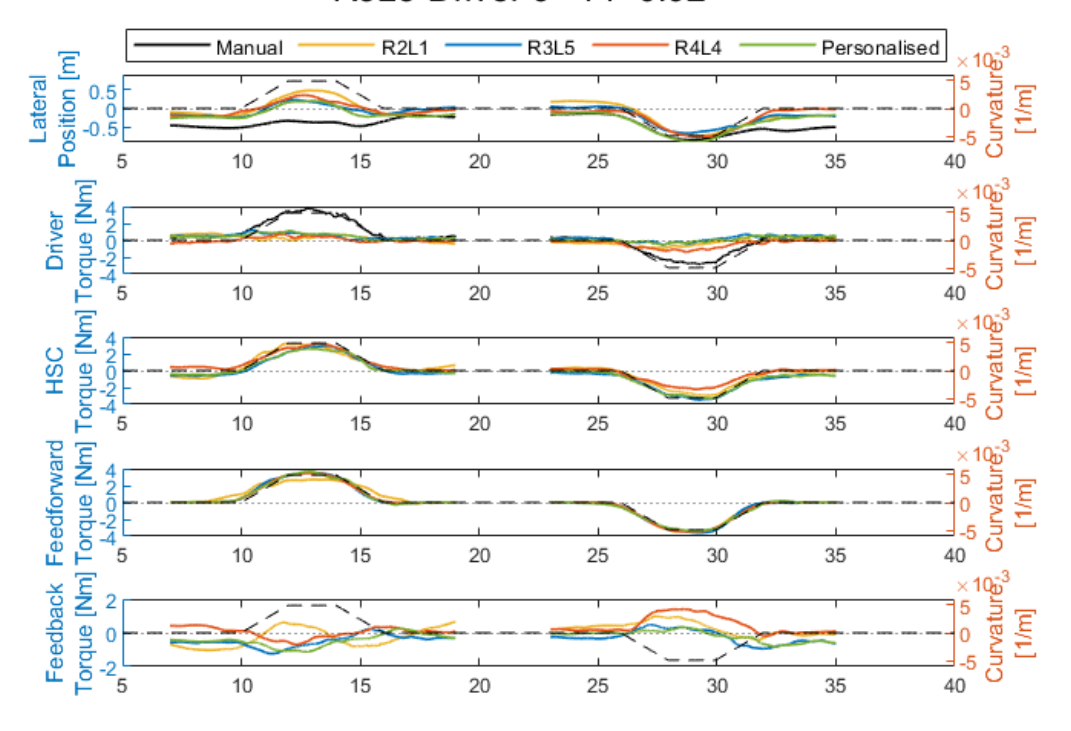


Figure B.99: Timeseries R3L5 driver 9 – FF 0.92

R3L5 Driver 9 - FF 0.92

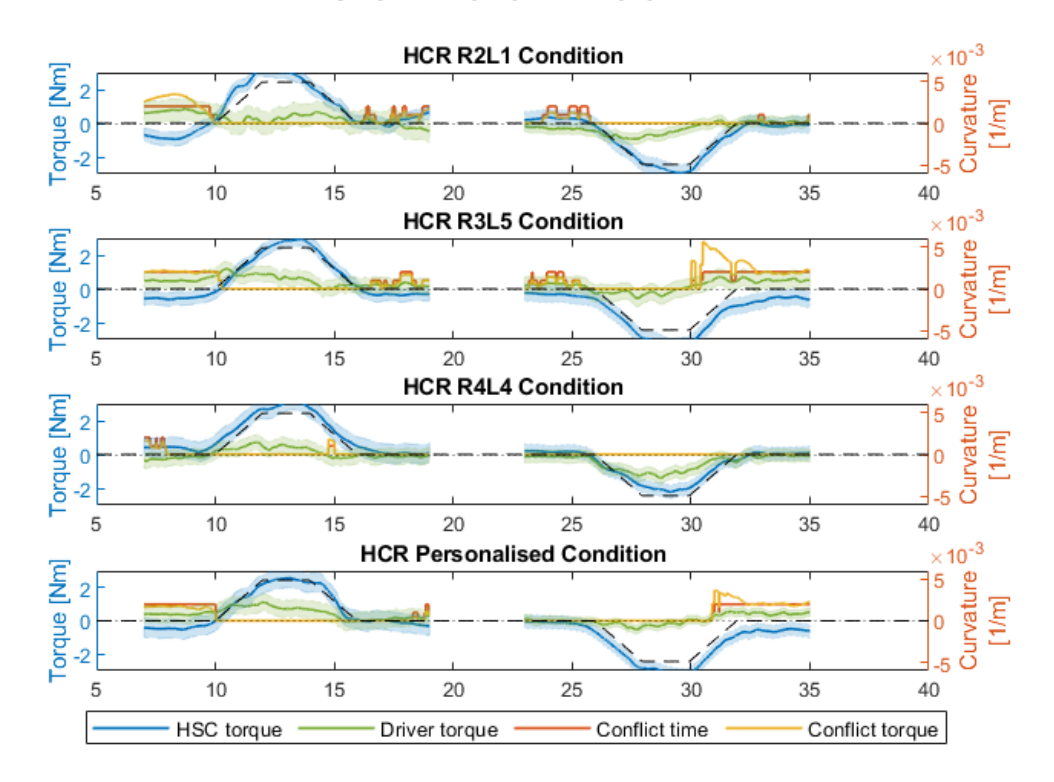


Figure B.100: Timeseries of conflict R3L5 driver 9 - FF 0.92

R3L5 Driver 10 - FF 0.5

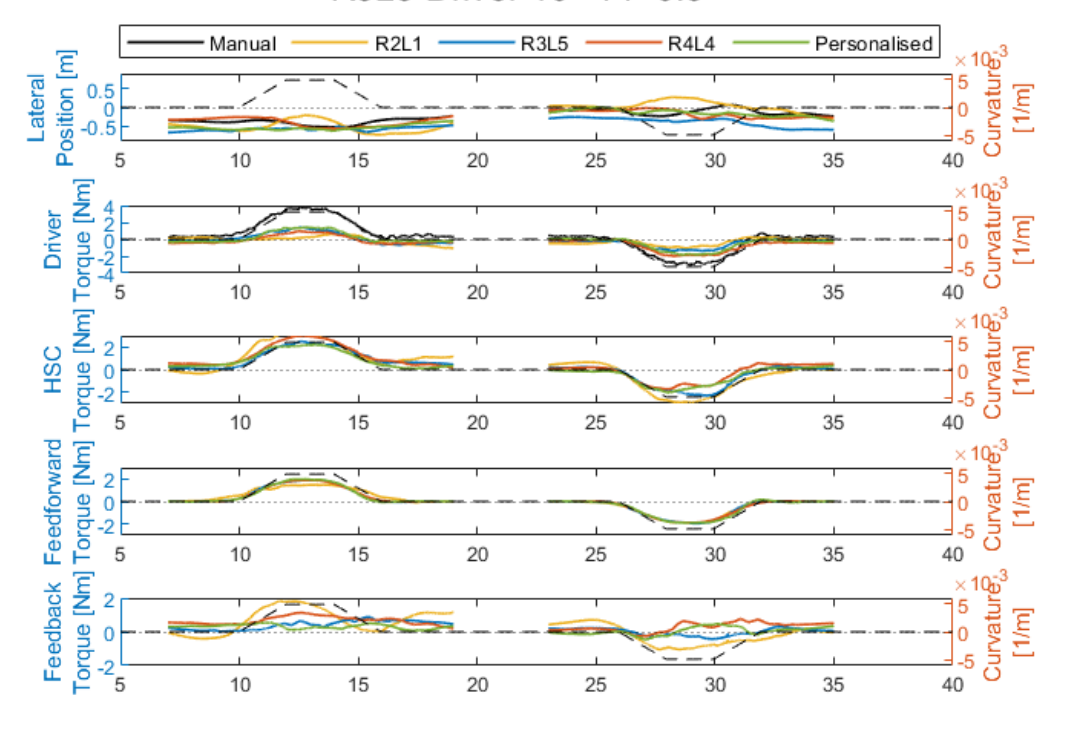


Figure B.101: Timeseries R3L5 driver 10 – FF 0.5

R3L5 Driver 10 - FF 0.5

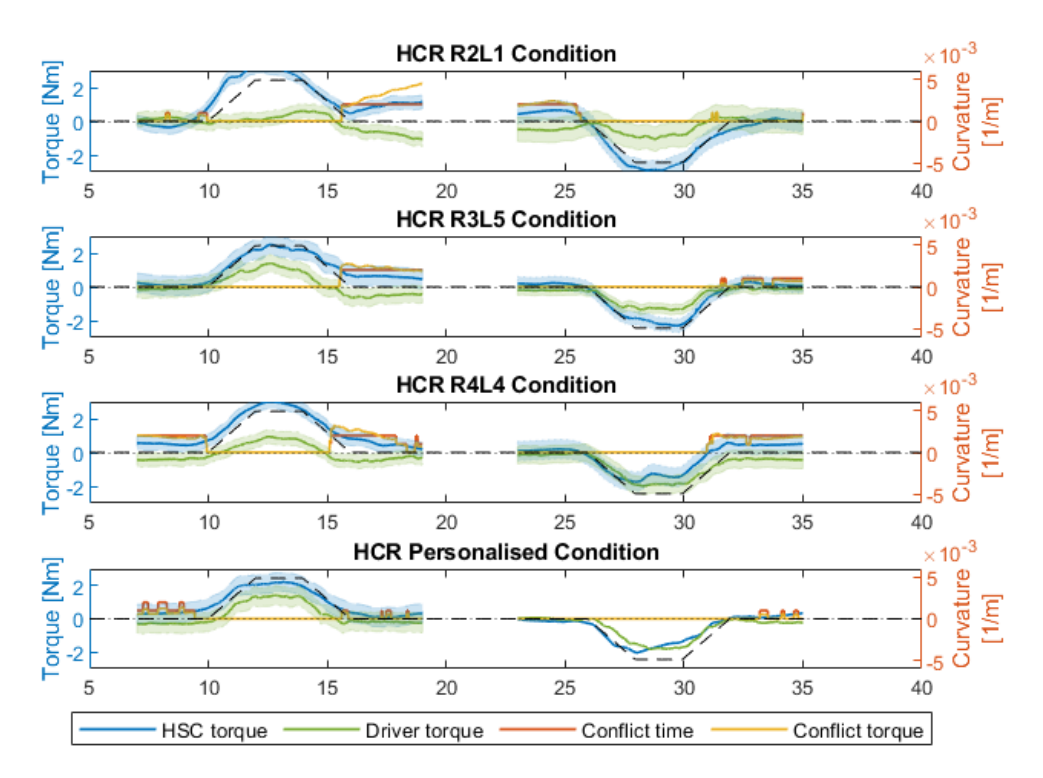


Figure B.102: Timeseries of conflict R3L5 driver 10 - FF 0.5

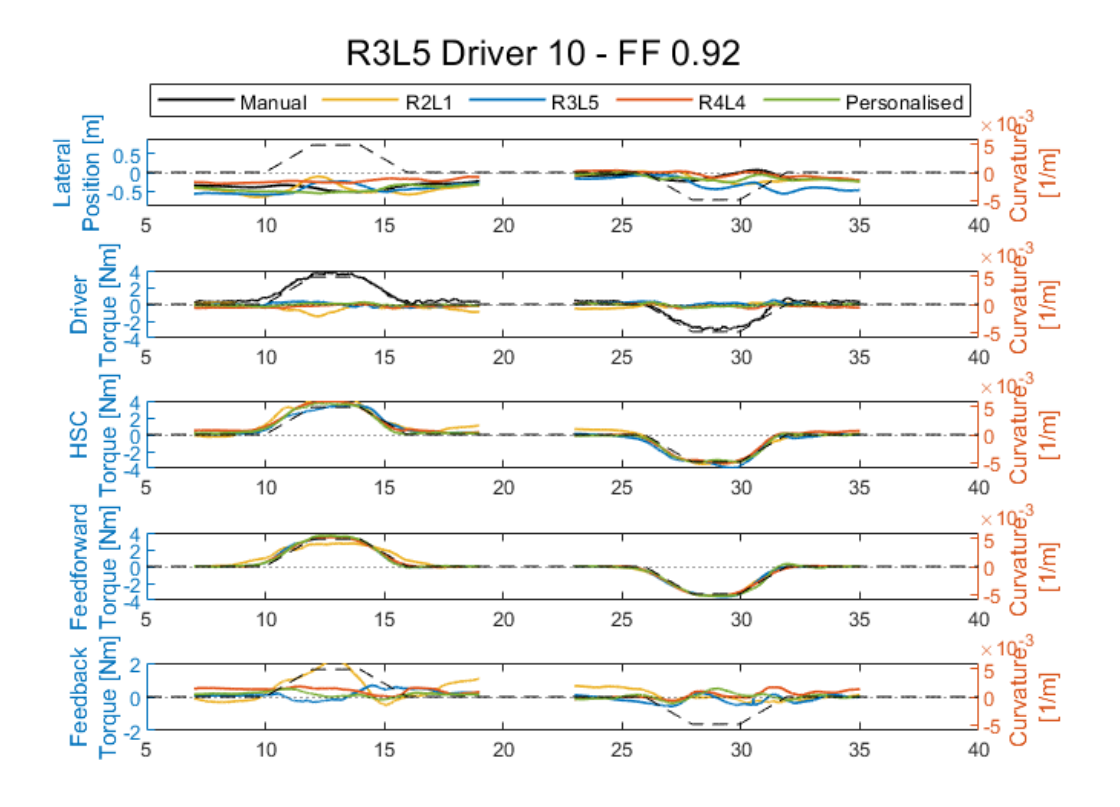


Figure B.103: Timeseries R3L5 driver 10 – FF 0.92

R3L5 Driver 10 - FF 0.92

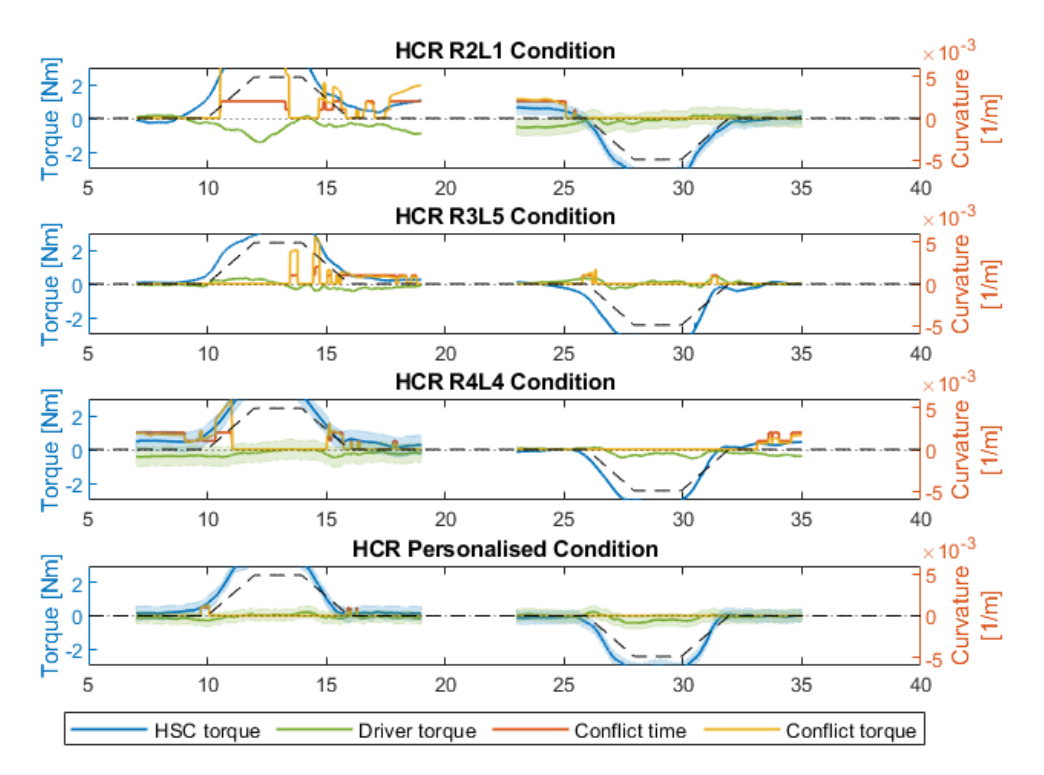


Figure B.104: Timeseries of conflict R3L5 driver 10 - FF 0.92

R3L5 Driver 11 - FF 0.5

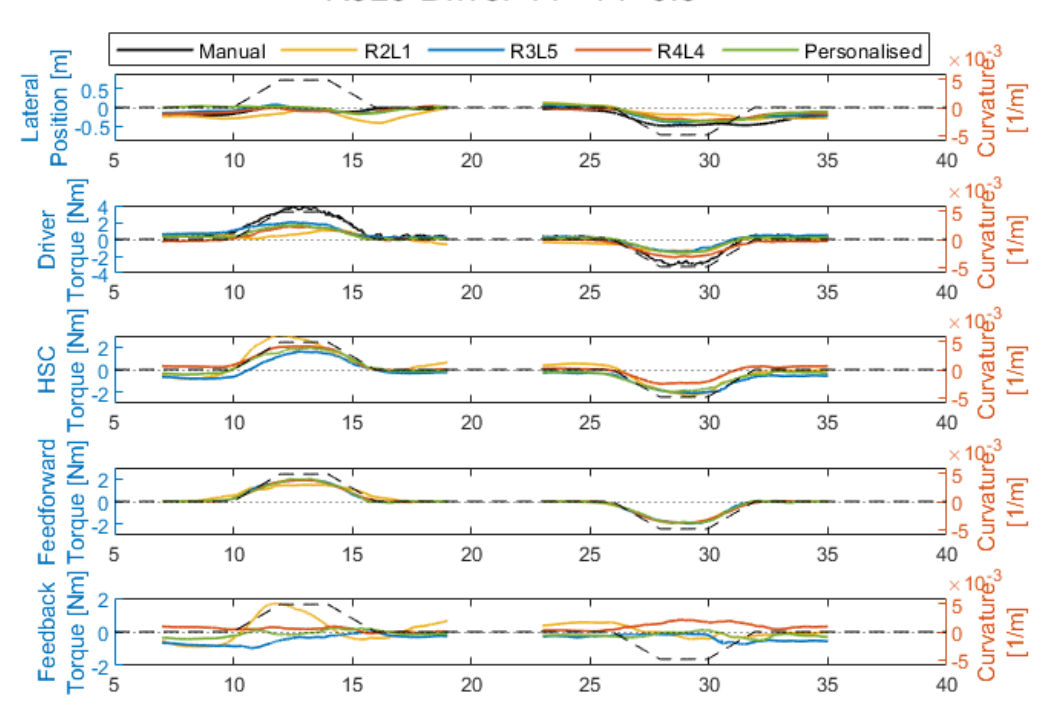


Figure B.105: Timeseries R3L5 driver 11 – FF 0.5

R3L5 Driver 11 - FF 0.5

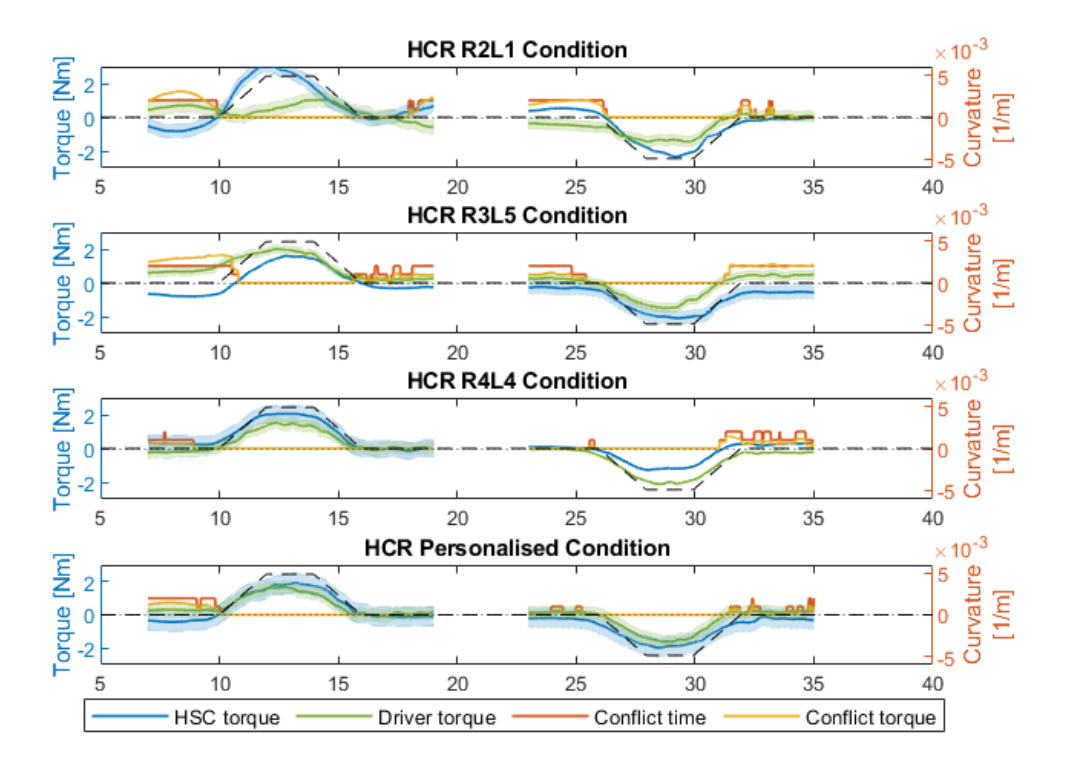


Figure B.106: Timeseries of conflict R3L5 driver 11 - FF 0.5

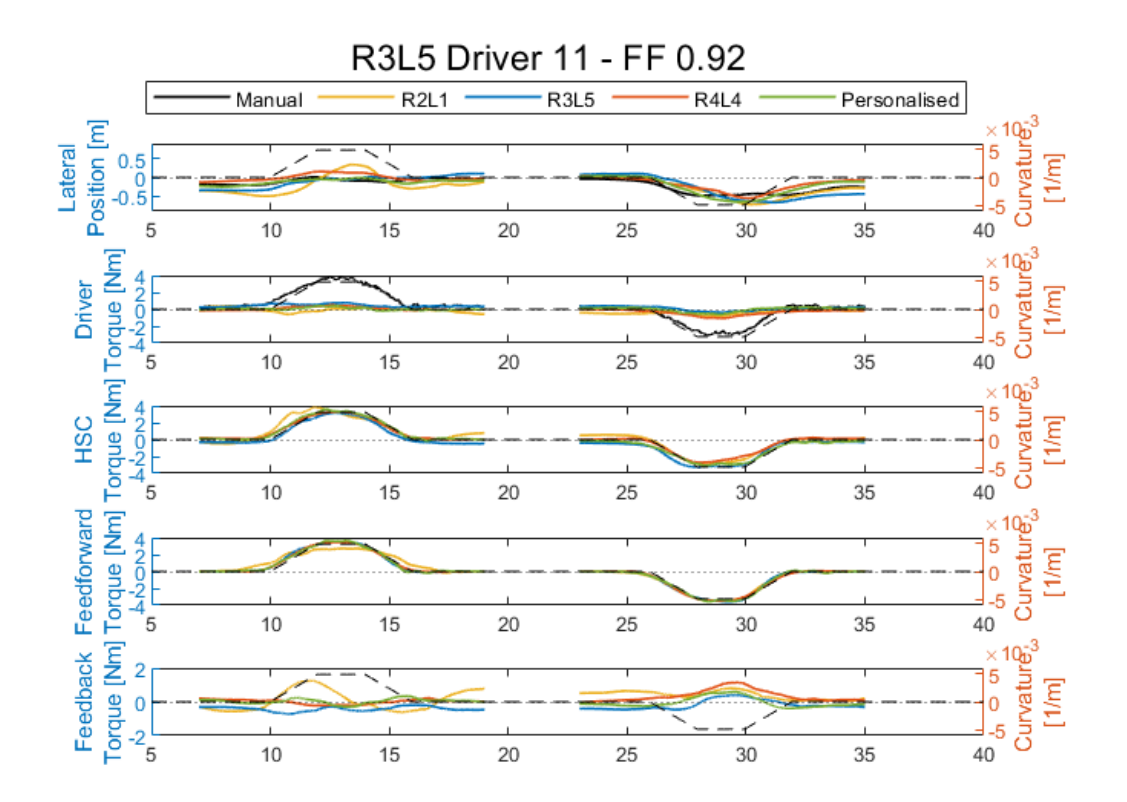


Figure B.107: Timeseries R3L5 driver 11 – FF 0.92

R3L5 Driver 11 - FF 0.92

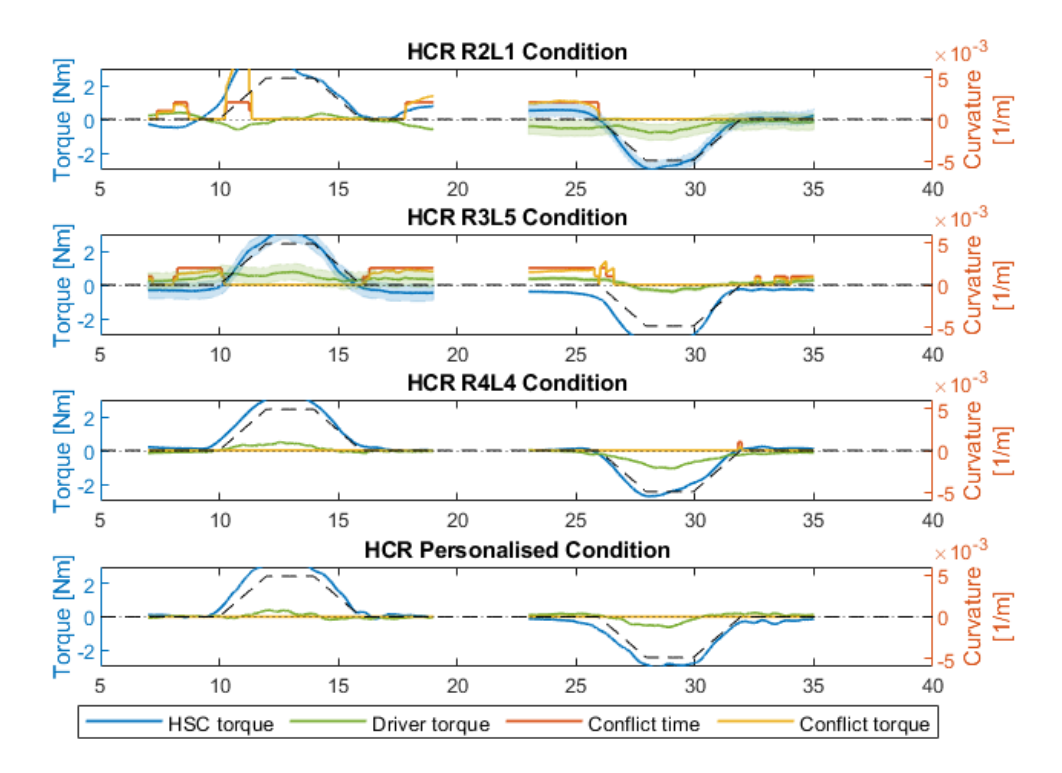


Figure B.108: Timeseries of conflict R3L5 driver 11 – FF 0.92

R3L5 Driver 12 - FF 0.5

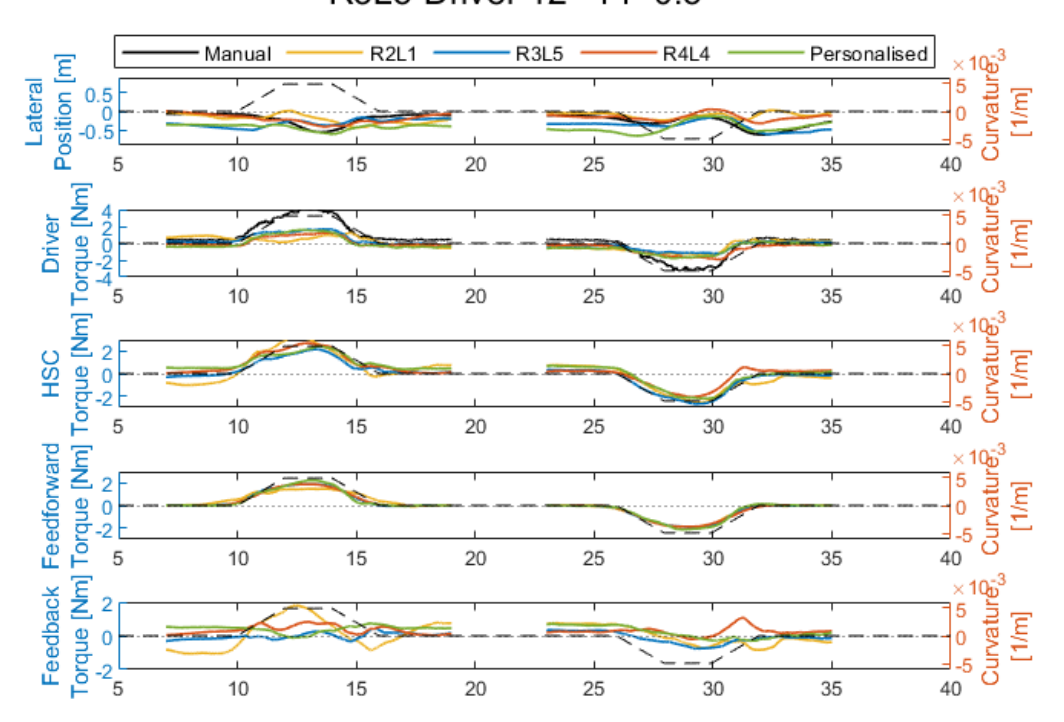


Figure B.109: Timeseries R3L5 driver 12 – FF 0.5

R3L5 Driver 12 - FF 0.5

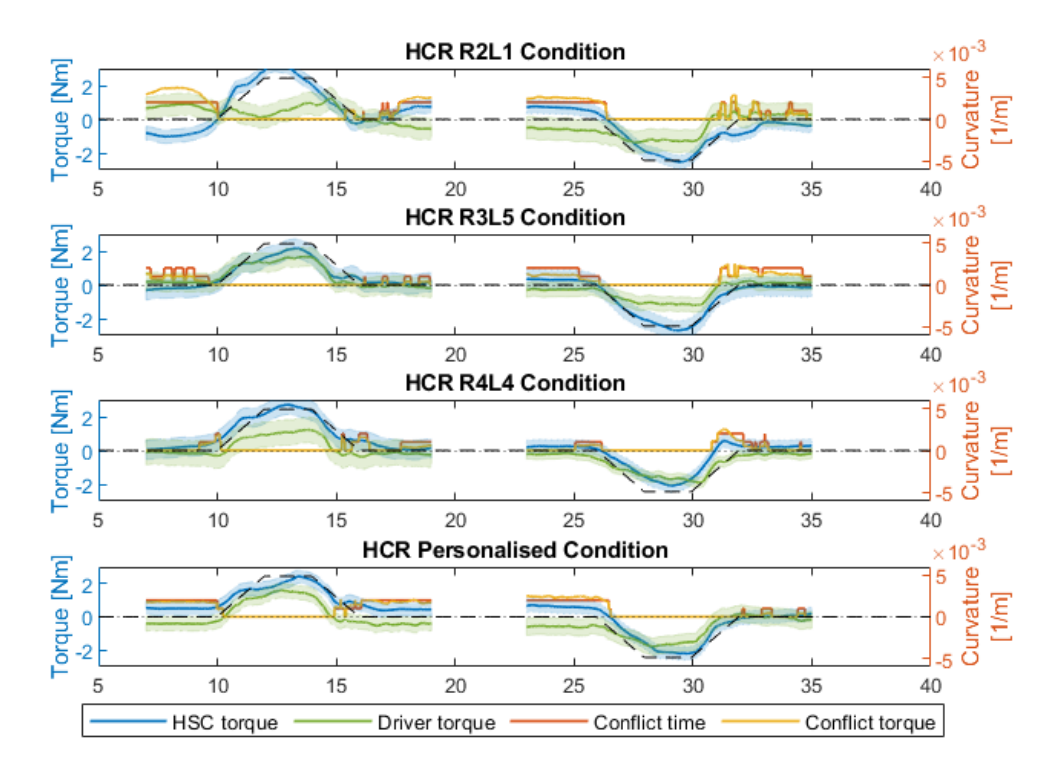


Figure B.110: Timeseries of conflict R3L5 driver 12 - FF 0.5

R3L5 Driver 12 - FF 0.92

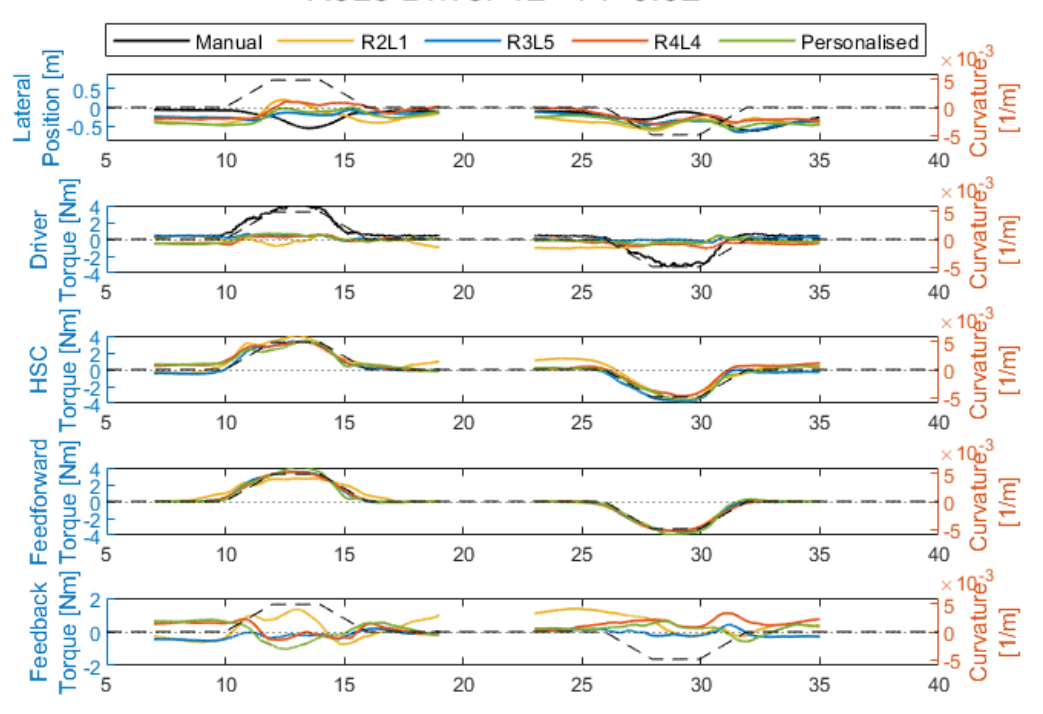


Figure B.111: Timeseries R3L5 driver 12 – FF 0.92

R3L5 Driver 12 - FF 0.92

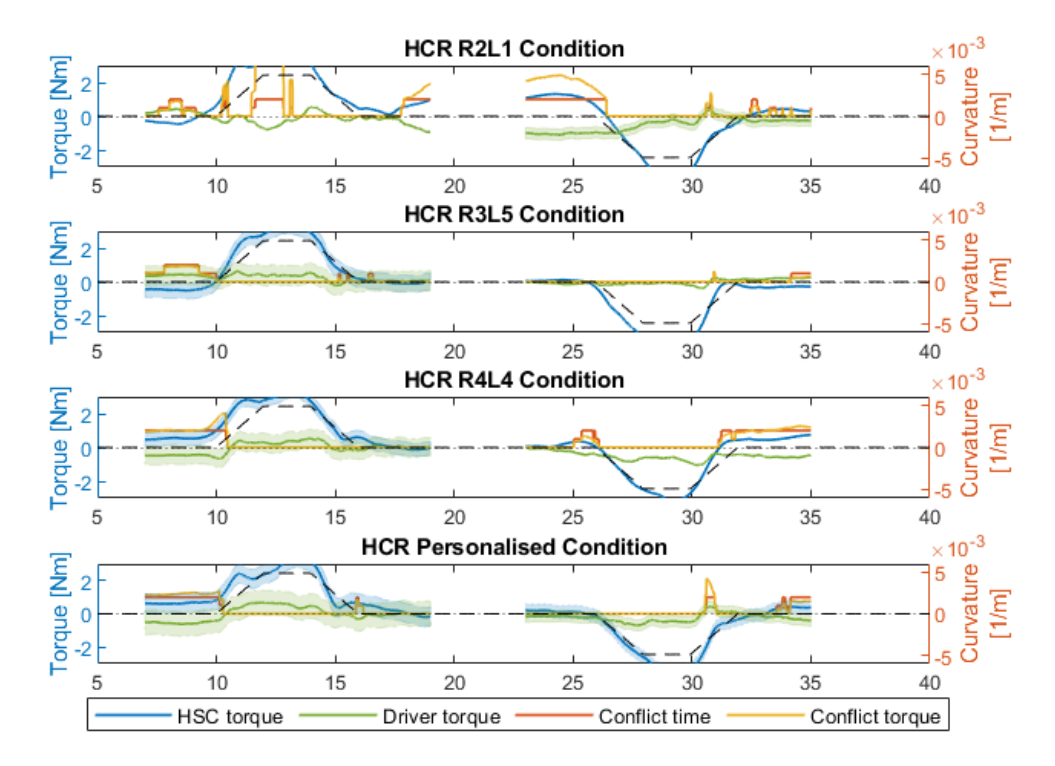


Figure B.112: Timeseries of conflict R3L5 driver 12 – FF 0.92

R3L5 Driver 13 - FF 0.5

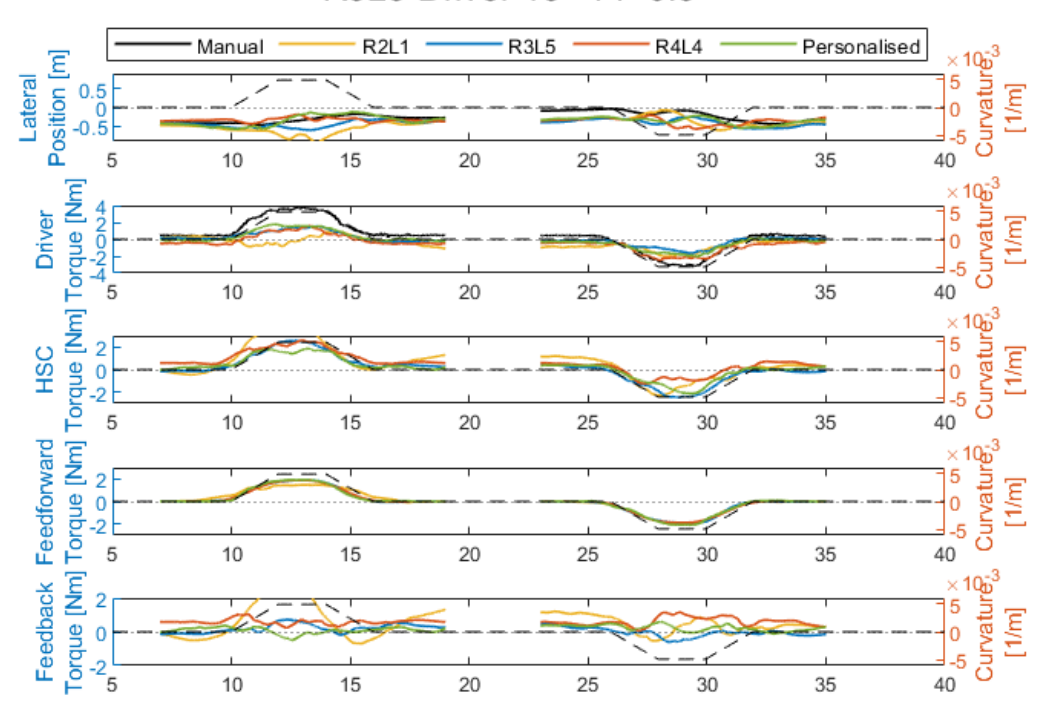


Figure B.113: Timeseries R3L5 driver 13 – FF 0.5

R3L5 Driver 13 - FF 0.5

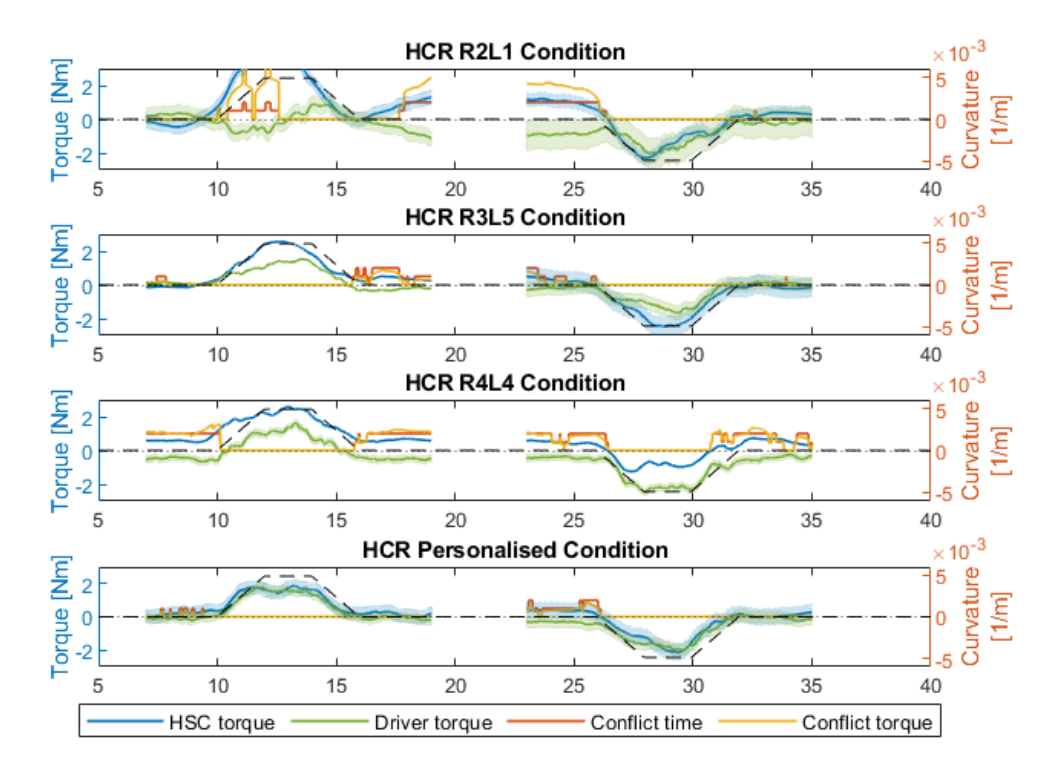


Figure B.114: Timeseries of conflict R3L5 driver $13 - FF\ 0.5$

R3L5 Driver 13 - FF 0.92 Manual R2L1 R3L5 Personalised Curvature) Position [m] 0.5 0 -0.5 -5 40 Torque [Nm] Torque [Nm] Torque [Nm] Torque [Nm] Driver [1/m] -5 40 Curvature 2 [1/m] ×10-5-0-5-0 Curvature0 Feedback Feedforward 2 0 -2 -4 5 [1/m] Curvature 2 -2 5

Figure B.115: Timeseries R3L5 driver 13 – FF 0.92

R3L5 Driver 13 - FF 0.92

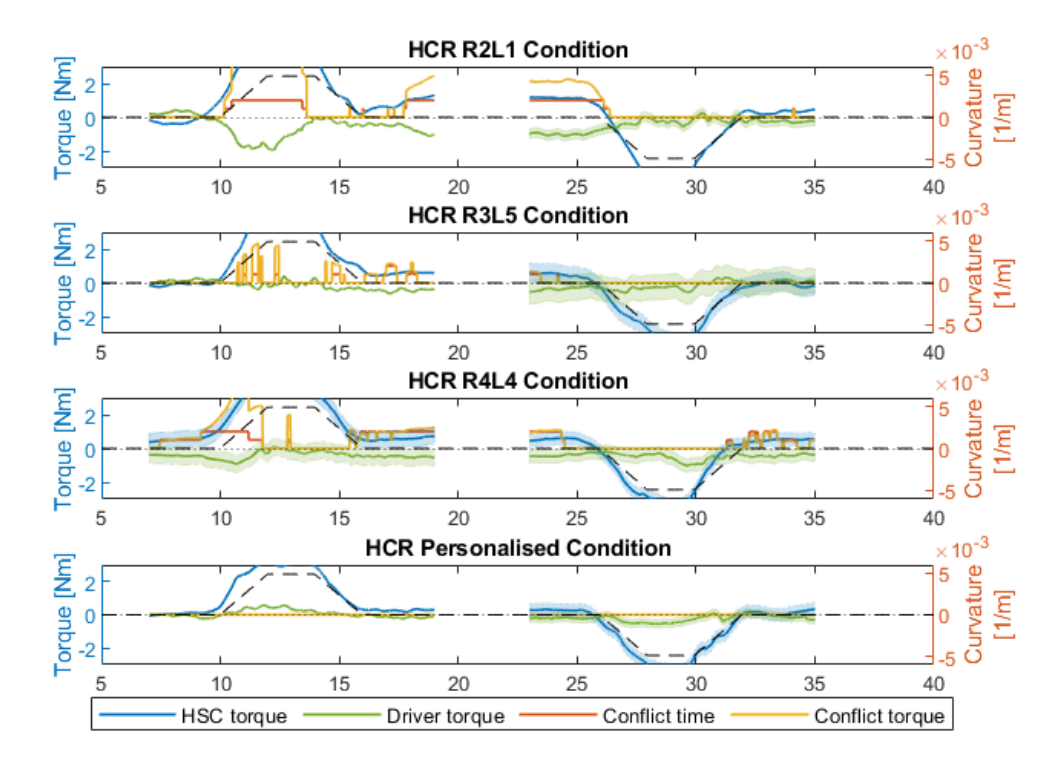


Figure B.116: Timeseries of conflict R3L5 driver 13 - FF 0.92

R3L5 Driver 14 - FF 0.5

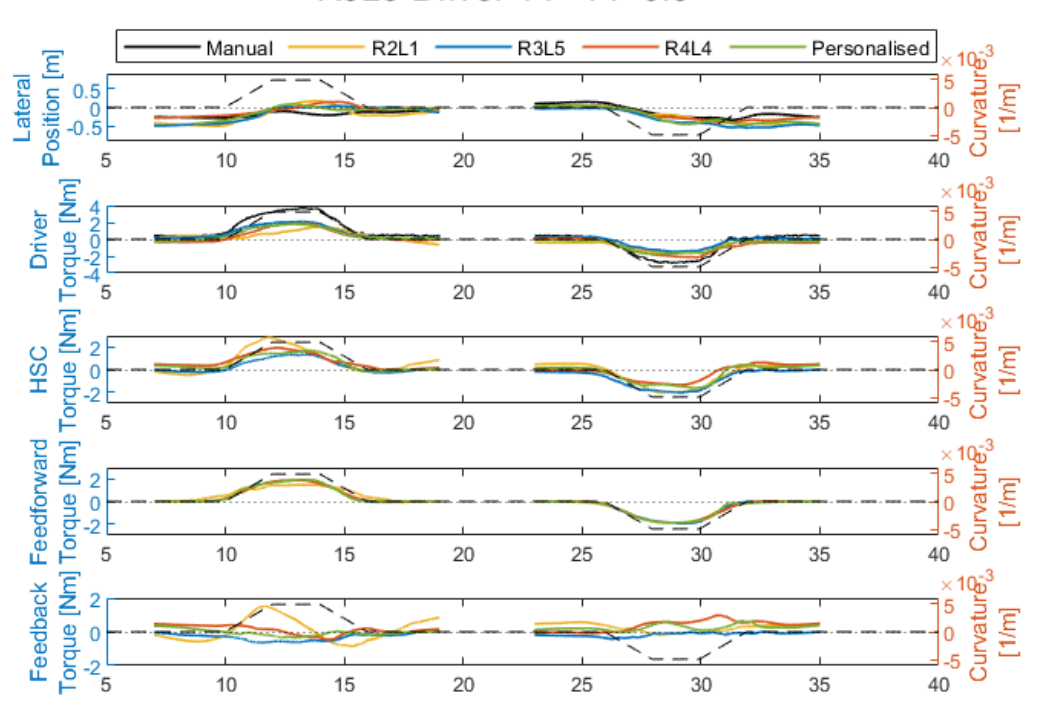


Figure B.117: Timeseries R3L5 driver 14 – FF 0.5

R3L5 Driver 14 - FF 0.5

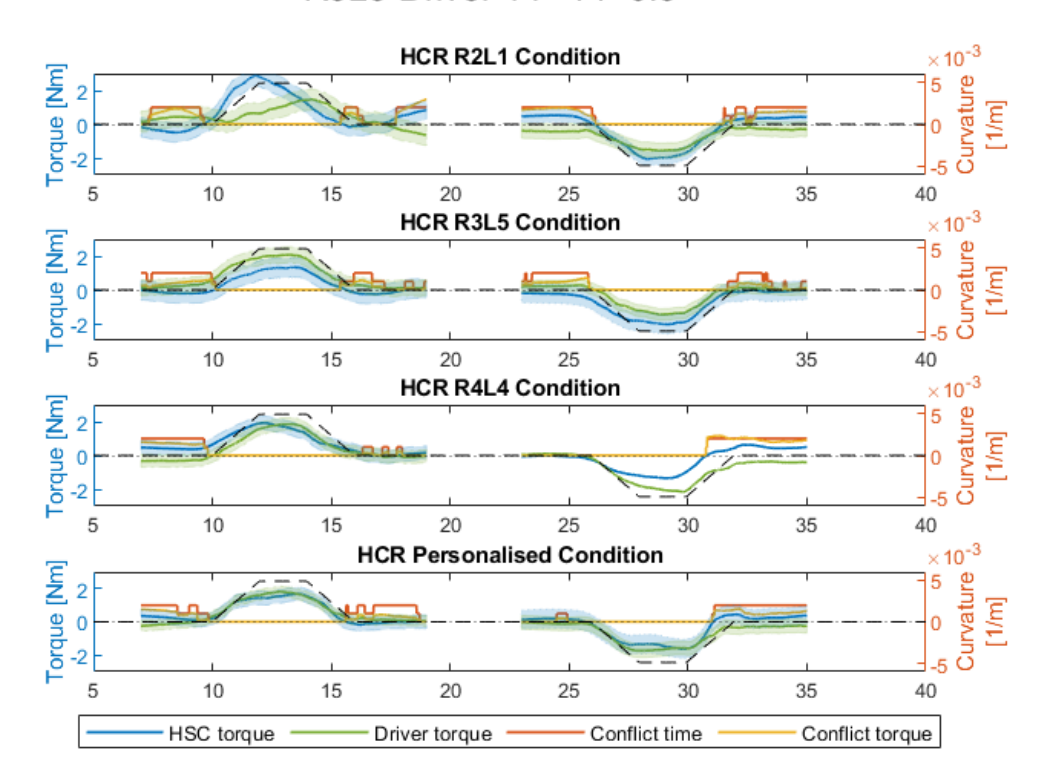


Figure B.118: Timeseries of conflict R3L5 driver 14 - FF 0.5

R3L5 Driver 14 - FF 0.92 R2L1 -R3L5 Manual R4L4 Personalised

Curvature. Position [m] 0.5 0 -0.5 -5 40 × 10-5-0 5-0 5-0 0-0-0 Torque [Nm] Torque [Nm] Torque [Nm] Torque [Nm] Driver [1/m] -5 40 × 10-3 5 0 -5 -0 Curvature 40 [1/m] ×10-5-0-5-0 Curvature0 Feedback Feedforward 2 0 -2 -4 5 [1/m] Curvature 2 -2 5

Figure B.119: Timeseries R3L5 driver 14 – FF 0.92

R3L5 Driver 14 - FF 0.92

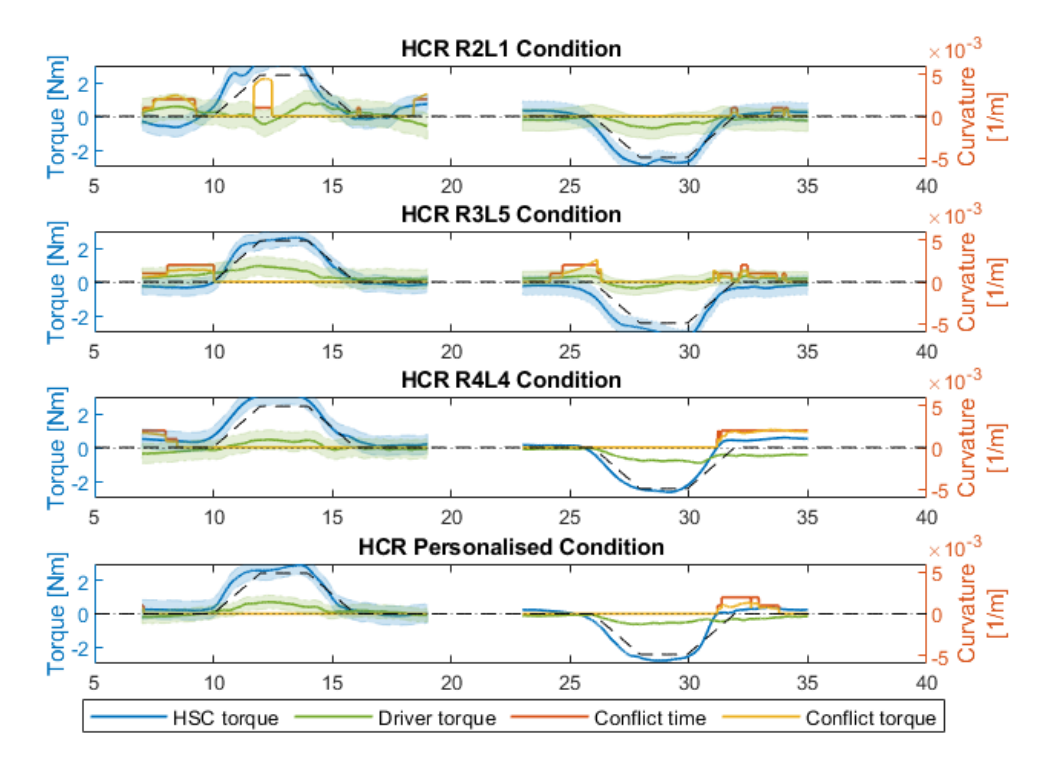


Figure B.120: Timeseries of conflict R3L5 driver 14 - FF 0.92

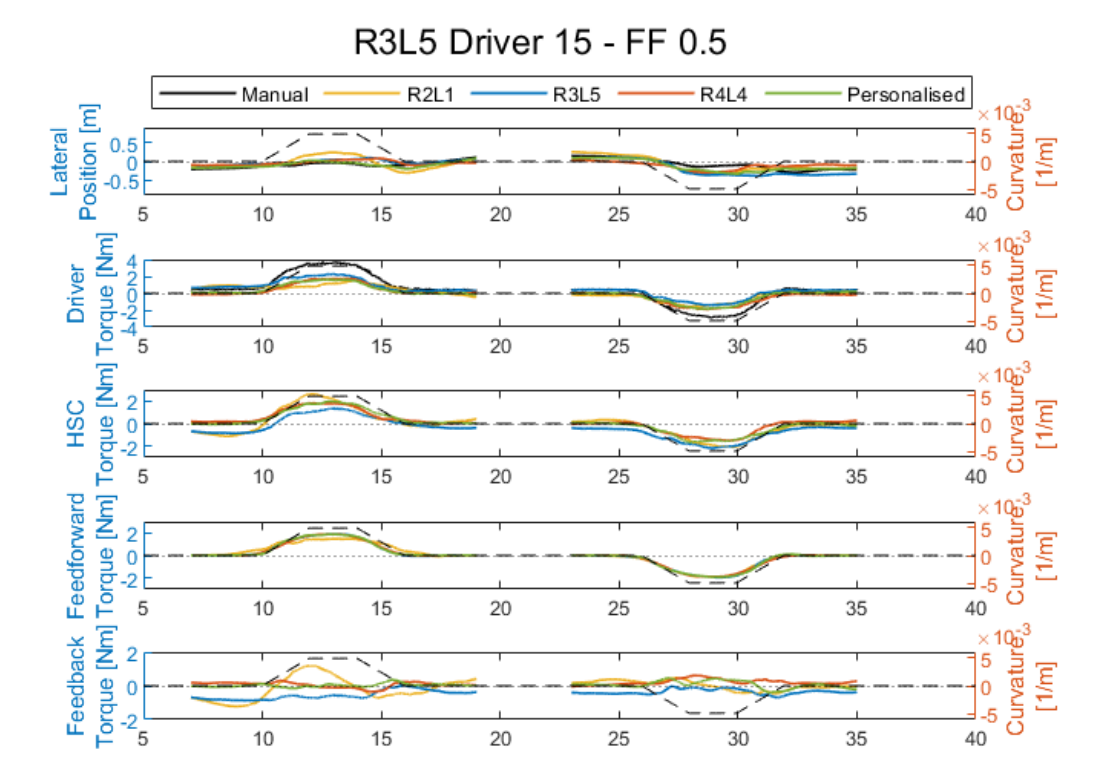


Figure B.121: Timeseries R3L5 driver 15 – FF 0.5

R3L5 Driver 15 - FF 0.5

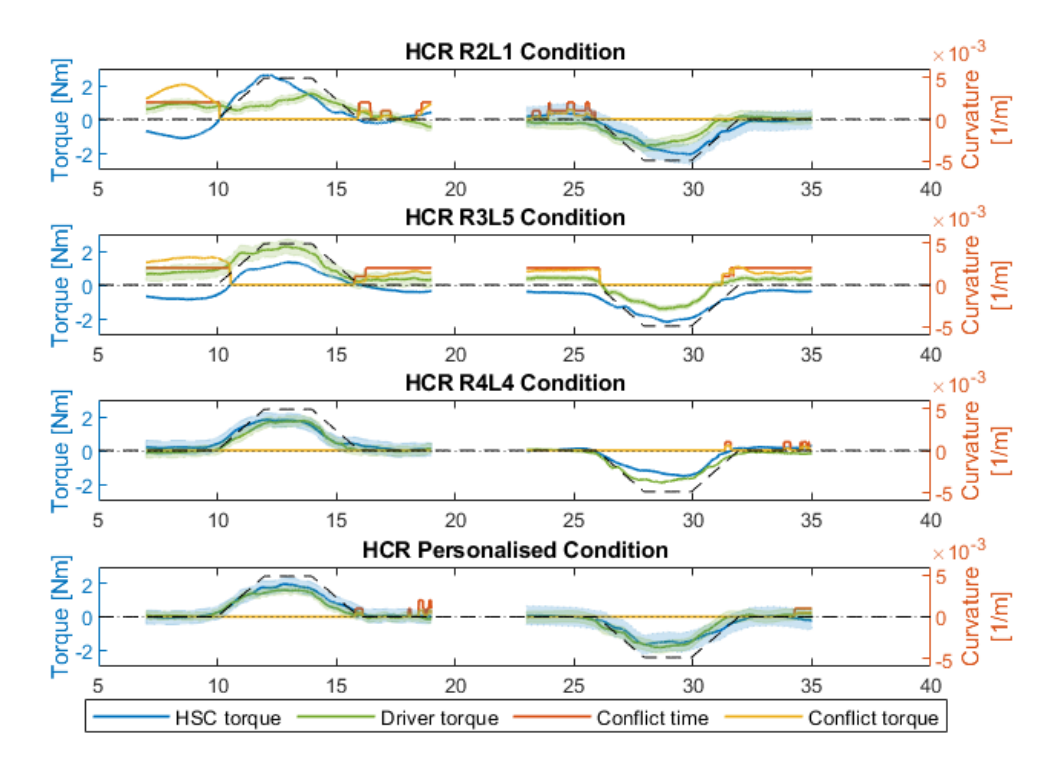


Figure B.122: Timeseries of conflict R3L5 driver $15 - FF\ 0.5$

R3L5 Driver 15 - FF 0.92

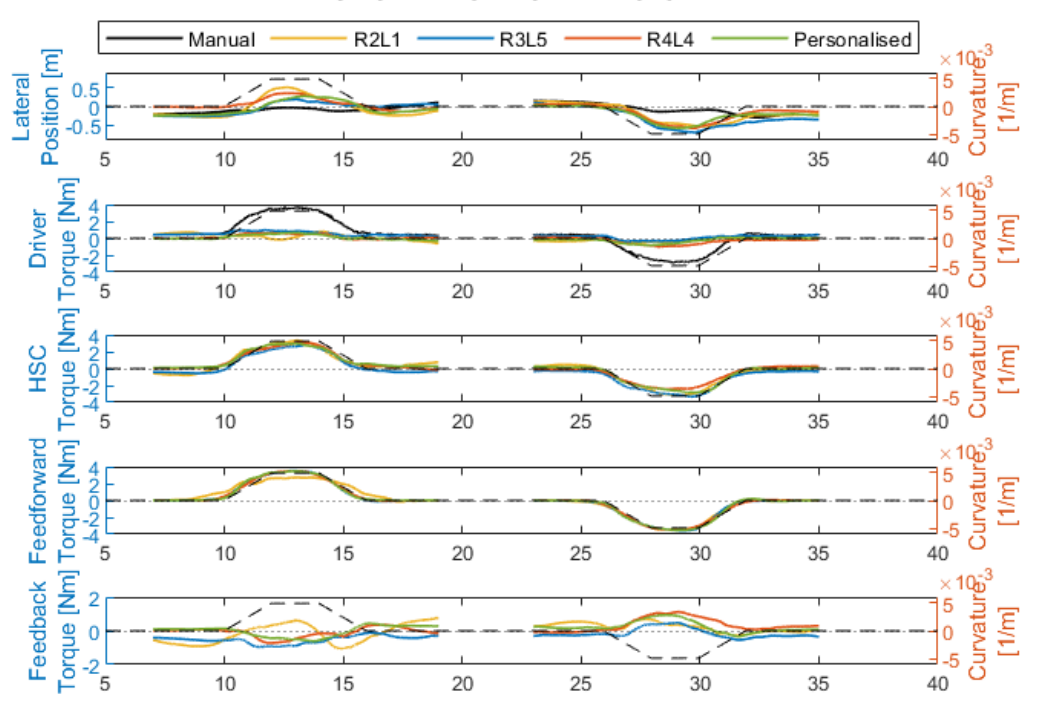


Figure B.123: Timeseries R3L5 driver 15 – FF 0.92

R3L5 Driver 15 - FF 0.92

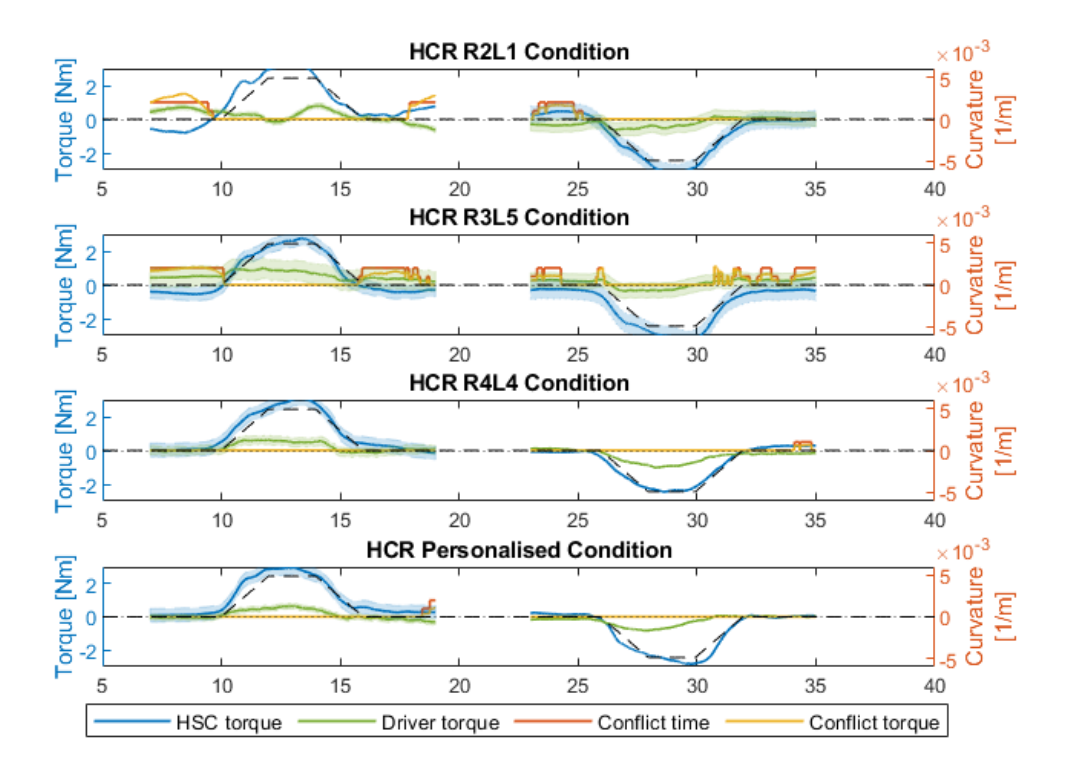
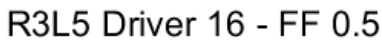


Figure B.124: Timeseries of conflict R3L5 driver 15 – FF 0.92



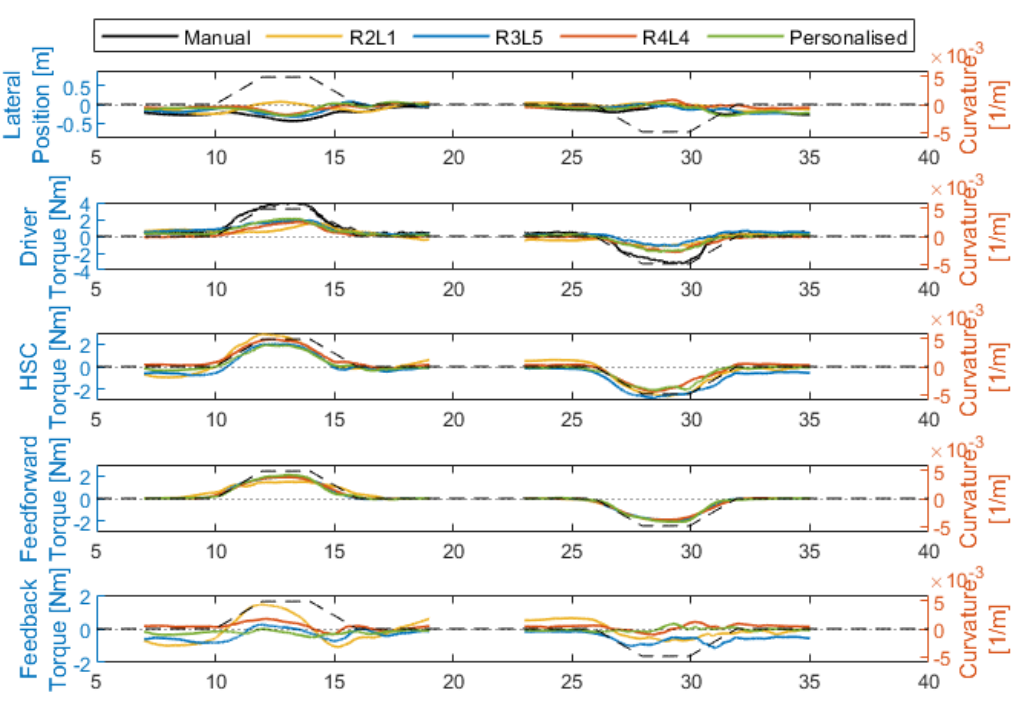


Figure B.125: Timeseries R3L5 driver 16 – FF 0.5

R3L5 Driver 16 - FF 0.5

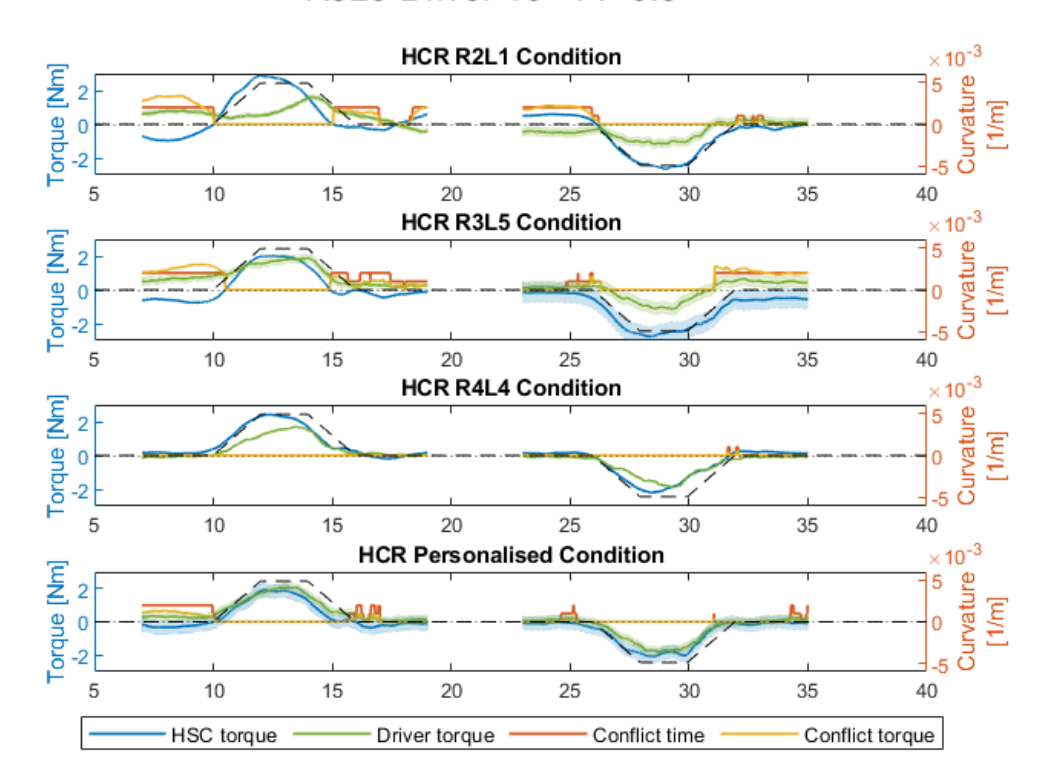


Figure B.126: Timeseries of conflict R3L5 driver 16 - FF 0.5

R3L5 Driver 16 - FF 0.92

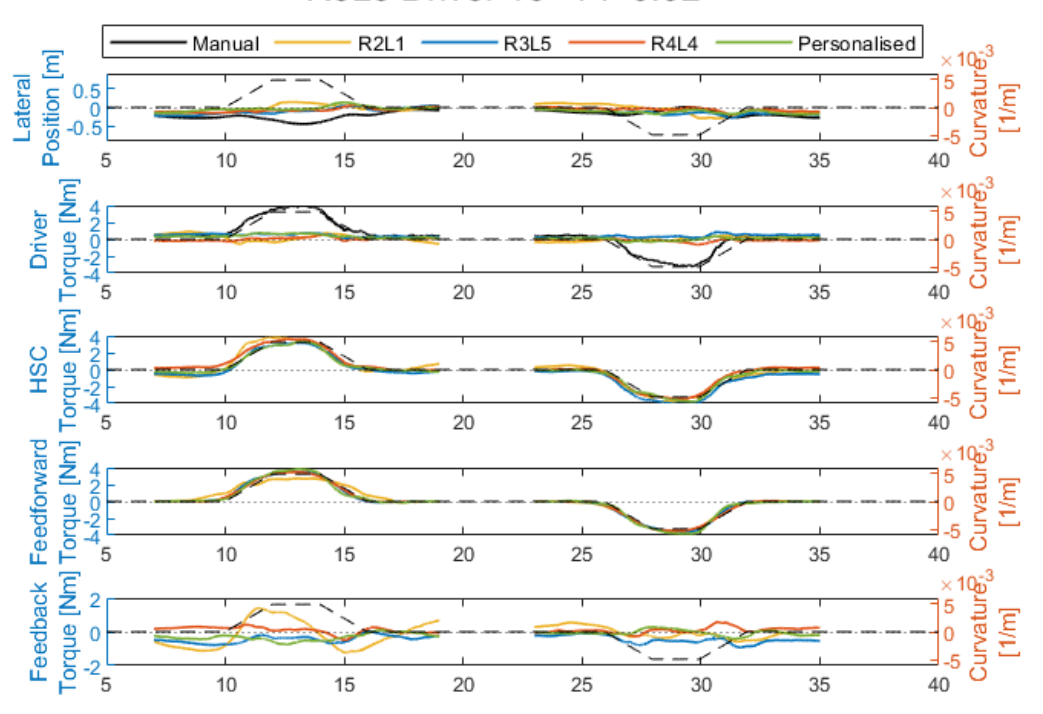


Figure B.127: Timeseries R3L5 driver 16 – FF 0.92

R3L5 Driver 16 - FF 0.92

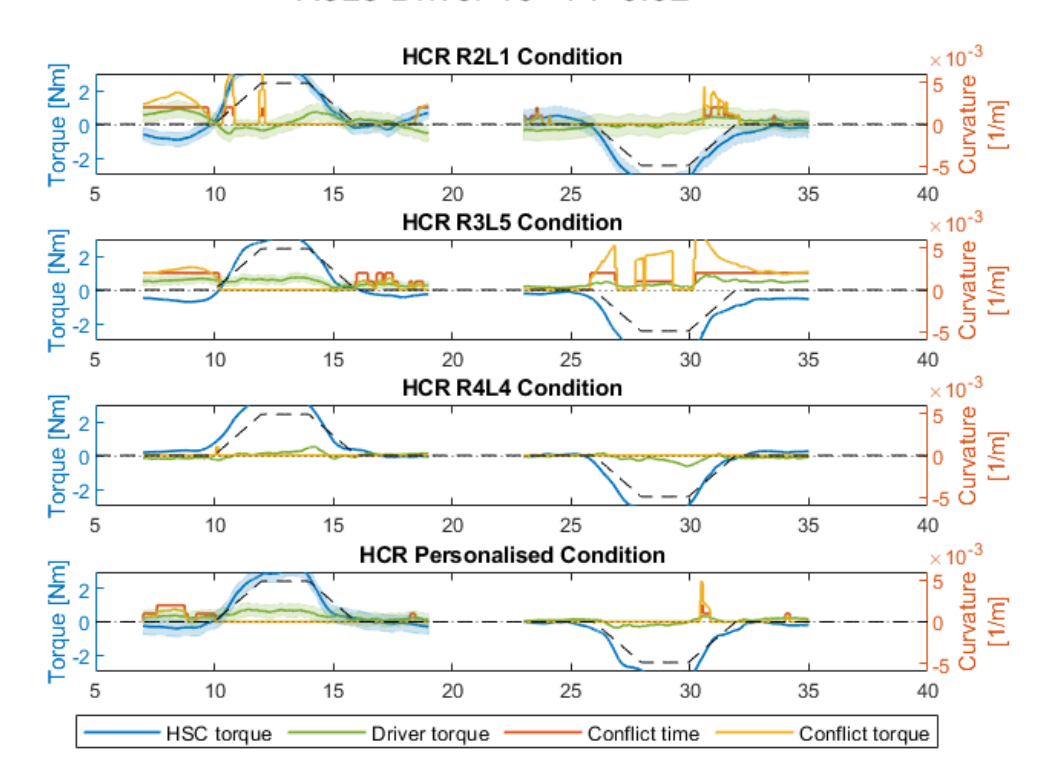
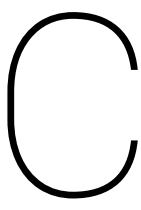


Figure B.128: Timeseries of conflict R3L5 driver 16 – FF 0.92



Questionnaire data

This appendix contains the results of the CARS and Van der Laan questionnaires for the haptic shared control experiment.

R2L1					R4L	4 - 0.9	92									R4L	_4 - 0.	.5									R3L	5 - 0.9
Participant #	R?L?	Cars	Confidence	Q1	Q2	Q3	Q4	Q5	Q6	Q7	Q8	Q9	Cars	Confidence	Q1	Q2	Q3	Q4	Q5	Q6	Q7	Q8	Q9	Cars	Confidence	Q1	Q2	Q3
4	R2L2	8	Α	1	1	1	1	1	1	1	1	0	9	Α	1	1	1	1	1	1	1	1	0	8	В	1	0	1
5	R2L1	7	В	0	-1	-1	-1	0	-1	0	-1	-1	4	С	-2	-2	-1	-2	-1	-2	-1	-2	2	9	Α	2	2	2
23	R2L1	7	Α	1	0	1	0	1	0	1	1	1	6	Α	-1	-1	0	-1	0	-1	-1	-1	1	9	Α	1	1	1
25	R2L1	7	Α	1	1	1	1	1	1	1	1	0	7	Α	1	1	0	0	1	1	1	1	0	7	Α	1	1	1
32	R2L2	8	Α	2	2	2	1	2	2	2	2	0	7	Α	1	1	0	1	0	0	0	0	0	9	Α	2	1	2
35	R2L2	9	С	0	-1	-1	-1	1	-1	1	0	-1	10	Α	2	2	1	1	1	0	1	0	0	8	С	1	-1	0
40	R2L2	7	Α	1	0	2	1	2	1	2	1	1	9	Α	2	2	2	2	2	1	2	1	2	9	Α	2	2	2
43	R2L1	10	Α	2	2	2	2	2	2	2	2	2	10	Α	1	2	1	-1	1	2	1	2	2	10	Α	2	2	2
59	R2L1	7	В	2	1	2	1	2	1	2	1	0	7	В	0	1	1	0	0	0	0	0	2	9	Α	2	1	2
61	R2L2	8	Α	1	1	0	1	0	0	1	0	-1	5	Α	-2	0	0	0	-2	0	0	-2	0	7	Α	1	1	1
65	R1L1	9	Α	1	1	1	1	2	1	2	1	2	6	В	0	-1	-1	0	0	0	0	-1	0	7	В	1	-1	-1
69	R2L2	9	Α	2	2	2	2	2	1	2	2	-1	6	В	0	1	0	1	0	1	0	1	-1	6	В	0	1	1
73	R2L2	10	Α	2	2	2	2	2	2	2	2	0	10	Α	2	2	2	2	2	2	2	2	0	10	Α	2	2	2
77	R2L2	9	Α	2	2	2	2	2	2	2	2	-1	9	Α	2	2	2	2	2	2	2	2	-1	8	Α	2	2	2
83	R2L1	8	В	1	1	1	1	2	2	1	1	1	4	В	-1	-1	-1	-1	0	0	-1	-1	0	9	Α	2	2	1
86	R2L2	8	Α	2	2	2	1	2	1	2	2	0	6	Α	1	0	-1	-1	1	-1	0	-1	1	9	Α	2	2	2
		_		_	_	_	_																	_				
		_	,,													D 41	1 0	-						-				- O.
R3L5					R4L	4 - 0.9	92			07	00	00	Cors		01		_4 - 0.		OF	06	07		00	Cors		01	R3L	2.0 - 5
R3L5 Participant #	R?L?	Cars	Confidence	Q1	R4L4 Q2	4 - 0.9 Q3	92 Q4	Q5	Q6	Q7	Q8	Q9	Cars	Confidence	Q1	Q2	Q3	Q4	Q5	Q6	Q7	Q8	Q9	Cars	Confidence	Q1	R3L!	Q3
R3L5 Participant # 3	R?L? R3L5	Cars 10	Confidence A	Q1 2	R4L4 Q2 2	4 - 0.9 Q3 2	92 Q4 2	Q5 1	Q6 2	1	1	0	9	Confidence A	0	Q2 1	Q3 0	Q4 1	0	1	0	Q8 1	0	10	Confidence A	2	R3L5 Q2 2	Q3 2
R3L5 Participant # 3 9	R?L? R3L5 R3L5	Cars 10 8	Confidence A A	Q1 2 1	R4L4 Q2 2 1	4 - 0.9 Q3 2 1	Q4 2 1	Q5 1 1	Q6 2 1	1 1	1 1	0 -2	9 6	Confidence A B	0 1	Q2 1 2	Q3 0 0	Q4 1 1	0 0	1 2	0	Q8 1 0	0 1	10 5	Confidence A B	2 0	R3L! Q2 2 -1	Q3 2 0
R3L5 Participant # 3 9 14	R?L? R3L5 R3L5 R3L5	Cars 10 8 9	Confidence A A B	Q1 2 1 2	R4L4 Q2 2 1	4 - 0.9 Q3 2 1 2	Q4 2 1 2	Q5 1 1 2	Q6 2 1 2	1 1 2	1 1 2	0 -2 1	9 6 7	Confidence A B C	0 1 0	Q2 1 2 0	Q3 0 0 1	Q4 1 1 0	0 0 0	1 2 0	0 0	Q8 1 0	0 1 0	10 5 8	Confidence A B	2 0 2	R3L ¹ Q2 2 -1 1	Q3 2 0 2
R3L5 Participant # 3 9 14 27	R?L? R3L5 R3L5 R3L5 R3L5	Cars 10 8 9 10	Confidence A A B A	Q1 2 1 2	R4L4 Q2 2 1 2 0	Q3 Q3 2 1 2	Q4 2 1 2	Q5 1 1 2	Q6 2 1 2	1 1 2 1	1 1 2 0	0 -2 1 0	9 6 7 10	Confidence A B C A	0 1 0 1	Q2 1 2 0	Q3 0 0 1 1	Q4 1 1 0	0 0 0 2	1 2 0 0	0 0 0 1	Q8 1 0 0	0 1 0 0	10 5 8 10	Confidence A B B	2 0 2 1	R3L Q2 2 -1 1	Q3 2 0 2 0
R3L5 Participant # 3 9 14 27 28	R?L? R3L5 R3L5 R3L5 R3L5 R3L5	Cars 10 8 9 10	Confidence A A B A C	Q1 2 1 2 1 0	R4L4 Q2 2 1 2 0	Q3 Q3 2 1 2 0	Q4 2 1 2 1 0	Q5 1 1 2 1	Q6 2 1 2 0	1 1 2 1	1 1 2 0 -1	0 -2 1 0 -2	9 6 7 10 6	Confidence A B C A A	0 1 0 1 -1	Q2 1 2 0 0 -1	Q3 0 0 1 1 -1	Q4 1 1 0 1 -1	0 0 0 2 1	1 2 0 0 -1	0 0 0 1 1	Q8 1 0 0 0 -1	0 1 0 0	10 5 8 10 9	Confidence A B B A	2 0 2 1 0	R3L5 Q2 2 -1 1 1	Q3 2 0 2 0 0
R3L5 Participant #	R?L? R3L5 R3L5 R3L5 R3L5 R3L5	Cars 10 8 9 10 10	Confidence A A B A C	Q1 2 1 2 1 0 2	R4L4 Q2 2 1 2 0	Q3 2 1 2 0 1	Q4 2 1 2 1 0	Q5 1 1 2 1 1	Q6 2 1 2 0 0	1 1 2 1 1 2	1 1 2 0 -1 1	0 -2 1 0 -2	9 6 7 10 6	Confidence A B C A A B	0 1 0 1 -1	Q2 1 2 0 0 -1 -1	Q3 0 0 1 1 -1	Q4 1 1 0 1 -1	0 0 0 2 1	1 2 0 0 -1 0	0 0 0 1 1	Q8 1 0 0 0 -1 0	0 1 0 0 1	10 5 8 10 9	Confidence A B B A C C	2 0 2 1 0 2	R3L! Q2 2 -1 1 0 2	Q3 2 0 2 0 0 0
R3L5 Participant #	R?L? R3L5 R3L5 R3L5 R3L5 R3L5 R3L5	Cars 10 8 9 10 10 8 7	Confidence A A B A C A	Q1 2 1 2 1 0 2	R4L4 Q2 2 1 2 0 0 1 1	Q3 Q3 2 1 2 0	Q4 2 1 2 1 0 1	Q5 1 1 2 1 1 1	Q6 2 1 2 0 0 1 1	1 1 2 1 1 2 2	1 1 2 0 -1	0 -2 1 0 -2	9 6 7 10 6	Confidence A B C A A A A B	0 1 0 1 -1 1 2	Q2 1 2 0 0 -1 -1 1	Q3 0 0 1 1 -1 0	Q4 1 1 0 1 -1 0	0 0 0 2 1 1 2	1 2 0 0 -1 0 2	0 0 0 1 1 0	Q8 1 0 0 0 -1 0	0 1 0 0 1 0 -1	10 5 8 10 9	Confidence A B A C A B	2 0 2 1 0 2 1	R3L5 Q2 2 -1 1 0 2 -1	Q3 2 0 2 0 0 2 -1
R3L5 Participant # 3 9 14 27 28 30 31 45	R?L? R3L5 R3L5 R3L5 R3L5 R3L5 R3L5 R3L5	Cars 10 8 9 10 10 8 7	Confidence A A B A C A A A	Q1 2 1 2 1 0 2 1 2	R4L4 Q2 2 1 2 0 0 1 1	Q3 Q3 2 1 2 0 1 1 1	Q4 2 1 2 1 0 1 1	Q5 1 1 2 1 1 1 1	Q6 2 1 2 0 0 1 1	1 1 2 1 1 2 2 2	1 1 2 0 -1 1 1	0 -2 1 0 -2 0 -1	9 6 7 10 6 6	Confidence A B C A A A C	0 1 0 1 -1	Q2 1 2 0 0 -1 -1	Q3 0 1 1 -1 0 1 -1	Q4 1 1 0 1 -1	0 0 0 2 1	1 2 0 0 -1 0 2 -1	0 0 0 1 1 0 1 -1	Q8 1 0 0 0 -1 0 1 -1	0 1 0 0 1 0 -1	10 5 8 10 9 10 5	Confidence A B B C A C A B B	2 0 2 1 0 2	R3LL Q2 2 -1 1 0 2 -1	Q3 2 0 2 0 0 0 2 -1 1
R3L5 Participant # 3 9 14 27 28 30 31 45	R?L? R3L5 R3L5 R3L5 R3L5 R3L5 R3L5 R3L5 R3L5	Cars 10 8 9 10 10 8 7 8 10	Confidence A A B A C A A A A A	Q1 2 1 2 1 0 2 1 2 2	R4L4 Q2 2 1 2 0 0 1 1	4 - 0.9 Q3 2 1 2 0 1 1	Q4 2 1 2 1 0 1	Q5 1 1 2 1 1 1	Q6 2 1 2 0 0 1 1	1 1 2 1 1 2 2	1 1 2 0 -1 1	0 -2 1 0 -2 0 -1	9 6 7 10 6 6	Confidence A B C A A A C B A	0 1 0 1 -1 1 2 -1	Q2 1 2 0 0 -1 -1 1	Q3 0 0 1 1 -1 0	Q4 1 0 1 -1 0 1 -1	0 0 0 2 1 1 2 -1	1 2 0 0 -1 0 2 -1 -1	0 0 0 1 1 0 1 -1	Q8 1 0 0 0 -1 0 1 -1	0 1 0 0 1 0 -1 0	10 5 8 10 9 10 5 9	Confidence A B B A C A B B B	2 0 2 1 0 2 1 1	R3L! Q2 2 -1 1 0 2 -1 1 0	Q3 2 0 2 0 0 2 -1 1 1
R3L5 Participant # 3 9 14 27 28 30 31 45 47	R?L? R3L5 R3L5 R3L5 R3L5 R3L5 R3L5 R3L5 R3L5	Cars 10 8 9 10 10 8 7	Confidence A A B A C A A A	Q1 2 1 2 1 0 2 1 2	R4L4 Q2 2 1 2 0 0 1 1 1 2	Q3 Q3 2 1 2 0 1 1 1 1	Q4 2 1 2 1 0 1 1 1	Q5 1 1 2 1 1 1 2 2	Q6 2 1 2 0 0 1 1 1 2	1 1 2 1 1 2 2 2 2	1 1 2 0 -1 1 1 2	0 -2 1 0 -2 0 -1 0 -1	9 6 7 10 6 8 5 7	Confidence A B C A A A C	0 1 0 1 -1 1 2 -1	Q2 1 2 0 0 -1 -1 1 0	Q3 0 0 1 1 -1 0 1 -1	Q4 1 0 1 -1 0 1 -1 0	0 0 2 1 1 2 -1	1 2 0 0 -1 0 2 -1	0 0 0 1 1 0 1 -1	Q8 1 0 0 0 -1 0 1 -1	0 1 0 0 1 0 -1	10 5 8 10 9 10 5	Confidence A B B C A C A B B	2 0 2 1 0 2 1 1 1	R3L Q2 2 -1 1 0 2 -1 1 0 2	Q3 2 0 2 0 0 0 2 -1 1
R3L5 Participant # 3 9 14 27 28 30 31 45	R?L? R3L5 R3L5 R3L5 R3L5 R3L5 R3L5 R3L5 R3L5	Cars 10 8 9 10 10 8 7 8 10 9	Confidence A A B A C A A A A A	Q1 2 1 2 1 0 2 1 2 2 1	R4L-Q2 2 1 2 0 0 1 1 1 2	Q3 2 1 2 0 1 1 1 1 2	Q4 2 1 2 1 0 1 1 1 2	Q5 1 1 2 1 1 1 2 2 1	Q6 2 1 2 0 0 1 1 1 2 1	1 1 2 1 1 2 2 2 2 0	1 1 2 0 -1 1 1 2 0	0 -2 1 0 -2 0 -1 0 -1	9 6 7 10 6 8 5 7	Confidence A B C A A B C B A C	0 1 0 1 -1 1 2 -1 1	Q2 1 2 0 0 -1 -1 1 0 0	Q3 0 0 1 1 -1 0 1 -1 0	Q4 1 0 1 -1 0 1 -1 0	0 0 2 1 1 2 -1 0	1 2 0 0 -1 0 2 -1 -1	0 0 0 1 1 0 1 -1 0 -1	Q8 1 0 0 0 -1 0 1 -1 0	0 1 0 0 1 0 -1 0 0	10 5 8 10 9 10 5 9 7	Confidence A B B A C A B B B A C A A A A A A A A A	2 0 2 1 0 2 1 1 1	R3L! Q2 2 -1 1 0 2 -1 1 0	Q3 2 0 2 0 0 2 -1 1 1 2
R3L5 Participant # 3 9 14 27 28 30 31 45 47 58	R?L? R3L5 R3L5 R3L5 R3L5 R3L5 R3L5 R3L5 R3L5	Cars 10 8 9 10 10 8 7 8 10 9	Confidence A A B A C A A A A B	Q1 2 1 2 1 0 2 1 2 2 1 2	R4L4 Q2 2 1 2 0 0 1 1 1 2 1 2	Q3 2 1 2 0 1 1 1 1 2	Q4 2 1 2 1 0 1 1 1 2	Q5 1 1 2 1 1 1 1 2 2 1 1 0	Q6 2 1 2 0 0 1 1 1 2 1 0 0	1 1 2 1 1 2 2 2 2 0 0	1 2 0 -1 1 1 2 0	0 -2 1 0 -2 0 -1 0 -1 0	9 6 7 10 6 6 8 5 7 8	Confidence A B C A A B A C B A C B A B	0 1 0 1 -1 1 2 -1 1 -1	Q2 1 2 0 0 -1 -1 1 0 0	Q3 0 0 1 1 -1 0 1 -1 0 0	Q4 1 1 0 1 -1 0 1 -1 0 0	0 0 0 2 1 1 2 -1 0 0	1 2 0 0 -1 0 2 -1 -1 0	0 0 0 1 1 0 1 -1 0 -1	Q8 1 0 0 0 -1 0 1 -1 0 0 0	0 1 0 0 1 0 -1 0 0 0	10 5 8 10 9 10 5 9 7 10 7	Confidence A B B A C A B B B A C A B B B B B B B B	2 0 2 1 0 2 1 1 1 1	R3L1 Q2 2 -1 1 0 2 -1 1 0 2 -1	Q3 2 0 2 0 0 2 -1 1 1 2 0
R3L5 Participant # 3 9 14 27 28 30 31 45 47 58 64 71	R?L? R3L5 R3L5 R3L5 R3L5 R3L5 R3L5 R3L5 R3L5	Cars 10 8 9 10 10 8 7 8 10 9 7 10	Confidence A A B A C A A A A A A A A A A A A A A A	Q1 2 1 0 2 1 2 2 1 1 2 2 1 1 2 2	R4L4 Q2 2 1 2 0 0 1 1 1 2 1 -1 2	Q3 2 1 2 0 1 1 1 1 2 1 0 2	Q4 2 1 2 1 0 1 1 1 2 1 0 1	Q5 1 1 2 1 1 1 2 2 1 0 2	Q6 2 1 2 0 0 1 1 1 2 1 0 1 1	1 1 2 1 1 2 2 2 2 0 0	1 1 2 0 -1 1 1 1 2 0 0	0 -2 1 0 -2 0 -1 0 -1 0 0 -2	9 6 7 10 6 8 5 7 8 8	Confidence A B C A A B A C B A C B A C C B A C C C C	0 1 0 1 -1 1 2 -1 1 -1 1	Q2 1 2 0 0 -1 -1 1 0 0 1	Q3 0 0 1 1 -1 0 1 -1 0 0 0	Q4 1 0 1 -1 0 1 -1 0 0 0	0 0 0 2 1 1 2 -1 0 0	1 2 0 0 -1 0 2 -1 -1 0 0	0 0 0 1 1 0 1 -1 0 -1 0	Q8 1 0 0 0 -1 0 1 -1 0 0 0	0 1 0 0 1 0 -1 0 0 0	10 5 8 10 9 10 5 9 7 10 7	Confidence A B B A C A B B B B B B B B B B B B	2 0 2 1 0 2 1 1 1 1 1	R3L1 Q2 2 -1 1 0 2 -1 1 0 2 -1 1 -1	Q3 2 0 2 0 0 2 -1 1 1 2 0
R3L5 Participant # 3 9 14 27 28 30 31 45 47 58 64 71 78	R?L? R3L5 R3L5 R3L5 R3L5 R3L5 R3L5 R3L5 R3L5	Cars 10 8 9 10 10 8 7 8 10 9 7 10 10	Confidence A A B A C A A A A A A A A A A A A A A A	Q1 2 1 2 1 0 2 1 2 2 1 1 2 2 1 1 2 1 1 2 1 1	R4L-Q2 2 1 2 0 0 1 1 1 2 1 -1 2 2	Q3 2 1 2 0 1 1 1 1 2 1 0 2 1 2 1 2 1 2 1 1 2 1 1 1 2 1 1 1 1	Q4 2 1 2 1 0 1 1 1 1 1 1 1 1 1 1 1 1 1 1 1	Q5 1 1 2 1 1 1 2 2 1 0 2 2	Q6 2 1 2 0 0 1 1 1 2 1 0 1 1	1 1 2 1 1 2 2 2 2 2 0 0 2 2	1 1 2 0 -1 1 1 2 0 0 1	0 -2 1 0 -2 0 -1 0 -1 0 -2 1	9 6 7 10 6 8 5 7 8 8 6 10	Confidence A B C A A B A C B A C B A C B A A A A A	0 1 0 1 -1 1 2 -1 1 -1 1 1	Q2 1 2 0 0 -1 -1 1 0 0 1 0 0 2	Q3 0 0 1 1 -1 0 1 -1 0 0 0 0	Q4 1 1 0 1 -1 0 1 -1 0 0 0 0 0	0 0 0 2 1 1 2 -1 0 0 1 1	1 2 0 0 -1 0 2 -1 -1 0 0	0 0 0 1 1 0 1 -1 0 -1 0	Q8 1 0 0 0 -1 0 1 -1 0 0 0 0 2	0 1 0 0 1 0 -1 0 0 0 0	10 5 8 10 9 10 5 9 7 10 7	Confidence A B B A C A B B B B B A A A A A A B B A A A A	2 0 2 1 0 2 1 1 1 1 1 -1	R3L: Q2 2 -1 1 0 2 -1 1 0 2 -1 1	Q3 2 0 2 0 0 2 -1 1 1 2 0 0

92									R3L	.5 - 0.	.5									R2L	1 - 0.	92									R2L
Q4	Q5	Q6	Q7	Q8	Q9	Cars	Confidence	Q1	Q2	Q3	Q4	Q5	Q6	Q7	Q8	Q9	Cars	Confidence	Q1	Q2	Q3	Q4	Q5	Q6	Q7	Q8	Q9	Cars	Confidence	Q1	Q2
1	1	0	1	0	1	9	Α	1	1	1	1	1	2	1	1	-1	7	В	0	-1	-1	-1	0	0	1	0	1	7	В	0	0
1	1	1	2	2	-1	6	В	-1	-2	-1	-1	-1	-2	0	-1	1	9	Α	1	1	1	1	1	1	1	1	-1	8	В	1	0
2	1	1	2	1	-1	8	Α	1	1	1	1	1	1	1	0	-1	9	Α	2	2	1	1	2	1	2	1	-1	7	В	1	0
1	1	1	1	1	0	7	Α	1	1	0	1	0	0	1	1	0	6	В	0	-1	0	-1	0	-1	1	-1	0	5	В	-1	-1
2	2	1	2	1	0	8	Α	1	1	1	1	1	0	1	1	0	9	Α	2	2	2	2	2	2	2	2	0	8	Α	2	1
-2	2	-1	1	-1	-1	8	В	0	0	0	0	0	0	1	0	-1	3	С	-2	-2	-2	-2	-2	-2	-2	-2	2	6	В	-1	-1
2	2	2	2	2	2	9	Α	0	2	1	1	-1	1	-1	2	0	10	Α	2	2	2	2	2	2	2	2	0	9	Α	2	2
2	2	2	2	2	1	10	Α	2	2	2	2	2	2	1	1	1	8	В	1	1	0	0	1	0	1	0	0	10	Α	2	2
2	1	2	1	2	0	6	В	0	1	0	0	0	0	0	1	0	9	Α	2	2	2	2	2	2	2	2	-1	6	В	0	0
1	1	1	1	0	0	5	Α	0	1	0	0	0	0	0	0	0	9	Α	1	1	1	1	1	1	1	0	-1	7	Α	1	1
-1	1	-1	1	-1	-1	7	В	0	0	0	0	0	0	0	0	0	7	В	1	-1	-1	-1	1	-1	1	-1	-1	9	Α	1	1
1	0	1	1	1	-1	6	В	0	1	0	1	0	1	0	1	-1	9	Α	2	1	1	2	2	1	1	2	-1	7	Α	1	1
2	2	2	2	2	0	10	Α	2	2	2	2	2	2	2	2	0	8	В	2	1	1	1	1	1	1	1	1	10	Α	2	2
2	2	2	2	2	-1	9	Α	2	2	2	2	2	2	1	2	1	8	Α	2	1	2	1	2	0	2	1	0	7	В	2	1
1	2	2	1	1	2	5	С	-1	-2	-2	-2	-1	-2	-1	-2	0	9	Α	2	1	2	2	2	1	2	1	2	1	В	0	0
2	2	2	2	2	0	7	Α	1	1	1	1	2	1	1	0	1	7	Α	1	0	0	-1	1	0	1	0	1	7	Α	1	-1
22									וכם	5 0	E									D 2 I	1 0	02									וכם
92	05	06	07	08	09	Cars	Confidence	01		.5 - 0. O3		Ω5	06	07	08	09	Cars	Confidence	01		1 - 0.		05	06	07	08	Ω9	Cars	Confidence	01	R2L
Q4	Q5 2	Q6 1			Q9 0	Cars	Confidence A	Q1 1	Q2	Q3	Q4	Q5 1	Q6 2	Q7 1	Q8 1	Q9 0	Cars 5	Confidence	Q1 0	Q2	Q3	Q4	Q5 1	Q6 -1	Q7 1	Q8 -2	Q9 1	Cars	Confidence B	Q1 1	Q2
	Q5 2 0	Q6 1 0	2	1	0	Cars 10	Α	1	Q2 2	Q3 1		1	2	Q7 1 -1	1	Q9 0 2	5	С	Q1 0 1				Q5 1	Q6 -1 1	Q7 1 2	Q8 -2 1	1	Cars 7 6	В	1	Q2 -1
Q4 1	2	1				10			Q2	Q3	Q4 1			-		0 2		C A	0	Q2 -2	Q3 -1 1	Q4 -2		-	1	-2 1	1 -2	7		1 0	Q2 -1 -1
Q4 1 0	2 0	1 0	2 -1	1 0	0 1	10 1	A C	1 -1	Q2 2 -2	Q3 1 -1	Q4 1	1 -2	2 -2	-	1 -2	0	5 8	С	0	Q2 -2 2	Q3 -1	Q4 -2 1	1	-1 1	1 2	-2	1	7 6	B B	1	Q2 -1
Q4 1 0 2	2 0 1	1 0 2	2 -1	1 0 1	0 1 2	10 1 6	A C C	1 -1 -1	Q2 2 -2 0	Q3 1 -1 0	Q4 1 -2 0	1 -2	2 -2 0	1 -1 -1	1 -2 0	0 2 -1	5 8 4	C A C	0 1 0	Q2 -2 2 -2	Q3 -1 1 -2	Q4 -2 1 -2	1 1 0	-1 1	1 2	-2 1 -2	1 -2 2	7 6 4	B B C	1 0 -1	Q2 -1 -1 -1
Q4 1 0 2 1	2 0 1 1	1 0 2 0	2 -1	1 0 1 1	0 1 2 1	10 1 6 10	A C C A	1 -1 -1 0	Q2 2 -2 0 1	Q3 1 -1 0	Q4 1 -2 0 1	1 -2 -1 1	2 -2 0 0	1 -1 -1 1	1 -2 0 0	0 2 -1 0	5 8 4 8	C A C A	0 1 0 0	Q2 -2 2 -2 -1	Q3 -1 1 -2 0	Q4 -2 1 -2 -1	1 1 0 0	-1 1	1 2	-2 1 -2 0	1 -2 2 0	7 6 4 8	B B C C	1 0 -1 1	Q2 -1 -1 -1 0
Q4 1 0 2 1	2 0 1 1 0	1 0 2 0 0	2 -1 2 1	1 0 1 1 -1	0 1 2 1 0	10 1 6 10 6	A C C A A	1 -1 -1 0 -1	Q2 2 -2 0 1 -1	Q3 1 -1 0 0 -1	Q4 1 -2 0 1 -1	1 -2 -1 1 -2	2 -2 0 0 -2	1 -1 -1 1 0	1 -2 0 0 -1	0 2 -1 0 1	5 8 4 8 9	C A C A C	0 1 0 0 1	Q2 -2 2 -2 -1 1	Q3 -1 1 -2 0 1	Q4 -2 1 -2 -1	1 1 0 0	-1 1	1 2 0 1	-2 1 -2 0 0	1 -2 2 0 -2	7 6 4 8	B B C C	1 0 -1 1 0	Q2 -1 -1 -1 0 -1
Q4 1 0 2 1 1	2 0 1 1 0 2	1 0 2 0 0	2 -1 2 1 1	1 0 1 1 -1	0 1 2 1 0	10 1 6 10 6 7	A C C A A B	1 -1 -1 0 -1	Q2 2 -2 0 1 -1	Q3 1 -1 0 0 -1 1	Q4 1 -2 0 1 -1	1 -2 -1 1 -2	2 -2 0 0 -2	1 -1 -1 1 0	1 -2 0 0 -1 -1	0 2 -1 0 1	5 8 4 8 9 7	C A C A C	0 1 0 0 1 2	Q2 -2 2 -2 -1 1	Q3 -1 1 -2 0 1	Q4 -2 1 -2 -1 0	1 1 0 0 1 1	-1 1 -2 0 0	1 2 0 1 1 2	-2 1 -2 0 0	1 -2 2 0 -2 0	7 6 4 8 8	B B C C A A	1 0 -1 1 0 2	Q2 -1 -1 -1 0 -1
Q4 1 0 2 1 1 2 -1	2 0 1 1 0 2	1 0 2 0 0 1 -1	2 -1 2 1 1 2	1 0 1 1 -1 2 0	0 1 2 1 0 0	10 1 6 10 6 7 9	A C C A A B	1 -1 -1 0 -1 1	Q2 2 -2 0 1 -1 -1	Q3 1 -1 0 0 -1 1	Q4 1 -2 0 1 -1 0	1 -2 -1 1 -2 1	2 -2 0 0 -2 0 2	1 -1 -1 1 0 1	1 -2 0 0 -1 -1	0 2 -1 0 1 1	5 8 4 8 9 7 5	C A C A C A B	0 1 0 0 1 2	Q2 -2 2 -2 -1 1 -1	Q3 -1 1 -2 0 1 1	Q4 -2 1 -2 -1 0 0 -1	1 1 0 0 1 1	-1 1 -2 0 0	1 2 0 1 1 2	-2 1 -2 0 0 0	1 -2 2 0 -2 0 0	7 6 4 8 8 9	B C C A A	1 0 -1 1 0 2 2	Q2 -1 -1 -1 0 -1 1
Q4 1 0 2 1 1 2 -1 1	2 0 1 1 0 2 1	1 0 2 0 0 1 -1 2	2 -1 2 1 1 2 1	1 0 1 1 -1 2 0 1	0 1 2 1 0 0 0	10 1 6 10 6 7 9	A C C A A B A	1 -1 -1 0 -1 1 2 -1	Q2 2 -2 0 1 -1 -1 2	Q3 1 -1 0 0 -1 1 1 -1	Q4 1 -2 0 1 -1 0 1	1 -2 -1 1 -2 1 2 -1	2 -2 0 0 -2 0 2	1 -1 -1 1 0 1 1	1 -2 0 0 -1 -1 1	0 2 -1 0 1 1 0	5 8 4 8 9 7 5	C A C A C A B	0 1 0 0 1 2 1 2	Q2 -2 2 -2 -1 1 -1 -1	Q3 -1 1 -2 0 1 1 0 2	Q4 -2 1 -2 -1 0 0 -1 2	1 1 0 0 1 1 1	-1 1 -2 0 0	1 2 0 1 1 2 1 2	-2 1 -2 0 0 0 0	1 -2 2 0 -2 0 0 -1	7 6 4 8 8 9 8	B C C A A C	1 0 -1 1 0 2 2 -2	Q2 -1 -1 -1 0 -1 1 2
Q4 1 0 2 1 1 2 -1 1 0	2 0 1 1 0 2 1 1	1 0 2 0 0 1 -1 2	2 -1 2 1 1 2 1 1	1 0 1 1 -1 2 0 1	0 1 2 1 0 0 0 0	10 1 6 10 6 7 9 1	A C C A A B A C	1 -1 -1 0 -1 1 2 -1	Q2 2 -2 0 1 -1 -1 2 0	Q3 1 -1 0 0 -1 1 1 -1	Q4 1 -2 0 1 -1 0 1 0	1 -2 -1 1 -2 1 2 -1	2 -2 0 0 -2 0 2 0	1 -1 -1 1 0 1 1	1 -2 0 0 -1 -1 1 1	0 2 -1 0 1 1 0 0	5 8 4 8 9 7 5 9	C A C A C A B A	0 1 0 0 1 2 1 2	Q2 -2 2 -1 1 -1 -1 2	Q3 -1 1 -2 0 1 0 2 0	Q4 -2 1 -2 -1 0 0 -1 2	1 1 0 0 1 1 1 1	-1 1 -2 0 0 0 -1 2	1 2 0 1 1 2 1 2	-2 1 -2 0 0 0 0 1	1 -2 2 0 -2 0 0 -1 1	7 6 4 8 8 9 8 3 8	B B C C A A C B	1 0 -1 1 0 2 2 -2	Q2 -1 -1 -1 0 -1 1 2 -2
Q4 1 0 2 1 1 2 -1 1 0 2	2 0 1 1 0 2 1 1 1 2	1 0 2 0 0 1 -1 2 0	2 -1 2 1 1 2 1 1 1 2	1 0 1 1 -1 2 0 1 1	0 1 2 1 0 0 0 0 0	10 1 6 10 6 7 9 1 8	A C C A A B A C B	1 -1 -1 0 -1 1 2 -1 1	Q2 2 -2 0 1 -1 -1 2 0 1	Q3 1 -1 0 0 -1 1 1 -1 1	Q4 1 -2 0 1 -1 0 1 0 1	1 -2 -1 1 -2 1 2 -1 1	2 -2 0 0 -2 0 2 0 1	1 -1 -1 1 0 1 1	1 -2 0 0 -1 -1 1 -1 1	0 2 -1 0 1 1 0 0 1	5 8 4 8 9 7 5 9 7	C A C A B A B	0 1 0 0 1 2 1 2 1 -1	Q2 -2 -2 -1 1 -1 -1 -1 2 0	Q3 -1 1 -2 0 1 1 0 2 0 -1	Q4 -2 1 -2 -1 0 0 -1 2 0 -1	1 0 0 1 1 1 1 1 -1	-1 1 -2 0 0 0 -1 2 0 -1	1 2 0 1 1 2 1 2 1 0	-2 1 -2 0 0 0 0 1 0 -1	1 -2 2 0 -2 0 0 -1 1	7 6 4 8 8 9 8 3 8	B B C C A A C B	1 0 -1 1 0 2 2 -2 1 1	Q2 -1 -1 -1 0 -1 1 2 -2 1
Q4 1 0 2 1 1 2 -1 1 0 2	2 0 1 1 0 2 1 1 1 2	1 0 2 0 0 1 -1 2 0 1 -1	2 -1 2 1 1 2 1 1 1 2 0	1 0 1 1 -1 2 0 1 1 0	0 1 2 1 0 0 0 0 0 1	10 1 6 10 6 7 9 1 8 9	A C C A B A C B	1 -1 -1 0 -1 1 2 -1 1 1	Q2 2 -2 0 1 -1 -1 2 0 1 1	Q3 1 -1 0 0 -1 1 1 -1 1	Q4 1 -2 0 1 -1 0 1 0 1 2	1 -2 -1 1 -2 1 2 -1 1 1	2 -2 0 0 -2 0 2 0 1 1	1 -1 -1 1 0 1 1	1 -2 0 0 -1 -1 1 -1 1	0 2 -1 0 1 1 0 0 1 0	5 8 4 8 9 7 5 9 7 7	C A C A B A B	0 1 0 0 1 2 1 2 1 -1	Q2 -2 2 -2 -1 1 -1 -1 -1 2 0 -1	Q3 -1 1 -2 0 1 0 2 0 -1 0	Q4 -2 1 -2 -1 0 -1 2 0 -1 -1	1 0 0 1 1 1 1 1 -1	-1 1 -2 0 0 0 -1 2 0 -1 -1	1 2 0 1 1 2 1 2 1 0	-2 1 -2 0 0 0 0 1 0 -1 0	1 -2 2 0 -2 0 0 -1 1 0	7 6 4 8 8 9 8 3 8 9 7	B B C C A A A B	1 0 -1 1 0 2 2 -2 1 1	Q2 -1 -1 -1 0 -1 1 2 -2 1 1
Q4 1 0 2 1 1 2 -1 1 0 2 -1 -1	2 0 1 1 0 2 1 1 1 2 0	1 0 2 0 0 1 -1 2 0 1 -1	2 -1 2 1 2 1 1 1 2 0	1 0 1 1 -1 2 0 1 1 0 0 -1	0 1 2 1 0 0 0 0 1 0 0	10 1 6 10 6 7 9 1 8 9 8	A C C A B A C B A	1 -1 -1 0 -1 1 2 -1 1 1 1	Q2 2 -2 0 1 -1 -1 2 0 1 1 0 2	Q3 1 -1 0 0 -1 1 1 -1 1	Q4 1 -2 0 1 -1 0 1 0 1 2 0	1 -2 -1 1 -2 1 2 -1 1 1	2 -2 0 0 -2 0 2 0 1 1	1 -1 -1 1 0 1 1	1 -2 0 0 -1 -1 1 -1 1 0	0 2 -1 0 1 1 0 0 1 0 0	5 8 4 8 9 7 5 9 7 7 7	C A C A B A B C	0 1 0 0 1 2 1 2 1 -1 0 -1	Q2 -2 2 -1 1 -1 -1 2 0 -1 -1	Q3 -1 1 -2 0 1 1 0 2 0 -1 0 -1	Q4 -2 1 -2 -1 0 -1 2 0 -1 -1 -1	1 0 0 1 1 1 1 1 -1 0 -1	-1 1 -2 0 0 0 -1 2 0 -1 -1 -1	1 2 0 1 1 2 1 2 1 0 0	-2 1 -2 0 0 0 0 1 0 -1 0 -1	1 -2 2 0 -2 0 0 -1 1 0 0	7 6 4 8 8 9 8 3 8 9 7 3	B C C A A C B A C	1 0 -1 1 0 2 2 -2 1 1 1	Q2 -1 -1 -1 0 -1 1 2 -2 1 1 -1 -1

.1 - 0	.5									Ow	า - 0.9	92									Ow	n - 0.	5					
Q3	Q4	Q5	Q6	Q7	Q8	Q9	Cars	Confidence	Q1	Q2	Q3	Q4	Q5	Q6	Q7	Q8	Q9	Cars	Confidence	Q1	Q2	Q3	Q4	Q5	Q6	Q7	Q8	Q9
0	0	0	-1	1	0	1	9	Α	2	1	1	1	2	1	1	1	0	10	Α	2	2	1	2	1	2	1	1	-1
1	0	0	0	1	0	0	10	Α	1	2	1	2	1	2	2	1	1	8	Α	1	1	1	1	1	0	1	1	0
1	0	1	0	1	1	-1	9	В	2	2	1	1	2	1	2	-1	-1	7	В	1	1	1	1	1	0	1	1	-1
-1	-1	0	-1	0	-1	0	7	Α	1	-1	0	-1	1	0	1	0	0	6	Α	0	0	0	1	0	0	1	0	0
1	2	2	2	2	2	1	8	Α	2	1	2	2	2	1	2	2	0	9	Α	2	2	2	1	2	2	2	2	0
-2	-2	0	-1	0	-1	1	10	Α	2	2	1	1	1	1	1	0	1	9	Α	1	1	1	1	0	0	1	1	0
2	2	2	2	1	2	1	8	Α	2	2	1	2	0	2	2	1	1	7	Α	2	1	1	2	0	1	2	2	0
2	2	2	2	2	2	1	7	В	1	0	0	-1	0	0	1	0	0	10	Α	2	2	2	2	1	2	1	2	0
-1	-1	-1	-1	0	-1	1	10	Α	2	2	2	2	1	2	2	2	-1	10	Α	2	2	2	2	1	2	1	2	-1
1	1	1	1	1	1	0	9	Α	1	1	1	1	1	0	1	1	-1	6	В	-1	-1	-1	-1	-1	0	-1	-1	0
1	1	2	1	1	1	2	7	В	1	0	0	0	1	0	1	0	0	7	В	0	0	0	0	0	0	0	0	0
1	1	1	1	2	1	-1	7	В	1	1	1	1	0	1	1	1	-1	8	Α	1	2	2	1	1	1	1	1	-1
2	2	2	2	2	2	1	10	Α	2	2	2	2	2	2	2	2	-1	10	Α	2	2	2	2	2	2	2	2	1
2	1	2	1	2	1	0	7	Α	2	1	2	1	2	1	2	1	0	10	Α	2	2	2	2	2	2	2	2	-1
0	0	0	1	-1	1	0	5	В	0	0	0	0	0	1	0	0	1	1	С	-2	0	0	0	-2	0	-2	0	0
0	-1	0	-1	0	-1	0	8	Α	2	2	2	1	1	2	2	2	0	6	Α	1	1	0	0	0	0	0	1	0
4 0	-									_	0.0	20									0	•	-					
.1 - 0.		OF	06	07	00	00	Core	Confidence	01		n - 0.9		OF	06	07	00	00	Cars	Confidence	01		n - 0.		OF	06	07	00	00
Q3	Q4	Q5	Q6	Q7	Q8	Q9	Cars	Confidence	Q1	Q2	Q3	Q4	Q5	Q6	Q7	Q8	Q9	Cars	Confidence	Q1	Q2	Q3	Q4	Q5	Q6	Q7	Q8	Q9
Q3 1	Q4 0	1	-1	2	0	-1	9	Α	1	Q2 1	Q3 2	Q4 1	2	1	2	1	0	8	В	1	Q2 1	Q3 1	Q4 1	0	1	1	0	0
Q3 1 -1	Q4 0 -1	1	-1 -1	2	0	-1 1	9 9	A A	1 2	Q2 1 2	Q3 2 2	Q4 1 2	2	1 2	2	1 2	0 -2	8 8	B A	1	Q2 1 1	Q3 1 1	Q4 1 1	0 1	1 1	1	0	0 -2
Q3 1 -1 -1	Q4 0 -1 -2	1 0 1	-1 -1 -2	2 0 1	0 0 -1	-1 1 2	9 9 7	A A B	1 2 1	Q2 1 2 -1	Q3 2 2 0	Q4 1 2 0	2 2 0	1 2 0	2 2 0	1 2 0	0 -2 1	8 8 6	B A C	1 1 -1	Q2 1 1 0	Q3 1 1 0	Q4 1 1 0	0 1 -1	1 1 0	1 1 -1	0 0	0 -2 0
Q3 1 -1 -1 1	Q4 0 -1 -2 -1	1 0 1	-1 -1 -2 0	2 0 1	0 0 -1 0	-1 1 2 0	9 9 7 10	А А В А	1 2 1	Q2 1 2 -1 0	Q3 2 2 0 1	Q4 1 2 0 1	2 2 0 1	1 2 0 0	2 2 0 2	1 2 0 1	0 -2 1 0	8 8 6 10	B A C A	1 1 -1 1	Q2 1 1 0	Q3 1 1 0	Q4 1 1 0	0 1 -1 1	1 1 0 1	1 1 -1 1	0 0 0	0 -2 0 0
Q3 1 -1 -1 1 0	Q4 0 -1 -2 -1	1 0 1 1	-1 -1 -2 0 -1	2 0 1 1	0 0 -1 0	-1 1 2 0	9 9 7 10 9	A A B A C	1 2 1 1 0	Q2 1 2 -1 0	Q3 2 2 0 1	Q4 1 2 0 1	2 2 0 1 0	1 2 0 0	2 2 0 2 1	1 2 0 1 -1	0 -2 1 0 -1	8 8 6 10 10	B A C A C	1 1 -1 1 0	Q2 1 1 0 0	Q3 1 1 0 0	Q4 1 1 0 0	0 1 -1 1 0	1 1 0 1	1 1 -1 1 0	0 0 0 0 -1	0 -2 0 0
Q3 1 -1 -1 1 0	Q4 0 -1 -2 -1 0	1 0 1 1 1 2	-1 -1 -2 0 -1	2 0 1 1 1 2	0 0 -1 0 0	-1 1 2 0 0	9 9 7 10 9	A B A C	1 2 1 1 0 2	Q2 1 2 -1 0 0 2	Q3 2 2 0 1 0	Q4 1 2 0 1 1 2	2 2 0 1 0	1 2 0 0 0	2 2 0 2 1	1 2 0 1 -1	0 -2 1 0 -1	8 8 6 10 10	B A C A C	1 1 -1 1 0 2	Q2 1 1 0 0 1 2	Q3 1 1 0 0 0 2	Q4 1 1 0 0 1 2	0 1 -1 1 0	1 1 0 1 1	1 1 -1 1 0 1	0 0 0 0 -1 1	0 -2 0 0 0
Q3 1 -1 -1 1 0 2	Q4 0 -1 -2 -1 0 1	1 0 1 1 1 2 2	-1 -1 -2 0 -1 1	2 0 1 1 1 2 2	0 0 -1 0 0 1	-1 1 2 0 0 1 -1	9 7 10 9 9	A B A C A	1 2 1 1 0 2 2	Q2 1 2 -1 0 0 2 2	Q3 2 2 0 1 0 2	Q4 1 2 0 1 1 2	2 2 0 1 0 1 2	1 2 0 0 0 1 2	2 2 0 2 1 1 2	1 2 0 1 -1 2	0 -2 1 0 -1 0 -1	8 8 6 10 10 9	B A C A C A	1 1 -1 1 0 2	Q2 1 1 0 0 1 2	Q3 1 1 0 0 0 2 1	Q4 1 1 0 0 1 2	0 1 -1 1 0 1	1 0 1 1 1	1 1 -1 1 0 1	0 0 0 0 -1 1 2	0 -2 0 0 0 0
Q3 1 -1 -1 1 0 2 1	Q4 0 -1 -2 -1 0 1 1	1 0 1 1 1 2 2	-1 -1 -2 0 -1 1 1	2 0 1 1 1 2 2	0 0 -1 0 0 1 1	-1 1 2 0 0 1 -1 2	9 7 10 9 9 10	A B A C A A	1 2 1 1 0 2 2 2	Q2 1 2 -1 0 0 2 2 2	Q3 2 2 0 1 0 2 1	Q4 1 2 0 1 1 2 1 2	2 2 0 1 0 1 2 2	1 2 0 0 0 1 2	2 2 0 2 1 1 2 2	1 2 0 1 -1 2 1	0 -2 1 0 -1 0 -1 -1	8 8 6 10 10 9 9	B A C A C A C	1 1 -1 1 0 2 1	Q2 1 1 0 0 1 2 2	Q3 1 1 0 0 0 2 1 -1	Q4 1 1 0 0 1 2 1	0 1 -1 1 0 1 1	1 1 0 1 1 1 1 -1	1 1 -1 1 0 1 1	0 0 0 0 -1 1 2 -1	0 -2 0 0 0 0 0
Q3 1 -1 -1 1 0 2 1 -2	Q4 0 -1 -2 -1 0 1 1 -2	1 0 1 1 2 2 -2	-1 -1 -2 0 -1 1 -1	2 0 1 1 1 2 2 -2	0 0 -1 0 0 1 1 -2	-1 1 2 0 0 1 -1 2	9 9 7 10 9 9 10 9	A B A C A A A	1 2 1 1 0 2 2 2 2	Q2 1 2 -1 0 0 2 2 2	Q3 2 2 0 1 0 2 1 2	Q4 1 2 0 1 1 2 1 2	2 2 0 1 0 1 2 2	1 2 0 0 0 1 2 1	2 2 0 2 1 1 2 2	1 2 0 1 -1 2 1 1	0 -2 1 0 -1 0 -1 -1	8 8 6 10 10 9 9 5 7	B A C A C A C B	1 1 -1 1 0 2 1 -1	Q2 1 1 0 0 1 2 2 0	Q3 1 1 0 0 0 2 1 -1	Q4 1 0 0 1 2 1 0 -1	0 1 -1 1 0 1 1 -1	1 0 1 1 1 1 -1 -1	1 1 -1 1 0 1 1 0 -1	0 0 0 0 -1 1 2 -1	0 -2 0 0 0 0 0 0
Q3 1 -1 -1 1 0 2 1 -2 1	Q4 0 -1 -2 -1 0 1 1 -2 1	1 0 1 1 2 2 -2 1 1	-1 -1 -2 0 -1 1 1 -1 1	2 0 1 1 1 2 2 -2 1 0	0 0 -1 0 0 1 1 -2 1 0	-1 1 2 0 0 1 -1 2 0	9 9 7 10 9 9 10 9	A B A C A A A	1 2 1 1 0 2 2 2 2 1	Q2 1 2 -1 0 0 2 2 2 2 1	Q3 2 0 1 0 2 1 2 1 2	Q4 1 2 0 1 1 2 1 2 2	2 2 0 1 0 1 2 2 1	1 2 0 0 0 1 2 1 1	2 2 0 2 1 1 2 2 2	1 2 0 1 -1 2 1 1 0	0 -2 1 0 -1 0 -1 -1 0	8 8 6 10 10 9 9 5 7	B A C A C A C B	1 1 -1 1 0 2 1 -1 0	Q2 1 1 0 0 1 2 2 0 0	Q3 1 1 0 0 0 2 1 -1 0	Q4 1 0 0 1 2 1 0 -1	0 1 -1 1 0 1 -1 -1 1	1 0 1 1 1 -1 -1	1 1 -1 1 0 1 1 0 -1	0 0 0 0 -1 1 2 -1 -1	0 -2 0 0 0 0 0 0 1
Q3 1 -1 -1 1 0 2 1 -2 1 1 0	Q4 0 -1 -2 -1 0 1 -2 1 1 -2	1 0 1 1 1 2 2 -2 1 1 0	-1 -1 -2 0 -1 1 1 -1 1 -1	2 0 1 1 1 2 2 -2 1 0	0 0 -1 0 0 1 1 -2 1 0	-1 1 2 0 0 1 -1 2 0 0	9 9 7 10 9 9 10 9 9	A B A C A A B	1 2 1 1 0 2 2 2 2 2 1 0	Q2 1 2 -1 0 0 2 2 2 2 1 -1	Q3 2 0 1 0 2 1 2 2 1 0	Q4 1 2 0 1 1 2 1 2 2 1 -1	2 2 0 1 0 1 2 2 1 1	1 2 0 0 0 1 2 1 1 1 -1	2 0 2 1 1 2 2 2 1 0	1 2 0 1 -1 2 1 1 0	0 -2 1 0 -1 0 -1 -1 0 0	8 8 6 10 10 9 9 5 7 9	B A C A C A C B A B	1 1 -1 1 0 2 1 -1 0 1	Q2 1 1 0 0 1 2 2 0 0 1	Q3 1 1 0 0 2 1 -1 0	Q4 1 1 0 0 1 2 1 0 -1 0	0 1 -1 1 0 1 -1 -1 1	1 0 1 1 1 -1 -1 0	1 1 -1 1 0 1 1 0 -1 0	0 0 0 0 -1 1 2 -1 -1 0	0 -2 0 0 0 0 0 1 0 0
Q3 1 -1 -1 1 0 2 1 -2 1 1 0 -1	Q4 0 -1 -2 -1 0 1 1 -2 1 1 -1	1 0 1 1 2 2 -2 1 1 0	-1 -1 -2 0 -1 1 1 -1 1 -1 -1	2 0 1 1 1 2 2 -2 1 0 0 -1	0 0 -1 0 0 1 1 -2 1 0 0	-1 1 2 0 0 1 -1 2 0 0 0	9 9 7 10 9 9 10 9 9	A B A C A A A A B A	1 2 1 1 0 2 2 2 2 2 1 0	Q2 1 2 -1 0 0 2 2 2 2 1 -1 1	Q3 2 2 0 1 0 2 1 2 2 1 0 1	Q4 1 2 0 1 1 2 1 2 2 1 -1 1	2 2 0 1 0 1 2 2 1 1 0	1 2 0 0 0 1 2 1 1 1 -1	2 0 2 1 1 2 2 2 1 0 2	1 2 0 1 -1 2 1 1 0 0	0 -2 1 0 -1 0 -1 -1 0 0 0	8 8 6 10 10 9 5 7 9 8 8	B A C A C A C B A	1 1 -1 1 0 2 1 -1 0 1 1	Q2 1 1 0 0 1 2 2 0 0 1 0 1	Q3 1 1 0 0 0 2 1 -1 0 1	Q4 1 1 0 0 1 2 1 0 -1 0 0	0 1 -1 1 0 1 -1 -1 1 1	1 0 1 1 1 -1 -1 0 0	1 1 -1 1 0 1 1 0 -1 0 1 2	0 0 0 0 -1 1 2 -1 -1 0	0 -2 0 0 0 0 0 1 0 0 0
Q3 1 -1 -1 1 0 2 1 -2 1 1 0 -1	Q4 0 -1 -2 -1 0 1 1 -2 1 1 -1 -2 -1	1 0 1 1 2 2 -2 1 1 0 -2	-1 -1 -2 0 -1 1 -1 1 -1 -1 -1	2 0 1 1 2 2 -2 1 0 0 -1 1	0 0 -1 0 0 1 1 -2 1 0 0 -2 -1	-1 1 2 0 0 1 -1 2 0 0 0 1 1	9 9 7 10 9 9 10 9 9 7 8 10	A B A C A A A A A A A A A A A A A A A A	1 2 1 1 0 2 2 2 2 2 1 0 1	Q2 1 2 -1 0 0 2 2 2 2 1 -1 1 1	Q3 2 2 0 1 0 2 1 2 2 1 0 1 2 2	Q4 1 2 0 1 1 2 1 2 2 1 -1 1 2	2 2 0 1 0 1 2 2 1 0 1 2 2	1 2 0 0 0 1 2 1 1 1 -1 1	2 2 0 2 1 1 2 2 2 1 0 2	1 2 0 1 -1 2 1 1 0 0 1 2	0 -2 1 0 -1 0 -1 -1 0 0 0	8 8 6 10 10 9 5 7 9 8 8 10	B A C A C A C B A B	1 1 -1 1 0 2 1 -1 0 1 1 1	Q2 1 1 0 0 1 2 2 0 0 1 0 1 0 1	Q3 1 1 0 0 0 2 1 -1 0 1 0 0	Q4 1 1 0 0 1 2 1 0 -1 0 0 0 0	0 1 -1 1 0 1 -1 -1 1 1 0	1 0 1 1 1 1 -1 -1 0 0	1 1 1 1 0 1 1 0 -1 0 1 2 -1	0 0 0 0 -1 1 2 -1 -1 0 0	0 -2 0 0 0 0 0 1 0 0 0 0 -1 0
Q3 1 -1 -1 1 0 2 1 -2 1 1 0 -1	Q4 0 -1 -2 -1 0 1 1 -2 1 1 -1	1 0 1 1 2 2 -2 1 1 0	-1 -1 -2 0 -1 1 1 -1 1 -1 -1	2 0 1 1 1 2 2 -2 1 0 0 -1	0 0 -1 0 0 1 1 -2 1 0 0	-1 1 2 0 0 1 -1 2 0 0 0	9 9 7 10 9 9 10 9 9	A B A C A A A A B A	1 2 1 1 0 2 2 2 2 2 1 0	Q2 1 2 -1 0 0 2 2 2 2 1 -1 1	Q3 2 2 0 1 0 2 1 2 2 1 0 1	Q4 1 2 0 1 1 2 1 2 2 1 -1 1	2 2 0 1 0 1 2 2 1 1 0	1 2 0 0 0 1 2 1 1 1 -1	2 0 2 1 1 2 2 2 1 0 2	1 2 0 1 -1 2 1 1 0 0	0 -2 1 0 -1 0 -1 -1 0 0 0	8 8 6 10 10 9 5 7 9 8 8	B A C A C A C B A	1 1 -1 1 0 2 1 -1 0 1 1	Q2 1 1 0 0 1 2 2 0 0 1 0 1	Q3 1 1 0 0 0 2 1 -1 0 1	Q4 1 1 0 0 1 2 1 0 -1 0 0	0 1 -1 1 0 1 -1 -1 1 1	1 0 1 1 1 -1 -1 0 0	1 1 -1 1 0 1 1 0 -1 0 1 2	0 0 0 0 -1 1 2 -1 -1 0	0 -2 0 0 0 0 0 1 0 0 0



Briefing and Consent Form

This appendix contains the experiment briefing and the consent form the participants were asked to sign.

Experiment Briefing

Drivers' acceptance of trajectory type in trajectory-driven haptic shared control

Thank you for participating in this experiment! The experiment, conducted in the Human-Machine Interaction Laboratory (HMI-Lab), analyses drivers' acceptance of different trajectory types in trajectory-driven haptic shared control, and tries to understand the relationship between these preferences and manual driving styles. The experiment consists of two parts: a manual driving experiment and, for a selected set of participants, also a haptic shared control experiment. This briefing will introduce you to the experiment and what is expected of you as a participant.

Experiment Goal

The goal of this experiment is to investigate drivers' acceptance of trajectory type in trajectory-driven haptic shared control. Advanced driver-assistance systems (ADAS) have the potential to increase driving safety for all road users, however, these systems will only be used if drivers accept and trust them. In order to investigate how to optimise this acceptance, a haptic shared control experiment is conducted. The results of the experiment should clarify how acceptance is optimised for drivers.

Experiment Task

In this task, you will drive a car <u>at fixed speed</u> on a road that curves a couple of times to the left and a couple of times to the right. It is your task to drive on the road as you normally would. In the first part of the experiment you will drive manually, so without any haptic feedback (forces) on the steering wheel. If you are selected for the second part of the experiment (based on your natural driving style), you will drive the same single-lane road with different settings of a haptic shared controller.

The car-side of the HMI-Lab consists of a car seat and control-loaded steering wheel by Nissan. The 180° field of view screens will display a single-lane road surrounded by trees with no other road users. The fixed speed of the car will be shown on the driver display.

In addition, while very unlikely for the current experiment, it is possible that some participants may develop nausea (simulator sickness) during the tests. In case you experience the first symptoms of simulator sickness (feeling very warm, sweating profusely, stomach awareness), you are instructed to inform the experimenter, as then experiment will, unfortunately, be discontinued.

Experiment Procedures

For the manual driving experiment, you will perform three repeated trials of the same simulated driving task. All runs have the same conditions. For the haptic shared control experiment, you will be subjected to several different types of haptic feedback. The different conditions will be presented to you in a random order. After you have completed a run for each condition once, you will be given a different random set of conditions, which is repeated until a satisfactorily consistent performance has been attained for all conditions. The researcher will keep track of your performance and will announce when the experiment has been completed.

Each driving run lasts about 180 seconds. Short breaks can be taken between runs to alleviate any discomfort that might occur due to controlling the side-stick or after sitting in a fixed position for a prolonged period of time. Longer breaks will be taken after every 9-12 runs, where you will be taken out of the simulator for 5-10 minutes. The experiment will last approximately 45 minutes.

For each driving trial, the subsequent procedure will be followed:

- 1. The researcher applies the settings for the next run.
- 2. The researcher checks whether the participant is ready to proceed (i.e., simulator sickness symptoms) and initiates the run after a countdown from 3 (3-2-1-go).
- 3. The participant performs the tracking task.
- 4. The participant will be notified of their performance in the completed run in terms of error score displayed on the primary flight display after the completed run.

Contact information researcher:Contact information research supervisorEmma GhysDr. ir. Daan Poole.p.j.ghys@student.tudelft.nld.m.pool@tudelft.nl+32 473 51 73 23+31 15 2789611

Thank you for participating!

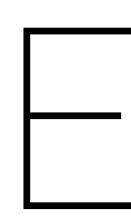
Experiment Consent Form

Driver's acceptance of trajectory type in trajectory-driven haptic shared control

I hereb	y confirm, by ticking each box, that:		
1.	(Emma Ghys) under supervision of Aerospace Engineering of TU Delft. I u	Deriment conducted by the researcher Dr.ir. Daan Pool from the Faculty of understand that my participation in this withdraw and discontinue participation	
2.	·	g and confirm that I understand the questions answered to my satisfaction.	
3.		lves performing a simple driving task in a erent settings of haptic (force) feedback	
4.	•	provided me with detailed safety and dware (simulator setup, control-loaded experiment.	
5.	during the tests and that in case I exp	nay develop nausea (simulator sickness) perience the first symptoms (i.e., feeling , I will inform the experimenter. I also e discontinued for this reason.	
6.		ot identify me by name in any reports or experiment, and that my confidentiality as ecure.	
7.	TU Delft Human Research Ethics Com regarding my participation in the e	nas been reviewed and approved by the mittee (HREC). To report any problems xperiment, I know I can contact the tion below or, if necessary, the TU Delft	
My Sig	nature	Date	
My Pri	nted Name	Signature of researcher	
Emr	tact information researcher: na Ghys j.ghys@student.tudelft.nl	Contact information research supervi Dr. ir. Daan M. Pool d.m.pool@tudelft.nl	<u>sor</u>

+32 473 51 73 23

+31 15 2789611



Attempts at New Conflict Definition

During the analysis of the results of the haptic shared control experiment, it was found that the conflict definition used was incomplete as it – in some scenarios – accounted for conflict caused by the feedforward torque, although this torque is not experienced by the drivers as punishing.

A first attempt at a new definition consisted of a comparison between the driver torque and the rescaled feedforward torque by the control system. The area difference between both curves indicates how much the driver's steering differs from the intended path of the haptic shared control system. Figure E.1 shows the driver torque and rescaled feedforward torque of an R3L5 driver. This driver is an example of an R3L5 driver that shows a high amount of conflicts for R3L5 guidance, but also rated the R3L5 guidance very high on the subjective rating scales.

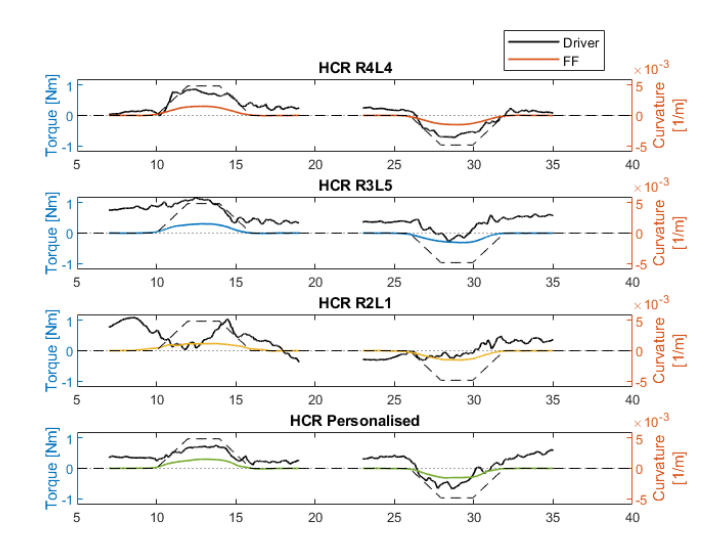


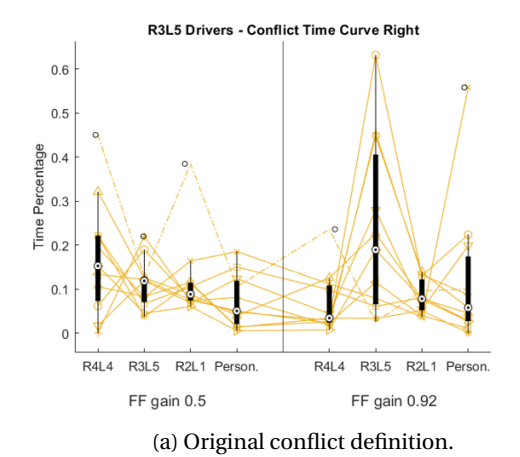
Figure E.1: Driver torque plotted against the rescaled feedforward torque of the controller for driver 3, an R3L5 driver.

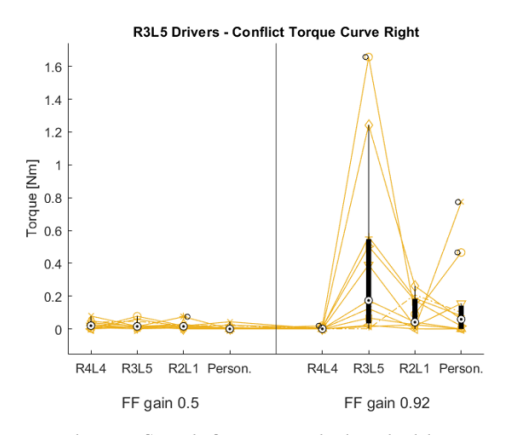
Additionally, Table E.1 shows the calculated area difference between both curves. The table shows that the area difference is largest for the R3L5 guidance, especially in the curve sections, indicating that this attempt at a new conflict definition is insufficient to solve the problem.

A second attempt at a new conflict definition included a threshold on the driver torque. The intention behind the threshold was that no conflict can be present if the driver follows the guidance and thus the driver torques are low. On the other hand, if the driver is actively steering and the driver torques are above the threshold, then conflict is possible. Since the driver torque in the prepositioning phase most often shows a steady, constant trend, it was decided to only add the threshold to the driver torques in the curve phase. The results of adding the threshold can be seen in Figure E.2. The left figure of Figure E.2 shows the conflict time over the different conditions for an R3L5 driver in the curve phase, while the right figure shows the results

Left Right Prep Curve Prep Curve R4L40.37122.3203 1.1578 1.5706 R3L5 3.8967 3.9939 1.9211 2.0124 R2L1 3.878 1.7736 1.3535 1.3327 Personalised 1.8621 1.9373 1.6492 1.135

 $\label{thm:eq:torque} \textbf{Table E.1: Area difference between driver torque and rescaled feedforward torque of driver 3.}$





(b) Conflict definition with threshold in curves

Figure E.2: Conflict time for R3L5 drivers for right curves.

with a threshold of 20% on top of the constant torque of the prepositioning phase. The figures show that the threshold also does not solve the issue of the high conflict values in R3L5, as the conflict remains high.